



UNIVERSITY OF
BIRMINGHAM

SPRAY, COMBUSTION AND EMISSION CHARACTERISTICS OF DIESEL FUEL

By

Fan Zhang

A thesis submitted to

The University of Birmingham

for the degree of

DOCTOR OF PHILOSOPHY

The University of Birmingham
School of Engineering
March 2013

UNIVERSITY OF
BIRMINGHAM

University of Birmingham Research Archive

e-theses repository

This unpublished thesis/dissertation is copyright of the author and/or third parties. The intellectual property rights of the author or third parties in respect of this work are as defined by The Copyright Designs and Patents Act 1988 or as modified by any successor legislation.

Any use made of information contained in this thesis/dissertation must be in accordance with that legislation and must be properly acknowledged. Further distribution or reproduction in any format is prohibited without the permission of the copyright holder.

ABSTRACT

The fuel blend of diesel and gasoline (dieseline) has been studied in the present work. In particular, it investigates spray characteristics of dieseline in a state-of-the-art fuel spray test rig, the performance of combustion and emissions, in a modern light duty compression-ignition (CI) engine.

Experimental results showed that the spray of dieseline fuel had similar tip penetration length as diesel at various back pressures and injection pressures while the penetration length of gasoline was shorter than diesel, due to vaporization. With an increase of the gasoline/diesel blending ratio, both the mean diameter and the SMD of the fuel droplets were decreased at the downstream injector nozzle. This is of benefit for fuel/air mixing and reducing particulate matter (PM) emissions.

When operating with dieseline, the engine's PM emissions were much less than with diesel in terms of mass and number. The PM emissions of dieseline were less sensitive to the variation of exhaust gas recirculation (EGR) ratio, as compared to diesel. With the usage of advanced injection timing and large amounts of EGR, both the NO_x and PM emissions of a G50 (50% gasoline in diesel by volume) fuelled partially premixed compression ignition (PPCI) engine, were reduced significantly at part load. Using split injection strategies gave more flexibility, than the single injection strategies, for the control of mixing strength and combustion phasing. However, the power density of dieseline fuelled PPCI operation was still limited by the NO_x reduction's dependence on EGR.

A novel concept, named Stoichiometric Dual-fuel Compression Ignition (SDCI) was investigated. The diesel and gasoline were blended internally through direct injection (DI) and

port fuel injection (PFI) respectively. EGR was used to operate the engine under stoichiometric condition, which thus allows the usage of a three-way catalyst for handling NO_x emissions. This removes the traditional NO_x-PM trade-off compromise in engine design and has the potential of being used to develop high power density engines and using low-cost after treatments to meet stringent emissions' legislation. The SDCI combustion can achieve better thermal efficiency than a diesel engines in a relatively wide load range (4.3 to 8 bar IMEP). The PM emissions of SDCI combustion were lower by up to 75% in number than the conventional CI diesel combustion. Overall, the SDCI concept was experimentally proved to be a very promising technique for optimising a CI engine's efficiency, emissions and noise without compromise of cost and power density.

ACKNOWLEDGEMENTS

First and foremost, I would like to thank my supervisor Professor Hongming Xu for his guidance and support throughout my PhD study. The help and suggestions from Professor Mirosław L. Wyszynski (associate supervisor) are also greatly appreciated.

I would also like to thank Professor Gautam Kalghatgi from Saudi Aramco for his helpful discussions, Roger Cracknell from Shell Global Solutions UK and Haiwen Song from Ford Motor Company for their technical advice and support.

Thanks also go to the laboratory technicians- Carl Hingley, Peter Thornton and Lee Gauntlett for their support with all test facility matters.

I am sincerely grateful to all of my colleagues at the Future Power System group for their support and companion. In particular, great thanks go to Dr Jun Zhang for his guidance during my first year of study, Dr Yanfei Li and Daliang Jing for their support in the dieseline spray study, Dr Guohong Tian and Dr Xiao Ma for their valuable discussions in my research, Soheil Zeraati Rezei for his help in engine modification and testing.

Finally, on a more personal level, I would like to thank my girlfriend, Qin Wang, for her patience and encouragement throughout my study in UK.

*I wish to dedicate this thesis to my family for their love and
great support along the way*

CONTENTS

ABSTRACT	I
ACKNOWLEDGEMENTS	III
CONTENTS	V
LIST OF ABBREVIATIONS	X
LIST OF FIGURES.....	XIII
LIST OF TABLES.....	XIX
LIST OF PUBLICATIONS	XX
CHAPTER 1 INTRODUCTION.....	1
1.1. Background.....	1
1.1.1. Energy Demand and Climate Change	1
1.1.2. Emission Legislation.....	3
1.1.3. Advanced Diesel Engine.....	5
1.1.4. Towards High Efficient and Clean Diesel Engine.....	6
1.2. Research Objectives.....	7
1.3. Thesis Outline	8
CHAPTER 2 LITERATURE REVIEW	10
2.1. Fuel Spray Characteristics	10
2.1.1. Spray Structure and Process.....	11
2.1.2. Tip Penetration and Cone Angle	14
2.1.3. Fuel Droplet Size.....	17
2.2. Diesel Combustion and Emissions Formation.....	18
2.2.1. Conceptual Model.....	18
2.2.2. Formation of Emissions.....	20

2.3. Partially Premixed Compression Ignition(PPCI).....	24
2.3.1. Introduction	24
2.3.2. Effects of Injection Strategies and Engine Hardware.....	27
2.3.3. Fuels for PPCI.....	29
2.3.4. Low Octane Gasoline Fuelled PPCI	30
2.3.5. Dieseline Fuelled PPCI.....	31
2.3.6. Real Time Fuel Design Through In-cylinder Blending.....	32
2.3.7. Diesel Stoichiometric Combustion	34
2.4. Summary	34
CHAPTER 3 EXPERIMENTAL SETUP	35
3.1. Spray Measurement	35
3.1.1. Fuel Injection System	36
3.1.2. Spray Visualisation	38
3.1.3. Phase Doppler Particle Analyzer(PDPA).....	39
3.2. Engine Test Rig.....	41
3.2.1. The Engine	41
3.2.2. Test Rig Control	42
3.2.3. Real Time Combustion Analysing System	44
3.2.4. Fuel Consumption Measurement and Calibration.....	45
3.2.5. Tested Fuels	46
3.3. Dual Fuel and Single Cylinder Engine Modification	47
3.3.1. Overview of the Single Cylinder Engine	47
3.3.2. Exhaust Manifold Modification.....	49
3.3.3. Intake Manifold Modification.....	49

3.3.4. Gasoline PFI System.....	50
3.3.5. Flag Signal for PFI System	51
3.4. Emissions Measurement Instruments	53
3.4.1. Gaseous Emissions Measurement.....	53
3.4.2. Particle Emissions Measurement.....	54
3.5. Data Processing.....	59
3.5.1. Heat Release Rate Analyses	59
3.5.2. Engine Efficiency Calculation.....	60
3.5.3. Specific Emissions Calculation	61
3.6. Summary	61

CHAPTER 4 DIESELINE SPRAY CHARACTERISTICS 63

4.1. Introduction	63
4.2. Fuel Spray Tip Penetration	64
4.2.1. Test Conditions.....	64
4.2.2. Effect of Gasoline/Diesel Blending Ratio.....	66
4.2.3. Effect of Back Pressure and Injection Pressure.....	68
4.2.4. Empirical Correlation for Dieseline Spray	70
4.3. Dieseline Fuel Droplets' Size and Velocity.....	73
4.3.1. Test Conditions.....	73
4.3.2. Effect of Gasoline/Diesel Blending Ratio	75
4.3.3. Fuel Droplets Size and Velocity Distribution.....	77
4.3.4. Effect of Injection Pressure	80
4.4. Conclusions	82

CHAPTER 5 CONVENTIONAL DIESEL LINE COMBUSTION..... 84

5.1. Dieseline Combustion Using Conventional Engine Strategies..... 84

5.1.1. Studied Fuels and Methods..... 85

5.1.2. Heat Release Rate Analysis 86

5.1.3. Combustion Performance 88

5.1.4. Regulated Emissions..... 93

5.1.5. Particle Number 96

5.2. Effect of Engine Conditions 98

5.3. Effect of Pilot Injection 101

5.4. Conclusions..... 106

CHAPTER 6 DIESEL LINE FUELLED PPCI COMBUSTION..... 108

6.1. Challenge of Achieving PPCI with Diesel..... 108

6.2. Single Injection Dieseline PPCI..... 110

6.2.1. Injection Timing and EGR Ratio Sweep..... 110

6.2.2. Effect of Injection Pressure 119

6.2.3. Engine Load Extension..... 121

6.3. Split Injection PPCI 123

6.3.1. Introduction 123

6.3.2. Effect of First Injection Quantity and Timing 125

6.3.3. Effect of Second Injection Timing 130

6.4. Conclusions..... 134

CHAPTER 7 IN-CYLINDER BLENDED DIESELINE COMBUSTION	136
7.1. Introduction.....	136
7.2. Dual Fuel Lean Burn.....	137
7.2.1. Effect of EGR and G/(G+D) Ratio.....	137
7.2.2. Combustion Phasing Sweep.....	142
7.2.3. Load Sweep	144
7.3. Stoichiometric Dual Fuel Compression Ignition (SDCI).....	149
7.3.1. Introduction	149
7.3.2. Engine Load Sweep.....	150
7.3.3. Impact of Gasoline Percentage	157
7.3.4. Impact of DI Timing	163
7.4. Conclusions.....	166
CHAPTER 8 SUMMARY, CONCLUSIONS AND FUTURE WORK.....	168
8.1. Summary and Conclusion	168
8.2. Future Work	171
8.2.1. CFD Simulation and Optical Diagnostic.....	171
8.2.2. Load Extension for PPCI Operation	171
8.2.3. Reliability of Using Dieseline in Common Rail Injection System ..	172
8.2.4. SDCI Combustion	172
LIST OF REFERENCES.....	173
APPENDIX A.....	185
APPENDIX B.....	185

LIST OF ABBREVIATIONS

AC	Alternating Current
AHR50	50% of cumulative apparent heat release
AIS	Adaptive Injection Strategies
ANR	Analyser Rack Unit
ATDC	After Top Dead Centre
BMEP	Brake Mean Effective Pressure
BSNO_x	Brake Specific Mono-nitrogen Oxides
BSHC	Brake Specific Hydrocarbon
BSCO	Brake Specific Carbon Mono-oxide
BTDC	Before Top Dead Centre
BTE	Brake Thermal Efficiency
Ca	Area Contraction Coefficient
Cv	Orifice Velocity Contraction Coefficient
CAD	Crank Angle Degree
CI	Compression Ignition
CMD	Count Mean Diameter
CMOS	Complementary Metal-Oxide-Semiconductor
CN	Cetane Number
CO	Carbon Mono-Oxide
CPC	Condensation Particle Counter
dQ	Change of Heat Release
dθ	Time Step Size in Degrees
dp	Change of In-cylinder Pressure
dv	Change of In-cylinder Volume
D_n	Injector Nozzle Diameter
DAQ	Data Acquisition
DMA	Differential Mobility Analyzer
DOC	Diesel Oxidation Catalyst
DPF	Diesel Particulate Filter
EC	Electrostatic Classifier
ECU	Engine Control Unit
EU	European Union

FID	Flame Ionization Dectector
FS	Full Scale
FSN	Filter Smoke Number
GDCI	Gasoline Direct-injection Compression Ignition
HEDGE	High Efficiency Diluted Gasoline Engine
HEV	Hybrid Electric Vehicle
HC	Hydrocarbon
HCCI	Homogenous Charge Compression Ignition
HCI	Homogeneous Charge Induced Ignition
ICE	Internal Combustion Engine
IFP	French Institute of Petroleum
IMEP	Indicated Mean Effective Pressure
IPCC	Intergovernmental Panel on Climate Change
ISCO	Indicated Specific Carbon Mono-oxide
ISFC	Indicated Specific Fuel Consumption
ISHC	Indicated Specific Hydrocarbon
ISNO_x	Indicated Specific Nitrogen Oxides
LDV	Light Duty Vehicle
LIEF	Laser Induced Exciplex Fluorescence
LNT	Lean NO _x Trap
LTC	Low Temperature Combustion
m_f	Fuel Mass Flow rate
MK	Modulated Kinetics
MPRR	Maximum Pressure Rise Rate
MCU	Main Control Unit
NEDC	New European Driving Cycle
NO	Nitric Oxide
NO₂	Nitrogen dioxides
NO_x	Nitrogen Oxides
OH	Hydroxyl
OVN	Oven Unit
P	Engine Power
P_{back}	Back Pressure
P_{inj}	Fuel Injection Pressure
P_{max}	Maximum In-cylinder Pressure
PAH	Polycyclic Aromatic Hydrocarbon

PCCI	Premixed Charge Compression Ignition
PDPA	Phase Doppler Particle Analyser
PFI	Port Fuel Injection
PPCI	Partially Premixed Compression Ignition
PM	Particulate Matter
PN	Particulate Number
Q_{HV}	Lower Fuel Heating Value
RCCI	Reactivity Controlled Compression Ignition
RON	Research Octane Number
RP	Rail Pressure
S	Spray Penetration Length
SCR	Selective Catalytic Reduction
SDCI	Stoichiometric Dual-fuel Compression Ignition
SI	Spark Ignition
SMD	Sauter Mean Diameter
SMPS	Scanning Mobility Particle Analyser
SOC	Start of Combustion
SOF	Soluble Organic Fraction
SOI	Start of Injection
SVS	Solenoid Valve System
t	Spray observing time
TDC	Top Dead Centre
UHC	Unburned Hydrocarbon
ULSD	Ultra-Low Sulfur Diesel
UNIBUS	Uniform Bulky Combustion System
V	Engine Volume
VIP	Variable Injection Pressure
VNT	Variable Nozzle Turbine
VVT	Variable Valve Timing
ρ_{amb}	Ambient Density
ρ_l	Liquid Fuel Density
Δp	Pressure difference between ambient and injection
θ	Spray Dispersion Angle
η_f	Thermal Efficiency
γ	Ratio of Specific Heats

LIST OF FIGURES

Figure 1.1 Global Energy Demand Forecast [1]	1
Figure 1.2 Global Primary Energy Consumption by Source and Sector, 2010 [2].....	2
Figure 2.1 Parameters of a spray [7].....	12
Figure 2.2 Schematic view of the diesel spray with a very short break-up length [11].....	14
Figure 2.3 Penetration versus time for vaporizing (the symbols) and non-vaporizing spray (the curves) Injection pressure 137 MPa, ambient gas temperature 451 K and 1000 K [14].....	15
Figure 2.4 Conceptual schematic of conventional diesel combustion [25]	19
Figure 2.5 Sketch of variation of NO _x with local mixture strength. Fuels can be premixed to different degrees depending on their ignition quality [35].....	22
Figure 2.6 Diagram showing the ϕ -temperature ranges for soot and NO _x formation and the regions for conventional diesel, HCCI, and diesel PCCI engines [47].....	26
Figure 2.7 Conceptual model for partially premixed low-temperature diesel combustion and the comparison to conventional diesel combustion model (heavy duty diesel engine) [48]	27
Figure 3.1 Schematic of spray test rig [128]	35
Figure 3.2 Schematic of Fuel Injection System	36
Figure 3.3 Major Components of Fuel Injection System: (a) Fuel pressure controller; (b) Solenoid injector; (c) Driver for solenoid injector.....	37
Figure 3.4: Phantom V710 Camera and its Specifications	38
Figure 3.5 Images of Spray. (a) Original image; (b) segmented and rotated image; (c) binary imag	39
Figure 3.6 Schematic of PDPA system [130]	40
Figure 3.7 Ford PUMA engine test bench [131].....	41
Figure 3.8 Schematic of the standard 4-cylinder Ford engine set-up and diagnostics.....	42
Figure 3.9 Front panel of Real Time Combustion Analysing Program	45
Figure 3.10 Calibration of fuel consumption reading from ECU.....	46
Figure 3.11 Schematic of Single Cylinder Dual Fuel Engine (Modified from 4-Cylinder PUMA Engine).	48
Figure 3.12 Modified Exhaust Manifold.....	49
Figure 3.13 Intake Manifold with PFI Injector Installed.....	50
Figure 3.14 Schematic of Gasoline PFI System	51

Figure 3.15 Input and Output Signals of D-Type Flip-Flop ACT374.....	52
Figure 3.16 Gas Flow Schematic for Horiba 7100DEGR.....	54
Figure 3.17 Gas Flow Schematic for Electrostatic Classifier with DMA [133].....	56
Figure 3.18 Schematic of DMS500 Two-stage Dilution System [134].....	58
Figure 3.19 DMS500 Particle Classifier and Charger [134]	59
Figure 4.1 Spray images of diesel, G50 and G100, injection pressure 500 bar, back pressure 15 bar ..	66
Figure 4.2 Effect of gasoline/diesel blending ratio on penetration length at injection pressure of 500 bar. (a) $P_{back}=15$ bar; (b) $P_{back}=30$ bar	67
Figure 4.3 Effect of gasoline/diesel blending ratio on tip penetration length at injection pressure of 1000 bar. (a) $P_{back}=15$ bar; (b) $P_{back}=30$ bar.....	68
Figure 4.4 Effect of back pressure on penetration length. (a) $P_{inj}= 500$ bar; (b) $P_{inj}=1000$ bar.....	69
Figure 4.5 Effect of injection pressure on penetration length.....	69
Figure 4.6 Comparison of experimental data with Naber and Siebers’s model at Injection pressure of 500 bar. (a) $P_{back}=15$; (b) $P_{back}=30$ bar.....	72
Figure 4.7 Comparison of experimental data with Naber and Siebers’s model at Injection pressure of 1000 bar. (a) $P_{back}=15$ bar; (b) $P_{back}=30$ bar.....	72
Figure 4.8 PDPA Testing positions.....	74
Figure 4.9 Example of unprocessed PDPA result, diesel fuel, Injection pressure: 1000 bar, sampling position: 40 mm downstream, (a) axial droplets velocity; (b) droplets diameter	74
Figure 4.10 Effect of gasoline/diesel blending ratio on droplets size sampling position: 40 mm downstream of jet nozzle. (a) Mean diameter; (b) SMD	76
Figure 4.11 Effect of gasoline/diesel blending ratio on axial mean velocity, sampling position: 40 mm downstream of jet nozzle. (a) $P_{inj}=500$ bar; (b) $P_{inj}=1000$ bar	76
Figure 4.12 Distribution of fuel droplets along axial direction, injection pressure: 750 bar. (a) mean diameter; (b) SMD	77
Figure 4.13 Fuel droplets size (SMD) distribution throughout the spray region at injection pressure of 750 bar. (a) Diesel; (b) G50; (c) G100	79
Figure 4.14 Droplets mean velocity of G50 along axial direction, injection pressure: 750 bar.....	80
Figure 4.15 Effect of injection pressure on droplets size, sampling position: 40 mm downstream. (a) Mean diameter; (b) SMD	81
Figure 4.16 Cumulative ratio against droplets diameter, sampling position: 40 mm downstream. (a) Varied injection pressure, fuel G50; (b) varied gasoline blending ratio, $P_{inj}= 500$ bar	82
Figure 5.1 EGR ratio and AHR50 with engine operated from 1.27 bar to 7.85 bar BMEP.....	85

Figure 5.2 In-cylinder pressure and heat release rate of the single injection diesel and G50 versus crank angle: (a) 1.38 bar BMEP; (b) 4.3 bar BMEP; (c) 7.85 bar BMEP	88
Figure 5.3 Combustion performances of base diesel, single injection diesel, G20 and G50 at different engine load. (a) Combustion delay; (b) COV	89
Figure 5.4 The combustion duration of base diesel, single injection diesel, G20 and G50 versus BMEP	90
Figure 5.5 The MPRR of base diesel, single injection diesel, G20 and G50 versus BMEP	91
Figure 5.6 The brake thermal efficiency and combustion efficiency of base diesel, the single injection diesel, G20 and G50 versus BMEP	92
Figure 5.7 Smoke, BSNO _x , BSHC and BSCO emissions of the base diesel, single injection diesel, G20 and G50 versus BMEP	95
Figure 5.8 Brake specific particle number total concentration of the base diesel, the single injection diesel, G20 and G50 versus BMEP	97
Figure 5.9 The particulate number and size distribution of the base diesel, the single injection diesel, G20 and G50	97
Figure 5.10 Particle count median diameter (CMD) of the base diesel, the single injection diesel, G20 and G50 versus BMEP	98
Figure 5.11 In-cylinder pressure and heat release rate of the single injection diesel and G50 versus crank angle: (a) 2 bar BMEP; (b) 4.3 bar BMEP	100
Figure 5.12 Combustion performances of G50 with pilot injection quantity of 0, 1.5 and 3 mm ³ /cycle. (a) Combustion delay; (b) MPRR	102
Figure 5.13 Effect of pilot injection quantity on In-cylinder pressure and heat release rate, 4.3 bar BMEP engine condition. (a) Diesel; (b) G50.	103
Figure 5.14 Trade-off between smoke and NO _x as pilot injection quantity varied	104
Figure 5.15 Accumulation mode and nucleation mode particle total concentration of diesel and G50 with varied pilot injection quantity at 2 bar, 3 bar and 4.3 bar BMEP	105
Figure 5.16 Particle count median diameter of diesel and G50 with varied pilot injection quantity at 2 bar, 3 bar and 4.3 bar BMEP	105
Figure 6.1 Diesel fuelled PPCI combustion in the current engine	109
Figure 6.2 Testing matrix for EGR ratio and injection timing sweep	111
Figure 6.3 Combustion delay versus injection timing at different EGR ratios	112
Figure 6.4 AHR50 and MPRR versus injection timing at different EGR ratios. (a) AHR50; (b) MPRR ..	113
Figure 6.5 Effect of injection timing at different EGR ratios on engine efficiency. (a) Combustion efficiency; (b) brake thermal efficiency	114
Figure 6.6 Smoke, BSNO _x , BSHC and BSCO emissions of G50 fuelled PPCI combustion at varied injection timings and EGR ratios	115

Figure 6.7 Effect of EGR ratios on particle number total concentration. (a) count median diameter (CMD); (b) and size distribution	116
Figure 6.8 Effect of injection timings on particle number total concentration. (a) count median diameter (CMD); (b) and size distribution	117
Figure 6.9 Trade-off between smoke and NO _x for diesel, G50 and G70 at 3 bar BMEP	118
Figure 6.10 Optimised G50 fuelled PPCI operation at 3 bar BMEP	119
Figure 6.11 Effect of injection pressure on combustion performances and emissions at 48% EGR and 23° BTDC SOI.....	120
Figure 6.12 Effect of injection pressure on particle emissions. (a) number size distribution; (b) total concentration and CMD.....	121
Figure 6.13 Trade-off between BSNO _x and smoke for G50 fuelled PPCI at 5.2 bar BMEP.....	122
Figure 6.14 G70 fuelled PPCI at 5.2 bar BMEP (marked point A in Figure 6.13).....	122
Figure 6.15 In-cylinder pressure, heat release rate and injection pulse for 3 bar BMEP. (a) 70%, 60% and 50% first injection quantity ratio (first injection timing was fixed at 18° BTDC); (b) 70% first injection quantity ratio (first injection timing varied from 68° BTDC to 97° BTDC)	126
Figure 6.16 Effect of different first injection quantity-ratios on combustion performances, 3 bar BMEP (a) Brake thermal efficiency; (b) MPRR	127
Figure 6.17 Smoke emissions of three different first injection quantity-ratios, 3bar BMEP.....	128
Figure 6.18 Brake specific NO _x of three different first injection quantity-ratios, 3bar BMEP	129
Figure 6.19 Effect of different first injection quantity-ratios on emissions, 3bar BMEP. (a) Brake specific total HC; (b) and brake specific CO	130
Figure 6.20 In-cylinder pressure, heat release rate and injection pulse for different second injection timings at 3 bar BMEP; second injection quantity ratio: 30%; first injection timing: 68° BTDC	131
Figure 6.21 Combustion phasing (AHR50) and BSNO _x emission for different second injection timings	132
Figure 6.22 Combustion delay and smoke emissions for different second injection timings	133
Figure 6.23 BSTHC and BSCO emissions for different second injection timings.....	133
Figure 7.1 In-cylinder pressure and heat release rate of in-cylinder blended diesel combustion for different EGR and G/ (G+D) ratios, IMEP 4.3 bar, AHR50 5° ATDC	138
Figure 7.2 Effect of different EGR and G/ (G+D) ratios on combustion performances, IMEP 4.3 bar, AHR50=5° ATDC. (a) MPRR; (b) combustion delay (deg)	139
Figure 7.3 Effect of different EGR and G/ (G+D) ratios on engine efficiency, IMEP 4.3 bar, AHR50 5° ATDC. (a) Combustion efficiency; (b) indicated efficiency	140
Figure 7.4 Smoke, ISNO _x , ISHC and ISCO for different EGR and G/ (G+D) ratios, IMEP 4.3 bar, AHR50 5° ATDC	141

Figure 7.5 In-cylinder pressure and heat release rate for different combustion phasing, IMEP 4.3 bar, EGR 36%, $G/(G+D)$ 0.52	142
Figure 7.6 Effect of different combustion phasing on engine performances, IMEP 4.3 bar, EGR 36%, $G/(G+D)=0.52$. (a) MPRR and combustion delay; (b) combustion efficiency and indicated efficiency	143
Figure 7.7 Effect of different combustion phasing on emissions, IMEP 4.3 bar, EGR 36%, $G/(G+D)$ 0.52. (a) Smoke and ISNOx; (b) ISCO and ISHC.....	144
Figure 7.8 Combustion characteristics for varied engine loads, EGR 22%	146
Figure 7.9 In-cylinder pressure and heat release rate for 2.1, 4.3 and 7.0 bar IMEP, EGR 22%, DI quantity 7.9 mg/stroke	146
Figure 7.10 Emission characteristics for varied engine loads, EGR 22%.....	147
Figure 7.11 Effect of varied engine loads on engine efficiency, EGR 22%. (a) Combustion efficiency; (b) indicated efficiency	148
Figure 7.12 SDCI Combustion analysis as the engine load sweeps. (a) In-Cylinder pressure; (b) heat release rate	152
Figure 7.13 Combustion duration and maximum pressure rise rate (MPRR) of load sweeps	152
Figure 7.14 Indicate specific fuel consumption (ISFC) and indicated thermal efficiency (ITE).....	153
Figure 7.15 Gaseous emissions of SDCI combustion for different engine loads. (a) ISCO and ISHC; (b) ISNOx	154
Figure 7.16 Combustion efficiency of SDCI combustion for different engine loads	155
Figure 7.17 PM and FSN data (a) PM size distribution; (b) Particle numbers of the accumulation and nucleation modes; (c) CMD of accumulation mode; (d) FSN	157
Figure 7.18 Combustion analyses at different gasoline percentages with a fixed injection timing (a) In-cylinder pressure; (b) ROHR.....	158
Figure 7.19 Efficiencies and combustion performances for varied gasoline percentages with a fixed DI timing (a) ISFC and ITE; (b) Combustion duration and MPRR.....	159
Figure 7.20 PM emissions at different gasoline percentages with a fixed injection timing (a) PM size distribution; (b) Particle number in accumulation and nucleation modes; (c) Particle count median diameter; (CMD) and smoke emission	160
Figure 7.21 Combustion analysis at different gasoline percentages with a fixed AHR50 (a) In-cylinder pressure; (b) ROHR	161
Figure 7.22 Efficiencies and combustion phase data at different gasoline percentages with a fixed AHR50: (a) ISFC and ITE; (b) Combustion duration and Max PRR	161
Figure 7.23 PM emissions at different gasoline percentages with a fixed AHR50 (a) PM size distribution; (b) Particle number in accumulation and nucleation modes; (c) CMD and FSN	162
Figure 7.24 Combustion analysis for the different DI injection timings (a) In-cylinder pressure; (b) ROHR.....	163

Figure 7.25 Impact of the DI injection timing on the ISFC, indicated thermal efficiency and combustion duration (a) ISFC and ITE; (b) Combustion duration and MPRR.....	164
Figure 7.26 Impact of the DI injection timing on the PM emissions (a) Normalised PM size distribution (b) Particle numbers of the accumulation and nucleation modes; (c) CMD and FSN	165
Figure B1 The torque and power characteristics of PUMA engine [131]	185
Figure B2 The block diagram of real time combustion analysing program	186
Figure B3 The front panel of Horiba remote control program	186
Figure B4 The block diagram of Horiba remote control program	187
Figure B5 The engineering drawing of PFI injector housing	187

LIST OF TABLES

Table 1.1 EU emissions' standard for light duty commercial vehicles, g/km	4
Table 1.2 Incremental costs for LDVs meeting European standards (2010 \$)	4
Table 3.1 PDPA specifications and operating parameters	40
Table 3.2 The Specifications of the standard 4-cylinder Ford engine.....	42
Table 3.3 Fuel Properties (~ means estimated value)	47
Table 3.4 Truth Table of D-Type Flip-Flop ACT374 [132].	52
Table 3.5 AVL 415S smoke meter specifications.....	55
Table 4.1 Test Conditions for spray penetration study	65
Table 5.1 Combustion performances of diesel and G50 at 2 bar, 3 bar and 4.3 bar BMEP	101
Table 5.2 Emissions of diesel and G50 at 2 bar, 3 bar and 4.3 bar BMEP.....	101
Table 6.1 Baseline single-injection strategy experimental results for 3 bar BMEP, AHR50: 3° ATDC, EGR: 45%	124
Table 7.1 Baseline and optimised (for efficiency) single injection diesel, 4.3 bar IMEP.....	137
Table 7.2 DI timing and gasoline percentages in the load sweeps	151

LIST OF PUBLICATIONS

1. **The Particle Emission Characteristics of a Light Duty Diesel Engine by Using Different Pilot Injections** Jun Zhang, Fan Zhang, Guohong Tian, Hongming Xu et al. SAE Technical Paper 2010-01-1959, 2010.
2. **The Application of Two Closely Coupled DPFs as the After-treatment System** Jun Zhang, Fan Zhang, Hongming Xu, Ritchie Daniel. SAE Technical Paper 2010-01-1939, 2010.
3. **The Particle Emissions Characteristics of a Light Duty Diesel Engine with 10% Alternative Fuel Blends** Jun Zhang, Hongming Xu, Guohong Tian, Fan Zhang, Phil Price. SAE International Journal of Fuels and Lubricants, 2010, 3(3): 438-452.
4. **Investigation into Light Duty Dieseline Fuelled Partially-Premixed Compression Ignition Engine** Fan Zhang, Hongming Xu, Jun Zhang, Guohong Tian, Gautam Kalghatgi. SAE International Journal of Engines, 2011, 4(1):2124-2134.
5. **Combustion and Emission Characteristics of a PPCI Engine Fuelled with Dieseline** Fan Zhang, Hongming Xu, Soheil Zaratti Rezari, Gautam Kalghatgi, Shijin Shuai. SAE Technical Paper 2012-01-1138, 2012.
6. **Characteristics of Light Duty Dieseline Fuelled Partially-Premixed Compression Ignition Engine.** Fan Zhang and Hongming Xu, Toward Clean Diesel Engine (TCDE) Conference 2011, Chester.
7. **Investigation of two-stage split-injection strategies for a Dieseline fuelled PPCI engine** Soheil Zaratti Rezari, Fan Zhang, Hongming Xu, Akbar Ghafourian et al. Journal of Fuel, Available online 28 November 2012, ISSN 0016-2361.
8. **A Study of Stoichiometric Dual-fuel Compression Ignition in a Single-Cylinder Diesel Engine** Xiao Ma, Fan Zhang, Hongming Xu and Shijin Shuai. Submitted to the Journal of Fuel.
9. **Experimental Investigation of Dieseline Spray Characteristics in a Common Rail Injection System** Fan Zhang, Daliang Jin, Yanfei Li and Hongming Xu. Prepared for the Journal of Fuel.

10. **Performance Characteristics of Diesel and Gasoline Blends in Partially Premixed Compression Ignition** Fan Zhang, Hongming Xu, Soheil Zaratti Rezari, Gautam Kalghatgi and Akbar Ghafourian. Prepared for the Journal of Automotive Engineering.

CHAPTER 1

INTRODUCTION

1.1. Background

1.1.1. Energy Demand and Climate Change

Energy demand and supply have been a concern since the 1980s as the global population grows quickly and the economy booms in emerging countries. Figure 1.1 illustrates the historical and the projected energy demand until 2050. It is shown that the world energy demand will increase by around 40% from the year 2010 to 2030. Fossil fuels will provide the main contribution during that period. After the year 2030, nuclear and renewable sources will increase considerably and fulfil the further increased demand. However, fossil fuels are expected to maintain their dominance as an energy source in the foreseeable future.

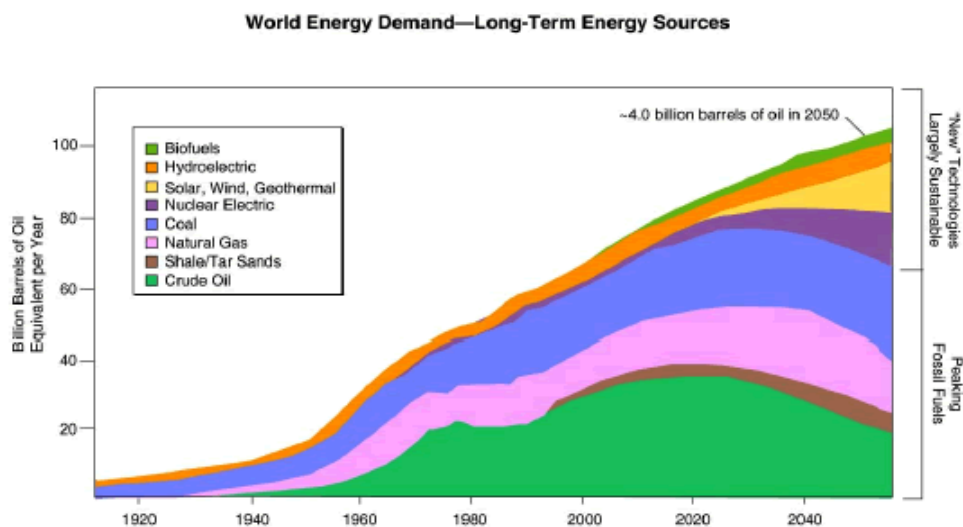


Figure 2.1 Global Energy Demand Forecast [1].

On considering the share of energy consumption by different sectors, it is shown in Figure 1.2 that the transportation sector consumed 28% of global total energy, which is just second to electricity power (40%), in 2010. In terms of energy source, 71% of liquid fuel went to the transportation sector. Driven by the oil price, government policy and technology development, it is supposed that more vehicles will be powered by electricity in the future [2]. Thus the transportation sector will use more electricity from coal, nuclear and renewable sources. The question is how many vehicles will be electrified. According to the projection from the European Parliament’s Committee [3], 59% of vehicles in 2030 will be still powered by an ICE and 13% will be HEVs, which contain an ICE, if CO2 limits are widely implemented, the oil price increases continuously and charging infrastructures are invested in. It can be expected that vehicles will still highly rely on liquid fossil fuel in the near future.

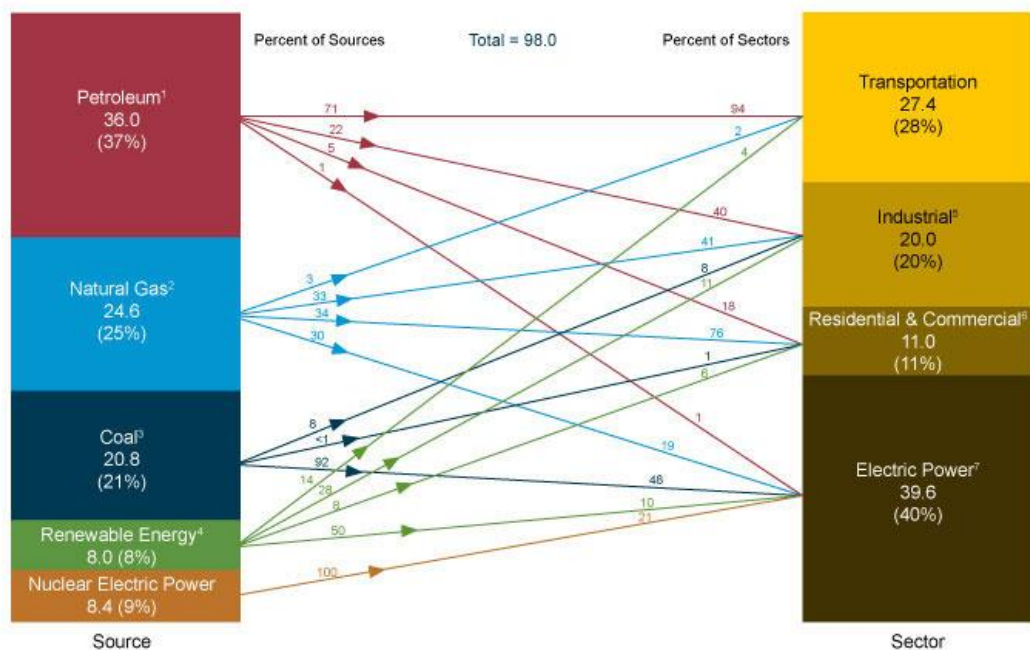


Figure 1.2 Global Primary Energy Consumption by Source and Sector, 2010 [2].

Apart from energy demand, climate change is another concern in recent years. As a result of fossil fuel combustion and deforestation, the green house gases’ (mainly CO2) concentration in the atmosphere has increased steadily since industrialization in western countries. The increasing concentration of CO2 is likely to be associated with climate change. The

intergovernmental panel on climate change (IPCC) advised that global CO₂ emissions must be reduced by 50% in 2050 to avoid the worst impact from climate change [4]. In 2007, the EU commissioned the reduction of CO₂ emissions by 20% by 2020, as compared to 1990. Aiming for the target for cars, CO₂ emissions will be limited to an average of 130 g/km in 2015 and it is proposed to decrease them further to 95g/km by 2020 [5].

Transferring to electric vehicles can definitely reduce CO₂ emissions effectively. However, as stated in the first two paragraphs of this chapter, fossil fuels will still be the dominant energy source and the ICE will take the major market share in the near future. Finding ways to utilise fossil fuel more efficiently and wisely in an ICE are critical and necessary. Much research has shown that there is great potential for efficiency improvement of internal combustion engines by adapting advanced technologies.

1.1.2. Emissions' Legislation

The Europe Union introduced emissions' regulation in 1992 and the standard has become more and more stringent since then. Table 1.1 presents the detailed EU emissions stages and the corresponding timeline for light duty vehicles. From 2000 to the present, the NO_x and PM emissions have been reduced by 85% and 90% respectively due to the regulation. A further aggressive 50% NO_x reduction will be applied in the coming Euro 6 in 2014. No further stringent regulation for toxic emissions is expected beyond Euro 6 but the CO₂ emissions are expected to be regulated. The USA and Japan have introduced similar emissions' standards as the EU and the emerging countries, such as China and India, are following.

Compared to gasoline engines, the stringent emissions' standard is more challenging for diesel engines. In gasoline engines the CO, THC and NO_x emissions can be removed

effectively by a cost effective three way catalyst, while the engine out PM level is already quite low. Diesel engine technology, as well as its cost, has largely been driven by the emissions' standard. The launch of Euro 5 has pushed all manufacturers to fit diesel engines with an expensive Diesel Particle Filter (DPF) and the coming Euro 6 will force the application of high cost Lean NOx Trap (LNT) or Selective Catalytic Reduction(SCR) .

Table 1.1 EU emissions' standard for light duty commercial vehicles, g/km

<i>Emissions</i>	<i>Date</i>	<i>CO(g/km)</i>	<i>NO_x(g/km)</i>	<i>PM</i>	<i>PN</i>
<i>Euro 1†</i>	1992.07	2.72 (3.16)	-	0.14 (0.18)	-
<i>Euro 2, IDI</i>	1996.01	1.0	-	0.08	-
<i>Euro 2, DI</i>	1996.01 ^a	1.0	-	0.10	-
<i>Euro 3</i>	2000.01	0.64	0.50	0.05	-
<i>Euro 4</i>	2005.01	0.50	0.25	0.025	-
<i>Euro 5a</i>	2009.09 ^b	0.50	0.18	0.005 ^f	-
<i>Euro 5b</i>	2011.09 ^c	0.50	0.18	0.005 ^f	6.0×10 ¹¹
<i>Euro 6</i>	2014.09	0.50	0.08	0.005 ^f	6.0×10 ¹¹

Source: <http://www.dieselnet.com/standards/eu/ld.php>, retrieved on 20/09/2012

An estimated cost of emissions' reduction technologies for light duty vehicles (LDVs) is presented in table 1.2. From Euro 4 to Euro 6, the additional cost for a gasoline engine is negligible, because a three way catalyst can handle most of the toxic emissions and no extra emission control equipment is needed. However, the fitting of a DPF and SCR, which is required to meet EURO 6, will more than double the total cost of emission control equipment.

Table 1.2: Incremental costs for LDVs meeting European standards (2010 \$)

Engine Type	Vehicle Class	Euro 1	Euro 1 to Euro 2	Euro 2 to Euro 3	Euro 3 to Euro 4	Euro 4 to Euro 5	Euro 5 to Euro 6	No control to Euro
Gasoline	4 Cylinders Vd=1.5L	\$142	\$63	\$122	\$25	\$10	--	\$362
Gasoline	4 Cylinders Vd=2.5L	\$232	\$3	\$137	\$15	\$30	--	\$417
Diesel	4 Cylinders Vd=1.5L	\$56	\$84	\$337	\$145	\$306	\$471	\$1399
Diesel	4 Cylinders Vd=2.5L	\$56	\$89	\$419	\$164	\$508	\$626	\$1862

Source: http://www.theicct.org/sites/default/files/publications/ICCT_LDVcostsreport_2012.pdf, Retrieved in 22/09/12

1.1.3. Advanced Diesel Engines

Diesel engines have been widely used in commercial vehicles because of their high fuel efficiency and the high torque they can offer at lower engine speeds. In Europe, thanks to significantly improved diesel engine technology since the last decade, more than 50% of the passenger car market is shared by diesel cars. Generally, diesel power cars consume half of the fuel consumed by similar size gasoline cars. The high efficiency of diesel engines results from its combustion characteristics.

The combustion inside diesel engines is very complicated and the process can be simplified as below: a liquid fuel spray jet enters the cylinder under high injection pressure at around TDC; the liquid fuel is broken up and atomised to small droplets resulting from cavitation, turbulence and the aerodynamic interactions at the liquid/gas interface; some of the small fuel droplets evaporate and form a gaseous fuel/air mixture; the mixture is compressed and ignited; the rest of the fuel droplets continue evaporating and the combustion flame is controlled by the mixing rate of evaporated gaseous fuel and air [24]. The nature of mixing controlled combustion and multi-point ignition helps diesel engines to avoid an engine knocking problem while being operated with a high compression ratio and high torque at low speed, both of which have a decisive effect on engine thermal efficiency. The inhomogeneous diesel/air mixtures make it possible to combust at an overall lean mixture. Thus diesel engines need not be throttled at part loads and there is quite low pump loss. However, in a gasoline engine, fuel is fully mixed with air and the overall lean mixture may result in misfire. Additionally, a three way catalyst in a gasoline engine is only efficient under stoichiometric conditions. Both of these facts make throttles indispensable for gasoline engines (VVT can partly reduce the dependence) and the pump loss increases, especially at low loads.

In order to meet emissions' legislations and achieve higher efficiency, many advanced technologies have been applied to modern diesel engines. High pressure common rail injection systems are widely equipped by diesel engines to reduce PM emissions. Intercooled EGR helps to reduce NO_x emissions effectively. A variable nozzle turbocharger (VNT) is used to raise the power output and fuel efficiency. An ECU can control all of this equipment and run the engine with optimised parameters. On the after-treatment side, DOC can reduce over 90% THC plus CO and a DPF can reduce 90% PM and PN. Combining these technologies, a Euro 5 diesel car can offer gasoline car-like emissions and comparable noise levels, while its efficiency is much higher than a gasoline car.

Although a lot of achievements have been made in the field of diesel engines, several challenges need to be overcome to maintain them as competitive power units for future vehicles. The biggest challenges are the increased diesel engine production cost (presented in table 1.2), which is caused by stringent emissions' legislation, and insufficient diesel fuel supply. Due to these challenges, many researchers are investigating new combustion modes and alternative fossil fuel for diesel engines, which is able to improve fuel efficiency and meet coming emissions' legislation without after- treatments.

1.1.4. Towards Clean Diesel Engines

In conventional diesel engines, the air/fuel mixture is highly inhomogeneous and there is a trade off between NO_x and particle emissions. Homogeneous charge compression ignition (HCCI) combustion was first researched on a gasoline engine to increase its fuel efficiency [6]. As emissions' legislations get more and more stringent, some researchers applied the HCCI concept in diesel engines in order to reduce NO_x and particle emissions simultaneously. However, after years of research, it was found that the operational window of diesel premixed

combustion is quite narrow as a result of diesel's auto-ignition characteristic. In recent years, the focus is on using alternative fossil fuel in diesel engines.

At the University of Birmingham, researchers firstly investigated the idea of designing fuel characteristics through blending gasoline with diesel (dieseline) and tested the blended fuel in a HCCI gasoline engine. This thesis extends the dieseline study into a diesel engine. The results show that particle emissions can be significantly reduced with dieseline fuel and NO_x can be reduced simultaneously if the engine runs on PPCI combustion mode.

1.2. Objectives and Approaches

The main purpose of this research is to develop a full understanding of dieseline fuel, from spray characteristics to combustion and emissions' characteristics, for both off-line diesel/gasoline blending and on-line in-cylinder blending. Ultimately the study aims to find proper injection strategies for dieseline fuel to eliminate the trade off between NO_x and particle emissions. The approaches include:

- Using a high speed camera and Phase Doppler Particle Analyser (PDPA) to measure the spray tip penetration length, cone angle, droplets size and velocity of dieseline fuel.
- Testing different diesel/gasoline blending fuel with conventional calibration strategies designed for diesel in a 4 cylinder diesel engine test rig.
- Investigating the effect of different injection strategies, including PPCI strategies and split injection strategies, on combustion performance and emissions' characteristics.

- Testing the combustion and emissions' characteristics of diesel/gasoline in-cylinder blending in a single cylinder dual-fuel engine (modified from a production 4 cylinder engine).

1.3. Thesis Outline

The thesis comprises eight chapters which cover different aspects of diesel engine study. In Chapter 2, the literature review is presented and this survey ranges from fundamental diesel combustion to the latest research progress on PPCI combustion, especially with the alternative fossil fuels. Following the literature survey, Chapter 3 introduces the testing equipment used in this study which includes the spray test rig and engine test bench.

In Chapter 4, the spray characteristics of different fuels, including neat gasoline, gasoline/diesel blends and neat diesel, are investigated on a common rail diesel injection system. The results compare the spray's tip penetration length, droplets size and velocity under different injection pressures and back pressures.

Chapter 5 concerns the combustion and emissions' characteristics of different gasoline/diesel blends in a production diesel engine. The test was carried out with a standard diesel calibration strategy and the combustion phases of blended fuels are adjusted to be the same as baseline diesel.

Chapter 6 focuses on the injection strategies for G50 (50% gasoline blends with diesel by volume) at medium operation load. Varied EGR ratios, injection timings and split injection strategies were tested. Simultaneous reduction of NO_x and PM was achieved with the usage of advanced injection timing and a large amount of EGR.

In Chapter 7, a new combustion mode named Stoichiometric Dual-Fuel Compression Ignition (SDCI) is developed. Within the new mode, EGR is used to adjust the intake air mass flow rate and the engine is operated under stoichiometric conditions. The principal fuel, gasoline, is injected via a PFI injector and a small quantity of diesel is directly injected into the cylinder at around TDC as a trigger for combustion. Several benefits can be gained from this new combustion mode. Firstly, NO_x, THC and CO emissions can be removed effectively by a cost effective three way catalyst since the combustion is stoichiometric. Secondly, the PM emissions' level is quite low as the principal fuel is gasoline and the gasoline /air mixture is homogeneous. Thirdly, the thermal efficiency of gasoline is tremendously increased by using it in a diesel engine. A summary of all the work is given in Chapter 8.

CHAPTER 2

LITERATURE REVIEW

This chapter aims to review available literature which is relevant to the conducted studies in this thesis. Firstly, a fundamental liquid fuel spray developing process, including break up and atomization, is introduced. It covers how the fuels' physical properties (viscosity and surface tension), injecting pressure and back pressure can affect spray penetration and droplets size. Secondly, the mechanisms of conventional diesel combustion and emissions formation are studied. Thirdly, the latest research of partially premixed combustion and stoichiometric combustion in CI engines is reviewed. In the final section of this chapter, the literature survey focuses on dual fuel partially premixed combustion.

2.1. Fuel Spray Characteristics

In compression ignition (CI) engines, fuel spray characteristics can largely affect the combustion performance and emissions through fuel distribution and its mixture formation process. Generally, the performance of fuel sprays can be evaluated by their macroscopic and microscopic characteristics. The former includes spray tip penetration, cone angle, tip velocity, spray area and the latter refers to droplet size, velocity, and size distribution.

2.1.1. Spray Structure and Process

In a basic sense, a spray is the introduction of a liquid jet, through a nozzle, into a gaseous environment. After injection, the liquid jet begins to interact with the surrounding gas and breaks up into numerous droplets. Figure 2.1 shows the main parameters that express the aspect of a spray, in which break-up length refers to the length of the continuous liquid column [7]. Under different injection velocities, break-up mechanisms are varied and they can be categorised into four regimes [8]. At low injection velocity, break-up is in the Rayleigh regime, which is due to the unstable growth of surface waves caused by surface tension and results in droplets larger than the jet diameter. As injection velocity is increased, the surrounding gas assists the perturbation of surface wave growth and leads to break-up. This is named the first wind-induced regime, resulting in droplets size at the order of the jet diameter. Further increase in injection velocity makes the liquid jet turbulent and perturbed at the nozzle exit. In this second wind induced regime, the average droplets size is much less than the jet diameter [8]. Further increase in injection velocity leads to break-up in the atomization regime, where jet disintegration completes at the nozzle exit [9]. In modern light duty diesel engines, break-up of fuel spray is in the atomization regime due to the high injection pressure (normally ranges from 300 bar to 2000 bar).

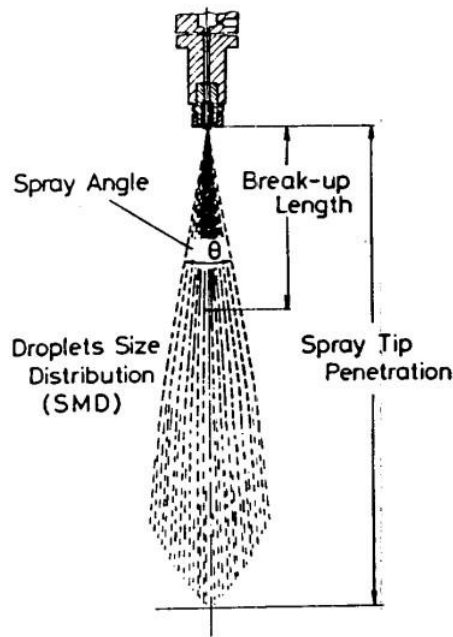


Figure 2.1 Parameters of a spray [7].

Lefebvre [8] used three dimensionless numbers to define different break-up regimes. They are Weber number - expressing the ratio of ambient gas dynamic forces to the surface tension, Reynold number - representing the ratio of inertial force to viscous force and Ohnesorge number - defining the ratio of internal viscous forces to surface tension force. The calculation equations for these dimensionless numbers are presented in Appendix A1 and the detailed criteria of break-up regimes can be found in [8].

To describe the break-up mechanism of the atomization regime of fuel spray, Arcoumanis et al. [9] introduced three models in their study:

- Aerodynamic-induced atomization: aerodynamic shear force between liquid/gas interface produces waves on the surfaces of the liquid jet and thus leads to atomization. Weber number can be used to determine the growth rate of waves and jet disintegration.
- Jet turbulence-induced atomization: the radical velocity component of turbulent flow leads to jet surface disruption. Jet disintegration is driven by turbulence and break-up can occur even when the liquid is injected to a vacuum condition.

- Cavitation-induced atomization: The collapse of cavitation bubbles causes perturbation of the liquid jet surface. The perturbation results in jet disintegration and small droplets formation.

Soteriou et al. [10] claimed that the predominant mechanism of spray jet atomization is cavitation while aerodynamic interaction assists the break-up. He presented two types of cavitation mechanism: dynamically induced cavitation and geometry induced cavitation. In the fuel spray, cavitation occurs when local fuel pressure suddenly overshoots or falls to its vapour pressure. Following that, small bubbles of vaporised fuel or dissolved air can be formed. Dynamically induced cavitation only occurs in transient flow and is usually caused by pressure change, resulting from valve movement. Geometry induced cavitation can occur both in steady flow and transient flow. It is initiated by local high velocities within separated boundary layers, which are generated by sudden changes in the flow path geometry [10]. The authors thought that geometry induced cavitation exists in standard direct injection nozzles and can produce opaque foam [10]. Fath et al. [11] showed that the collapse of cavitation bubbles help the air entrainment and thus intensify aerodynamic interaction between liquid/gas interfaces.

In a review from Smallwood and Gulder [12], it was concluded from experimental data that the liquid jet exiting from the nozzle hole atomizes completely at the exit of the nozzle or within, at most, a few nozzle diameters, as shown schematically in Figure 2.2. The authors presented that nozzle cavitation and turbulence-driven instabilities are the dominant break-up mechanisms. Cavitation can help jet break-up in two aspects: the bursting and collapsing of vapour cavities contribute to the fuel masses disintegration at the exit of the nozzle hole; and cavitation intensifies flow turbulence through the nozzle hole and increases fuel jet instability.

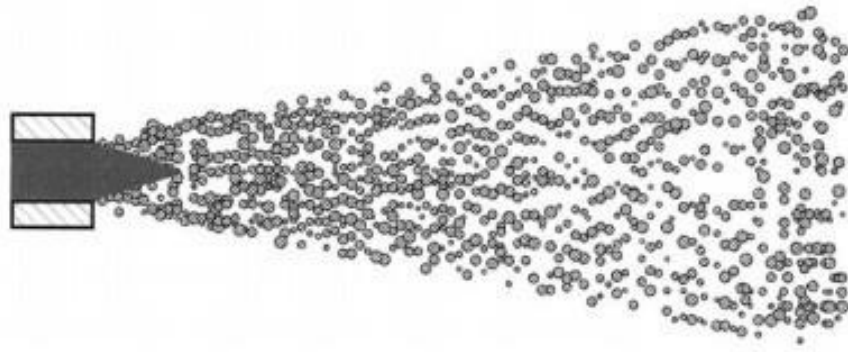


Figure 2.2 Schematic view of the diesel spray with a very short break-up length [11].

2.1.2. Tip Penetration and Cone Angle

Spray penetration and cone angle greatly influence combustion. If the penetration length is too long and the cone angle is too narrow, fuel may impinge on the piston or wall, resulting in lower combustion efficiency and higher soot emissions. In the case of short penetration, fuel can't travel deeply in the combustion chamber and the utilisation of air will be poor. Penetration length and cone angle can be affected by several parameters such as nozzle configurations, injection parameters, ambient conditions and fluid properties. Calculation equations have been proposed by Hiroyasu, Siebers and many other researchers [7,14,15]. In a recent study, Klein-Douwel et al. [15] reviewed these equations and presented a general form for non-vaporizing spray (effects of fuel properties were not included).

$$S \propto \rho_{gas}^{m_s} \times \Delta P^{n_s} \times d_n^{\alpha_s} \times t^{\beta_s} \times \tan^{-0.5 \frac{\vartheta}{2}} \quad \text{Equation 2.1}$$

$$\tan \frac{\vartheta}{2} \propto \rho_{gas}^{m_\vartheta} \times \Delta P^{n_\vartheta} \times d_n^{\alpha_\vartheta} \times t^{\beta_\vartheta} \quad \text{Equation 2.2}$$

Where ρ_{gas} is ambient gas density, ΔP is the pressure difference between injection and ambient, d_n is nozzle diameter of injector, t is the time after injection, ϑ is spray angle. The

exponents of each parameter are varied in different researcher's study and Klein-Douwel et al. [15] presented a summary of these exponents in their study.

Siebers and Naber [14] investigated the effects of gas density and vaporization on penetration and dispersion of diesel spray. The authors found that higher gas density can increase spray dispersion, which results in more entrained air and lower penetration velocity. The effect of fuel vaporization on penetration was studied by testing diesel spray under different ambient temperatures, which are 451 K and 1000 K. As shown in Figure 2.3, it was found that vaporization can reduce penetration length by 20% at low ambient gas density, which was 3.3 kg/m^3 . However, the difference was negligible at high ambient gas density, which were 28.6 and 58.6 kg/m^3 . It was hypothesized by the authors that the gas mixture was cooled by fuel vaporization and thus its density increased, resulting in lower tip velocity of newly injected fuel.

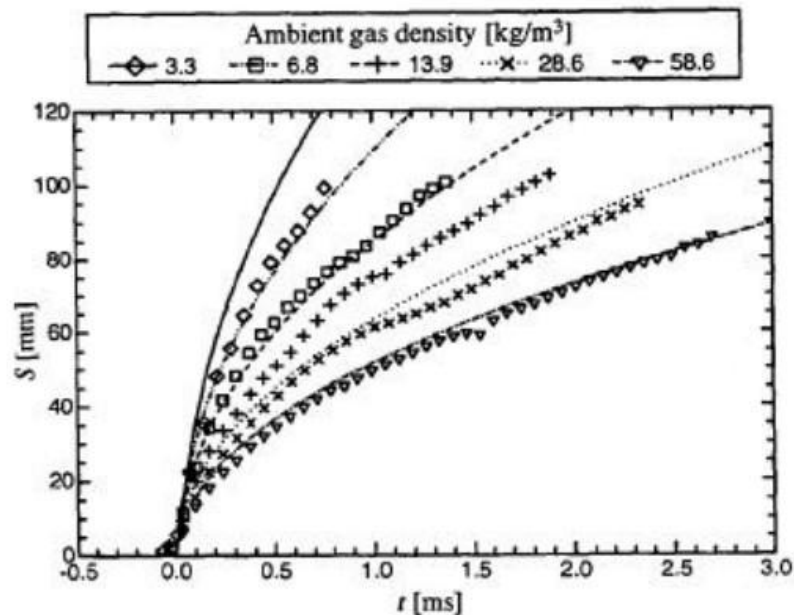


Figure 2.3 Penetration versus time for vaporizing (the symbols) and non-vaporizing spray (the curves). Injection pressure 137 MPa, ambient gas temperature 451 K and 1000 K [14]

Regarding the effects of fuel properties on spray macroscopic characteristics, fuel density is the most influential property [7, 9, 14]: lower fuel density could result in wider cone angle and shorter penetration length. Reitz and Bracco [9] presented that fluid kinematic viscosity and surface tension can effect spray penetration length and cone angle but have a lesser effect than fluid density. Chang and Farrel [16] tested three fuels with different viscosities under an injection pressure of 90 MPa. They found that the effect of viscosity on penetration length and cone angle was small. Zink et al. [17] studied fuel property's influence on spray formation by measuring the spray momentum of twenty one different fluids. They concluded that the influence of the fluid's density and kinematic viscosity was dependent on the rail pressure: at low rail pressure of 40 MPa, both higher density and higher viscosity can increase momentum thus penetration length; however at high rail pressure of 120 MPa, density had a pronounced influence while the influence of viscosity was small.

Matsuoka et al. [18] used LIEF (Laser Induced Exciplex Fluorescence) techniques to analyse spray vapour-liquid separation of commercial diesel and light diesel (which has similar physical properties to gasoline: lower kinematic viscosity, density and boiling points) under simulated engine conditions (50 MPa, 873 K). It was reported that light diesel had shorter liquid penetration, shorter vapour penetration and wider spray angle. From an optical engine test, it was found that by using light diesel, the dense mixture packets that with more than 2 of equivalence ratio were reduced as compared to commercial diesel .A more recent study conducted by Payri et at.[19] showed no clear difference between diesel and gasoline in terms of penetration length and cone angle of non-evaporative spray (both of the two fuels were injected by a diesel common rail injection system).

2.1.3. Fuel Droplets Size

As discussed in section 2.1.1, diesel spray is atomised into a numerous number of droplets near the nozzle exit [13]. The droplets diameter and size distribution can strongly affect liquid fuel evaporation and their mixing with air. Several types of mean diameter were used to describe the droplets size [20]. Among them, median diameter (D_{10}) and sauter mean diameter (SMD, D_{32}), which is the ratio of volume to surface and thus determines the evaporation rate, were most commonly used in engine research.

The size of spray droplets is dependent on the break-up mechanism, which can be affected by injection parameters, injector configuration and fluid property. Results from Hiroyasu et al. [7] showed that SMD decreased as injection pressure increased. However, the reduction was very small as injection pressure was further increased above 50 MPa. It was also shown by Hiroyasu and Tabata [7, 21] that SMD increased with increase of ambient pressure when injection pressure was above 5 MPa.

Gulder and Smallwood's [22] results showed that there was little variation of droplets' diameter with time and axial distance, which suggested that atomization finished near the exit and secondary break-up (mainly caused by aerodynamic interaction) contributes little to the spray break-up. In the radial direction, there was not a solid conclusion on droplets' size distribution. In Smallwood's et al. [22] review, it was expected that radial droplets' size distribution would become a balance between the non-evaporating break-up (large droplets on the periphery) and evaporation (small droplets on periphery).

There is very limited literature that covers the investigation of fuel property's effect on droplets' size. It was shown by Tabata et al. [21] that increased viscosity caused an increase in

SMD. Yule et al. [23] compared the droplets' size of diesel and a diesel/kerosene blend, using PDPA (Phase Doppler Particle Analyser) techniques. He concluded that within the normal range of diesel fuel quality, there was no sizeable difference on droplet diameter.

2.2. Diesel Combustion and Emissions Formation

Conventional diesel combustion is a complicated, multiphase and turbulent process. As the liquid fuel jet penetrates across the combustion chamber and atomises into small droplets, part of the liquid fuel evaporates and is mixed with the surrounding hot air. Premixed combustion starts at the local fuel/air mixture pockets which have a high equivalence ratio since in-cylinder temperature is above fuel auto-ignition temperature. Following that, diffusive combustion happens at the spray periphery and it is controlled by the fuel/air mixing rate. The rate of fuel-air mixing is largely affected by the spray pattern, droplets' distribution and turbulent flow inside the combustion chamber [24]. In order to optimise the combustion and reduce emissions, it is important to understand the fundamental combustion process and emissions' formation mechanisms inside the cylinder, such as ignition starting location, equivalence ratio distribution and various emissions' formation regions.

2.2.1. Conceptual Model

Based on laser diagnostics results of an optical diesel engine, Dec [25, 26] proposed the conceptual model of early stage mixing-controlled combustion, which has been widely referred for describing the combustion process of a diesel engine. According to the model, firstly, a fuel-rich (equivalence ratio 2~4) premixed flame starts at the leading portion of the fuel jet, resulting in formation of small particles and Polycyclic Aromatic Hydrocarbons (PAH). Then, as fuel injection continues, a diffusion flame forms at the jet periphery between

the products of premixed combustion and the surrounding air. The diffusive flame is almost stoichiometric combustion and flame temperature is high (nearly 2600 K). After the entrained hot air inside the spray is consumed by the premixed burning, combustion will be fully ‘mixing-controlled combustion’.

Figure 2.5 presents a conceptual schematic of mixing-controlled combustion. Soot initially formed at the premixed flame and the highest concentration is at the head vortex region, as soot grows and moves down the jet. Part of the soot can be oxidised by OH radical which is formed at the diffusive flame. Thermal NO is formed during mixing-controlled combustion since the flame temperature is high and oxygen is available in the surrounding air.

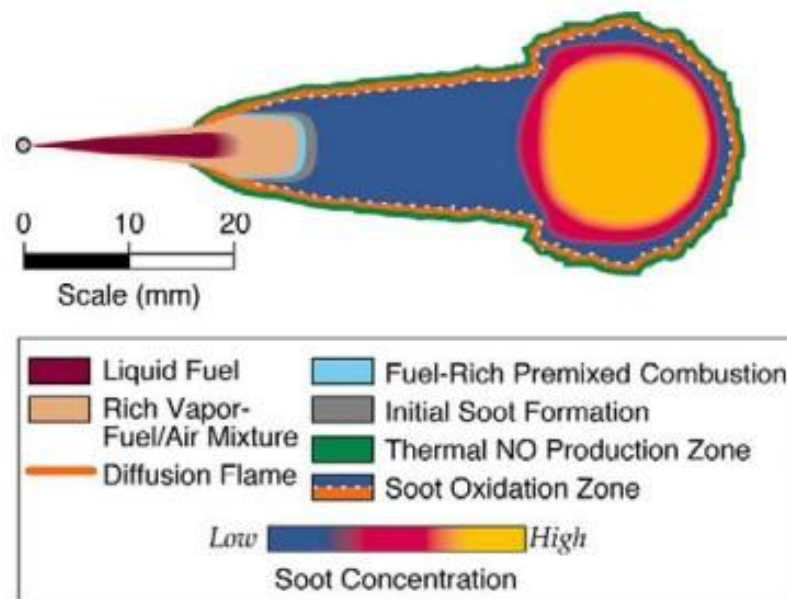


Figure 2.4 Conceptual schematic of conventional diesel combustion [25].

2.2.2. Formation of Emissions

Four types of emissions are regulated under current legislation for diesel engines, including particulate matter, oxide of nitrogen, carbon monoxide and hydrocarbons. General formation mechanisms of these emissions are introduced in the following paragraphs.

Based on the size, particles from engines can be categorised into three modes. They are nucleation mode (<50 nm), accumulation mode (50 – 1000 nm) and coarse mode (>1000 nm) [27]. Nucleation mode particles are mainly soluble organic fraction (SOF) and some investigators suggested that solid kernels exist in them as well [28]. Due to the irreproducible nature of nucleation mode particles, there was very limited knowledge about them. Most research attention has been focused on the accumulation mode particles which consist of a solid carbonaceous core (soot), with some volatile compounds adhered. Coarse mode particles are mainly formed by the other two types of particles.

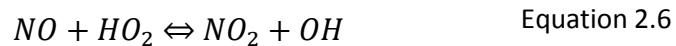
Soot formation is favoured in a fuel-rich (equivalence ratio above 2) and high temperature environment (temperature above 1300 K). As described in Dec's conceptual model for diesel [25], soot forms in a premixed flame and is oxidised during mixing-controlled combustion in a conventional diesel engine. Various parameters can affect soot emission such as injection pressure, combustion phase, EGR ratio, charge pressure and oxygenated compound of fuel etc [28-30]. Pickett and Siebers [31] applied laser-extinction techniques to investigate the effect of ambient temperature, ambient pressure and injection pressure on soot emissions. They concluded that the quantity of air entrained upstream of the premixed flame was the decisive parameter. In a real engine, carbonaceous particles (soot) are formed during the combustion process and grow by agglomeration during the exhaust process. The volatile compounds nucleate into new particles during the exhaust process as the temperature of the exhaust gas lowers [32]. To reduce particle emissions from the tailpipe and meet emissions' legislation, all

current generation diesel engines (Euro 5) are equipped with a high pressure common rail injection system and diesel particulate filter (DPF) [33].

The most accepted formation mechanism of nitric oxide (NO) in a diesel engine is thermal formation [24]. Zeldovich [34] suggested that the reaction equations for NO formation are as below:



In diesel engines, part of the NO can be oxidised to NO₂ as the NO cools down in the expansion stroke. The NO₂ to NO_x ratio are normally 10 to 30 percent depending on the loads [24]. The conversion reaction is as below [24].



According to Dec's conceptual model [25], the NO production rate is highest at the jet periphery of the diffusion flame. This is because of the diffusive flame being almost stoichiometric combustion, which is ideal for NO production (adiabatic flame temperature is high and there is a source of oxygen). However, it was also claimed by Dec [25] that most of NO production may occur at the later part of the mixing-controlled burn or in hot-gas regions after combustion ends, since NO production is a relatively slow process. Although a premixed flame doesn't generate NO directly in conventional diesel combustion, it still plays an important role in final NO emissions. Higher premixed combustion intensity can cause the diffusive flame temperature to rise, resulting in higher NO [35].

Heywood [24] suggested that NO was mainly produced during the start of combustion until the peak of in-cylinder pressure. As combustion proceeds and in-cylinder temperature increases, the burned gases are compressed to maximum temperature, which is favoured by NO formation. As demonstrated in Figure 2.5, NO_x emission is highly dependent on local mixture strength [36]. Either over-lean or over-rich local mixture would result in low NO_x emissions.

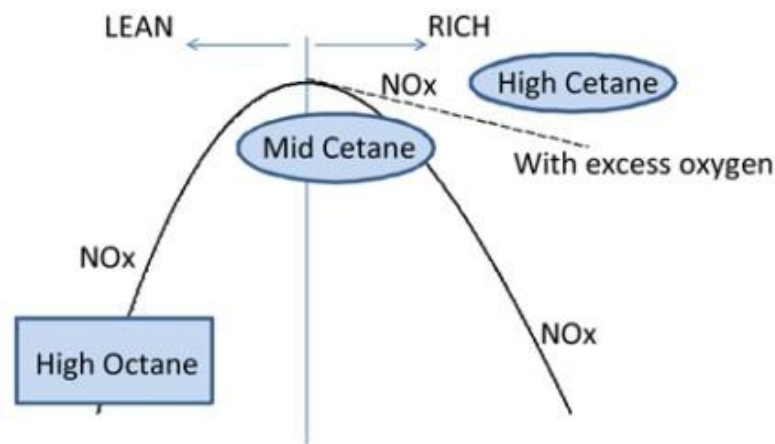


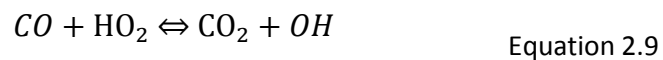
Figure 2.5 Sketch of variation of NO_x with local mixture strength. Fuels can be premixed to different degrees depending on their ignition quality [35]

To reduce NO_x emissions, the most commonly used technique in the current generation of diesel engines is exhaust gas recirculation (EGR). A high EGR ratio can reduce flame temperature by decreasing the intake oxygen concentration and increasing the heat capacity of in-cylinder gases (exhaust contains CO₂, its heat capacity is higher than oxygen and nitrogen) [24].

Basically, the unburned hydrocarbon (HC) and carbon monoxide (CO) emissions, products of incomplete combustion, are very low at high operation load for conventional diesel engines. As the load decreases, HC and CO emissions increase since the equivalence ratio decreases and bulk-gas temperature goes down. It was found that HC can't be oxidized completely

under temperatures of 1200 K and CO requires 1500 K to achieve complete combustion [37]. These temperatures are independent of the original fuel structure [38].

HC can be emitted from several sources in diesel engines, including over-lean mixing, under-mixing, fuel impingement on piston bowl/wall, quenching of combustion flame on the cylinder wall and even from evaporated lubricant oil, etc [24]. Over-lean mixing mainly happens in the ignition-delay period, when part of the fuel/air mixture becomes too lean to support flame propagation. During the combustion process, part of the fuel/air mixture could be too rich to be ignited [24] and thus is emitted as HC emissions. Regarding CO emissions, Heywood [24] proposed that they mainly formed in fuel-rich mixtures and are independent of combustion temperature as there is not enough oxygen to complete CO oxidization. Khan illustrated [39] that CO can be formed in overly lean mixtures as well when the combustion temperature is between 800-1400 K. This is due to CO oxidization being highly dependent on temperature. The most important pathways of CO oxidization are as below [39].



Sjöberg and Dec [39] illustrated that OH radicals are the main source of CO oxidization. The concentration of OH radicals is largely affected by charge temperature. At low charge temperature, the OH concentration is relatively low, resulting in slow CO oxidization. Cost-effective diesel oxidization catalysts (DOC) are commonly equipped with modern diesel engines in order to reduce HC and CO emissions.

2.3. Partially-Premixed Compression Ignition (PPCI)

2.3.1. Introduction

As presented in Section 2.2, conventional diesel engines suffer high particles and NO_x emissions due to the nature of diffusive combustion. Faced with stringent emissions' legislation, extensive research efforts have been focused on premixed diesel combustion, which is able to eliminate particles and NO_x emissions simultaneously. Basically, there are two types of premixed diesel combustion: homogeneous charge compression ignition (HCCI) and partially premixed compression ignition (PPCI) (also named as low temperature combustion (LTC)). For the former, early direct injection (the injection timing is usually more than 100 CAD BTDC) and port injection (intake air heating is required to assist diesel vaporization) are commonly used to form a homogeneous fuel/air mixture [40-43]. However, the difficulty of combustion phase control and low volatility of diesel fuel make diesel HCCI not readily implemented. Therefore, researchers and manufacturers are paying more attention to PPCI, whose combustion phase is directly controlled by injection timing while its emissions are similar to HCCI.

PPCI differs from conventional diesel combustion in that it has a larger amount of premixed charge and lower flame temperature when combustion begins. This can be demonstrated by Figure 2.6. Conventional diesel combustion starts with low temperature fuel-rich premixed combustion, which is in the soot formation region, and then is dominated by relatively high temperature stoichiometric diffusive combustion, which is in the NO_x formation region. In order to avoid the soot and NO_x formation regions, the local fuel/air mixture packets need to be shifted from the conventional diesel area to the PPCI area. Several methods can facilitate this; the main methods are to decrease oxygen concentration and ambient temperature of the

charge [44]. Lower oxygen concentration (by increasing exhaust gas recirculation (EGR) ratio etc.) slows the chemical reaction and thus extends the ignition delay, which allows for longer mixing time before rapid heat release starts [24]. The maximum flame temperature is reduced due to the additional heat capacity of the diluted charge and thus NO_x emissions fall substantially. The effect of lower oxygen concentration on soot emissions is complicated as it depends on soot formation and oxidization. Figure 2.6 illustrated that soot mainly formed at temperatures above 1300 k and equivalence ratio of 2-4. As oxygen concentration decreases, more charge is required to maintain the equivalence ratio. It was found by Pickett and Siebers [45] that the average equivalence ratio at lift-off remained approximately constant, which resulted from the self-cancelling effect of longer ignition delay and lower oxygen concentration. Kook et al. [44] observed that the final soot emissions firstly increased and then decreased as the EGR ratio rose. From low to moderate EGR ratios, the increase of soot emissions was supposed to occur because of the reduced soot oxidation due to the lower oxygen concentration and lower flame temperature [44]. From moderate to high EGR ratios, soot emissions went down since the combustion temperature was reduced further and soot formation was suppressed to a greater degree than soot oxidation [26].

With ambient temperature reduced (by advancing or retarding injection timing, reducing compression ratio or using a more powerful intake cooler), the maximum achievable temperature of local fuel packets can be decreased at a given equivalence ratio [46]. Thus, the ignition delay would be extended and local equivalence ratios would be decreased. By checking the total soot luminosity, it was found that soot formation was reduced with a lower ambient temperature (by advancing or retarding injection timing) [44]. Some other techniques can also be used to enhance the fuel/air mixing, such as increasing injection pressure and changing piston bowl geometry [31, 48-50].

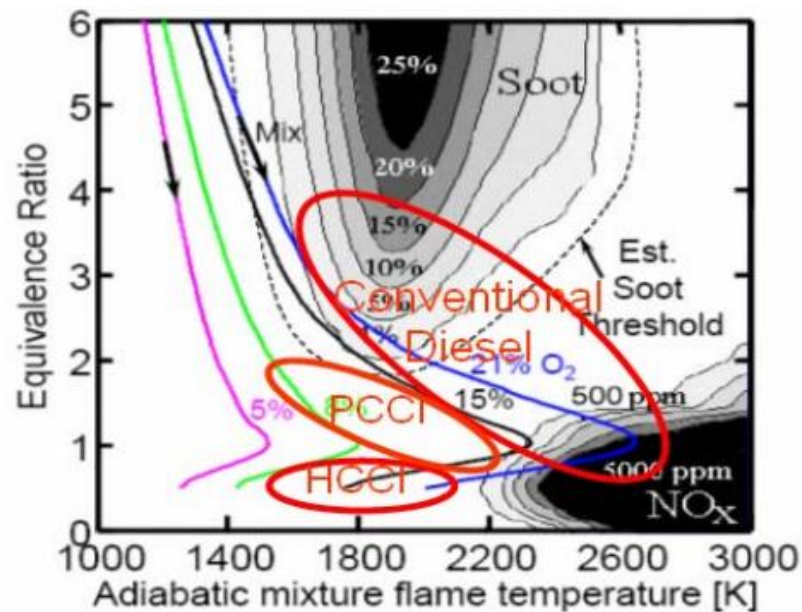


Figure 2.6 Diagram showing the ϕ -temperature ranges for soot and NO_x formation and the regions for conventional diesel, HCCI, and diesel PCCI engines [47].

To help understand the in-cylinder process of LTC (or PPCI), Musculus et al. [51] updated Dec's conceptual model [25] to cover LTC combustion, which is shown in Figure 2.7. For LTC, fuel jets penetrate further into the combustion chamber and impinge on the wall. The wall wetting is a potential source of HC emissions. The main products of first stage ignition are formaldehyde (CH_2O), H_2O_2 , CO and HC. Soot is not formed during this period due to low flame temperature and enhanced mixing. Second stage ignition starts after the injection ends and the products of first stage ignition are further oxidized during this period. Some soot is present in the head vortex region due to fuel-rich mixtures in the piston bowl. However, most of it is oxidized at around 40 CADs after the start of injection [51].

Although PPCI combustion is very effective in reducing NO_x and particle emissions, there are several challenges. Firstly, the operational conditions are limited to low to medium loads since EGR replaces some of the intake air and the overall fuel/air mixture would be too rich at high loads [52]. Secondly, the UHC and CO emissions are high, which is caused by low temperature of the flame, wall wetting and some over-lean fuel/air mixture pockets near the

nozzle exit [53]. Various strategies and methods are being tested to overcome the challenges. They are introduced in the following sections.

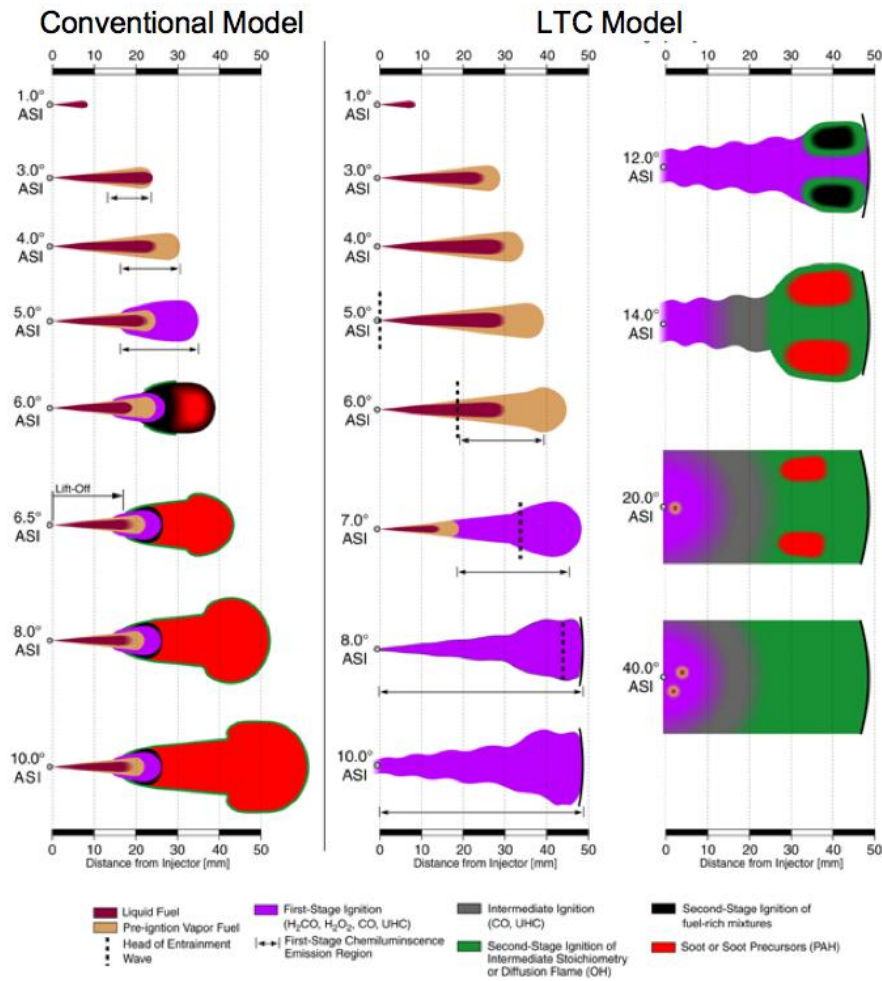


Figure 2.7 Conceptual model for partially premixed low-temperature diesel combustion and the comparison to conventional diesel combustion model (heavy duty diesel engine) [48].

2.3.2. Effects of Injection Strategies and Engine Hardware

As discussed in section 2.3.1, PPCI combustion requires lower oxygen concentration and lower ambient temperature. Current generation diesel engines are capable of achieving PPCI combustion at part loads by using EGR with fuel injection either earlier or later than conventional diesel engines [44]. Kimura et al. [54-56] utilises high EGR ratio, late injection timing (closed to or after TDC) and a toroidal combustion chamber (helps to increase swirl ratio) to promote premixing and reduce combustion temperature. The combined techniques

were named as the Modulated Kinetics (MK) concept and have been successfully implemented to Nissan's (Japanese automotive company) production engine.

For PPCI combustion with early fuel injection (usually around 20-30 CADs BTDC), even more EGR is required, as compared to late injection PPCI, in order to prolong the ignition delay further and avoid ignition before TDC [44]. However, too much EGR would limit the PPCI operation range at low loads. By lowering the compression ratio of PPCI engines to 14:1 or 15:1, some researchers successfully avoided early ignition and reduced the dependence of EGR [57-59]. Fuel impingement on the piston bowl/wall, causing poor mixing and emissions, is another issue for early injection. It was found that fuel impingement can be reduced by boosting the intake to higher pressure [60] or increasing the diameter of the piston bowl [50, 61].

Hasegawa et al. [62 63] combined the early injection and late injection strategies and developed the Uniform Bulky Combustion System (UNIBUS). In UNIBUS, a portion of the fuel is injected at around 50 ° BTDC to form a cold flame and the rest of the fuel is injected after TDC, acting as a combustion trigger. The high temperature reaction of the first injection was avoided by choosing proper injection timing, injection quantity, IVC timing and intake temperature. Low NO_x and near zero smoke emissions were achieved in UNIBUS. It has to be noted that the wall impingement problem still exists for split injection PPCI combustion. To resolve this problem, Sun and Reitz [64 65] developed adaptive injection strategies (AIS) and a variable injection pressure (VIP) system. The VIP system was capable of switching injection pressure between low and high during the same engine cycle. Low pressure was used for the early injection to reduce wall impingement and high pressure for the second injection was to extend load capability. Kokjohn et al. [66] found that UHC emissions can be

significantly reduced by replacing high pressure (860 bar) early injection (around 50° BTDC) with low pressure (100 bar) early injection.

2.3.3. Fuels for PPCI

Diesel fuels have low volatility and high auto-ignition quality, which make it unfavourable for premixed combustion and limit the operating range. Pesant et al. [67] tested two fuel matrixes, which had different auto-ignition quality, volatility and chemical composition. He concluded that the PPCI operating range can be extended by reducing the fuel's cetane number (CN) and increasing fuel's volatility. Cheng et al. [68] studied the effect of fuel volatility on early injection PPCI combustion in an optical diesel engine. The ignition quality of tested fuels was kept almost the same and the volatility was varied. It was found that a higher level of high volatility content resulted in less liquid fuel impingement, less poor fires, and thus less smoke emissions, particularly with the injection timing earlier than 30° BTDC. Kalghatgi et al. [69, 70] investigated low cetane number diesel (CN 24, boiling range similar to diesel, 75% aromatic content) in a single cylinder research diesel engine and found that it produces almost zero smoke emissions, which was similar to gasoline with research octane number (RON) 84, at different engine speeds and loads. They concluded that the resistance of auto-ignition was far more important than volatility in terms of smoke emissions' reduction if fuel's cetane number was sufficiently low (below 30 in their case). More literature about the effect of fuels' properties on PPCI combustion can be found on [18, 71-73]. Many researchers used biodiesel in PPCI as it was produced from sustainable resources [57, 74-77]. Experimental results have shown that, as compared to conventional diesel fuel, biodiesel was able to reduce cyclic variability and better sustain high EGR rates in late injection PPCI combustion due to its high cetane number and oxygen compound [74, 75]. Additionally, it was found that the soot, CO

and UHC emissions of biodiesel-fuelled PPCI combustion was lower than conventional diesel [57].

2.3.4. Low Octane Gasoline Fuelled PPCI

Compared to diesel fuel, gasoline possesses much higher auto-ignition resistance and higher volatility, which make it an ideal fuel for PPCI combustion. In a series of tests, Kalghatgi et al. [78-85] has demonstrated that gasoline fuel can be successfully run in a diesel engine under PPCI mode. In [78], low smoke emissions (FSN 0.36) and low fuel consumption (ISFC 178 g/kW.h) was achieved under 14.86 bar IMEP, by injecting gasoline near TDC and using 2 bar intake pressure and 32% EGR. Achieving such low smoke emissions at high loads was very challenging with diesel fuel. Additional experiments show that pilot injection can help to reduce the maximum pressure rise rate of gasoline fuelled PPCI and the operating load with low emissions was extended to 15.95 bar IMEP in [79]. According to Kalghatgi's explanation, there was a range where the combustion phase can be controlled by varying injection timing at each operating condition. Too early or too late injection might cause misfire and these phenomenon were defined as 'premixed too much'. In Kalghatgi's papers, it was shown that long ignition delay of gasoline fuelled PPCI can't reduce NO_x emission significantly and it was even higher than diesel at high loads. The reduction of NO_x still highly depended on the usage of EGR.

Researchers from Lund University extensively studied gasoline and ethanol fuelled PPCI combustion in light duty and heavy duty diesel engines [86-92]. In [86], higher than 45% indicated efficiency was achieved in the load range of 6 and 17 bar IMEP while the smoke was maintained below FSN 0.1 and NO_x was below 20 ppm. Three factors contributed to the good results: high boost (from 2.6 bar to 3.2 bar), 50% EGR and double injections (similar to

UNIBUS, one early injection and one late injection as combustion trigger) [86]. The main issues were reported as the high pressure rise rate [15 bar/deg] at high load and the difficulty of extending operation to a lower load. According to Lund's concept, NO_x and soot emissions can be simultaneously avoided as long as there is the correct equivalence ratio and EGR combination with fuel in the boiling point range of gasoline [87].

Researchers from Delphi Corporation (a company that supplies fuel injection systems) tested a gasoline direct injection compression ignition (GDCI) engine at 6 bar IMEP with the application of up to 3 injection events [93]. The results show that a triple-injection strategy with optimised injection timings and quantities produced better fuel economy and lower NO_x emissions than single and double injections. In [94], the GDCI engine was extensively operated from 2 bar to 18 bar IMEP and at different speeds. Smoke less than FSN 0.1, NO_x less than 0.2 g/kW.h and diesel-like efficiency were achieved at all tested conditions. The triple-injection strategies, VVT (variable valve timing) technology and specially manufactured injector were claimed to be the key enablers [94]. Researchers at Argonne National Laboratory optimised double injection strategies for gasoline fuelled PPCI with loads ranging from 2 bar to 12 bar IMEP [95]. Groups at the University of Wisconsin performed detailed CFD studies of gasoline fuelled PPCI as well as tests in a heavy duty diesel engine [96, 97]. Weall and Collings studied gasoline fuelled PPCI at low load and low speed [98].

2.3.5. Dieseline Fuelled PPCI

Gasoline and diesel have opposite properties in terms of volatility and self-ignitability. In 2005, researchers at the University of Birmingham firstly investigated the idea of altering fuel characteristics through blending gasoline with diesel and the resulting fuel was named

'Dieseline'. Originally, the studies focused on utilising dieseline fuel in a HCCI engine equipped with a port fuel injection system. It was found that increasing proportions of diesel in the diesel-gasoline mixture reduced the ignition delay and increased combustion stability [99,100].

As described in section 2.3.3, PPCI combustion favours fuels which have higher auto-ignition resistance and higher volatility than diesel. Thus, the dieseline concept was adapted to PPCI combustion by a research group at the University of Birmingham and other research organisations [101, 102]. Weall and Collings [103] used dieseline fuel to obtain low emissions from an operating PPCI engine. It was confirmed that dieseline (with 50% gasoline in this case) can increase the upper load limit of PPCI operation to 7 bar BMEP while high HC and CO emissions were an issue for low loads. Han et al. [104] found that intake boost can shift the entire dieseline PPCI operation to higher loads and the increase of EGR can extend it to lighter loads. In [105], the results show that the dependence of soot reduction on high injection pressure was reduced by using dieseline fuel. This thesis will follow Weall and Han's work and conduct deeper and wider investigation regarding dieseline fuelled PPCI combustion.

2.3.6. Real-Time Fuel Design Through In-cylinder Blending

Designing fuel properties can be achieved not only by blending diesel and gasoline off-line, which is presented in section 2.3.5, but also possible through in-injector blending (a special injector is required), or in-cylinder blending (direct injection plus port injection). The latter seems to be able to give the engine more flexibility for optimization and combustion control. According to Bessonette et al. [106], the best fuel for HCCI operation at high and low loads is different. For instance, at 16 bar BMEP the fuel should have a cetane number of ~27 while a

cetane number of ~45 was required at below 2 bar BMEP operation. Several research organisations are investigating the techniques that use port injected gasoline and direct injected diesel to achieve real-time control of fuel reactivity.

Researchers at the University of Wisconsin and Oak Ridge National Laboratory found that the combustion phasing of dual-fuel PPCI (also named as reactivity controlled compression ignition (RCCI)) was controlled by fuel reactivity and the pressure rise rate can be controlled by the fuel stratification. Both modelling and experimental results show that optimum conditions were achieved with splitting direct injection into two: 60% of total diesel amount at around 60° BTDC and the rest at 30° BTDC [107, 108]. Optical diagnostics' results illustrated that the combustion initiated with high reactivity fuel and then progressed to low reactivity fuel while the combustion speed of low and high reactivity fuel was found to be the same [109]. At high loads, the dependence of a high EGR ratio for NO_x reduction was not reduced and this would decrease the maximum achievable load [110].

Researchers at Southwest Research Institute also performed dual-fuel PPCI tests within the project HEDGE (High Efficiency Diluted Gasoline Engine) [111-113]. HEDGE is different from RCCI in two aspects. Firstly HEDGE was operated under stoichiometric conditions, which enables the usage of a three way catalyst (very efficient in reducing NO_x, UHC and CO emissions simultaneously). Secondly micro pilot diesel (cetane number 76) was injected at around TDC to ignite the gasoline. Similar tests were conducted at Tsinghua University under the name of HCII (Homogeneous Charge Induced Ignition) [114,115]. It was reported that HCII mode can extend the lean burn limit of gasoline to air excess ratio 3.5 and the smoke was significantly reduced as compared to a diesel engine.

2.3.7. Diesel Stoichiometric Combustion

As reviewed in previous sections, PPCI engines have shown a great potential of meeting stringent emissions' regulations on NO_x and smoke without after-treatments. However, the techniques highly depend on usage of EGR and limit the maximum load. Lee et al. [116,117] suggested running a diesel engine under stoichiometric conditions, thus a cost-effective three way catalyst can be used to eliminate NO_x, UHC and CO emissions simultaneously. A combination of intake throttle and EGR was used to regulate the oxygen supply and maintain stoichiometric conditions [118, 1119]. A 98.7% conversion efficiency of NO_x was reported in [118] while the UHC and CO levels were also reduced significantly. The main issues of this technique were poor fuel efficiency and high smoke emissions. Around 7% sacrifice in fuel consumption caused by incomplete combustion and high smoke level 1.0 g/kg-fuel were reported [119]. In this thesis, the elimination of fuel efficiency and a smoke emissions' penalty through dual-fuel combustion is investigated in Chapter 8.

2.4. Summary

In summary, this chapter reviews the latest research progress of modern clean diesel engine technologies and the associated fuels. The major areas include the discussion of the effect of fuel properties on spray penetration length and droplets size, the fundamental diesel combustion and emissions formation mechanism and the progression towards PPCI engines to reduce NO_x and particulate emissions simultaneously. In particular, the focus is on the PPCI engines that utilise low-cetane fuel and dual fuel. Investigations from other institutions show that they are more suitable for PPCI operation than diesel in terms of load extension and toxic emissions reduction. This introduces the main motivation of this thesis, which is to investigate the spray, combustion and emissions characteristics of diesel fuel and the associated injection strategies in a PPCI engine.

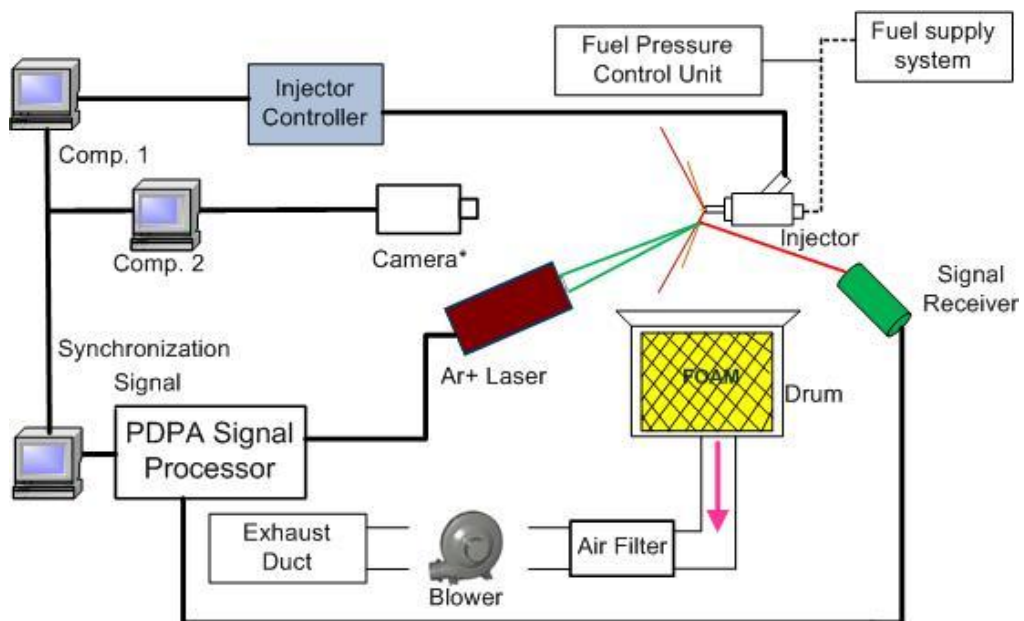
CHAPTER 3

EXPERIMENT SETUP

This chapter introduces all of the equipment and data processing programmes used in this study. Most of the experiments are done in a diesel engine test bench and a spray test rig. Detailed information of the test rigs and relevant instruments are presented in the rest of this chapter.

3.1 Spray Measurement

The spray test rig can be divided into four subsystems: fuel injection system, high speed camera, Phase Doppler Particle Analyser (PDPA) and a ventilation system. The connections between the four subsystems are shown in Figure 3.1. The control signals of the injector, camera and PDPA are synchronised.



* The Image test was done with injector placed in vessel

Figure 3.1 Schematic of spray test rig [128].

The spray visualisation test was carried out with the injector placed in a pressurised vessel. It has four optical access ports, one bottom view round window with a diameter of 68 mm and three elliptical windows with a diameter of 25.4mm×40 mm. Spray images were taken from the bottom view window and two 500w xenon lamps were put beside the ellipse windows as continuous light sources. The vessel can be pressurized up to 45 bar by filling with pure nitrogen gas. The PDPA test was done in ambient atmosphere conditions and it was not viable to carry it out in the vessel due to the limited optical access area and low data rate. All other testing conditions of the PDPA test were kept the same as the spray visualisation test.

3.1.1. Fuel Injection System

Figure 3.2 presents a schematic of the fuel injection system. A production high pressure fuel pump driven by a 5.5kw three phase AC motor was used to produce up to 2000 bar fuel pressure for a common rail. The AC motor was controlled by a three phase frequency convertor and the rail pressure was controlled by a common rail control unit (photo shown in Figure 3.3).

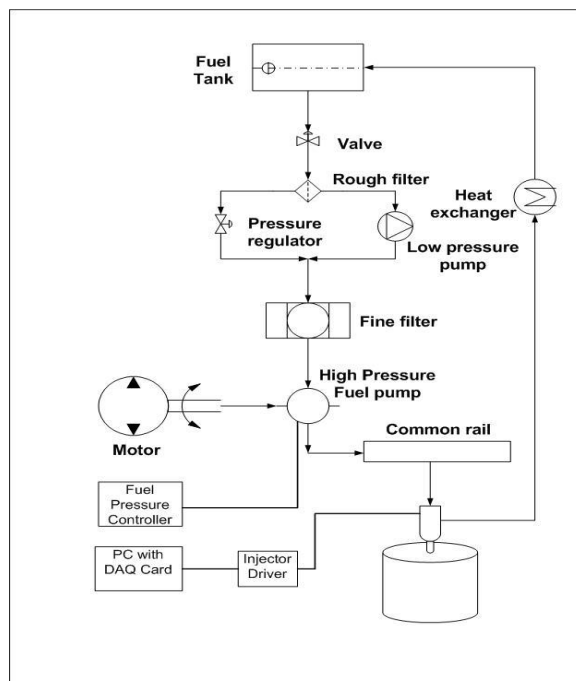
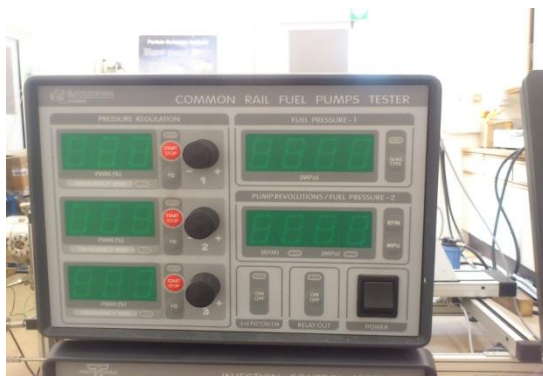


Figure 3.2 Schematic of Fuel Injection System.

The injector, Figure 3.3 b, used in the spray measurements is the same as the injector on the author's engine test bench. It is a solenoid injector (Model: Denso SPEC 3) with 7 holes and 0.15 mm diameter. The injector was controlled by electrical pulses, which were generated from a DAQ PCI NI6023E card. The pulse width and frequency can control the injection duration and frequency respectively. As the power output from a DAQ card is quite small and a special pulse shape is required by the injector, a solenoid injector driver was used to amplify and shape the pulses. Photos of the fuel pressure controller, solenoid injector and driver are shown in Figure 3.3.



(a)



(b)



(c)

Figure 3.3 Major Components of Fuel Injection System: (a) Fuel pressure controller; (b) Solenoid injector; (c) Driver for solenoid injector.

3.1.2. Spray Visualisation

A high speed Phantom V710 CMOS camera was used to capture spray images throughout the spray visualisation test. The specifications and a photo of the camera are shown in Figure 3.4. Due to the hardware limit of this CMOS camera, there is a trade-off between shutter speed and picture resolution. It was found that the speed of 18003 frames per second (fps) can give out a good enough resolution 608×600 for this spray visualisation application. Normally the injection duration of a modern diesel engine is from 600 μ s to 800 μ s. The speed of 18003 fps means that the camera can capture images every 55 μ s. Therefore 10 to 15 images can be captured while the injector lift valve opens. These images can illustrate the spray development process clearly.



Resolution	600×608
Speed	18003 fps
Colour expression gradations	Monochrome 8 bit and 12 bit
Lens	Nikon, 105 mm focus length
Imaging device	1280×800 CMOS sensor

Figure 3.4: Phantom V710 Camera and its Specifications.

Spray penetration length and cone angle are the most used parameters in quantifying spray macroscopic characteristics. They can be got by processing and analysing the spray images with matlab. Figure 3.5 presents an example of image processing procedures. The left hand side image is an original spray image and it has seven jets as shown. Among the jets, the left

corner jet has the highest brightness and thus was studied. The middle image, which contains the chosen single jet, was taken by segmenting and rotating the original image. The right hand side image is a binary image and it was converted from the middle image by thresholding. In this image, the pixel value of the spray is 1 and the background is 0. The spray tip position can be detected by finding the point which is farthest to the injector's tip position and with a pixel value of 1. The spray cone angle can be calculated out from its boundary but the results were not reliable (limited by the calculation algorithm) in this study and not presented in Chapter 4.

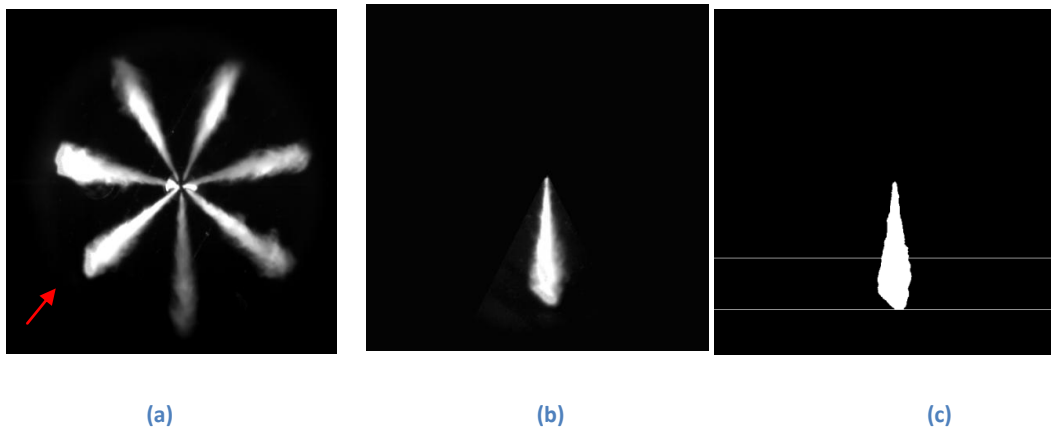


Figure 3.5 Images of Spray, (a) original image, (b) segmented and rotated image, (c) binary image.

3.1.3. Phase Doppler Particle Analyzer(PDPA)

A PDPA is an accurate and reliable instrument in measuring droplet size and velocity. The technique is based on the phase Doppler principle. A schematic of a PDPA system is shown in Figure 3.6. As seen from the figure, a measurement volume is formed by two focused laser beams. When a droplet travels through the measurement volume, lasers would be scattered and their frequency and phase would be changed. Three detectors can capture the refracted and reflected light. Then the processor compares the frequency and phase of the received light to the source lasers. Droplet velocity is related to the light frequency, which is received by

one of the detectors. Droplet diameter can be calculated out from the phase difference between the signals from the two detectors [129].

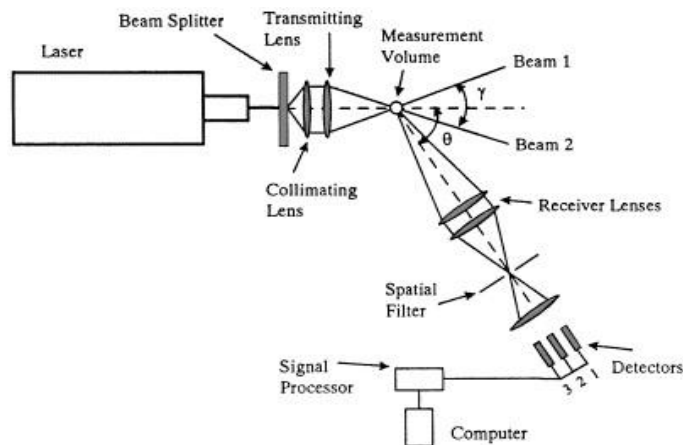


Figure 3.6 Schematic of PDPA system [130].

The PDPA used in this study were from DANTEC and they were fitted in a DANTEC 3D traverse system. Thus the measurement volume can be placed at different positions of the spray accurately, allowing for droplet size and velocity distribution measurement throughout the spray. The PDPA can only measure single particles. If two or more droplets are inside the measurement volume, the measurement would be rejected by the processor and result in a decreased data rate. It was noticed during the test that the data rate was very low at the position near the injector tip, which was because of the droplets being dense. The specifications and parameters of the PDPA are presented in table 3.1

Table 3.1 PDPA specifications and operating parameters

Wave length	514.5 nm
Beam diameter	2.2 mm
Transmitter optics	310 mm
Receiver optics	310 mm
Expander ratio	1.950
Beam spacing	37 mm
Frequency shift	4.00 MHz
Receiver type	112 mm Fiber PDPA
Scattering Mode	Refraction
Spatial filter	0.025 mm
Laser power	1.2 w

3.2. Engine Test Rig

The whole engine test bench was built by the author's colleague Jun Zhang in 2007 for Jaguar Land Rover's 'CONCEPT' project. The author upgraded this engine test bench afterwards. This section presents the specification of the engine test bench and focus on its upgrading. The detailed information regarding the test bench configuration, such as the water cooling system, drive shaft installation and dynamometer control, can be found in Jun Zhang's PhD thesis [131].

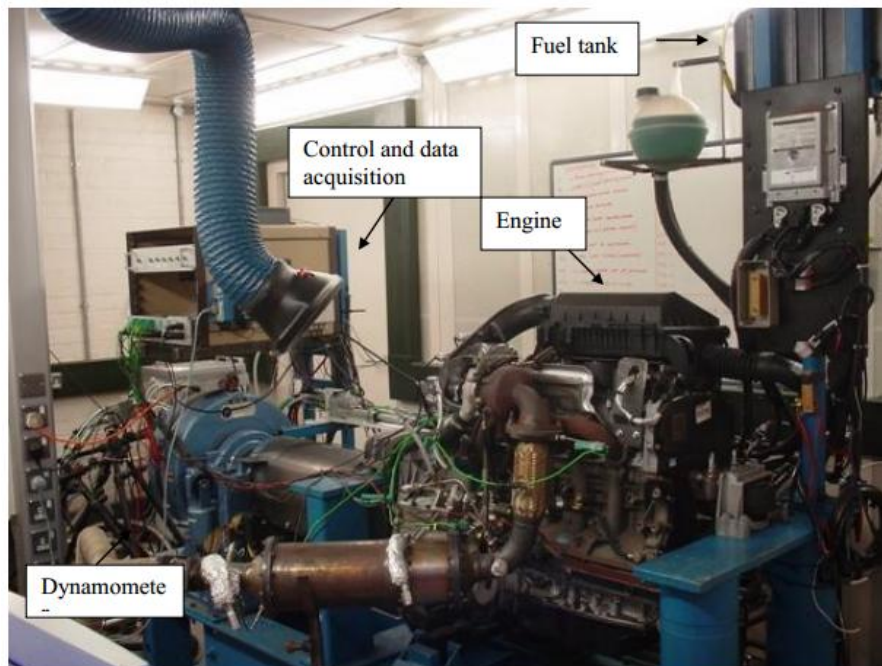


Figure 3.7 Ford PUMA engine test bench [131].

3.2.1. The Engine

The engine used for the experiments was a standard 4-cylinder Ford engine equipped with a modern common rail injection, a variable nozzle turbocharger (VGT) and a dual camshaft. The engine coolant was cooled by laboratory water and coolant temperature was fixed

between 77 °C to 85 °C by a thermal valve. The engine’s EGR cooler was modified to use laboratory water instead of coolant (fixed at 20 °C) to decrease its temperature more. Engine combustion air with a fixed temperature of 25 °C was supplied to the air intake duct. The compression ratio was maintained the same as the original production setup: 16.6. A schematic of the engine test bed is shown in Figure 3.8 and the specifications of the engine are given in Table 3.2. The torque and power characteristics of this PUMA engine are presented in Appendix B, Figure B1.

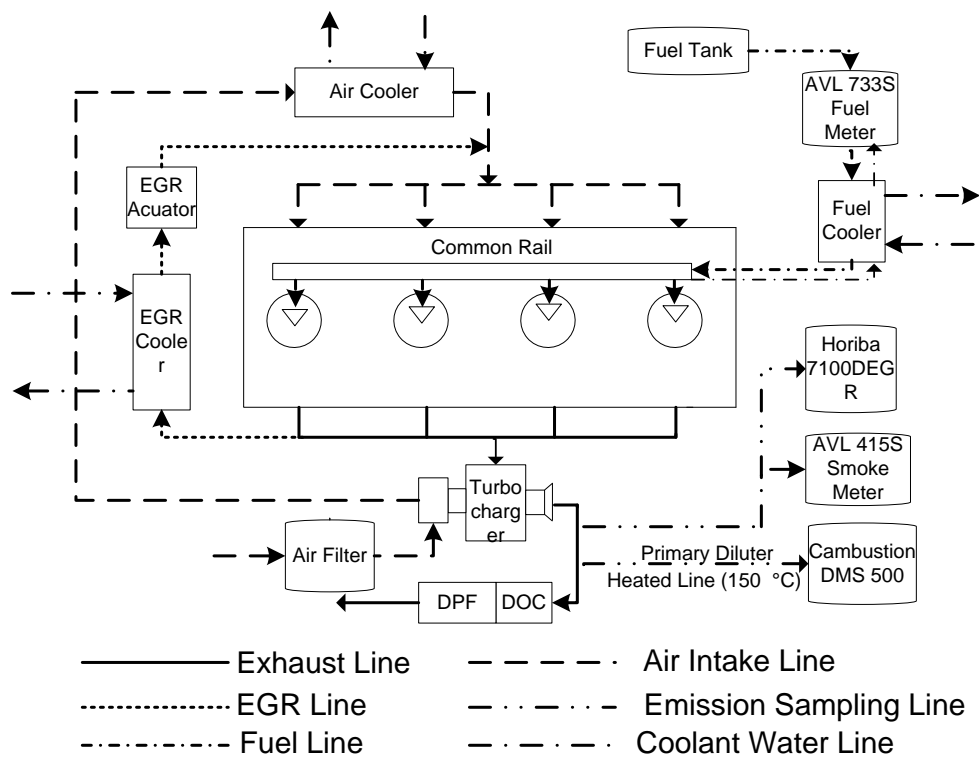


Figure 3.8 Schematic of the standard 4-cylinder Ford engine set-up and diagnostics

Table 3.2 The Specifications of the standard 4-cylinder Ford engine

Bore	86 mm
Stroke	94.6 mm
Compression Ratio	16.6
Engine Capacity	2198 cc
Max Power	96 KW (±5%) @ 3500 rpm
Max Torque	310 NM (±5%) @ 1600-2500 rpm
Injector type	Common Rail, Direct Injection

3.2.2. Test Rig Control

The engine test rig control system can be divided into two major parts: dynamometer control and engine control. The dynamometer controller is from SCHENCK and it has two modes, which are speed mode and torque mode. In the speed mode, a speed is settled manually and the engine will accelerate to this speed if the fuel flow rate is increased, either by pushing the acceleration pedal or by controlling the ECU directly. Further increasing the fuel flow rate will raise the engine torque instead of speed. Throughout the engine test in this study, the dynamometer speed mode was used.

The engine control system consists of two independent subsystems: an actuator for acceleration pedal control and calibration software ATI VISION for real time ECU control. The actuator can be operated with 0-5V analogue voltage signals, which are supplied by a National Instrument card USB 6218. Thus the requested position of the acceleration pedal can be achieved by giving the actuator a corresponding voltage signal. Compared to the acceleration pedal control, ATI VISION controls the engine operation parameters more independently and precisely; which include the number of injection pulses (up to 5) in each engine cycle, injection timing, duration, rail pressure, EGR valve position and the angle of VNT nozzle. Detailed information of the dynamometer controller and ATI VISION can be found at Jun Zhang's PhD thesis [131].

3.2.3. Real Time Combustion Analysing System

A real time combustion analysing system was developed by the author to monitor the engine combustion performances, which include in-cylinder pressure, indicated mean effective pressure, maximum pressure rise rate, heat release rate and combustion phase AHR50. The system has four major parts: a Kistler quartz pressure transducer (type 6542Q18X2) with amplifier, a shaft encoder (type A500/016 from AMI Elektronik), a National Instrument PCI6251 card and a real time signal processing and displaying program written with Labview.

The pressure transducer was placed in the first cylinder glow plug port. It can generate electrical charge at a frequency of 160k HZ when pressurised by the in-cylinder gas. A charge amplifier was used to convert the electrical charge to proportional voltage, which can be sampled by an analogue voltage input port of PCI6251 card at every crank angle. The shaft encoder was connected to the crank shaft by a double beam stainless steel coupling. It can produce two types of pulses: one pulse every crank angle degree used as clock input for the DAQ card and one pulse every revolution, which was combined with the camshaft pulse to trigger pressure data acquisition. Detailed information on using the crankshaft and camshaft pulse to generate a stable pulse at every engine cycle (two crankshaft revolutions) will be introduced in section 3.3 of this chapter.

The signal processing program is able to analyse in-cylinder pressure and give out critical combustion information every second, such as IMEP, AHR50 and maximum pressure rise rate (MPRR). The analysing function is achieved by a matlab script, which is integrated into the Labview program. Detailed calculation methods can be found in section 3.5.1 of this chapter. The front panel of the program is presented in Figure 3.9 and the block diagram,

which shows how the signal is processed and analysed, can be found in the Appendix B, Figure B2.

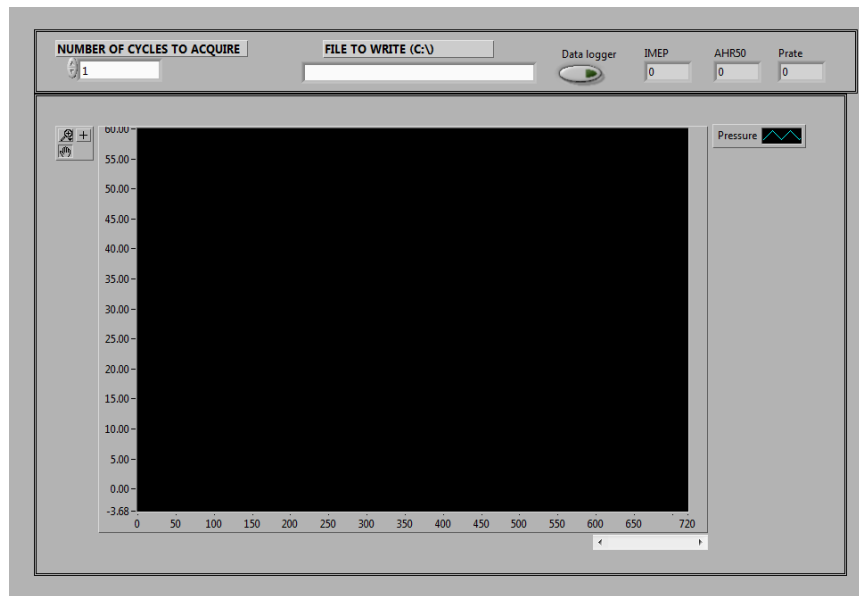


Figure 3.9 Front panel of Real Time Combustion Analysing Program.

3.2.4. Fuel Consumption Measurement and Calibration

Fuel consumption was measured by an AVL 733S fuel balance and fuel was cooled by an AVL 752 fuel cooling system in order to get accurate results. With longer measuring time, the measurement error can be reduced. It was found that repeatable fuel consumption results can be got with 20 seconds sampling time when the engine was operated with diesel. However, dieseline requires as long as 120 seconds measuring time to get repeatable results. This is due to dieseline having higher vapour pressure and a lower boiling point, resulting in vapour bubble inside the fuel line and measurement fluctuation.

To find out the relationship of the fuel consumption reading between the ECU and fuel meter, a calibration has been conducted. The engine was run under different speeds and loads to cover full operation range. Figure 3.10 shows that the ECU reading is quite linear to the fuel meter reading, so a reasonably accurate fuel mass flow rate can be predicted based on the

ECU reading and the equation obtained from Figure 3.10. The reason for carrying out this is that there are two independent fuel injection systems in this engine (a PFI injection system has been integrated into the engine and it will be introduced in the following section 3.3), while only one fuel meter is available. In Chapter 5 and 6, fuel consumption of diesel and dieseline were measure by the fuel meter directly. In Chapter 7, fuel consumption of gasoline via PFI injection was measured by the AVL fuel meter and diesel fuel consumption was obtained from the calibrated ECU reading.

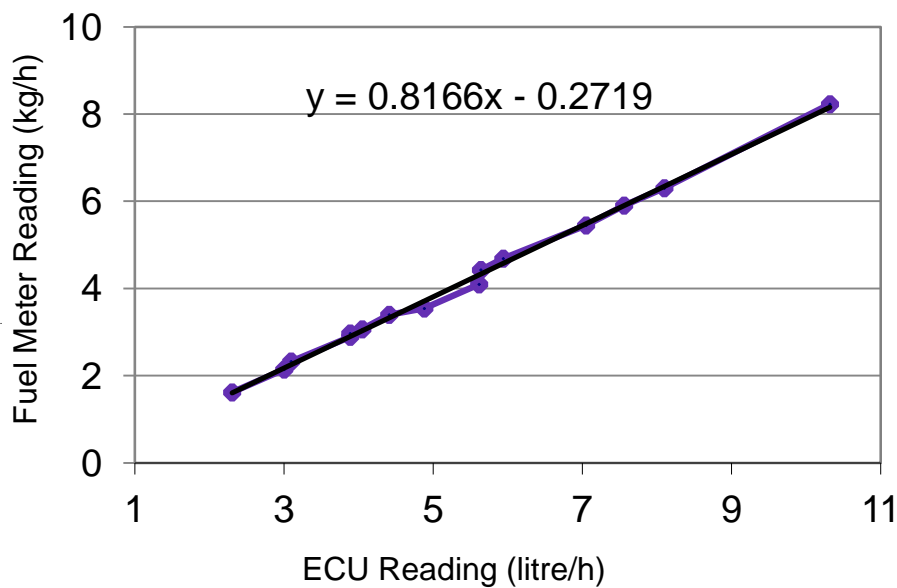


Figure 3.10 Calibration of fuel consumption reading from ECU.

3.2.5. Tested Fuels

Five types of liquid fuels were used in the experiments, namely: neat diesel, gasoline, 20% (G20), 50% (G50) and 70% (G70) gasoline blended with diesel by volume. The neat diesel was the European standard diesel (Specification EN590) and the gasoline was 95 octane gasoline (ULG95) with sufficient lubricity additive (300 ppm by volume). The neat diesel, gasoline, and additive are supplied by Shell Global Solutions, UK. The cetane number of the blended fuels were taken as proportionate to their blending ratio and the cetane number of the gasoline was assumed to be 15 [103]. Fuel properties are listed in Table 3.3. Boiling points of

diesel range from 160 to 340 °C and gasoline ranges from 40 to 160 °C. Blended fuels were expected to have wide boiling ranges, from 40 to 340 °C.

Table 3.3 Fuel Properties (~ means estimated value)

Test Fuel	Diesel	G20	G50	G70	Gasoline
Cetane Number	51	~45	~35	~26	~15
Density (g/ml at 15 °C)	0.84	0.82	0.79	0.763	0.73
Lower Heating Value (MJ/kg)	42.5	~42.7	~43.2	~43.5	44.0
Viscosity(mm ² /s at 40 °C)	2.90	2.08	1.12	0.72	0.50
Surface Tension (mN/m at 20 °C)	28.9	-	-	-	21.6
Vapour pressure (hPa at 20 °C)	<0.1	-	-	-	300-900

3.3. Dual-fuel Single Cylinder Engine Modification

To investigate the combustion and emission characteristics of in-cylinder blended gasoline/diesel, a gasoline PFI system was added to the first cylinder of PUMA engine. The intake and exhaust manifolds were modified to enable the engine run under single cylinder dual fuel engine mode.

3.3.1. Overview of the Single Cylinder Engine

Two modification methods have been tried. One method is unplugging the injectors of three cylinders and trying to run the engine only with the first cylinder. Since no motor was connected to the crankshaft, engine starting was a big problem for this method. Modifying the engine starting strategy, such as increasing the fuel rate and EGR rate (to increase the EGR temperature) during the cranking cycle, was tried, but the engine still could not be started. The second method was to separate the intake air and exhaust gas of the first cylinder from the

other three cylinders. This method was more realistic for the current engine configuration and proved to be successful. Figure 3.11 shows a schematic of a single cylinder dual fuel engine after modification.

In order to minimise modification work and cost, the existing intake and exhaust manifold were modified instead of manufacturing new manifolds. As shown in Figure 3.17, a metal plate (labelled 8) was inserted into the intake manifold after cylinder 1 to stop intake-air flowing to the other three cylinders. Two holes with diameters of 40 mm were drilled at the intake manifold and filter paper was attached to it, allowing fresh air from the ambient atmosphere to flow to cylinders 2, 3 and 4.

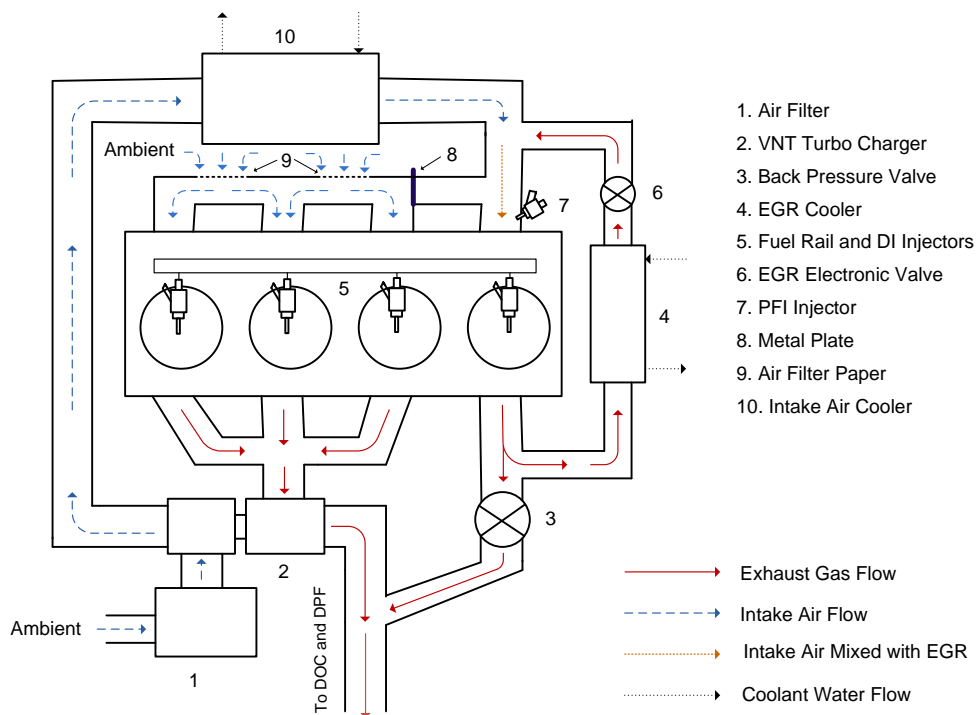


Figure 3.11 Schematic of Single Cylinder Dual Fuel Engine (Modified from 4-Cylinder PUMA Engine).

3.3.2. Exhaust Manifold Modification

As shown from Figure 3.12, the exhaust manifold of cylinder 1 was cut off from the rest and the cut ends were blocked by welding cast iron on them. With the modified manifold, the exhaust of cylinders 2, 3 and 4 would flow through the VNT turbo charger while the exhaust of cylinder 1 joins them after the turbo charger. When the engine ran, cylinders 2, 3 and 4 were used to drive the turbo charger and supply boost pressure to cylinder 1; the pressure can be controlled by the nozzle angle of the turbo charger. A stainless steel gate valve was used to increase the exhaust back pressure of cylinder 1 and force the exhaust to flow through the EGR line. The EGR ratio was controlled by an electronic valve, which was originally supplied with the engine.

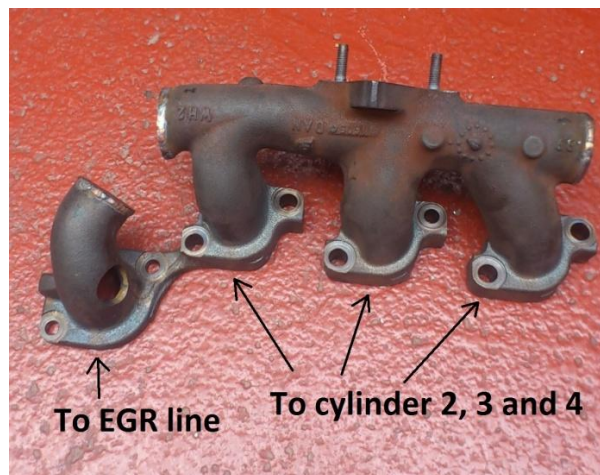


Figure 3.12 Modified Exhaust Manifold.

3.3.3. Intake Manifold Modification

The most challenging part of setting up a PFI system for this production engine was attaching a PFI injector on the intake manifold because the engine is compact. The injector fitting position and its angle need to be carefully chosen, to avoid any conflict with the engine block while the fuel spray direction should be toward the intake valve. Figure 3.13 presents the intake manifold with the PFI injector installed. The injector is fitted to a specially

manufactured adaptor and this adaptor is bolted to the intake manifold. Chemical metal (a super strong filler) is used to seal the adaptor. An engineering drawing for the adaptor of the PFI injector is presented in Appendix B, Figure B5.



Figure 3.13 Intake Manifold with PFI Injector Installed.

3.3.4. Gasoline PFI System

Figure 3.14 presents a schematic of the gasoline PFI system. The fuel line was pressurised by an out-tank injection pump (type: WalbroTCP020/1) and regulated to 2.5 bar by an adjustable fuel regulator. The injector was from DENSO (model: AJ5BR) and controlled by a Labview program with a DAQ card (Model: PCI 6251). The DAQ card can collect a clock signal from the shaft encoder, which was coupled to the engine crankshaft, and a flag signal from a D – type flip-flop (using shaft encoder zero pulse and camshaft signal as input, details of this will be introduced in the following paragraph). After receiving the two types of signal, a counter of the DAQ card is programmed to output pulses, which are of the desired width and at the required time. As the power output of the DAQ card is not sufficient to drive the PFI injector, a driver was used to amplify the injector controlling pulse.

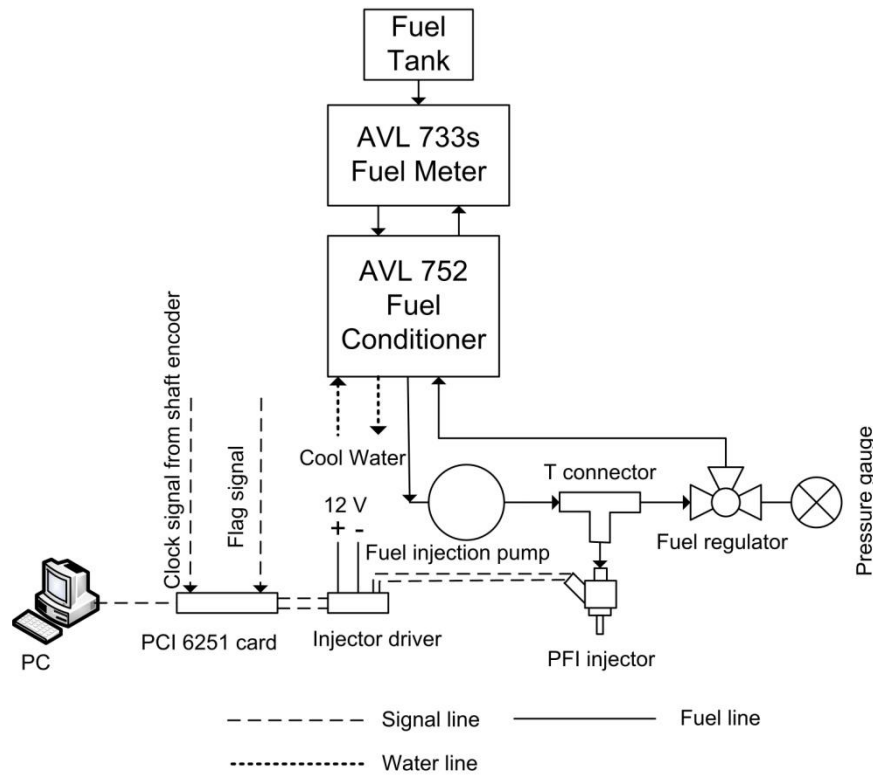




Figure 3.14 Schematic of Gasoline PFI System.


3.3.5. Flag Signal for PFI system

Getting a stable and accurate flag signal is fundamental for injection timing control. A crank shaft encoder zero pulse cannot be used as a flag signal since it contains two pulses in every engine cycle. A cam phase sensor, which is coupled to the camshaft, produces one pulse in each engine cycle. However, the signal is not stable and drifts slightly. This is unacceptable because injection timing needs to be exactly precise. The problem was resolved by using a D-type flip-flop ACT374 to combine the good points of the two signals. Table 3.2 shows the truth table of the flip-flop and Figure 3.15 gives an example of input and output signals of the flip-flop. The camshaft signal was obtained from the engine ECU and it can be observed that the camshaft pulse is much wider than the crankshaft pulse. The trick of getting a stable flag signal is to place the crankshaft pulse inside the camshaft pulse by adjusting the relative position between crankshaft and encoder. As seen from Figure 3.15, the rising edge of the flag

signal is decided by the crankshaft pulse rising edge, which is very stable, while its frequency is the same as the camshafts' pulses.

Table 3.4 Truth Table of D-Type Flip-Flop ACT374 [132].

INPUTS			OUTPUTS	
			374	534
\overline{OE}	CP	Dn	Qn	\overline{Qn}
L		H	H	L
L		L	L	H
L	L	X	QO	QO
H	X	X	Z	Z

H = High level (steady state)
 L = Low level (steady state)
 X = Don't care
 = Transition from low to high level
 QO = The level of Q before the indicated steady-state input conditions were established
 Z = High impedance

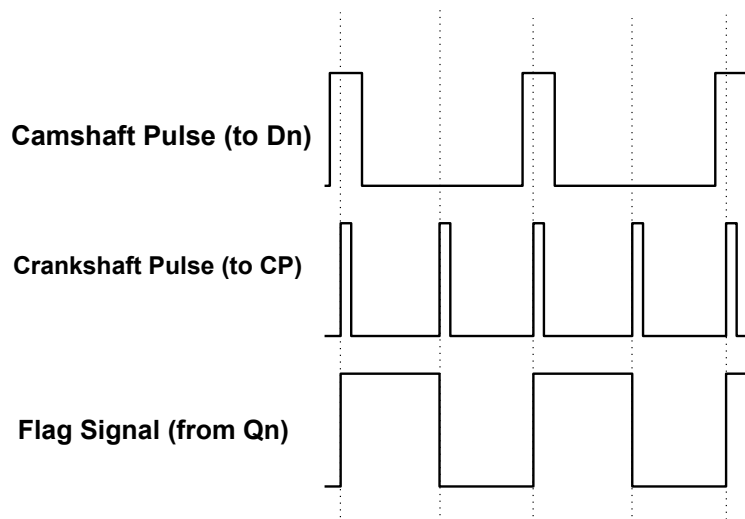


Figure 3.15 Input and Output Signals of D-Type Flip-Flop ACT374.

3.4. Emissions' Measurement Instruments

3.4.1. Gaseous Emissions' Measurement

A Horiba MEXA-7100DEGR emission analyser was used to measure exhaust gaseous emissions, including NO_x, HC, CO and O₂, as well as the EGR ratio (by measuring intake and exhaust CO₂ concentrations simultaneously). Figure 3.16 presents the main units and gas flow of the Horiba 7100DEGR. Calibration gases were supplied to the solenoid valve system (SVS) and then to each analyser in the analyser rack unit (ANR) and oven unit (OVN) respectively. A calibration procedure was conducted before every test to minimise the measurement errors. The exhaust gases were heated to 190 °C in the sampling line in order to avoid condensation of hydrocarbons and water. A flame ionization detector (FID), which is located in the OVN unit, was used to measure the concentrations of HC (in terms of CH₄). Exhaust gases from the OVN were sent to a sample handling unit to remove water vapour and then measured by each gas analyser inside the ANR. The measurement error of each analyser is 1% of their measurement ranges and the results presented in this thesis are averaged over 60 measurements. A Horiba remote control program, which was written with Labview, was developed by the author to get averaged measurements quickly. The program uses LAN cable to build communication between the host computer and the Horiba Main Control Unit (MCU) while the command protocol was taken from the Horiba user guide book. The front panel and a block diagram of the Horiba remote controller can be found in the Appendix B, Figure B3 and B4.

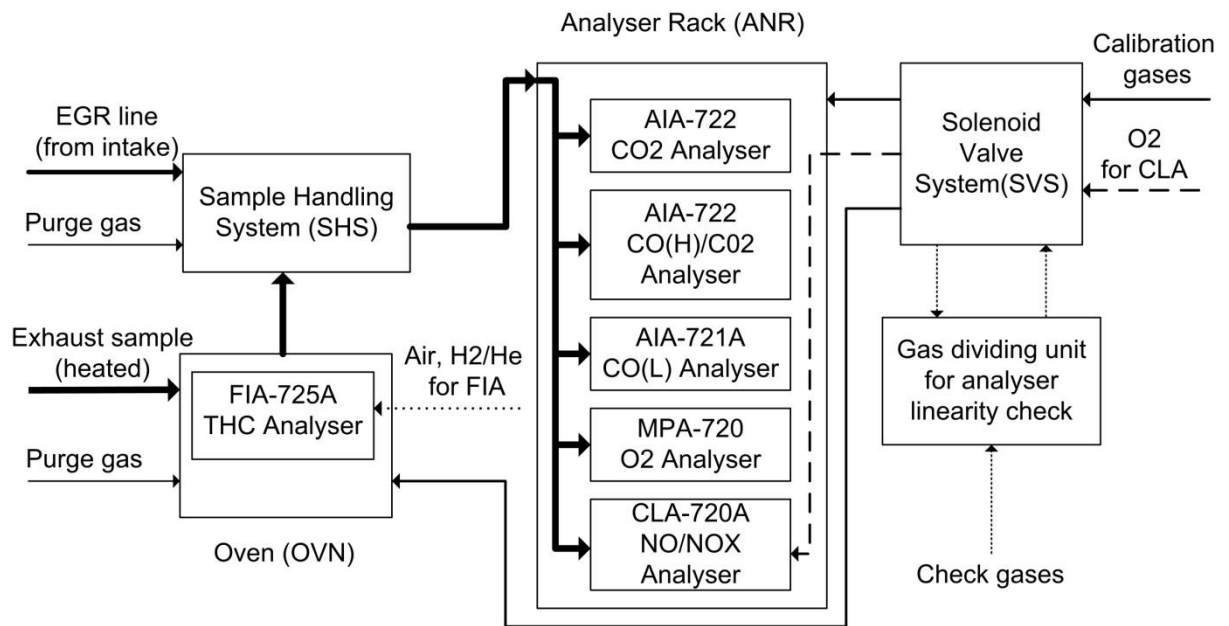


Figure 3.16 Gas Flow Schematic for Horiba 7100DEGR.

3.4.2. Particle Emissions' Measurement

Three pieces of equipment were used to measure particle emissions throughout the tests carried out in this thesis. They were a Smoke Meter 415SG002 from AVL, a Scanning Mobility Particle Analyser (SMPS) (Model 3936) from TSI and a DMS500 Fast Particle Analyser from Cambustion. Details of this equipment will be introduced in the rest of this section.

Smoke Meter

An AVL Smoke Meter 415SG002 is able to measure engine exhaust soot concentration. Its principle is as follows: a subset of exhaust gases is taken from the exhaust line via a probe and sucked through filter paper in 6 seconds, a reflect meter is used to measure the blackening of the filter paper and the result ranges from 0 (unloaded clean filter paper) to 10 (fully loaded with soot and absolutely black). The blackening of the filter paper is output as a Filter Smoke

Number (FSN). Soot concentration (unit: mg/m³) and pollution level (unit: %) can be calculated based on the FSN and is output by a smoke meter. The specifications of the AVL 415S smoke meter are presented in table 3.5.

Table 3.5 AVL 415S smoke meter specifications

Measurement Range	FSN: 0-10 Soot Concentration: 0-32000 mg/m ³ Pollution level: 0-100%
Resolution	0.001 FSN, 0.01 mg/m ³ , 0.01%
Repeatability	$\sigma < +/- (0.005 \text{ FSN} + 3\% \text{ of measurement value})$
Exhaust Back Pressure	-100—400 mbar
Sampling Time	6 seconds
Permissible exhaust temperature at sampling point	600 °C max

SMPS

A SMPS 3096 was used to measure particle number and size distribution. It consists of a Model 3080 Electrostatic Classifier (EC), a Model 3775 Condensation Particle Counter (CPC) and two Differential Mobility Analyzers (DMAs), one Model 3081 DMA (measuring range 10-1000 nm) and one Model 3085 DMA (measuring range 2-150 nm). As particle number total concentration of a diesel engine exhaust is very high, the exhaust sample was diluted by a 379020A diluter from TSI before entering the SMPS, to get the best measuring accuracy and avoid damage to the instrument.

The engine exhaust raw gas is firstly drawn into the diluter, where a disk with hemispheric cavities rotates on a steel block. The steel block has two aerosol channels, one is the raw gas channel and the other is the air channel. Then a well defined amount of raw gas in every disk

cavity is transported to the dilution air channel. The dilution ratio can be controlled by the disk rotating speed and dilution ratio 78:1 was used in the tests. Dilution air was heated to 150 °C to evaporate liquid particles before and during dilution, avoiding condensation of the former liquid particle matter. Finally, the diluted raw gas is sent to the SMPS for particle number and size distribution measurement.

Figure 3.17 illustrates the gas flow inside the EC and DMA, which are designed to extract a known size fraction of submicrometer particles from incoming raw gas. Inside the EC, particles above a known particle size are removed by an impactor. A Kr-85 neutralizer is used to charge the aerosol flow, making the particles have different electrical mobility depending on their electrical mobility diameter. Particles within a narrow range of electrical mobility can exit through a small slit at the bottom of the DMA and transfer to the CPC. The rest of the particles are either collected by the central negatively charged rod or bypassed to the exhaust.

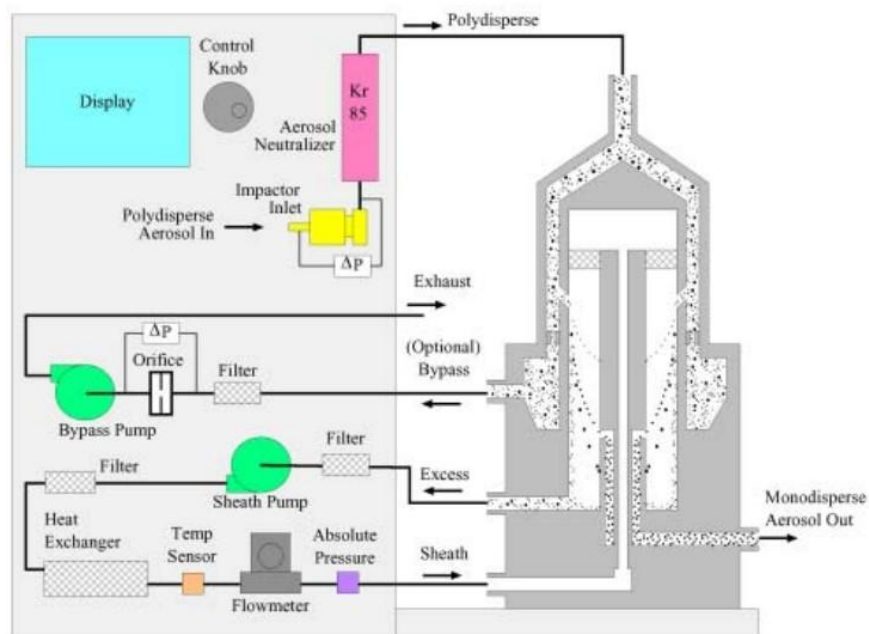


Figure 3.17 Gas Flow Schematic for Electrostatic Classifier with DMA [133].

In the CPC, the particles, whose size range is known from the DMA, firstly enter a saturated butanol vapour and then the vapour saturated aerosol flows into a cold condenser. The butanol vapour condenses onto the particles and the particles grow into large droplets, which are large enough to be counted optically. The particle number and size scanning time was set to 120 seconds in the tests.

DMS500

As the diluter of the SMPS was broken down several times and the repairing process took a long time after some of the tests, a DMS500 was used to measure the particle number and size distribution in part of the tests. Compared to the SMPS, a DMS500 has a much shorter measuring time (0.1 seconds) and is good for transit tests. The dilution system of a DMS500 is shown in Figure 3.18. It consists of two stages: the exhaust is primarily diluted in the heated (150 °C) sampling head by 5 bar compressed air in the first stage and further diluted by a rotating disk diluter in the second stage. The dilution ratio of the first stage is 5:1 and the sampling line is heated to 150 °C. The purpose of this is to avoid particle condensation in the sampling line, which may result in a sampling line blocking problem. The dilution ratio of the second stage can be varied by adjusting the rotating disk speed and a proper dilution ratio was chosen in the tests to maintain the particle concentration of the diluted exhaust at a suitable range.

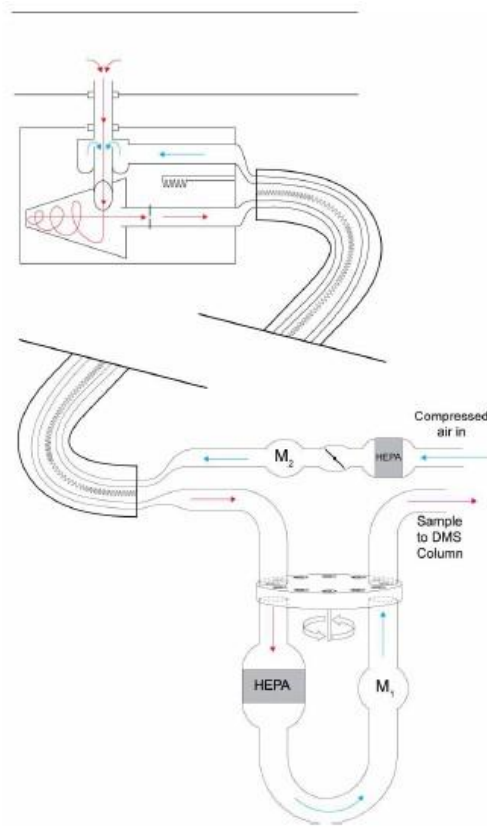


Figure 3.18 Schematic of DMS500 Two-stage Dilution System [134].

As shown in Figure 3.19, a DMS500 has an aerosol charger and particle electrical mobility classifier. The particles are positively charged before entering the classifier, which contains a high voltage electrode. The positively charged particles are repelled by the positive high voltage electrode towards the electrometer detectors. Small particles are more mobile and hence more easily deflected. Larger particles are less mobile and land on a detector further along the classifier. The detected particles will remain on the electrode rings until removed by the periodic instrument cleaning.

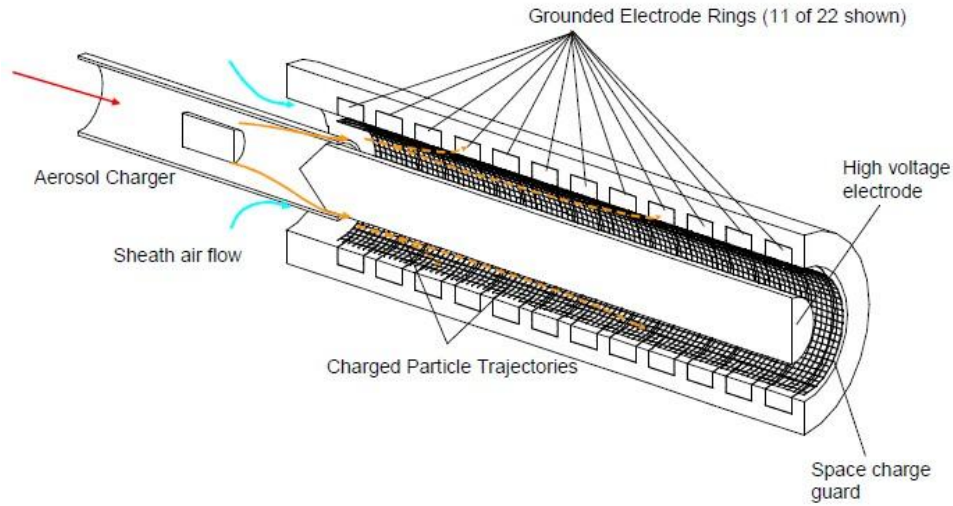


Figure 3.19 DMS500 Particle Classifier and Charger [134].

3.5. Data Processing

The data processing of the engine test was performed by a Matlab GUIDE program which is developed by the author. The input of the program is: engine operating condition, in-cylinder pressure, fuel consumption and emissions. The heat release rate, combustion performances which include ROPR, combustion delay, phasing and duration, engine efficiency and normalised emissions can be outputted by the program. The related calculation methods are introduced as follows.

3.5.1. Heat Release Rate Analysis

The heat release rate was calculated from the averaged results of 50 complete engine cycles' in-cylinder pressure data, which was collected by the Real Time Combustion Monitoring Program (introduced in section 3.2.3 of this chapter). The calculation equation is from Heydood [24] and it is:

$$\frac{dQ}{d\theta} = \frac{\gamma}{\gamma-1} p \frac{dV}{d\theta} + \frac{1}{\gamma-1} V \frac{dp}{d\theta} \quad (\text{Equation 3.1})$$

Where γ is the ratio of specific heats c_p/c_v . d_v and d_p are change of engine volume and pressure respectively during specific crank angle.

AHR50 is used to indicate the combustion phase and it is defined as the crank angle at which 50% of total heat release occurs. Combustion delay is the crank angle difference between start of injection (SOI) and AHR50. Combustion duration is the crank angle difference between AHR10 and AHR90.

3.5.2. Engine Efficiency Calculation

Calculation equations of indicate and brake thermal efficiency were taken from Heydood's work [24] and they are:

$$\eta_f(\%) = \frac{P(\text{kw}) \times 3.6}{\dot{m}_f(\text{kg/h}) \times Q_{HV}(\text{MJ/kg})} \quad (\text{Equation 3.2})$$

$$P(\text{kw}) = \frac{\text{mep}(\text{bar}) \times V_d(\text{litre}) \times N(\text{rev/s}) \times 10}{n_R} \quad (\text{Equation 3.3})$$

Where η_f = Brake (or Indicated, according to the choice of mep) thermal efficiency

\dot{m}_f = fuel mass flow rate

Q_{HV} = lower fuel heating value, the value is 42.5 for diesel, 44 for gasoline

mep = IMEP or BMEP, the results are corresponding to indicated or brake thermal efficiency respectively

V_d = engine capacity, which is 2.2 L for the engine used

N = engine speed

n_R = number of crank revolutions for each power stroke per cylinder (2 was chosen).

The calculation equation of combustion efficiency is as follows:

$$\eta_c = \frac{\sum Q_{LHV_i} x_i}{[\dot{m}_{fuel}/(\dot{m}_{fuel} + \dot{m}_{air})] Q_{LHV_{fuel}}} \quad (\text{Equation 3.4})$$

where x_i and Q_{LHV_i} represent the mass fractions and lower heating values (LHV), respectively, of HC, CO, NO and H₂. For this work, $Q_{LHV_{HC}}$ has been treated as equal to $Q_{LHV_{fuel}}$.

3.5.3. Specific Emissions' Calculation

The gaseous emissions' level measured by the Horiba are in terms of part per million (ppm). This is not an effective indicator of the emissions' level at various engine conditions since the exhaust mass flow rate and engine power output change. To evaluate the emissions' level more effectively, specific emissions were used, which is defined as the mass flow rate of pollutant for each unit power output [24]. The following is an example of specific hydrocarbon emissions' calculation.

(Equation 3.5)

$$\text{Specific HC emission}(g/kw.h) = \frac{\text{mass flow rate of HC}(g/h)}{\text{indicate(or brake) power output}(kw)}$$

(Equation 3.6)

$$\text{Mass flow rate of HC}(g/h) = \text{Mass flow rate of exhaust}(g/h) \times \frac{\text{HC molar mass}}{\text{exhaust mean molar mass}}$$

The power output was calculated from equation 3.3. The exhaust mass flow rate was deduced by adding the fuel mass flow rate and the intake air mass flow rate. The mean molar mass of exhaust gases was calculated according to the molar fraction of each exhaust component [24].

3.6. Summary

This chapter describes the entire test facilities involved in the experiments. They consist of two major test rigs: fuel spray test rig, which includes a high speed camera and a 2D PDPA system, and a 2.2 litre diesel engine test bench, where all the engine tests were conducted. In addition, the emissions' measurement instruments and data processing methods are introduced in detail.

Several major upgrades have been implemented to the engine test bench by the author after it was built by its previous operator, Jun Zhang. Firstly, a real time combustion analysing program was developed using Labview to monitor combustion performances, which include in-cylinder pressure, heat release rate, IMEP, pressure rise rate and combustion phase AHR50. Additionally, an AVL fuel meter and conditioner were integrated to the fuelling system and precise fuel consumption measurement was achieved. Finally, the author built a PFI injection system for the engine's first cylinder and the 4-cylinder production engine was modified to a single cylinder diesel engine by modifying the intake and exhaust manifolds.

CHAPTER 4

DIESELINE SPRAY CHARACTERISTICS

This Chapter examines the spray characteristics of dieseline under different injection pressures and back pressures. The tip penetration length of dieseline spray was measured using a high speed camera. The atomisation quality of dieseline fuel was evaluated in terms of droplets size and velocity using the PDPA technique.

4.1. Introduction

Dieseline and gasoline fuelled CI engines were experimentally studied by several research organisations. The results showed that smoke emissions were significantly reduced and the PPCI operating range was extended [78, 103-105]. Numerous researchers have demonstrated that the spray characteristics of diesel and diesel-like fuel play an important role in emissions' formation of direct injection CI engines [31, 45]. For example, over-penetration can cause piston bowl/cylinder wall wetting and thus increase particle, UHC and CO emissions; particle emissions can be effectively reduced with better spray atomization. Quite a few studies tested dieseline or gasoline spray in high pressure common-rail injection systems. The objective of this study is to investigate the behaviour of the injection and atomization process using dieseline/gasoline in a common rail injection system. It is believed that the fundamental findings of this chapter assist to explain the engine tests results of Chapters 5, 6 and 7. Additionally, the provided data can help to CFD code validation and engine design optimisation for further research.

4.2. Fuel Spray Tip Penetration

4.2.1. Test Conditions

Five fuels were tested in a pressurised vessel. They were neat diesel, neat gasoline (G100), 20% (G20), 50% (G50) and 70% (G70) gasoline blended in diesel by volume. The fuels' properties have been given in Chapter 3, section 3.2.5. Table 4.1 presents the test conditions of the spray penetration study. The injection pressure and injection duration were chosen based on the PUMA engine's (the engine tested in Chapters 5, 6 and 7) calibration map and they cover the whole engine operating range. With the increased ratio of gasoline in diesel, the injection system used in this study can't achieve its maximum injection pressure, because the pump used for producing the pressure was designed for diesel and it had a lower performance for gasoline. The back pressures in this study were chosen based on the actual ambient air density inside the cylinder of the PUMA engine when the fuel injection started. For example, when the engine was operated at 4 bar IMEP and fuel injection started at TDC, the in-cylinder pressure was 50 bar and the temperature was around 550 ° C. The corresponding air density was 21.2 kg/m³. Advanced injection timing corresponds to lower ambient density while higher engine load (the turbocharger began working and intake pressure was increased to up to 2.5 bar) corresponds to higher ambient density. The ambient temperature was at 20 ±2 ° C and the chosen ambient densities of this test are supposed to represent the lowest and highest possible air density inside the engine cylinder. At each testing condition, images of 10 sprays were captured by the high speed camera, which is introduced in Chapter 3, at frequency of 18003 fps. The averaged results are presented throughout this section.

Table 4.1 Test Conditions for spray penetration study

Test Fuel	P_{inj} (MPa)	P_{back} (MPa)	Ambient Density (kg/m^3)	Injection Duration(μs)
Diesel	50/75/100/125/150	1.5/3.0	17.8/35.6	600
G20	50/75/100/125/150	1.5/3.0	17.8/35.6	600
G50	50/75/100/125	1.5/3.0	17.8/35.6	600
G70	50/75/100/125	1.5/3.0	17.8/35.6	600
Gasoline (G100)	50/75/100	1.5/3.0	17.8/35.6	600

Figure 4.1 shows the spray images of diesel, G50 and G100 at injection pressure of 500 bar and back pressure of 15 bar. To determine the spray tip penetration length, a matlab imaging process programme was used to convert the grey images to binary images, where pixel value of 1 represents spray region and 0 represents background. The spray tip position can be detected by finding the point which is farthest to the injector's tip position and with pixel value 1. The spray length is defined as the length between the tip position of the spray and injector.

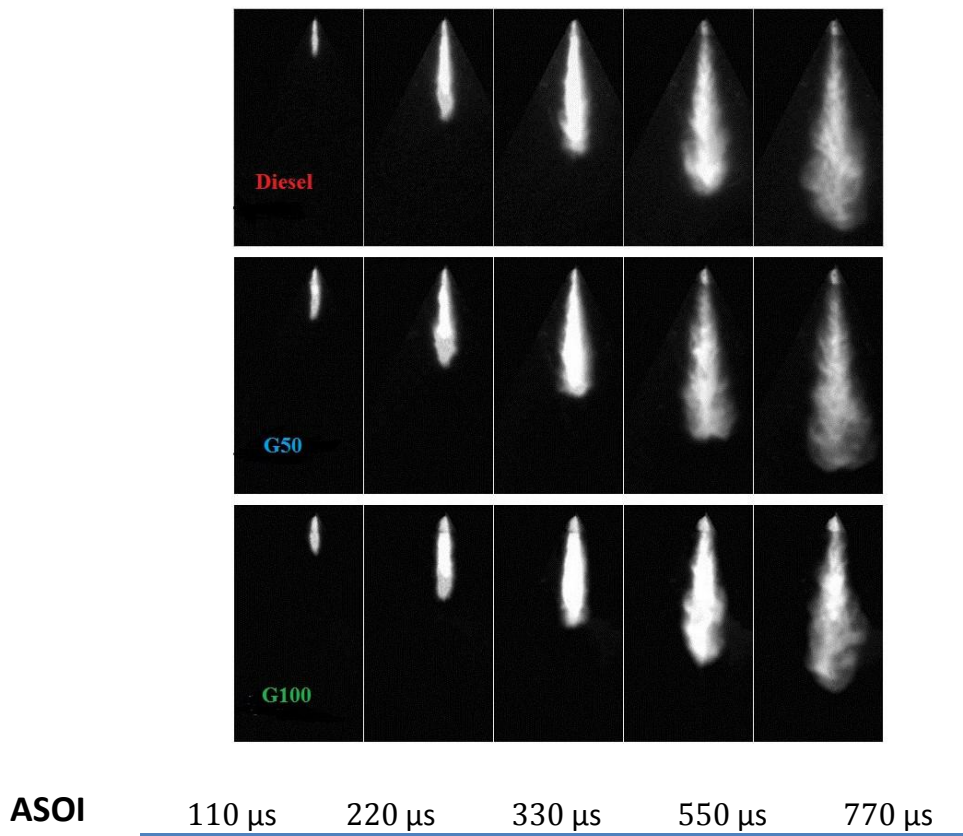


Figure 4.1 Spray images of diesel, G50 and G100, injection pressure 500 bar, back pressure 15 bar.

4.2.2. Effect of Gasoline/Diesel Blending Ratio

Figure 4.2 shows the penetration length of different gasoline/diesel blends with injection pressure of 500 bar. As shown in Figure 4.2 a, at 15 bar back pressure, the increase of gasoline ratio reduced the tip penetration length, particularly after 300 μ s ASOI. At the end of the injection event, the penetration length of diesel was 2 mm longer than G50 and 7 mm longer than gasoline. The main reason for this was believed to be the lower volatility and higher density of diesel, as compared to G50 and G100. Higher density of diesel gave it higher initial momentum and thus longer penetration length [14, 17] during the initial stage while lower volatility made it more difficult to lose mass and thus momentum in evaporation and break-up. Spray atomization processes may also play an important role. Gasoline has lower viscosity, which helps to atomise liquid fuel to small droplets [17] during secondary

break-up and increase the surface area. This could increase the interaction between ambient air and liquid droplets, resulting in shorter penetration length. Additionally, gasoline has much higher vapour pressure than diesel and it is supposed to be more favourable for cavitation formation inside the injector. Recent studies have demonstrated that cavitation is the main break-up mechanism for current high pressure common rail injection systems [12]. The stronger cavitation of gasoline might help the atomisation process and thus shorten its penetration length. The differences of penetration length between diesel and dieseline were significantly reduced by increasing the back pressure to 30 bar, which is shown in Figure 4.2 b. It was observed that the penetration length of gasoline was less sensitive to the increase of back pressure than neat diesel and dieseline. This is to be dicussed in a later section 4.2.3.

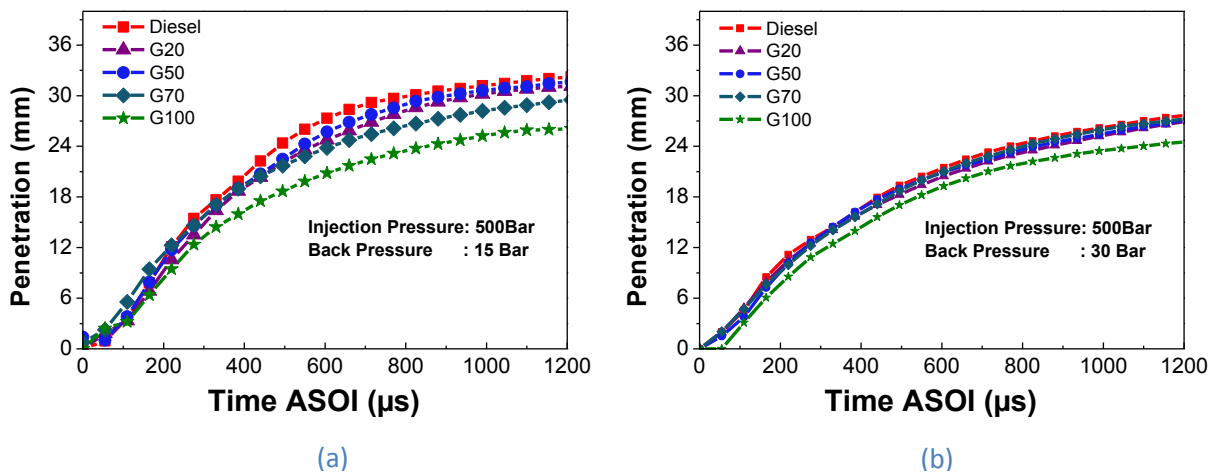


Figure 4.2 Effect of gasoline/diesel blending ratio on penetration length at injection pressure of 500 bar. (a) $P_{back}=15$ bar; (b) $P_{back}=30$ bar.

Figure 4.3 compares the penetration length of diesel and dieseline at 1000 bar injection pressure. The diameter of the vessel is 69 mm and penetration length longer than 34.5 mm cannot be observed. The spray penetration length became constant in the late stage because of the wall impingement at this high injection pressure. Similar to the case of 500 bar injection pressure, the penetration length differed little between fuels until 250 μs ASOI and after that time the fuel with higher gasoline fraction had shorter penetration length. However, the

difference was reduced as compared to the case 500 bar injection pressure, because the influence of viscosity became smaller at higher injection pressure. Similar phenomena were also found in [16, 17]. At 450 μs ASOI, diesel's penetration length was 2 mm longer than G50 and 5.5 mm longer than gasoline (G100) at 15 bar back pressure. Increasing the back pressure to 30 bar reduced the differences significantly, shown in Figure 4.3 b.

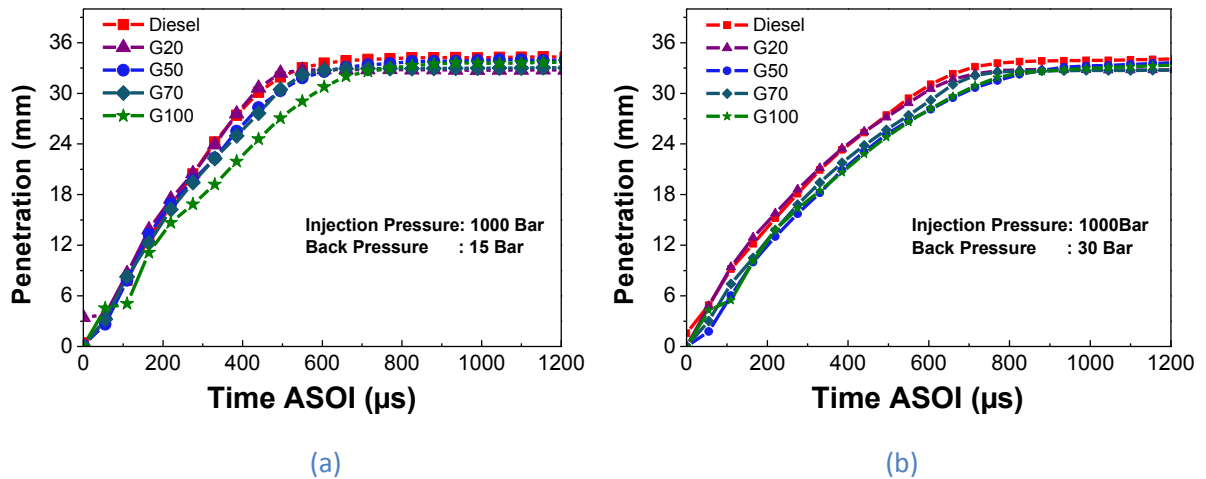


Figure 4.3 Effect of gasoline/diesel blending ratio on tip penetration length at injection pressure of 1000 bar. (a) $P_{\text{back}}=15$ bar; (b) $P_{\text{back}}=30$ bar.

4.2.3. Effect of Back Pressure and Injection Pressure

Figure 4.4 shows the effect of back pressure on spray tip penetration length for diesel, G50 and G100. Before the transient time (liquid column was dominating the spray region with respect to the entrained air [7]), the change of back pressure had little effect on penetration length as the spray was dense and the momentum was high. After the transient time, very clear reductions of penetration length were observed for diesel and G50. However, the effect of back pressure on G100's penetration was much smaller as compared to diesel and G50. A similar phenomenon was also found with tests under 1000 bar injection pressure. It was believed that the high volatility and low boiling points range of gasoline resulted in this observation. A possible reason is as follows: the G100 droplets can vaporize much faster and lose their momentum quicker than diesel and G50 as they move toward downstream; however,

higher back pressure results in less vaporization but more drag force for G100; the two effects cancel each other out and thus the G100's penetration length remains when back pressure is increased.

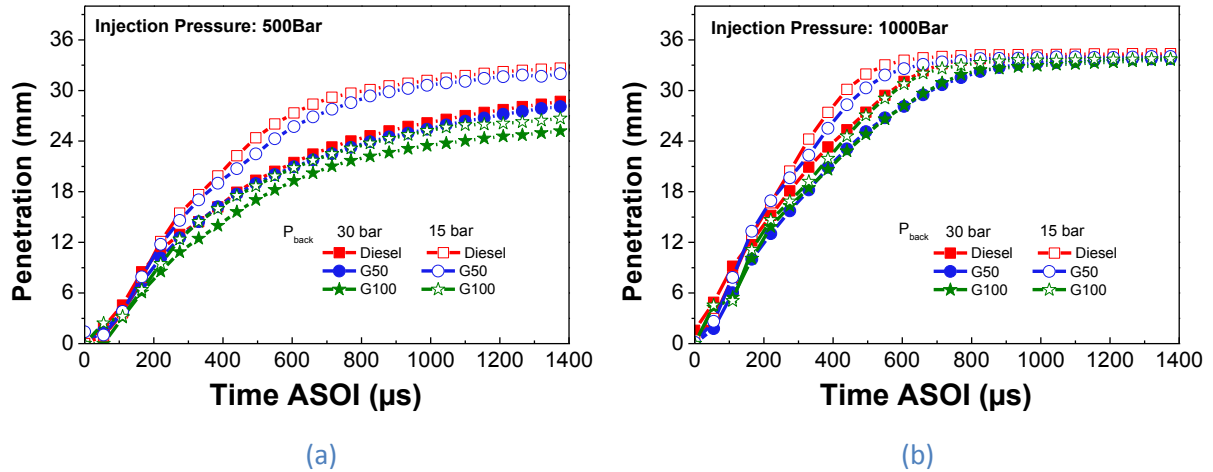


Figure 4.4 Effect of back pressure on penetration length. (a) $P_{inj}=500$ bar; (b) $P_{inj}=1000$ bar.

It is shown in Figure 4.5 that when injection pressure was increased, the penetration length of G50 and G100 were increased at a similar scale, which was due to the higher pressure difference and consequently higher initial momentum. The results indicate that, as compared to back pressure, injection pressure plays a more important role in affecting the penetration length of G100, under the presented testing conditions. G50's penetration lengths were found to be similar to diesel when injection pressure and ambient pressure were varied (shown in Figure 4.4).

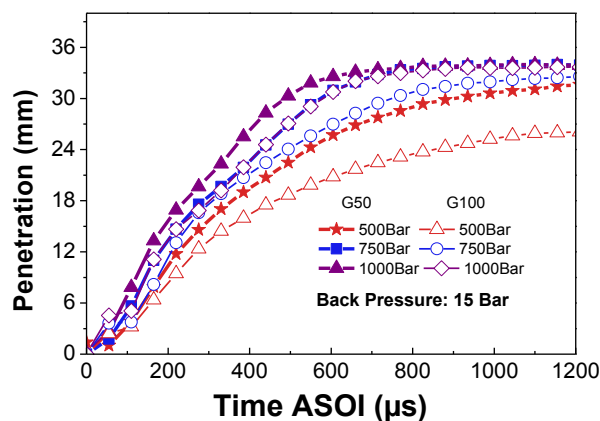


Figure 4.5 Effect of injection pressure on penetration length.

4.2.4. Empirical Correlation for Dieseline Spray

Numerous empirical equations have been proposed by different researchers to predict diesel fuel penetration. Hiroyasu et al. [7] proposed correlations for diesel fuel that included different penetrations laws depending on the region. In the nozzle's near field region and before the spray breaks up, the expression is as below:

$$S = 0.39 \times \left(\frac{2 \times (P_{inj} - P_{back})}{\rho_l} \right)^{0.5} \times t \quad (\text{Equation 4.1})$$

where S is spray penetration length, P_{inj} is injection pressure, P_{back} is back pressure, ρ_l is fuel density and t is the observing time. After the spray breaks up, ambient density plays an important role and the expression is:

$$S = 2.95 \times \left(\frac{P_{inj} - P_{back}}{\rho_{amb}} \right)^{0.25} \times (D \times t)^{0.5} \quad (\text{Equation 4.2})$$

where ρ_{amb} is the ambient density and D is nozzle diameter.

Wakuri [126] and Dent's [127] models, which were similar to Hirayasu's model but included the effect of ambient temperature, were also widely accepted and used. Recently, Nabber and Siebers [14] followed these models and presented dimensional form equations which included the estimation of arbitrary constant in their model.

Before the spray breaks up,, the expression is:

$$S = C_V \times \left(\frac{2 \times (P_{inj} - P_{back})}{\rho_l} \right)^{0.5} \times t \quad (\text{Equation 4.3})$$

After the spray breaks up, the expression is:

$$S = \left(\frac{C_v \times C_a^{0.5}}{a \times \tan \theta / 2} \right)^{0.5} \times \left(\frac{P_{inj} - P_{back}}{\rho_{amb}} \right)^{0.25} \times (D \times t)^{0.5} \quad (\text{Equation 4.4})$$

The break-up time is as below:

$$t_{break} = \frac{(C_a/2)^{0.5}}{C_v \sqrt{\tan \theta}} \times \frac{\rho_l \times D}{(P_{inj} - P_{back})^{0.5}} \quad (\text{Equation 4.5})$$

where C_v is the orifice velocity contraction coefficient and C_a is area contraction coefficient. Their values depended on the injector tip design. θ is the spray dispersion angle, a has a constant value of 0.66. The meaning of the other parameters are the same as explained for Hiroyasu's model.

In this study, Naber and Siebers's model was used. As discussed in the previous section, for G100, the ambient density appears less effective than injection pressure when spray was at the far field region, a free exponent n was given to ambient density in Equation 4.4. Considering the injector used in this study was different from Naber and Sieber's, free coefficients $K1$ and $K2$ were given to Equation 4.3 and Equation 4.4 and the values were kept the same for each fuel. Matlab fitting toolbox was used to find the value of n for each fuel separately. The modified equations are as below:

$$S_{Before\ break-up} = K1 \times \left(\frac{2 \times (P_{inj} - P_{back})}{\rho_l} \right)^{0.5} \times t \quad (\text{Equation 4.6})$$

$$S_{After\ break-up} = K2 \times (P_{inj} - P_{back})^{0.25} \times (\rho_{amb})^n \times (D \times t)^c \quad (\text{Equation 4.7})$$

Figure 4.6 and Figure 4.7 compares the experimental data with the Naber and Siebers's model at varied conditions. The lines represent the modelled penetration and the points represent the experimental data. As shown in Figure 4.6, the model fitted very well with the experimental results at injection pressure of 500 bar. The exponent n is -0.23 and -0.24 for diesel and G50 respectively while it is -0.28 for G100. This confirms that the ambient density (back pressure) has less effect on G100 than diesel and G50 in the far field region, which is discussed in section 4.2.3. At 1000 bar injection pressure, the model underestimated the penetration length of all three fuels. One possible reason is that this model does not properly take into account

the role of injection pressure and the exponent of pressure difference in Equation 4.6 for the far field region probably needs to be adjusted. Also, according to Naber and Siebers's model, the spray break-up lengths doesn't change with injection pressure. This is not accurate and the spray was supposed to have longer break-up length as injection pressure increased. Limited by the speed of the camera (18003 fps) in this study, very few images were got in the nozzle near field region. To find the proper spray break-up length, more investigations into the spray characteristic in this region should be carried out. Detailed study of this topic is out of the scope of the present thesis.

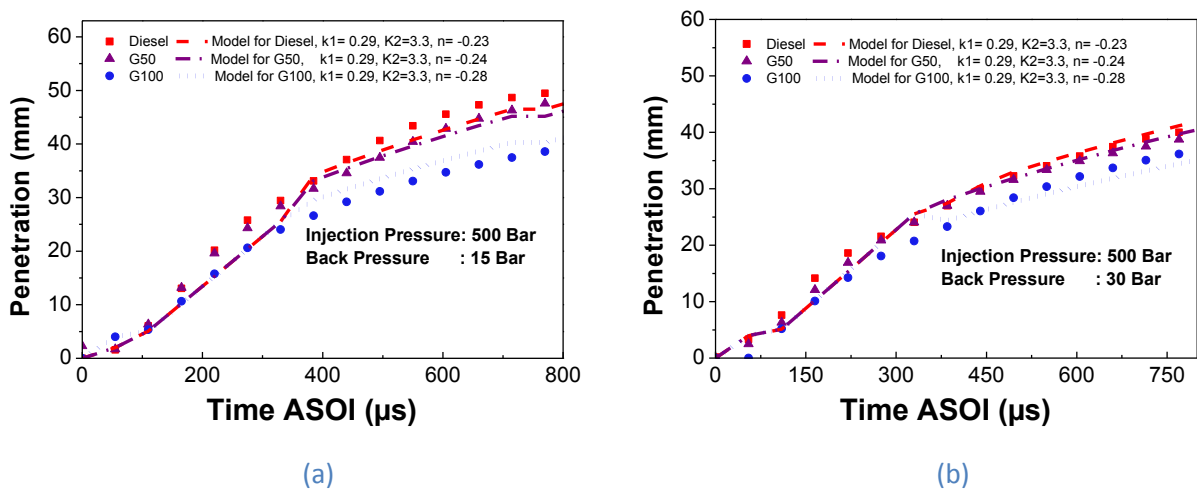


Figure 4.6 Comparison of experimental data with Naber and Siebers's model at Injection pressure of 500 bar. (a) $P_{\text{back}}=15$; (b) $P_{\text{back}}=30$ bar.

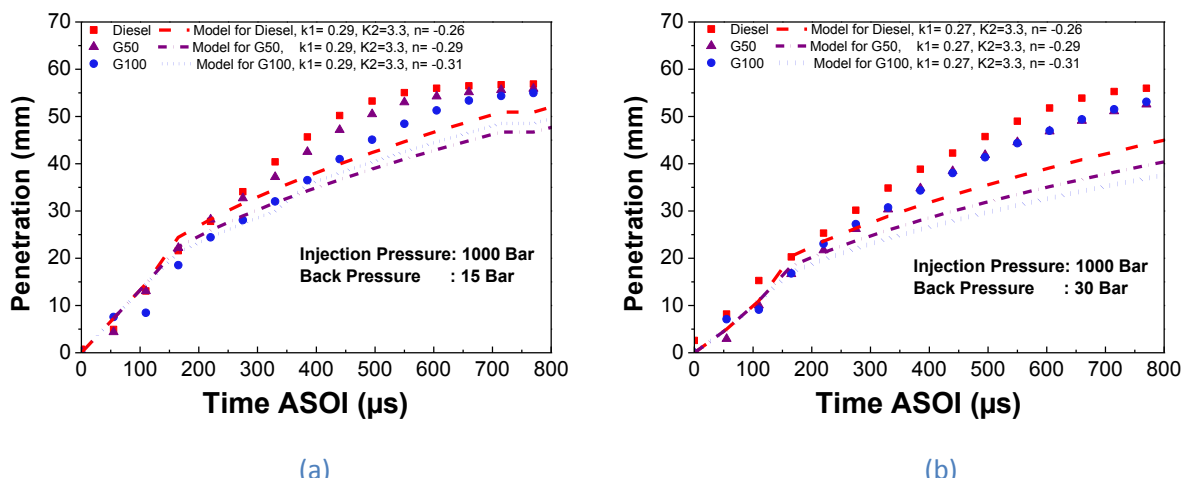


Figure 4.7 Comparison of experimental data with Naber and Siebers's model at Injection pressure of 1000 bar. (a) $P_{\text{back}}=15$ bar; (b) $P_{\text{back}}=30$ bar.

4.3. Dieseline Fuel Droplets' Size and Velocity

This section aims to investigate the atomization characteristic of dieseline spray using the PDPA technique. A comparison of dieseline to neat diesel was made in terms of fuel droplets' size and velocity. The effects of injection pressure and gasoline/diesel blending ratio on fuel droplets' size and distribution were studied.

4.3.1. Test Conditions

The tested fuels and selected injection pressure here were exactly the same as for the spray penetration test. However, instead of injecting the fuel into a pressurized vessel, this test was conducted in the open air. One reason is that the optical access window of the high pressure vessel was too small for PDPA application. Another reason is that PDPA measurement data rate in the vessel is very low, due to refraction of laser beams when they passed through the glass windows. Hiroyasu and Tabata [7, 21] have shown that fuel droplets' diameter increased with increase of ambient pressure. It can be expected that the droplets' diameter presented here would be bigger if the tests were conducted in a pressurized vessel.

As demonstrated in Figure 4.8, fuel droplets were sampled in different positions in the spray region. A scan of the whole spray for each fuel was only conducted at an injection pressure of 750 bar. For the other injection pressures, the central axes were scanned. To minimize the errors, 200 sprays were tested at each sampling position and averaged results are presented in this section.

Figure 4.9 demonstrates an example of unprocessed PDPA results for diesel spray at 1000 bar injection pressure. Valid data was obtained at 0.9 milliseconds after the injection signal and

the delay was partly caused by the delay of needle lift and partly by the jet travelling time. The velocity of droplets decreased quickly with time and the mean velocity (red dot line in Figure 4.9) was calculated out in this study with the time bin of 0.1 milliseconds. For droplets size, there was no clear indication that it changes with time. In diesel engines, combustion happens in a few milliseconds after injection starts, and thus only the droplets that measured within 3 milliseconds after the start of injection were investigated.

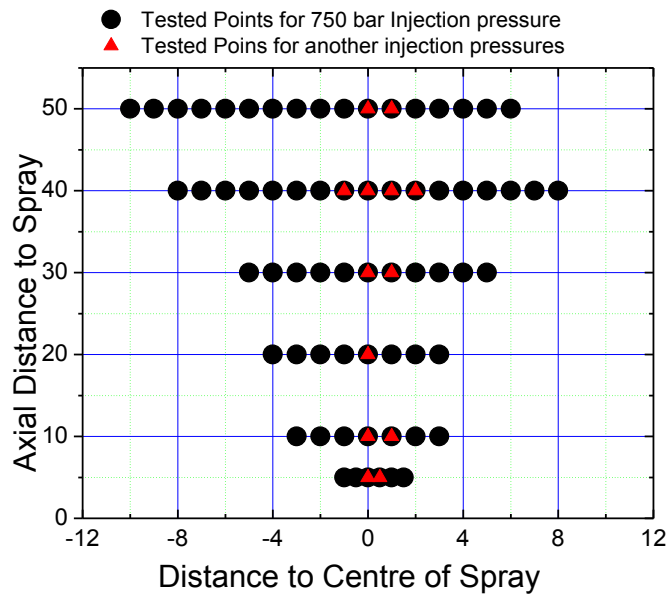


Figure 4.8 PDPA Testing positions

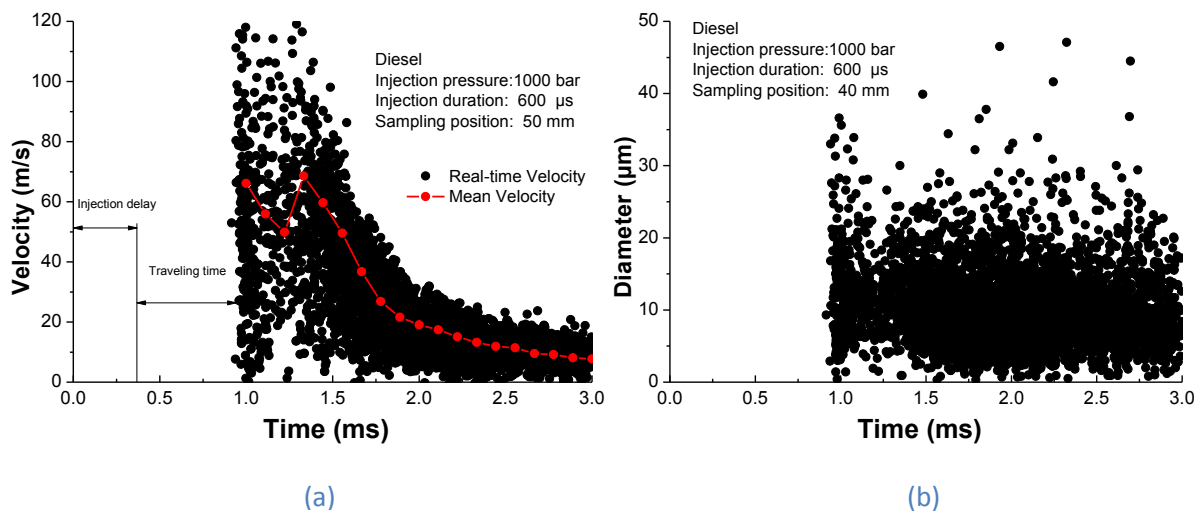


Figure 4.9 Example of unprocessed PDPA result, diesel fuel. Injection pressure: 1000 bar, sampling position: 40 mm downstream. (a) axial droplets velocity; (b) droplets diameter.

4.3.2. Effect of Gasoline/Diesel Blending Ratio

This section compares the droplets' size and velocity of different fuel blends at 40 mm downstream of the jet nozzle. The comparison between fuels at other locations is made in the following section 4.3.3.

Generally, with an increase of the gasoline/diesel blending ratio, both mean diameter and sauter mean diameter (SMD) decreased, shown in Figure 4.10. At 1000 bar injection pressure, the SMD peaked at 50% gasoline ratio and this was thought due to experiment error. SMD indicates volume/surface ratio and thus the spray evaporation quality, which has a strong effect on fuel/air mixing and combustion. Two factors may contribute to the droplets' size reduction in diesel fuel: evaporation and atomization. Gasoline, which was blended in diesel, has a higher evaporation rate than diesel at a given temperature. When travelling towards downstream, gasoline contents in diesel fuel droplets can vaporize quicker than diesel, resulting in reduced diameter. Better atomisation makes gasoline's droplets smaller than diesel. For modern high pressure common rail injection systems, spray atomization processes can be divided into two stages: primary break-up and secondary break-up. It has been reported by several researchers that the cavitation inside injector nozzles, which is caused by the rapid change of pressure, is probably the dominant mechanism for primary break-up [10-12]. As compared to diesel, gasoline has higher vapour pressure (70 kPa for gasoline and 1 kPa for diesel at 20 ° C) and is more favourable to form vapour bubble. Gasoline may have stronger cavitation than diesel inside the injector and thus better spray atomization at the injector exit. Internal flow needs to be studied to confirm this assumption. Lower viscosity of gasoline fuel may also contribute to its smaller droplets' size. During the spray secondary break-up, aerodynamic shear-generated disturbance plays a major role [13].

The fuels with lower viscosity have higher instabilities at the liquid/gas phase interface and thus better atomization [21].

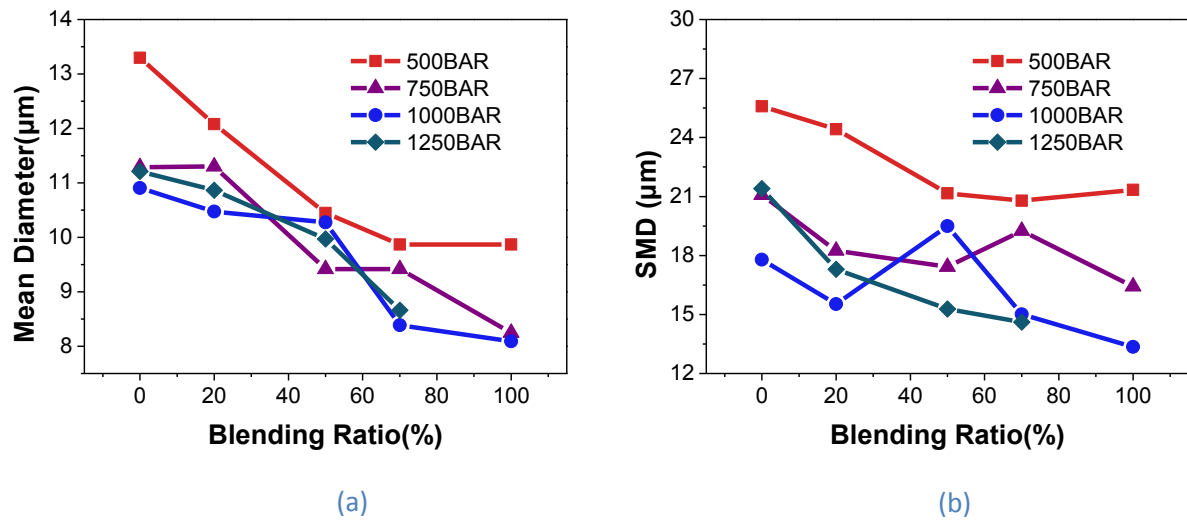


Figure 4.10 Effect of gasoline/diesel blending ratio on droplets size at sampling position 40 mm downstream of jet nozzle. (a) Mean diameter; (b) SMD

Figure 4.11 demonstrates the axial mean velocity of diesel fuel at injection pressures of 500 bar and 1000 bar. The droplets' velocity for all fuels decreased rapidly with time, which was due to the increasing amount of entrained air as injection continues. At 500 bar injection pressure, diesel fuel had quite similar droplets' velocity while the velocity of gasoline droplets were lower during the injection event. This agrees with diesel penetration results as demonstrated in section 4.3: G100 had shorter penetration length than other fuels. At 1000 bar injection pressure, no clear differences between fuels were observed.

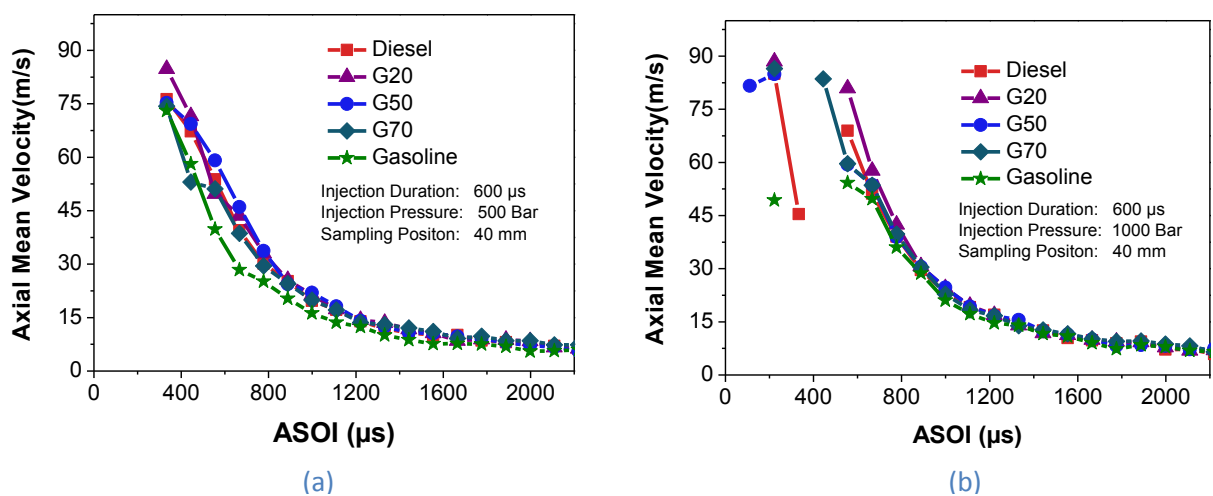


Figure 4.11 Effect of gasoline/diesel blending ratio on axial mean velocity, sampling position: 40 mm downstream of jet nozzle. (a) $P_{inj}=500$ bar; (b) $P_{inj}=1000$ bar.

4.3.3. Fuel Droplets Size and Velocity Distribution

To evaluate the atomisation quality of diesel fuel throughout the spray region, fuel droplets' size and velocity distribution were investigated. Figure 4.12 compares the droplets' size at different axial positions. It was found that the droplets' mean diameter decreased sharply when the sampling position moved from 5 mm to 10 mm downstream. This should be due to the interaction between air and liquid fuel, which would cause secondary break-up of fuel droplets. At further downstream of the jet tip, the droplets' mean diameter didn't change much. However, in terms of SMD, the droplets' size of the three fuels decreased continuously with the sampling position moving downstream. As compared to diesel and G50, the G100 droplets' size decreased much quicker, which was presumably due to its relatively high evaporation rate.

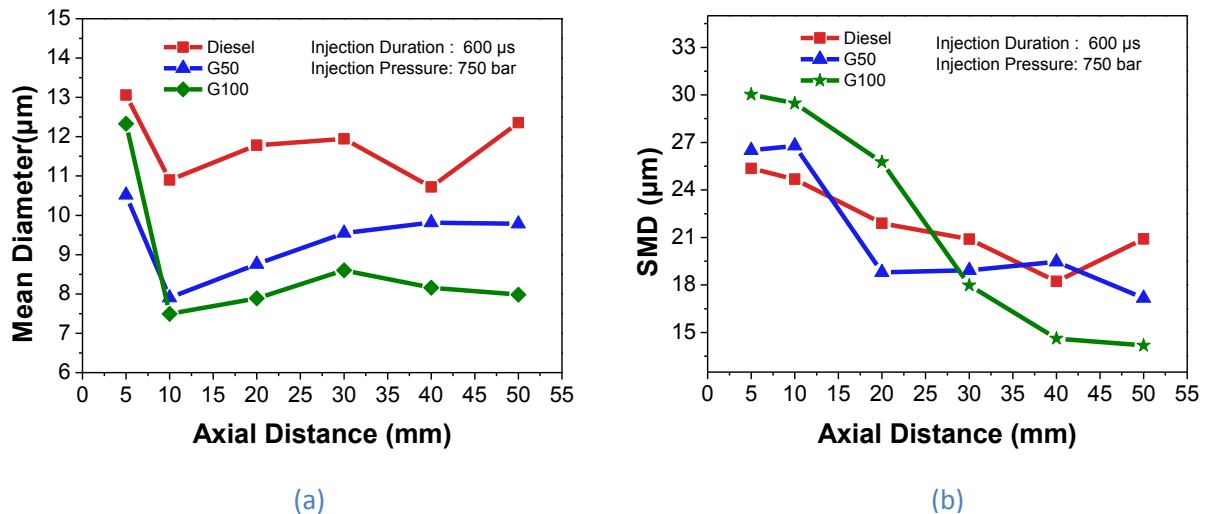
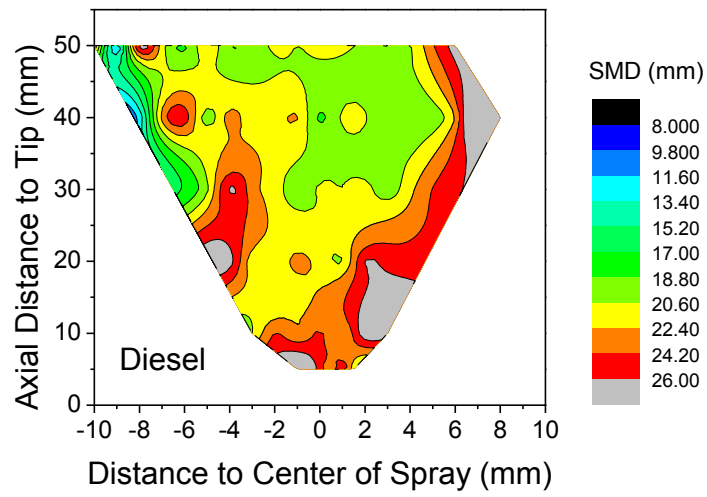


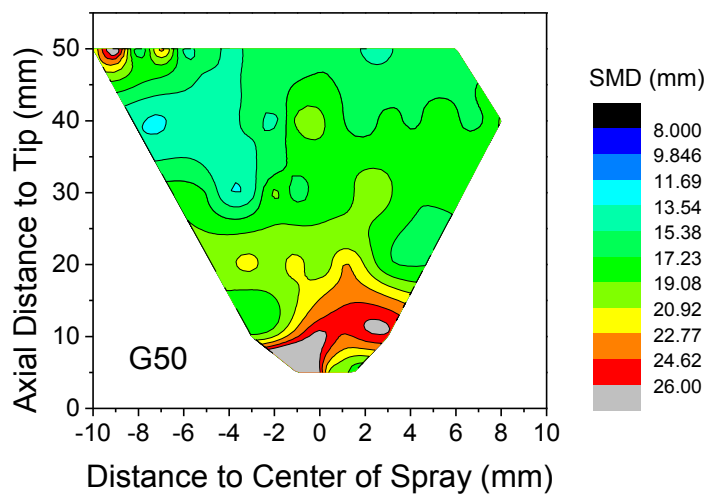
Figure 4.12 Distribution of fuel droplets along axial direction, injection pressure: 750 bar. (a) mean diameter; (b) SMD

Figure 4.13 demonstrates the droplets' size (SMD) distribution of diesel, G50 and G100 throughout the spray region. Generally, for diesel, the droplets at the periphery were larger than at the centreline, which agrees with the finding in [22]. One explanation for this is the larger droplets were brought to the periphery by the vortex motion, which was due to the relative movement of surrounding gas and droplets, at the spray tip. Different to the case of

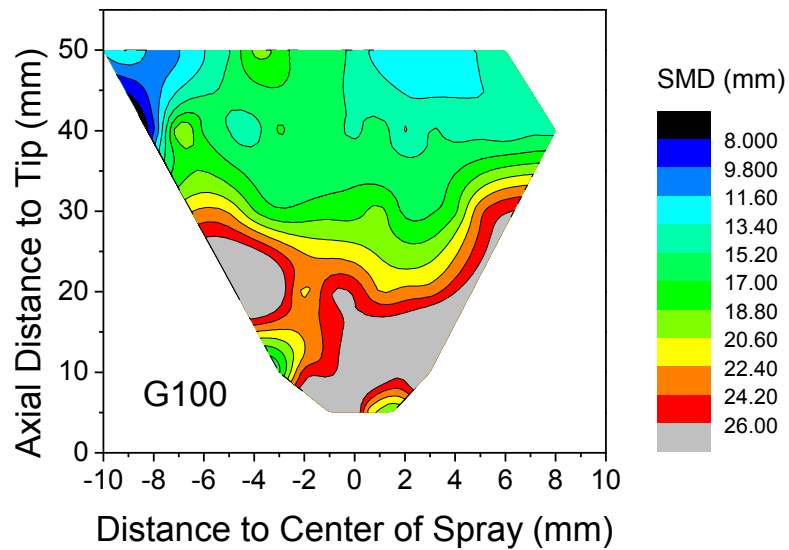
diesel, the droplets' size of G50 and G100 near the injector nozzle region, were much larger than downstream, while the centreline and periphery had similar droplets size. For G100, the droplets at the periphery had more chances to mix with air and had a higher evaporation rate than at the centreline. This could cancel the effect of spray tip vortex motion and balance the droplets' size in the radial direction. As discussed in section 4.2, G100 had shorter penetration length than diesel due to its higher volatility and lower density. As compared to upstream, droplets of G100 spray downstream were much smaller since they evaporated to the gas phase when moving away from the injector tip. It is interesting that the G100's droplets at jet upstream had smaller mean diameter (shown in Figure 4.10) but larger SMD than diesel. A possible reason is that the small gasoline droplets at upstream evaporated to gases phase quickly and only relatively large droplets were left, which brought up the SMD.



(a)



(b)



(c)

Figure 4.13 Fuel droplets size (SMD) distribution throughout the spray region at injection pressure of 750 bar. (a) Diesel ;(b) G50; (c) G100.

As shown in Figure 4.14, the fuel droplets' velocity increased at first and then decreased rapidly with time, because the initial droplets at the spray tip were decelerated by the surrounding gas. The following droplets had less contact with the surrounding gas and thus had higher velocity. As compared to downstream, the droplets' peak velocity at upstream was higher but decelerated quicker. The deceleration can be associated to the dense ambience generated in front of the droplets by the proceeding droplets, which exerts higher drag on the droplets. Also, the spray was denser near the injector nozzle and thus more collisions may occur. Similar phenomena were also found for other fuels at varied injection pressures.

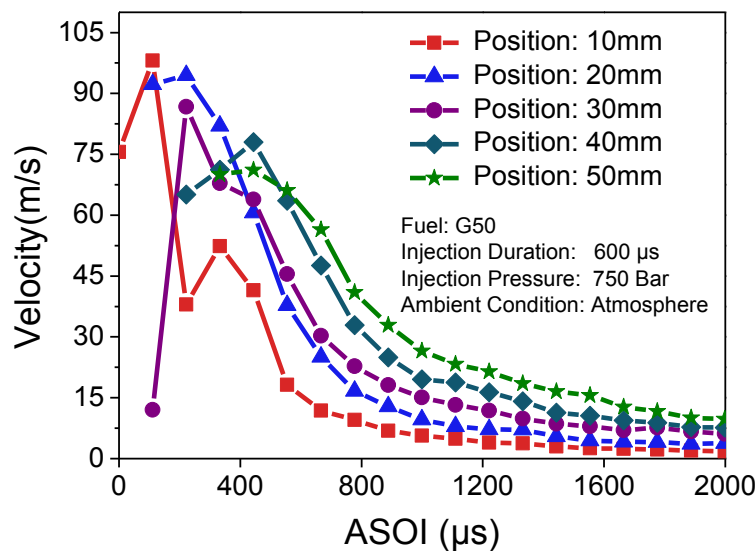


Figure 4.14 Droplets mean velocity of G50 along axial direction, injection pressure: 750 bar.

4.3.4. Effect of Injection Pressure

The effect of injection pressure on droplets' mean diameter and SMD are presented in Figure 4.15. It is shown that with increase of injection pressure, the droplets' mean diameter decreased, but just a little. For example, the diesel droplets' mean diameter decreased from 13.2 μm to 11.2 μm when injection pressure was increased from 500 bar to 1500 bar. However, in terms of SMD, the droplets' size decreased significantly as injection pressure

increased. This can be explained by Figure 4.16, which gives the cumulative ratio of the droplets' size at a sampling position of 40 mm downstream. As shown in Figure 4.16 a, the increase of injection pressure narrowed the range of droplet diameter: the portion of largest and smallest droplets decreased while the mean diameter almost kept the same. Higher injection pressure can increase the instability of liquid fuel spray and thus aerodynamic interaction, which helps secondary break-up of large droplets. It is interesting that higher injection pressure has reduced the number of small fuel droplets as well. That could be caused by the evaporation of small fuel droplets. In section 4.3.2, it was demonstrated that the droplets' diameter can also be reduced by increasing the gasoline/diesel blending ratio. Unlike increasing injection pressure, it is shown in Figure 4.16 b that increasing the gasoline/diesel blending ratio shifted the trace of cumulative ratio of the droplets' diameter towards the small size end. In this case, evaporation plays a major role, which reduced the size of both large and small droplets.

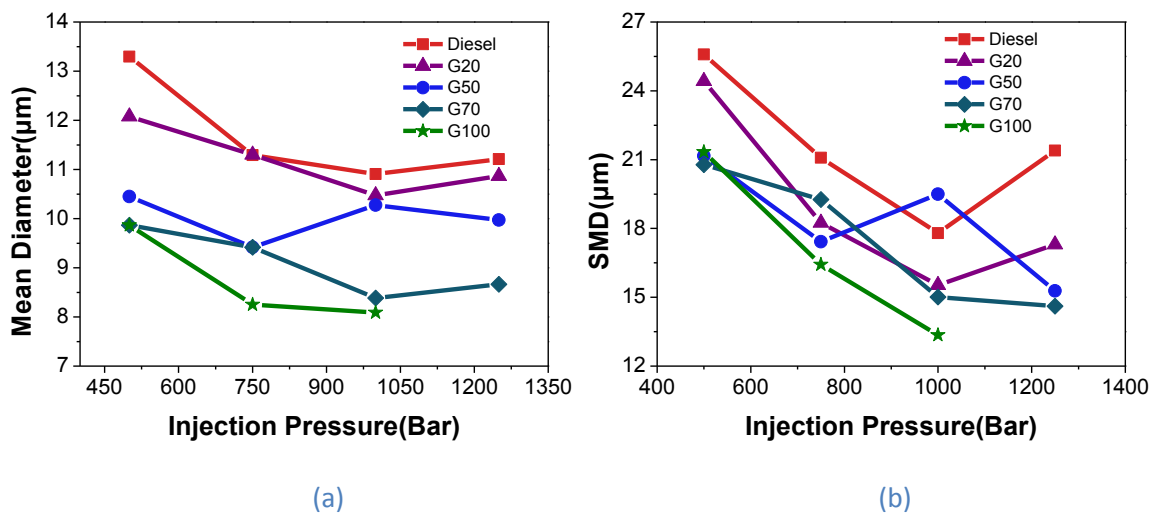


Figure 4.15 Effect of injection pressure on droplets size, sampling position: 40 mm downstream. (a) Mean diameter; (b) SMD.

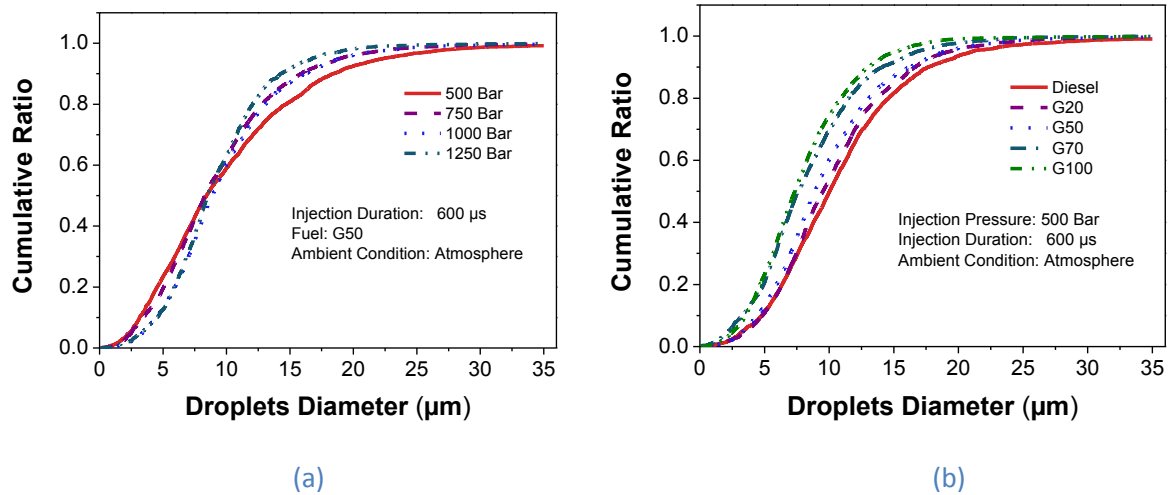


Figure 4.16 Cumulative ratio against droplets diameter, sampling position: 40 mm downstream. (a) Varied injection pressure, fuel G50; (b) varied gasoline blending ratio, $P_{inj} = 500$ bar.

4.4. Conclusions

The macroscopic and microscopic characteristics of dieseline spray have been studied in this section. The effect of the gasoline/diesel blending ratio, injection pressure and back pressure on spray tip penetration length were investigated. To evaluate the atomisation quality of dieseline spray, the fuel droplets' size and velocity were measured under atmospheric conditions using PDPA techniques. Fuel droplets and size distribution throughout the spray were also studied. The conclusions drawn from experimental results are as below:

1. At 15 bar back pressure, gasoline (G100) has a shorter penetration length than diesel due to the vaporization while the difference between G70, G50, G20 and diesel are small. It seems that a small quantity of diesel in the gasoline fuel can modify the spray penetration length and the lower volatility of diesel results in this. At 30 bar back pressure, penetration length of gasoline (G100) is similar to diesel,
2. As compared to diesel, the penetration length of gasoline (G100) is less sensitive to the change of back pressure. Higher back pressure resulted in less gasoline

vaporization but more drag force. The two effects seems to cancel each other out and thus cause little change of gasoline's penetration length in the downstream,

3. With an increase of the gasoline/diesel blending ratio, the mean diameter and SMD of the fuel droplets are decreased downstream of the injector nozzle. Fuel droplets of G70, G50, G20 and diesel have similar axial velocity while gasoline droplets have slightly lower axial velocity,
4. For all tested fuels, higher injection pressure improves the atomisation: the SMD was reduced by 7 to 10 mm as injection pressure increased from 500 bar to 1000 bar; the mean diameter was decreased as well but much less significantly than SMD,
5. For diesel, the droplets at the spray periphery are larger than at the centreline. For G50 and gasoline (G100), relatively large droplets appeared near the jet nozzle region and the diameter is significantly reduced downstream. As the sampling position moves towards downstream, axial initial velocity of G50 droplets decreases and the final velocity increases.

CHAPTER 5

CONVENTIONAL DIESEL LINE COMBUSTION

This chapter addresses the combustion characteristics of baseline diesel engine. In particular, different gasoline/diesel blends were tested using same control strategy, with engine loads ranging from 1.38 bar BMEP to 7.85 bar BMEP. The engine was also operated with optimised combustion phase without EGR and a comparison of diesel and G50 was conducted. Finally, the effect of pilot injection on combustion and emissions of G50 was investigated.

5.1. Dieseline Combustion Using Conventional Engine Strategies

The test engine used here was originally calibrated to meet Euro 4 emission regulations (Regulation No 715/2007, amended by 692/6008 and 595/2009). The strategy was to reduce NO_x emission inside the cylinder and handle smoke with diesel particle filter (DPF). A diesel oxidization catalyst (DOC) was also equipped to eliminate HC and CO emissions. To reduce NO_x from combustion, high levels of EGR was applied at low loads and combustion phase was retarded at high loads, which are shown in Figure 5.1. Dieseline was tested in the engine following this strategy.

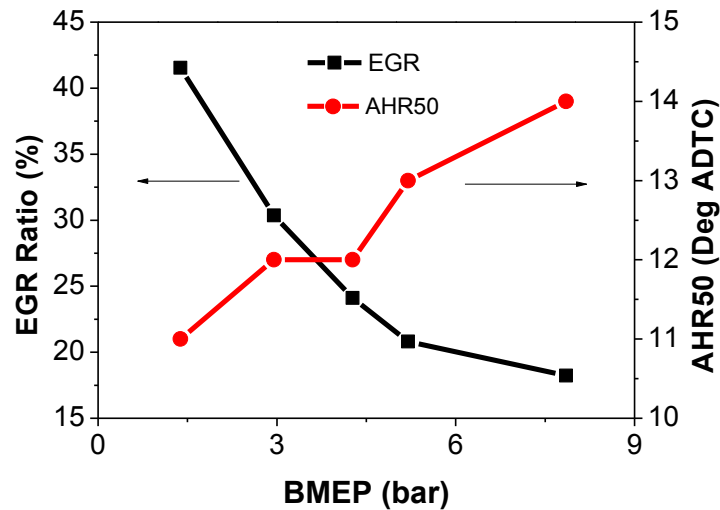


Figure 5.1 EGR ratio and AHR50 with engine operated from 1.27 bar to 7.85 bar BMEP

5.1.1. Studied Fuels and Methods

Three types of blends were used in the experiments, namely: neat diesel (G0), 20% (G20) and 50% (G50) gasoline blended with diesel by volume. The neat diesel was the European standard diesel (EN590) and the blended gasoline was 95 octane gasoline (ULG95) with sufficient lubricity additive. The cetane number of the blended fuels were taken as proportionate to their blending ratio and the cetane number of gasoline was assumed to be 15 [103]. Some of the fuel properties are listed in Table 3.2, Chapter 3. The boiling point of diesel ranges from 160 to 340 °C, while the boiling point of gasoline ranges from 40 to 160 °C. Blended fuels were expected to have wide boiling ranges and the detailed data were presented by Weall and Collings [103].

Five engine operating conditions were selected from the original engine calibration map which was transformed from respective operation points of the New European Driving Cycle (NEDC) at the studied engine speed. The engine speed was fixed at 1800 rpm and the loads were 1.38, 2.95, 4.3, 5.2 and 7.85 bar BMEP. The fluctuations of the engine speed was below ± 10 rpm and it was ± 0.02 bar BMEP for the load. During the tests, the base diesel was firstly

tested for the original calibration strategy (with a quantity of $1.5 \text{ mm}^3/\text{cycle}$ pilot injection starting at around 20 CAD before top dead centre (BTDC)). The single injection diesel, G20 and G50 tests were carried out with their EGR ratio and AHR50 adjusted to be the same to the baseline diesel (by changing the injection timing), which are shown in Figure 5.1. Adjusting AHR50 of diesel combustion to be the same as diesel baseline is critical in this study. Muether et al. [120] observed that for premixed combustion, the effect of fuel properties, particularly on thermal efficiency and noise, can be distinguished by maintaining a constant centre of combustion (AHR50) when testing different fuels.

5.1.2. Heat Release Rate Analysis

The in-cylinder pressure, heat release rate and injection signals (from the engine control unit (ECU)) of the single injection diesel and G50 at three engine loads are plotted versus CAD in Figure 5.2. From the spray test results reported in Chapter 4, a 0.3 ms delay (3.2 CAD at a speed of 1800 rpm) between injection signal and actual injection event was observed. Thus, the actual injection event may be a few crank angles latter than that presented. At the low load of 1.38 bar BMEP, the start of high temperature heat release for both diesel and G50 blend were after the end of the fuel injection event. This indicates that the engine combustion was in partially-premixed compression ignition (PPCI) mode. Two factors contributed to the separation between fuel injection and start of combustion at low load: usage of 42% EGR and short injection duration. Figure 5.2 (a) shows that G50 blend has lower heat release rate peak compared to diesel fuel. G50, with a longer combustion delay (shown in Figure 5.3) has more time to mix with air. When the global mixture strength is lean, as is the case at this low load condition (air excess ratio was 2.2), more locally burning mixture packets will be near the global mixture strength and hence lean. This will increase the combustion duration and reduce pressure rise rate which will be shown later. The lower boiling range and cooling factor of

gasoline in diesel may also play a role in reducing G50 peak heat release at 1.38 bar BMEP engine load (gasoline enthalpy of vaporization is 305 kJ/kg and it is 270 kJ/kg for diesel).

As shown in Figure 5.2 (b), the end of injection for diesel and G50 were closer to the start of combustion at the medium load of 4.3 bar BMEP as compared to 1.38 bar BMEP. The heat release rate curves for both diesel and G50 show a single peak and they nearly coincide. As the engine load increased to 7.85 bar BMEP, it was observed in Figure 5.2 (c) that diesel combustion process was partially overlapped with the fuel injection event, thus indicating long combustion duration and a low heat release peak. In contrast to diesel, injection event of G50 was separated from the combustion process and a relatively high heat release rate peak appeared. That was supposedly because a higher fraction of the local air/G50 mixture packets was close to the global equivalence ratio ($\lambda = 1.28$), which was nearly stoichiometric, due to the improved mixing. Similar trend were also observed by Kalghatgi et al. [81]: at 4 bar IMEP, gasoline had lower heat release peak than n-heptane (whose cetane number is very close to diesel); however, at 10 bar IMEP, heat release peak of the former was much higher than that of diesel (CN56) [81].

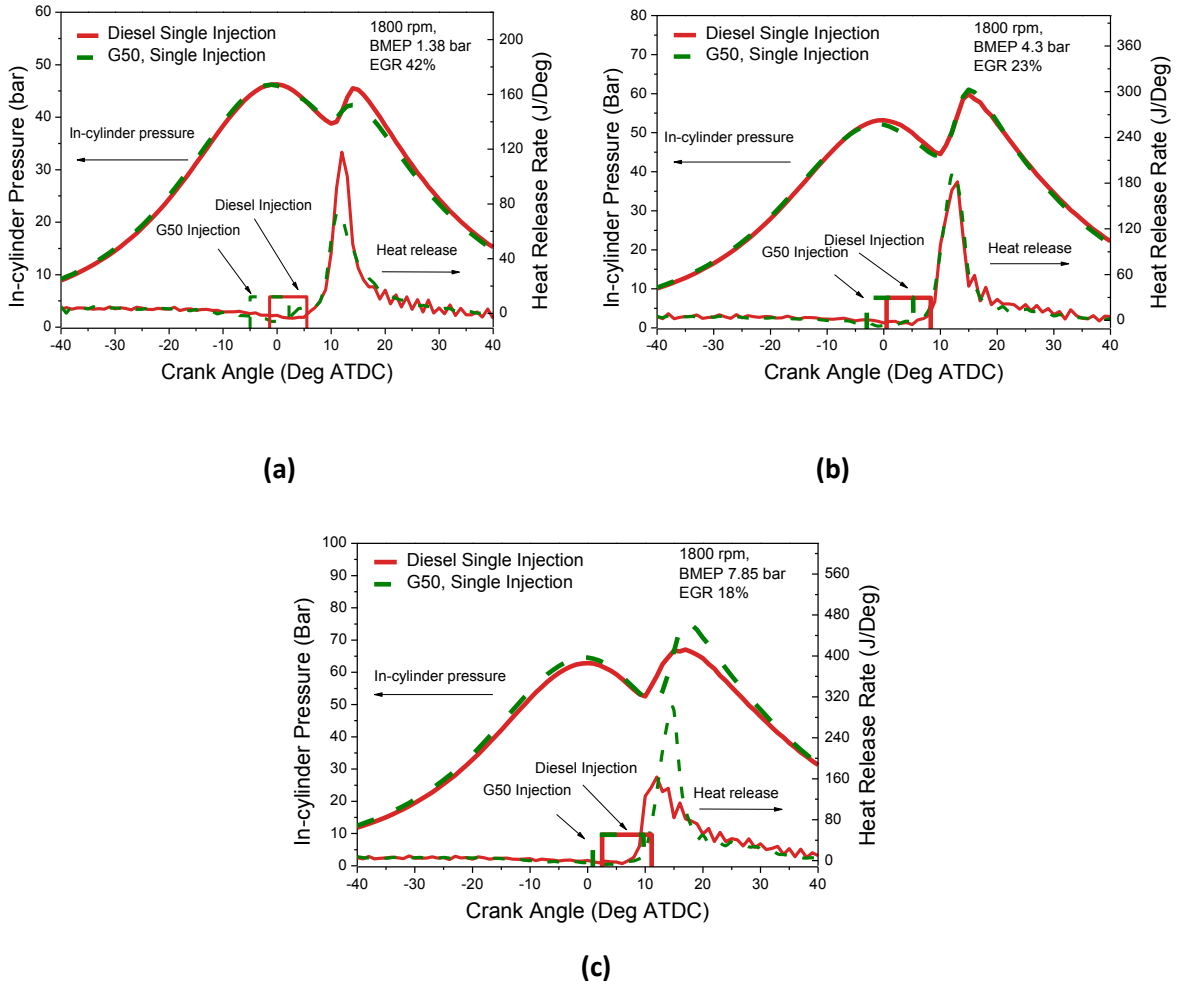


Figure 5.2 In-cylinder pressure and heat release rate of the single injection diesel and G50 versus crank angle: (a) 1.38 bar BMEP, (b) 4.3 bar BMEP, (c) 7.85 bar BMEP.

5.1.3. Combustion Performance

Combustion delay, defined as the crank angle difference between the start of injection and AHR50, are presented in Figure 5.3 for different diesel/gasoline blends as the BMEP was varied. It was shown by Kalghatgi et al. [81, 85] that combustion delay is a good parameter for understanding the fuel effects on combustion performance of compression ignition engines. Longer combustion delay means more fuel is premixed with air at the time of combustion. Figure 5.3a shows that combustion delay increased with higher gasoline ratio in the blend. At the lowest load, the combustion delay for G50 was 5 CA degrees longer than the single

injection diesel fuel. The reason is that gasoline is much more resistant to auto ignition and dieseline has lower cetane number than diesel. As the load increased, the combustion delay of both the neat diesel and dieseline decreased since the EGR ratio decreased (shown in Figure 5.1). Another possible reason for this is the cylinder wall became much hotter with the increase of engine load and thus assisted to fuel auto-ignition. At the highest load tested, the difference of combustion delay between neat diesel and G50 became much smaller (by around 2 CAD). For the diesel fuel with a pilot injection, the pilot combustion heated up the in-cylinder charge before the main injection occurred and the combustion delay was lower than for the single injection case. The coefficient of variations (COV) of IMEP for G50 at the load conditions of 1.38 and 2.95 bar BMEP were high (around 5%), shown in Figure 5.3 b. The relatively longer combustion delay of G50 was expected to be responsible for its high IMEP variation: long combustion delay can weaken the link between injection and combustion and thus may cause instability of combustion phase. However, as the engine load increased and the combustion delay reduced, the COV of G50 fell below 2.2%, which was marginally higher than base diesel (1.5%).

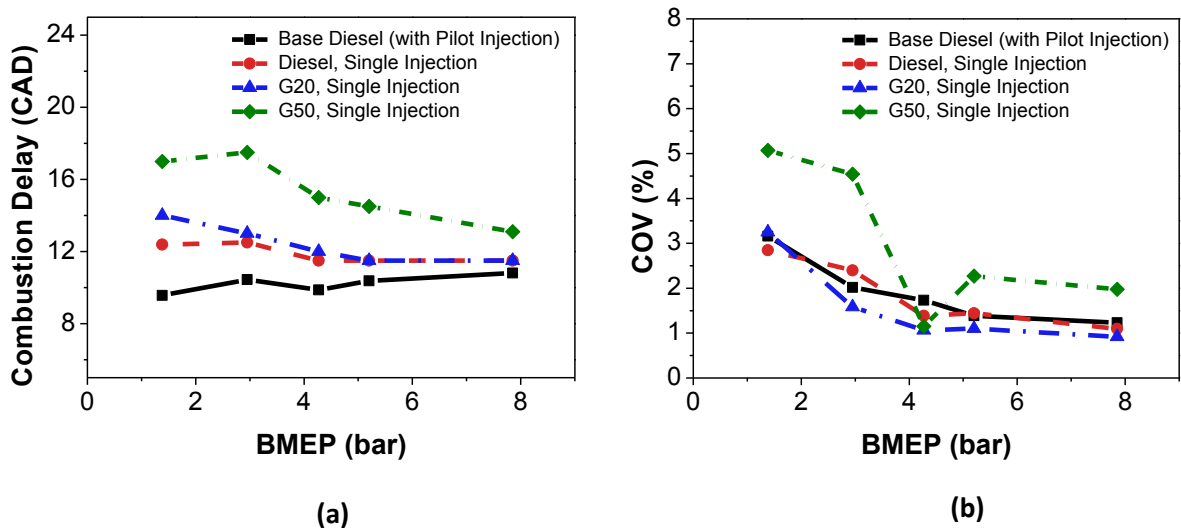


Figure 5.3 Combustion performances of base diesel, single injection diesel, G20 and G50 at different engine load. (a) Combustion delay; (b) COV of BMEP

The combustion durations, defined as crank angle differences between start of combustion (when the heat release rate goes up from a negative value to a positive value [25]) and 95% mass fraction burn (MFB 95) for different fuels, are presented in Figure 5.4. G50 case had longer combustion duration at low loads and shorter combustion duration at medium loads compared to diesel. G50 was better premixed with air compared with diesel at all tested loads because of its confirmed longer combustion delay as shown in Figure 5.3. The trend of combustion duration of G50 at low and medium loads can be explained as follows: at lower loads, the longer ignition delay of G50 led to some local mixture packets that were over-lean before combustion started. Hence, the burning rate was lower and combustion duration was longer than diesel. At medium loads, the local air/G50 mixture packets were expected to be closer to stoichiometric condition (overall equivalence ratio ~ 1.28) and have a high burning rate and short combustion duration. Unlike G50, it was observed that G20 had slightly shorter combustion duration than diesel at all the tested loads.

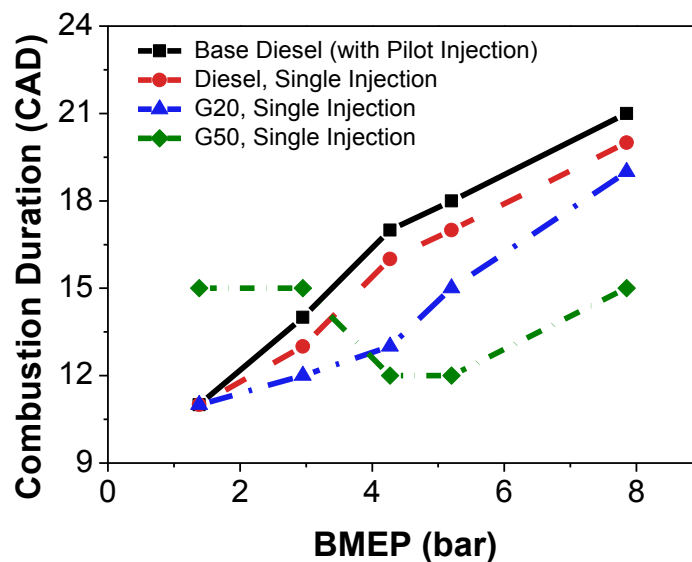


Figure 5.4 The combustion duration of base diesel, single injection diesel, G20 and G50 versus BMEP

The maximum pressure rise rate (MPRR), which can induce combustion noise, is presented in Figure 5.5. The MPRR of the base diesel with a pilot injection was maintained at low levels as the load increased because the pilot injection shortened the combustion delay and reduced

the premixed combustion and subsequently reduced the burning rate. This is in contrast to the case of single injection of diesel fuel where the MPRR climbed to a high level at medium engine loads. MPRR of G50, as compared to diesel with single injection, presented different trends at low and high loads. It can be seen from Figure 5.5 that G50 combustion was quieter than diesel at low loads. As BMEP was increased to higher values (>4.3 bar), the MPRR of G50 was much higher than that of diesel. There are two factors that can affect pressure rise rate at a given engine condition: one is combustion phasing and the other is burning rate [24]. Since combustion phasing was fixed for all the fuels, the different burning rate of diesel and dieseline was expected to cause their differences on MPRR. Similar to the explanation given for Figure 5.4, leaner local air/fuel mixture resulted in lower burning rate of G50 than diesel at low loads. At higher loads, the burning rate of G50 was higher than diesel and the MPRR is high. For automotive engines, a high MPRR is not favorable because of the noise. Reduction of MPRR at high loads can be achieved by using higher percentage of EGR and multiple injections which distribute air/fuel mixture in long durations and shape the heat release curve [79].

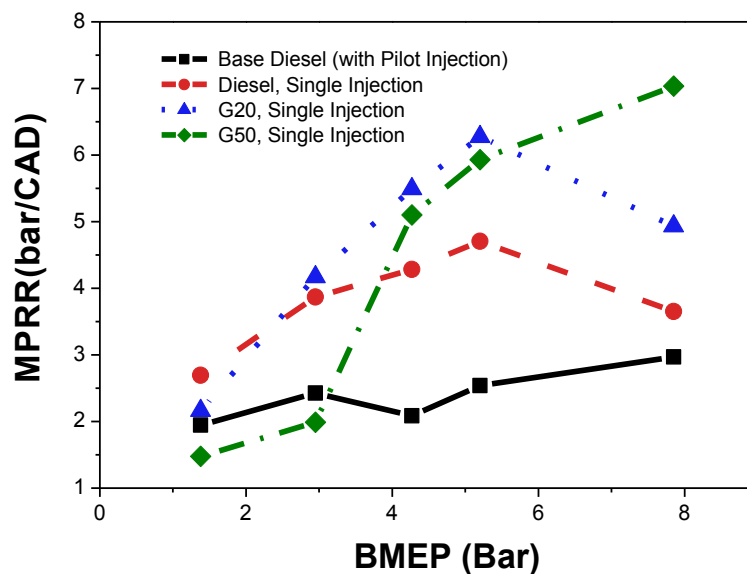


Figure 5.5 The MPRR of base diesel, single injection diesel, G20 and G50 versus BMEP

Figure 5.6 shows that the brake thermal efficiency (BTE) of all fuels increased with increase of engine loads. At 1.38 BMEP, G50's BTE was two percent lower than diesel whereas in the case of lower gasoline content G20, it was similar to diesel under varied loads. As shown in Figure 5.6, the combustion efficiency of single injection diesel was 98.1% while G50 had much lower combustion efficiency 93.8%. The incomplete combustion of G50, probably caused by over-mixing of some G50/air mixture packets, can be the reason for its low combustion efficiency and thus low BTE. Advancing the combustion phase and reducing EGR ratio, which will be discussed in section 5.3, can increase G50's BTE. Figure 5.6 shows that, with engine loads increased, the differences of combustion efficiency between G50 and diesel became substantially small and G50's BTE was close to that of diesel when BMEP was higher than 2.95 bar.

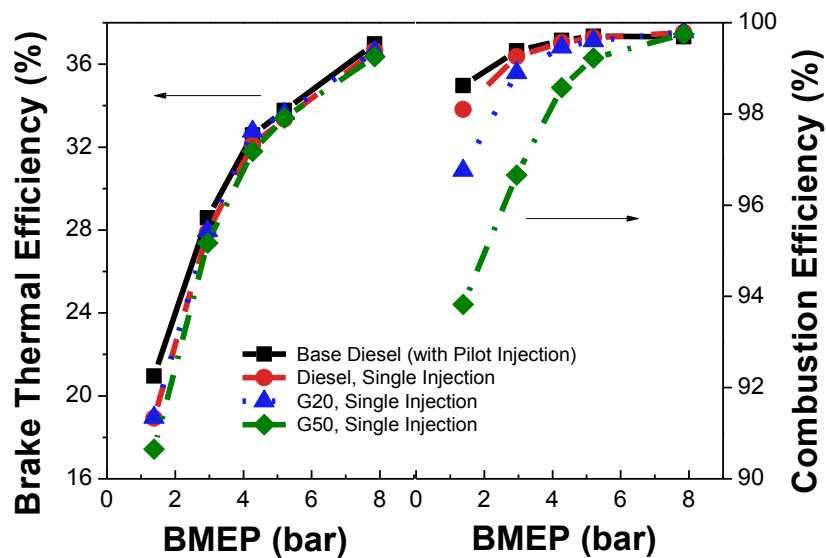


Figure 5.6 The brake thermal efficiency and combustion efficiency of base diesel, the single injection diesel, G20 and G50 versus BMEP

5.1.4. Regulated Emissions

Figure 5.7 presents four types of emissions of neat diesel and dieseline, including smoke, NO_x , HC and CO. The single injection produced low smoke (below FSN 0.5) up to 5.2 bar BMEP compared to the case of diesel baseline. Smoke emissions of the single injection diesel and G20 climbed sharply, similar to the base diesel, as the load was increased to 7.8 bar BMEP, while G50 maintained its low smoke emission. This can be explained by the fact that at lower loads, start of combustion for all three fuels began after the end of injection which resulted from the relatively high EGR ratio and short injection duration associated with lower in-cylinder temperature. Soot formation is favored in a fuel-rich (equivalence ratio above 2) and high temperature environment (temperature above 1300 K) [25]. The separation of injection and combustion in the case of PPCI, as in this study, improved the local air/fuel mixture and reduced the smoke emission. At higher loads, the ignition delays of diesel and G20 were not long enough to separate the start of combustion from injection while for G50 this separation was achievable which can explain low smoke of the G50 (below FSN 0.5). This explanation is supported by the findings in the literature [78-83].

G50 had wider boiling range and longer combustion delay than neat diesel. Longer combustion delay results in longer mixing time, thus reduces soot emissions. It is possibly that the lower volatility of G50 also contributed to soot reduction as reported here. Kalghatgi *et al.* [81, 83] found that the fuel volatility was not important for smokeless combustion if the fuel cetane number was sufficiently low. They investigated low cetane number (CN) diesel (CN 24, similar boiling range to diesel, 75% aromatic) in a single cylinder research diesel engine and found that it produces low smoke emission similar to RON 84 gasoline [81, 83]. The spray test results reported in Chapter 4 have shown that, as compared to diesel, dieseline fuel had slightly shorter penetration length and better atomization, most probably due to

evaporation. Matsuoka et al. [18] observed that the fuel volatility and spray characteristics can also effect the smoke emission. He used LIEF (Laser Induced Exciplex Fluorescence) techniques to analyze spray vapour-liquid separation of commercial diesel and light diesel (similar physical properties to gasoline: lower kinematic viscosity, density and boiling points) under a simulated engine condition (50 MPa, 873 K). It was found that, as compared to commercial diesel, shorter liquid penetration of light diesel reduced fuel impingement on the piston bowl and thus reduced smoke emission [18]. It was also found that higher volatility of light diesel helped to reduce smoke: the dense mixture with equivalence ratios more than 2 reduced quickly after the end of injection [18].

NO_x emissions, Figure 5.7, showed similar trends as pressure rise rates, Figures 5.5, when the load was swept from low to medium. At low loads of up to 4.3 bar BMEP, G50 produced less NO_x than diesel while the trend reversed at higher loads. At low loads, large amount of EGR was used and fuel injection event was completely separated from combustion, which indicated the engine was operated in PPCI mode. According to [121], for PPCI combustion, NO_x is likely formed throughout the jet cross section instead of jet periphery. Thus the mixing strength inside fuel jet may strongly affect NO_x formation. As introduced in Chapter 2, Figure 2.5, both over-lean and over-rich mixture can result in low NO_x emissions. Compared to diesel, G50 was much better premixed with air and some over-lean mixture packets may form inside fuel jet. Excess air for G50 inside spray jet may reduce the combustion temperature and reduced the NO_x formation. At higher loads, for diesel, the combustion was dominated by diffusive flame propagation, which is evident by its heat release rate shown in Figure 5.2. In this case, NO_x was mainly formed in jet periphery and strongly affected by in-cylinder temperature [25]. For G50, there was higher portion of premixed combustion, which was volumetric ignition rather than flame propagation. The volumetric ignition can warm up the ambient air quickly and thus may increase G50's NO_x formation during its diffusive

combustion process. Additionally, premixed combustion of G50 may also be a resource of NO_x and made G50 to have higher NO_x than diesel.

Regarding hydrocarbon and carbon monoxide emissions of diesel fuels, they were much higher than that of diesel at low loads. However, as the load was increased, they became close to that of base diesel. The high concentrations of hydrocarbon emissions for diesel at low loads were supposed to be caused by the higher portion of local mixture packets being over-lean which resulted in incomplete combustion. This can be mitigated to some extent by reducing the injection pressure [82]. Increased engine load reduced the excess air and shortened the combustion delay, shown in Figure 5.3, which made local burning mixtures closer to stoichiometric condition and thus increased bulk gas temperature, resulting in lower HC and CO emissions.

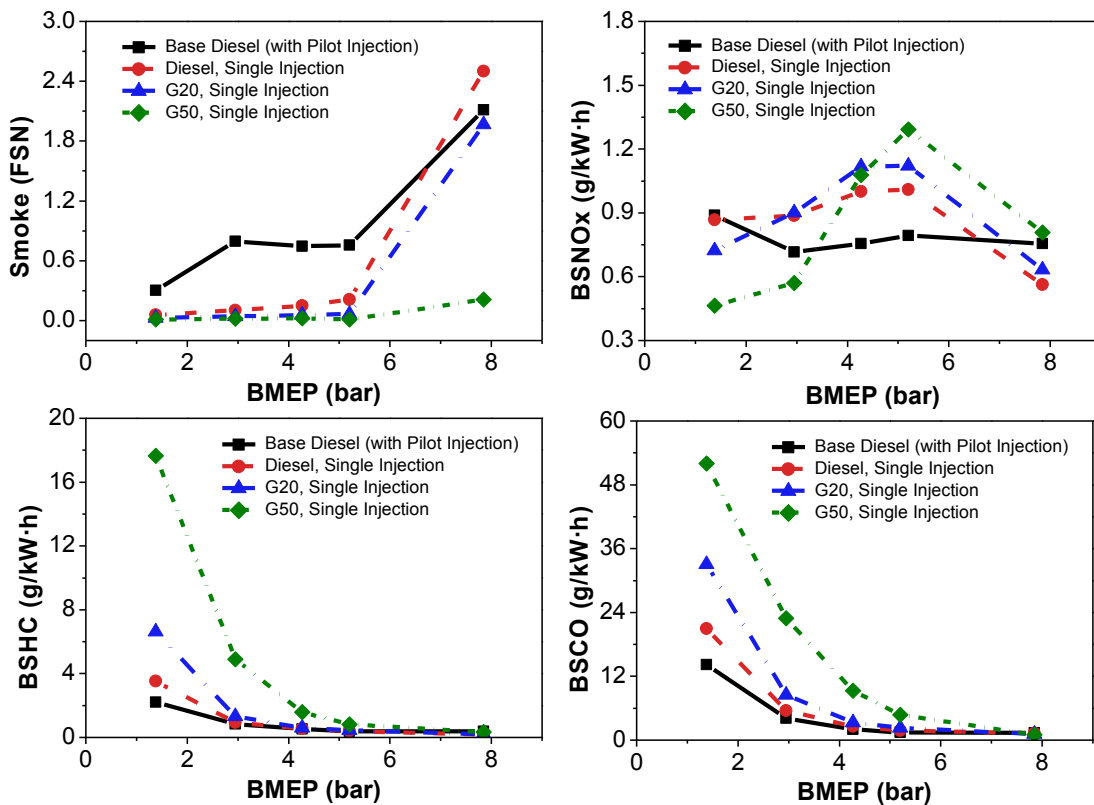


Figure 5.7 Smoke, BSNO_x, BSHC and BSCO emissions of the base diesel, single injection diesel, G20 and G50 versus BMEP

5.1.5. Particle Number

To investigate the effect of gasoline mixing with diesel on PM emission characteristics, particle number and size distribution were measured with DMS500 and investigated in this section.

Figure 5.8 represents the particle number (PN) concentrations of diesel and dieseline in terms of stacked bars. Each bar represents the total PN emissions from a particular measurement and these bars are divided into the nucleation and accumulation modes respectively, going from top to bottom. Up to 5.2 bar BMEP, the total particle number of single injection diesel was reduced by around 70-40% compared to the case of diesel baseline. The reduction in accumulation mode particles was much more significant than in nucleation mode particles. Single injection had longer combustion delay and more entrained air inside the fuel jet when combustion began than diesel baseline. Thus the local equivalence ratio of single injection was lower and less carbonaceous particles were formed during the fuel-rich premixed combustion process. On the other hand, some fuel droplets might have escaped from the high temperature zone of combustion and formed organic particles (nucleation mode particles) as a result of increased premixed combustion proportion. The effect of pilot injection on G50 combustion will be studied in later section 5.3 of this chapter. At medium load of 7.85 bar BMEP, the total particles number was similar to the case of base diesel and single injection diesel, where particles were dominated by accumulation mode.

As shown in Figure 5.8, increased portion of gasoline in diesel reduced the particle number total concentration dramatically. Compared to base diesel, G50 produced 90% less particles in terms of number up to 5.2 bar BMEP load and the reduction was approximately 50% at higher load of 7.85 bar BMEP. The improved premixed combustion of G50, which was caused by its

high volatility and low cetane number, is expected to be mainly responsible for the particulate number reduction [18, 83]. More detailed particle size and number distribution of different fuels at varied engine loads are presented in Figure 5.9.

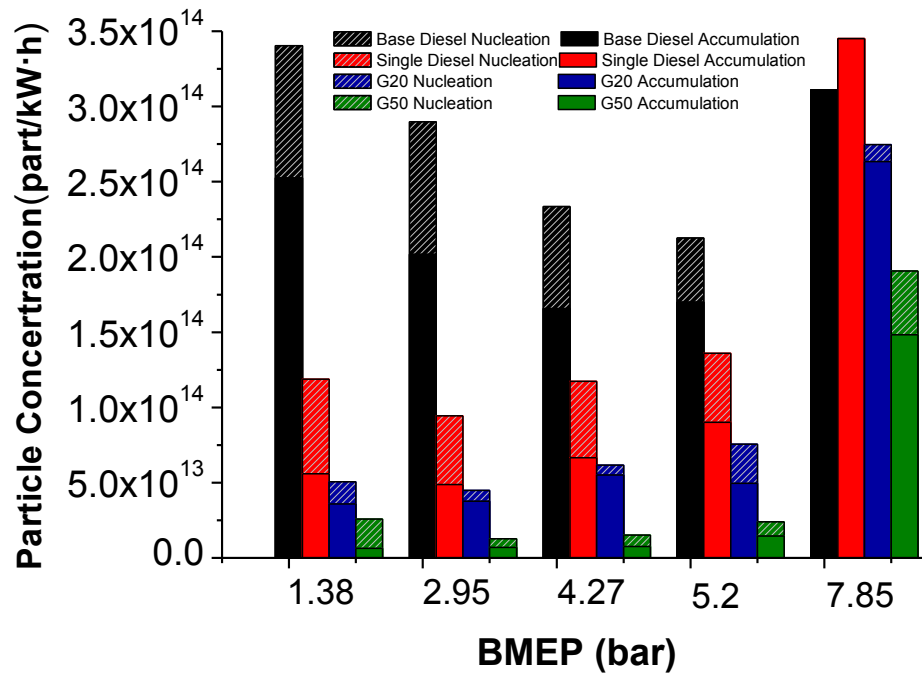


Figure 5.8 Brake specific particle number total concentration of the base diesel, the single injection diesel, G20 and G50 versus BMEP

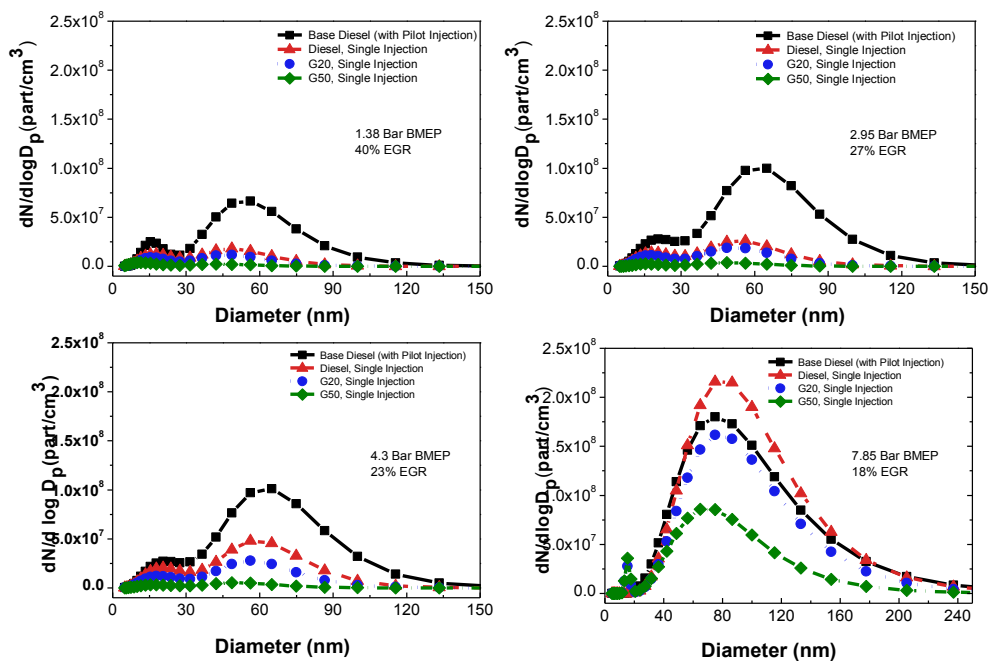


Figure 5.9 The particulate number and size distribution of the base diesel, the single injection diesel, G20 and G50

Figure 5.10 shows that the particulate count median diameter (CMD) of base diesel was increased from 46 to 75 nm as the engine load was increased from 1.38 to 7.85 bar BMEP. The increase of particulate size was supposed due to the reduced portion of well-premixed fuel/air packets, resulting from the reduced combustion delay and increased overlap between fuel injection and combustion, shown in Figures 5.2 and 5.3 respectively. Single injection diesel and G20 had similar particulate CMD which varied from 23 to 73 nm, depending on load. This is probably because they have quite similar combustion delay as shown in Figure 5.2. For G50, the particulate CMD was increased from 14 to 61 nm as the engine load increased from 1.38 to 7.85 bar BMEP. In contrast to the case of diesel, the particulate CMD of G50 was reduced by 20% to 50%, corresponding to the medium and low loads.

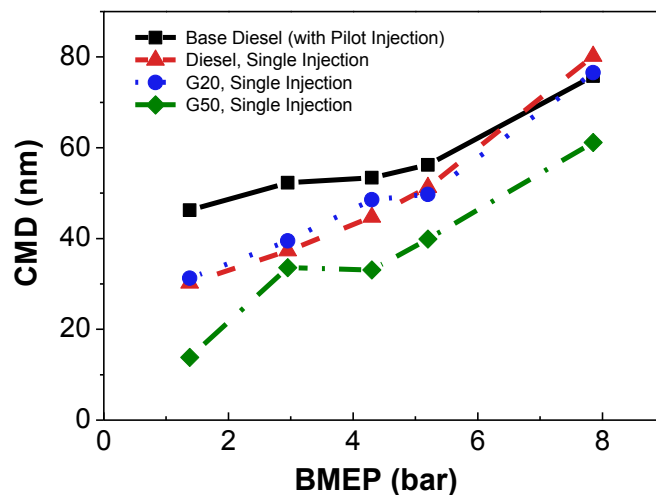


Figure 5.10 Particle count median diameter (CMD) of the base diesel, the single injection diesel, G20 and G50 versus BMEP

5.2. Effect of Engine Conditions

In the previous section, the combustion performance and emissions of diesel and dieseline were compared at varied loads with combustion phase and EGR ratio adjusted to the same as for the original calibration of diesel baseline. It was found that, at low loads, G50 had lower combustion efficiency and MPRR than diesel. At medium loads, the combustion of G50 was

much more rapid than diesel, resulting in high MPRR and high NO_x emissions. For the engine's original calibration, EGR ratio was reduced as engine loads increased. Thus it is not sure whether the different trends of G50 at low and medium loads were caused by changed EGR ratio or changed engine loads. In this section, diesel and G50 were compared with EGR ratio set to zero. The combustion phasing (AHR50) of diesel and G50 were adjusted to achieve the best fuel economy with the maximum pressure rise rate (MPRR) limited under 10 bar/deg for safety concern. The injection pressure was fixed at 500 bar and the engine was operated at three loads: 2 bar, 3 bar and 4.3 bar BMEP.

Figure 5.11 compares the in-cylinder pressure and heat release rate of diesel and G50 at 2 bar and 4.3 bar BMEP. The results show a similar phenomenon to that demonstrated in Section 5.2: at 2 bar BMEP, G50 had lower heat release rate peak and lower MPRR than diesel while the trend reversed at 4.3 bar BMEP. This indicates that the different trends of G50 at low and medium loads were at least dependent on engine operating conditions. EGR ratio may also have applied an effect. Table 5.1 presents that the combustion delay of G50 were around 3 crank angle degrees longer than that of diesel, both at 2 bar and 4.3 bar BMEP. Thus the mixture strength of G50 should be quite similar at these two loads and the over-mixing and under-mixing argument, discussed in Section 5.2, is not suitable here. Two explanations of G50's different trend at low and medium loads are proposed: one is that with increase of engine load for G50, the in-cylinder temperature increased, resulting in higher flame speed of gasoline, which was blended in the diesel fuel; on the other hand, higher engine load means larger quantity of diesel was injected into the cylinder that provided more ignition points for gasoline, which probably increased the burning rate of gasoline. More detailed optical diagnostics will help to check the proposed assumptions in the future work.

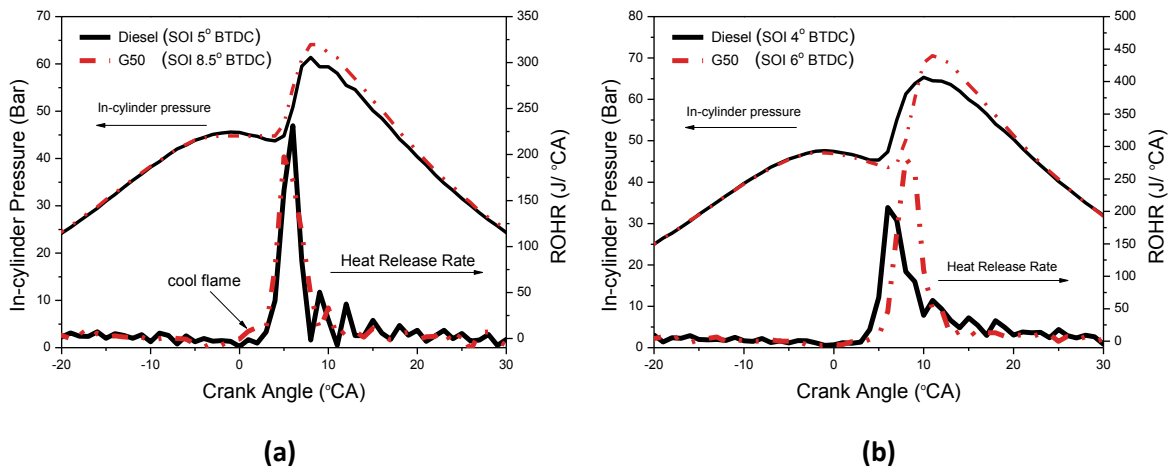


Figure 5.11 In-cylinder pressure and heat release rate of the single injection diesel and G50 versus crank angle: (a) 2 bar BMEP, (b) 4.3 bar BMEP

Table 5.1 and 5.2 listed the combustion performance and emission results of diesel and G50 at 2 bar, 3 bar and 4.3 bar BMEP. It is shown that G50 had similar indicated efficiency and brake thermal efficiency as diesel. At 2 bar BMEP, the combustion efficiency of G50 at 95.6% was lower than that of diesel at 98.9%. That was resulted from incomplete combustion of G50, which is evident by the relatively high HC and CO emissions shown in Table 5.2. With increasing load, the combustion efficiency of G50 became close to that of diesel, reaching around 99%. As expected, G50 exhibited extremely low smoke emission (below FSN 0.01) at all tested loads. However, since EGR ratio was set to zero and combustion phasing were optimized to achieve best fuel economy, NO_x emissions and MPRR were very high.

Regarding PN, G50 emitted much more small particles than diesel in this case, shown in Table 5.2. It was found that over 95% of particles emitted by G50 were in nucleation mode, which was mostly consisted by liquid droplets of unburned hydrocarbons [122]. A diesel oxidization catalyst should be able to remove them effectively. The CMD of G50 was constantly around 6 nm when engine load was increased. For diesel, the CMD increased from 25 nm to 52 nm as the BMEP increased from 2 bar to 4.3 bar.

Table 5.1 Combustion performances of diesel and G50 at 2 bar, 3 bar and 4.3 bar BMEP

Fuel	BMEP	AHR50(BTDC)	MPRR(bar/deg)	Combustion delay (deg)	Combustion Efficiency	Indicated Efficiency	BTE
Diesel	2 bar	5	8.7	10	98.9%	39.0%	26.2%
Diesel	3 bar	5	8.7	10	99.4%	42.5%	33.7%
Diesel	4.3 bar	6	7.7	10	99.5%	42.3%	36.3%
G50	2 bar	5	7.6	13.5	95.6%	40.2%	26.5%
G50	3 bar	5	9.8	13	98.7%	40.0%	33.0%
G50	4.3 bar	7	10.1	13	99.1%	41.6%	35.7%

Table 5.2 Emissions of diesel and G50 at 2 bar, 3 bar and 4.3 bar BMEP

Fuel	BMEP	BSNO _x (g/kW.h)	BSHC (g/kW.h)	BSCO (g/kW.h)	Smoke (FSN)	Particle total number(part/kW.h)	Particle CMD(nm)
Diesel	2 bar	7.3	1.81	6.79	0.019	2.83E14	25.48
Diesel	3 bar	6.4	0.86	1.98	0.096	3.25E14	49.15
Diesel	4.3 bar	5.7	0.68	1.35	0.213	3.28E14	52.15
G50	2 bar	8.5	7.87	34.71	0.009	2.16E15	6.37
G50	3 bar	9.7	1.83	7.02	0.005	1.08E15	6.13
G50	4.3 bar	9.0	1.49	4.05	0.013	1.11E15	6.07

5.3. Effect of Pilot Injection

Currently, pilot injection is widely used in diesel engines to lower combustion noise and NO_x emissions. As demonstrated in Section 5.3, single injection G50 had high MPRR. Thus pilot injection strategy was implemented to G50 in this study for reduction of MPRR. The tested engine loads were exactly the same as in Section 5.2, which was 2 bar, 3 bar and 4.3 bar BMEP respectively. The pilot injection quantities were 0 mm³, 1.5 mm³ and 3 mm³ every engine cycle at each load respectively. The pilot injection timing was fixed at 25° BTDC. The main injection timings were adjusted to get the same combustion phasing as listed in Table 5.1.

According to Figure 5.12, the combustion delays of G50 were reduced by 0.5 to 2 crank angle degrees with usage of 1.5 mm³/cycle pilot injection quantity at low and medium loads respectively. Compared to the case without pilot injection, further increasing the pilot injection quantity to 3mm³/cycle reduced the combustion delay of G50 by 3 crank angle degrees. Regarding the MPRRs, they were below 6 bar/deg for G50 at all tested loads when 3mm³/cycle pilot injection quantity was used, which were comparable to the case of base diesel (standard 1.5 mm³/cycle pilot injection).

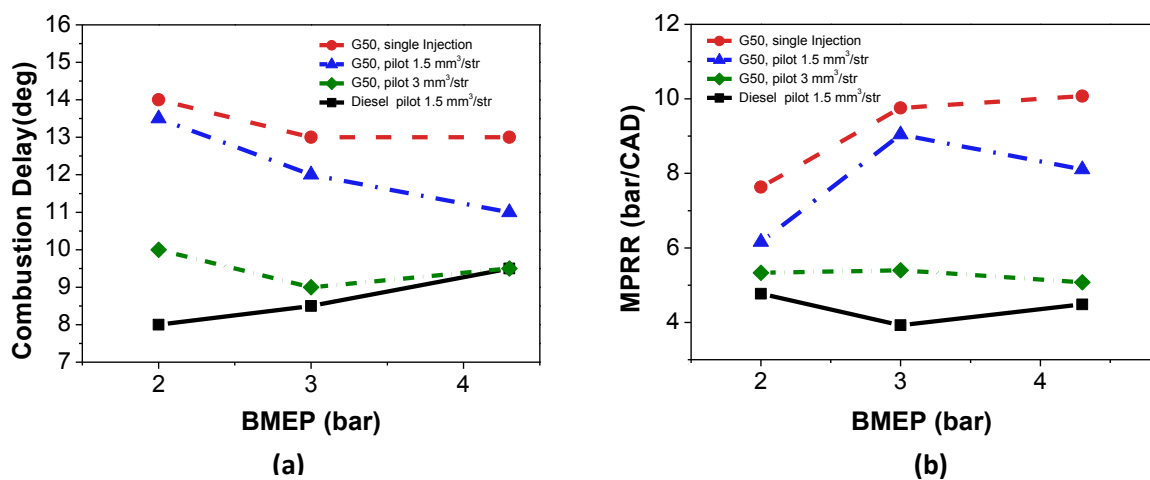


Figure 5.12 Combustion performances of G50 with pilot injection quantity of 0, 1.5 and 3 mm³/cycle. (a) Combustion delay; (b) MPRR

Figure 5.13 shows the in-cylinder pressure and heat release rate of diesel and G50 with varied pilot injection quantity at 4.3 bar BMEP. For both diesel and G50, increased pilot injection quantity lowered the heat release rate peak and prolonged the combustion duration. This is because the pilot injection helped to reduce premixed combustion, which is volumetric ignition and rapid, and increase diffusive combustion of diesel. For diesel, a clear pilot combustion was observed from the heat release rate curve when 3mm³/cycle pilot injection quantity was used. However, for G50, it seems such pilot combustion didn't appear. G50 had higher resistance to auto-ignition and higher volatility than diesel, which probably made the pilot injected fuel over-mixed with surrounding air and weakened the pilot combustion. Further increasing the pilot injection quantity can promote G50's pilot combustion. This

finding has been reported by the author in [101]. Extended pilot injection studies (split injection) of G50 will be reported in Chapter 6.

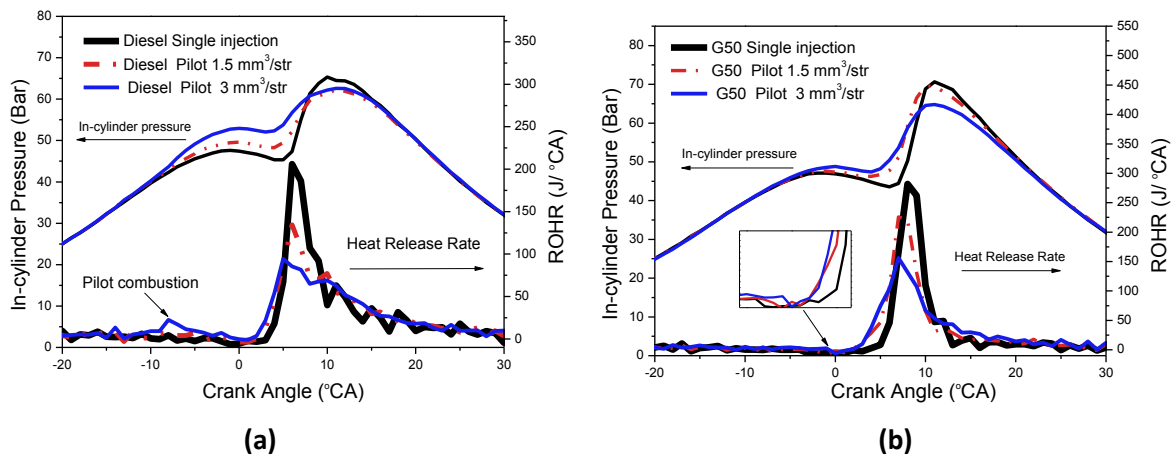


Figure 5.13 Effect of pilot injection quantity on In-cylinder pressure and heat release rate, 4.3 bar BMEP engine condition. (a) Diesel; (b) G50.

It is shown in Figure 5.14 that increasing pilot injection quantity has effectively reduced NO_x emissions but with penalty in smoke emissions. For G50 at 2 bar and 3 bar BMEP, the smoke penalties were minimal as compared to the benefits of NO_x reduction. However, at 4.3 bar BMEP, G50's smoke emissions increase dramatically with the increase of pilot injection quantity. As discussed in Section 5.2, pilot combustion warmed up in-cylinder gases and thus reduced the ignition delay of the main injection fuel which favoured soot formation. To sum up, G50 produced less smoke and higher NO_x than diesel when pilot injection was applied.

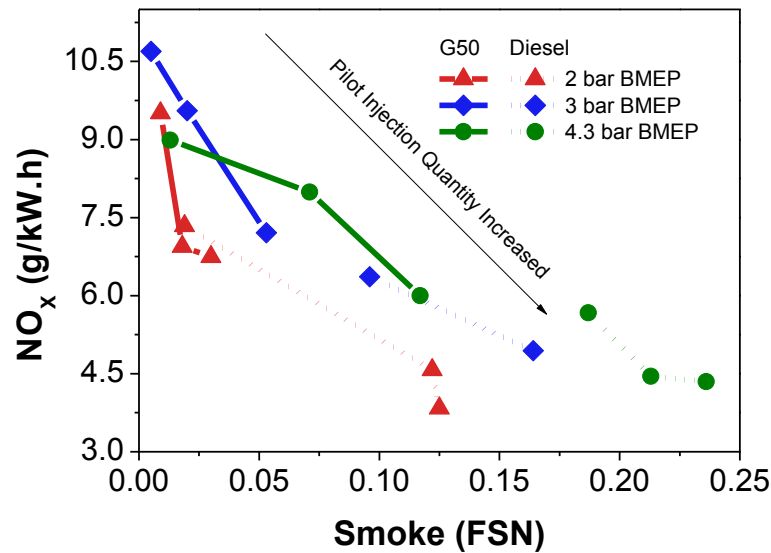


Figure 5.14 Trade-off between smoke and NO_x as pilot injection quantity varied

Figure 5.15 demonstrates the PN emissions of diesel and G50 combustion with pilot injection quantities varied from 0 to 3 mm³/cycle. The heights of shadow bar and solid bar represents the concentrations of nucleation and accumulation mode particles, respectively. Pilot injections of diesel, increased the number of accumulation mode particles and thus the total number, compared to single injections. G50's accumulation mode particle numbers were far less than diesel's at given engine conditions. However, G50 produced more nucleation mode particles than diesel and soared in the total number concentrations, except for the case of 4.3 bar BMEP with pilot injections. Because of the dominant nucleation mode particles, the particles CMD of G50 were small (around 6 nm) at most tested conditions, shown in Figure 5.16. At 4.3 bar BMEP with 3 mm³/cycle pilot injection, the CMD of G50's particles was 45 nm.

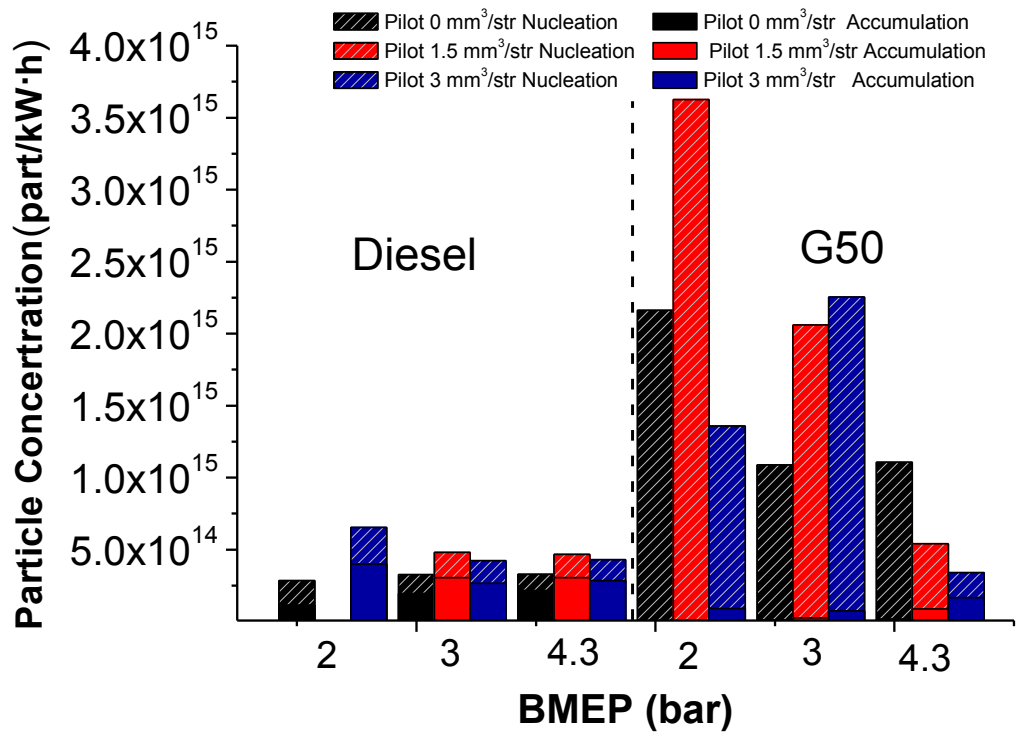


Figure 5.15 Accumulation mode and nucleation mode particle total concentration of diesel and G50 with varied pilot injection quantity at 2 bar, 3 bar and 4.3 bar BMEP

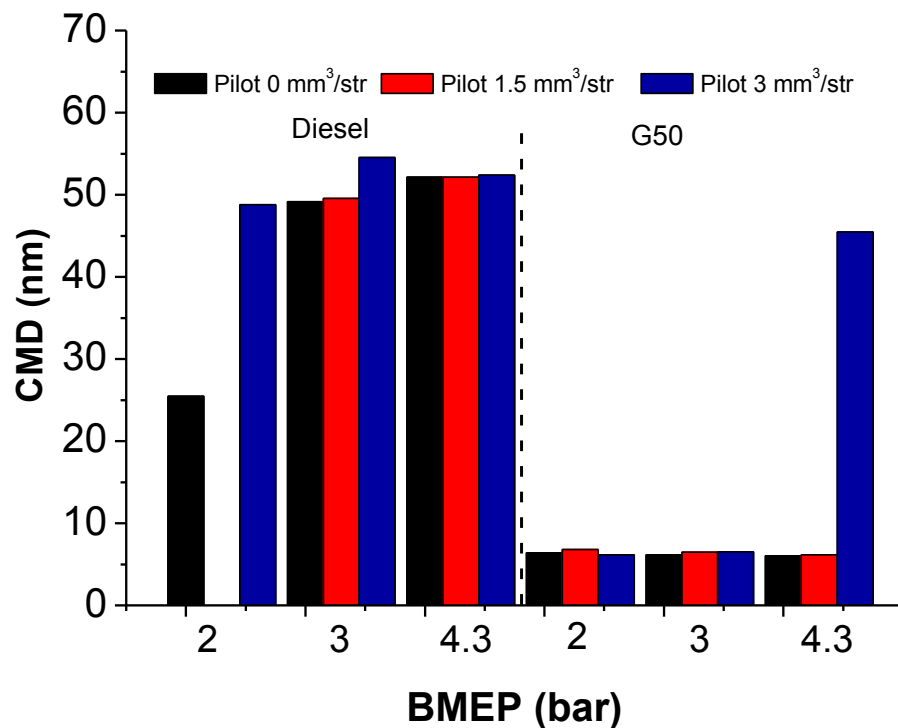


Figure 5.16 Particle count median diameter of diesel and G50 with varied pilot injection quantity at 2 bar, 3 bar and 4.3 bar BMEP

5.4. Conclusions

Combustion and emission characteristics of dieseline fuel were investigated this Chapter. The results illustrated how dieseline was different from diesel while operating the engine conventionally calibrated strategies for diesel. The results also revealed that single injection without EGR strategy and pilot injection alongside a main injection strategy. The findings are listed as following:

Conventional Calibration Strategies

1. The total PN concentration of G20 was reduced by 30 to 70% and CMD was reduced by up to 50% at the low load (1.38 bar BMEP). However, no reduction in CMD was found at the medium load (7.85 bar BMEP). For G50, the total PN concentration was reduced by 50 to 90% and CMD was reduced by 25 to 75% at medium and low loads, respectively,
2. Under original calibration strategies, smoke emissions of G20 and G50 were below FSN0.1 from 1.38 to 5.2 bar BMEP engine load conditions. At higher load of 7.85 bar BMEP, the smoke emission of G50 was maintained at low level of FSN 0.5 while G20 had a higher smoke (FSN 2.0) emission, which was similar to the diesel baseline,
3. The NO_x emission decreased by 50% at low loads and increased by 20% at medium loads for G50 compared to base diesel. G20 had similar NO_x emissions as single injection diesel. HC and CO emissions were substantially higher at low loads for G20 and G50, but they decreased to the diesel baseline level in higher load ranges,
4. Compared to diesel, dieseline fuels had lower MPRR and peak heat release rates at low loads while the trend reversed at medium loads. Increase of gasoline ratio in dieseline blends increased combustion delay. For G50, combustion delays were 4 to 7 crank angle degree longer than that of diesel.

Without EGR

5. With the combustion phasing optimised to achieve best fuel economy, the MPRR and heat release rate peak of G50 were lower than that of diesel at 2 bar BMEP and the trend reversed at higher loads (3 bar and 4.3 bar BMEP). G50's combustion delay was 3 crank angle degrees longer than that of diesel at all of the tested engine conditions,
6. The combustion efficiency of G50 was 3 percent lower than that of diesel at 2 bar BMEP while they were similar at 3 bar and 4.3 bar BMEP. G50 had similar optimized brake thermal efficiency to diesel.

Pilot Injection

7. Pilot injection effectively reduced the combustion delay of G50 and thus the MPRR. With the usage of 3 mm³/cycle pilot injection, G50's combustion delay was reduced by 4 crank angle degrees while MPRR was reduced by 3 to 5 bar/deg compared to the case without pilot injection,
8. The number of accumulation mode particles was increased with the usage of pilot injection for G50 and diesel. G50 produced high PN concentrations in nucleation mode particles at 2 bar and 3 bar BMEP. At 4.3 bar BMEP, increase of pilot injection quantity reduced the PN concentrations of nucleation mode particles.

To summarize, the obvious benefit of using dieseline in a conventional diesel engine is the reduction of smoke number, particle number and particle size. However, as compared to diesel, without optimization, dieseline combustion showed much higher THC and CO emissions than diesel at low loads. At medium to high loads, the high combustion noise is the main issue for dieseline combustion while pilot injection was proved to be an effective technique in resolving this problem. Next chapter investigates the effect of different injection parameters on dieseline combustion and an optimized result is presented.

CHAPTER 6

DIESEL FUELLED PPCI COMBUSTION

In this chapter, diesel fuelled partially-premixed compression ignition (PPCI) combustion was studied in a light duty 4 cylinder diesel engine. The objective of this investigation was to reduce a diesel engine's NO_x and particulate emissions simultaneously, while maintaining its high fuel economy by utilising advanced injection strategies and large amounts of cooled exhaust gas recirculation (EGR). In particular, the effects of different EGR ratios, injection timing and injection pressure on PPCI combustion were investigated first. Following that, the focus was on split injection strategies where the effects of split ratio and first-stage injection timing were examined.

6.1. Challenge of Achieving PPCI with Diesel

Conventional diesel engines suffer from high smoke and NO_x emissions due to the nature of dominated diffusive combustion [25]. Much research has shown that it is possible to reduce diesel engines' smoke and NO_x emissions simultaneously by strengthening the fuel/air mixing level and reducing combustion temperature [51-56]. However, as introduced in Chapter 2, special techniques are required to prolong the ignition delay and consequently improve the premixing process. Reducing compression ratio, increasing cooled EGR and increasing injection pressure are the most commonly used techniques, which however reduce engine efficiency [123]. Even with all of these techniques, extending the PPCI combustion load range to higher loads is still a challenge, because increased EGR replaces some of the intake air which makes the overall air/fuel mixture too rich and deteriorates the smoke emission.

Figure 6.1 shows the in-cylinder pressure and heat release rate of diesel fuelled PPCI combustion in the current engine (compression ratio 16.6). EGR ratio of 45% was used to reduce combustion temperature and thus NO_x emissions. Fuel with an injection pressure of 900 bar was injected to the cylinder at 20 ° BTDC to prolong combustion delay and suppress smoke emission. The problem was that diesel was too easy to be auto-ignited and combustion happened before the piston approached top dead centre, which resulted in a high pressure rise rate (12 bar/deg) and low indicated thermal efficiency (32.4%). The smoke emission was another issue: although the injection event was well separated from combustion and a high injection pressure of 900 bar was applied, the smoke emission (FSN 1.45) was just comparable to the diesel baseline (FSN 2.43). This was mainly due to the relatively low oxygen concentration (some of the fresh air was replaced by EGR), which weakened the soot oxidization process.

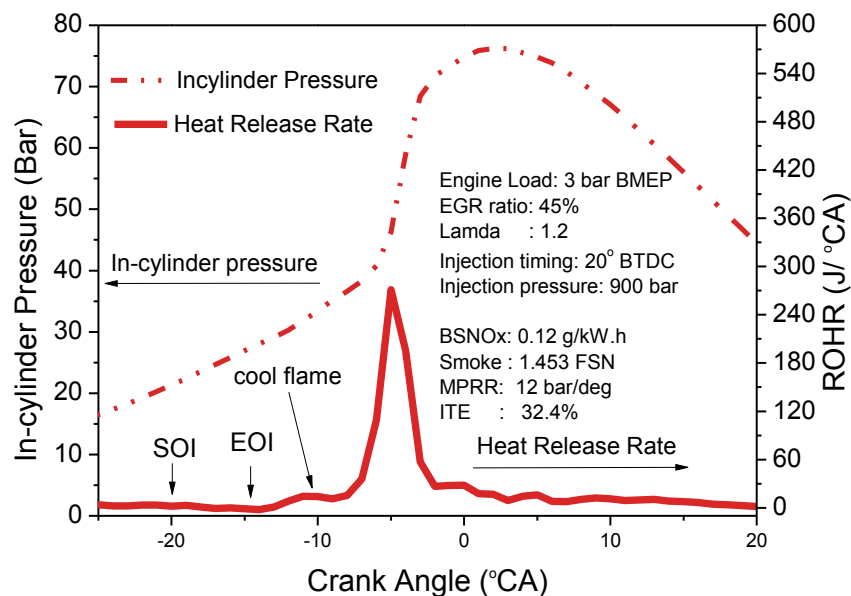


Figure 6.1 Diesel fuelled PPCI combustion in the current engine

In Chapter 5, it was demonstrated that dieseline fuel has a longer combustion delay and much lower smoke emissions than diesel. However, the results showed that NO_x emissions were still high for dieseline fuel when operating the engine with conventional calibration strategies which were designed for diesel. The basic idea of this chapter was to use a high EGR ratio to

suppress NO_x emissions and find out whether the low smoke emissions of dieseline combustion could be maintained. Apart from that, the long combustion delay of dieseline is expected to postpone the combustion phasing until after top dead centre, which is of benefit for achieving high indicated thermal efficiency and low pressure rise rate.

6.2. Single Injection Dieseline PPCI

In order to achieve PPCI combustion with dieseline fuel, firstly, injection timing and EGR ratio sweep for G50 (50% gasoline blended with diesel by volume) were performed at an engine condition of 3 bar BMEP. Then, the effect of injection pressure was examined. Finally, PPCI combustion fuelled by G70 (70% gasoline blended with diesel by volume) was tested at a higher load condition of 5.2 bar BMEP.

6.2.1. Injection Timing and EGR Ratio Sweep

Testing Matrix

The testing engine condition point was recommended by the engine OEM and selected from the NEDC driving cycle, which was a speed of 1800 rpm and load of 52 Nm (3 bar BMEP). The EGR ratio varied from 40% to 50% and the injection timing varied from 8° to 28° BTDC. The exact testing injection timings and EGR ratios are presented in Figure 6.2. At injection timings of 8° and 13° BTDC, more than 45% EGR wasn't tested since the combustion phasing was too late, which resulted in unacceptable engine stability and low indicated thermal efficiency (less than 35%).

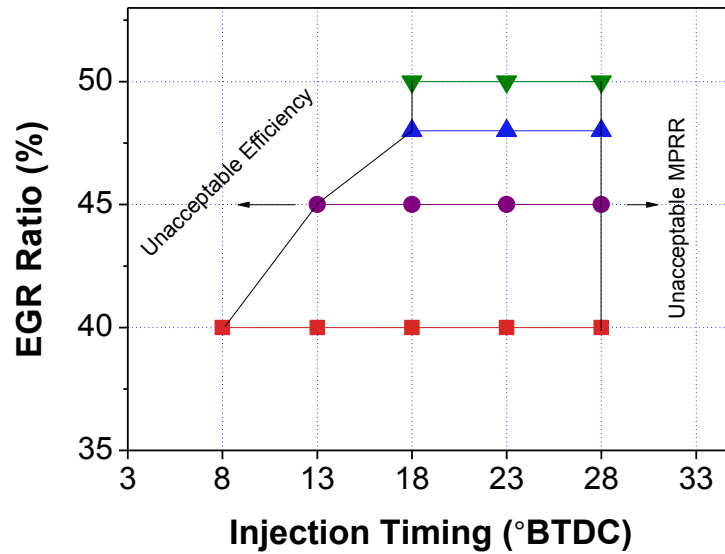


Figure 6.2 Testing matrix for EGR ratio and injection timing sweep

Combustion Performance

The effects of EGR ratio and injection timing on combustion delay are shown in Figure 6.3. Generally, the combustion delay increased with the advancing of the injection timing. For example, advancing the injection timing of G50 from 18° to 28° BTDC resulted in an increased combustion delay by 5 CAD for the tested EGR ratios. However, the combustion delay of G50 decreased by 4 CAD as the injection timing was advanced from 8° to 13° BTDC at an EGR ratio of 40%. This is due to the combustion delay being negatively related to ambient temperature. It has been found in [44] that peak in-cylinder temperature occurs around 12° BTDC rather than at TDC due to heat loss during compression. The in-cylinder temperature was higher as the fuel spray entered the cylinder later (until 12° BTDC), which reduced the combustion delay. It was also found that a higher EGR ratio increased the combustion delay. The main reason was that EGR replaced some of the fresh air and reduced intake oxygen concentration, which slowed the chemical reactions. Additionally, EGR increased the intake CO₂ concentration and thus the intake heat capacity which decreased the

temperature rise from early low-temperature reactions. The combustion delay of G50 at an injection timing of 28° BTDC and EGR ratio of 50% was 16 CAD longer than base diesel, which gave G50 a long premixing time.

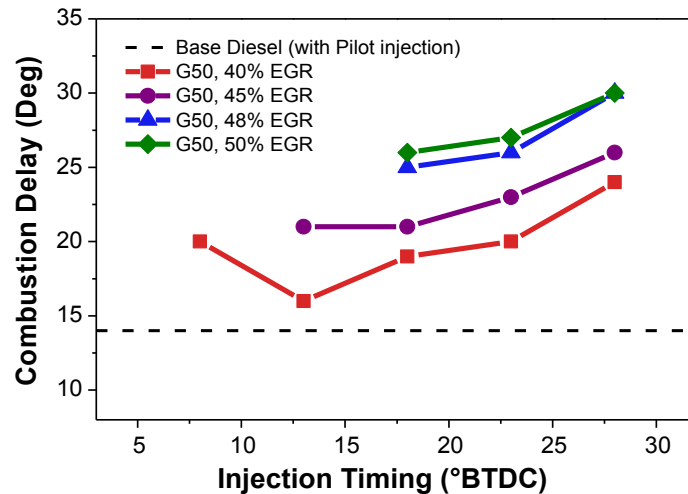


Figure 6.3 Combustion delay versus injection timing at different EGR ratios

Regarding the combustion phasing (AHR50) and maximum pressure rise rate (MPRR), it is shown in Figure 6.4 that the AHR50 advanced and MPRR increased as the injection timing was advanced. Therefore the combustion phasing was still directly controlled by the injection event for G50 fuelled PPCI, even though the combustion delay was relatively long compared to the case of conventional diesel. Advancing the injection timing from 8° to 23° BTDC resulted in a rapid increase of MPRR. However, the further advance of injection timing to 28° BTDC didn't increase the MPRR. Two factors can affect MPRR: burning rate and combustion phasing [24]. As the injection timing was advanced from 23° to 28° BTDC, the combustion delay was increased by almost 4 CAD, as shown in Figure 6.3, which probably caused over-mixing of air with fuel and thus the slowed chemical reactions. During the same period, combustion phasing remained almost the same since the long combustion delay cancelled the effect of advanced injection timing. It can be expected that if the injection timing was further advanced, the ignition delay would much more lengthened and the

combustion phase would be retarded. Therefore less EGR will be enough to keep the combustion phasing after TDC while injection timing is very advanced. This probably helps widen the PPCI operating range (more oxygen is available for the combustion). However, the fuel spray wall impingement would be an issue and the injector spray angle needs to be optimised. To conclude, G50 fuelled PPCI combustion does increase the MPRR compared to base diesel, due to the advanced combustion phasing.

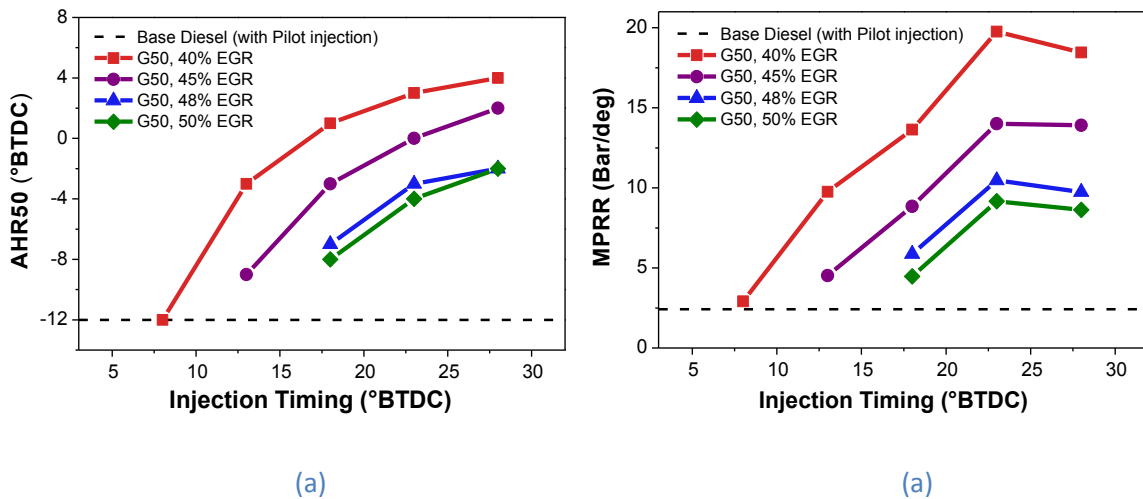


Figure 6.4 AHR50 and MPRR versus injection timing at different EGR ratios. (a) AHR50; (b) MPRR.

Figure 6.5 shows the combustion efficiency and brake thermal efficiency while the injection timing and EGR ratio were varied. The combustion efficiency of G50 fuelled PPCI operation was up to 3% lower than the case of base diesel. This was due to the reduced combustion temperature and prolonged mixing time. Advancing the injection timing can shorten the gap to below 1%. The highest brake thermal efficiency (BTE) of G50 PPCI was 30% (occurred at 50% EGR and injection timing of 28° BTDC), which was measurably higher than the case of base diesel (28.6%). The advanced combustion phasing, which increased the expansion ratio, contributed to the rise of BTE. For an EGR ratio of 40%, BTE peaked at 13° BTDC and then went down with the advancing of injection timing. This can be explained by Figure 6.4: the combustion phasing was at before top dead centre when the fuel injection was placed earlier than 13° BTDC.

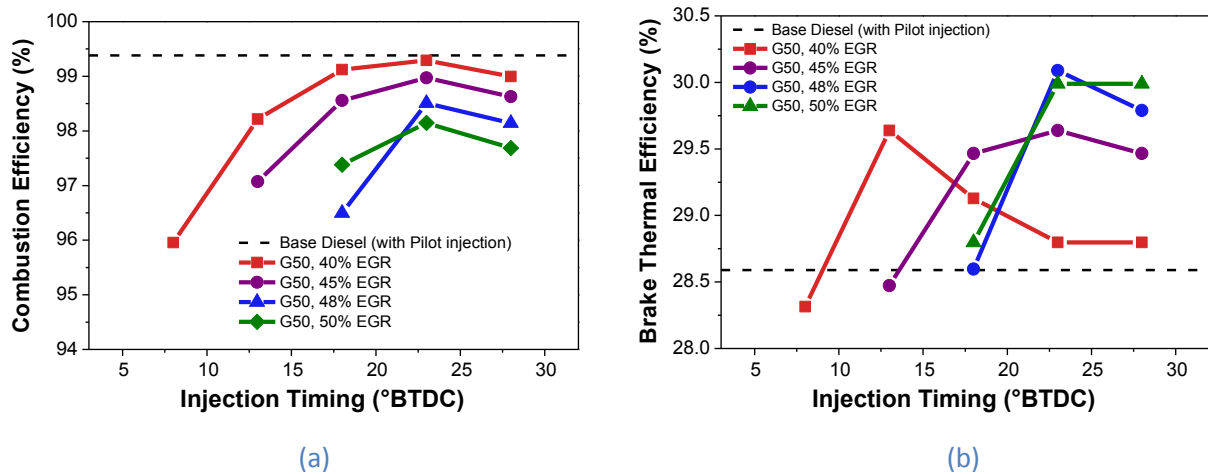


Figure 6.5 Effect of injection timing at different EGR ratios on engine efficiency. (a) Combustion efficiency; (b) brake thermal efficiency.

Regulated Emissions

Figure 6.6 presents the smoke, BSNO_x, BSHC and BSCO emissions of G50 fuelled PPCI operation. Almost zero smoke was achieved at the tested injection timings and EGR ratios. It is important to mention that lambda was only 1.1 at an EGR ratio of 50%. Three factors contributed to the low smoke emission: relatively low combustion temperature, high volatility of G50 fuel and long combustion delay (30 CAD), which was due to the advanced injection timing and G50's low cetane number. For diesel, it was not possible to achieve smokeless combustion at such low lambda in the current engine. In terms of NO_x emissions, as the injection timing was advanced for 40% EGR, NO_x emissions increased significantly and exceeded diesel base line at SOI of 23° BTDC. However, with the increase of EGR ratio, NO_x emissions became less sensitive to injection timing. For 50% EGR, BSNO_x stayed as low as 0.05 g/kW.h, regardless of tested injection timings. As discussed in the previous section, the main reason is the high EGR ratio reduced the oxygen concentration and retarded the combustion phasing, both of which lowered the combustion temperature.

As shown in Figure 6.6, G50 fuelled PPCI operation had higher BSHC and BSCO emissions than baseline diesel. However, they were reduced with the advancing of the injection timing.

For 50% EGR and SOI of 23° BTDC, BSHC and BSCO emissions were 3 times higher than baseline diesel, which were acceptable considering the benefits of BTE, smoke and NOx emissions.

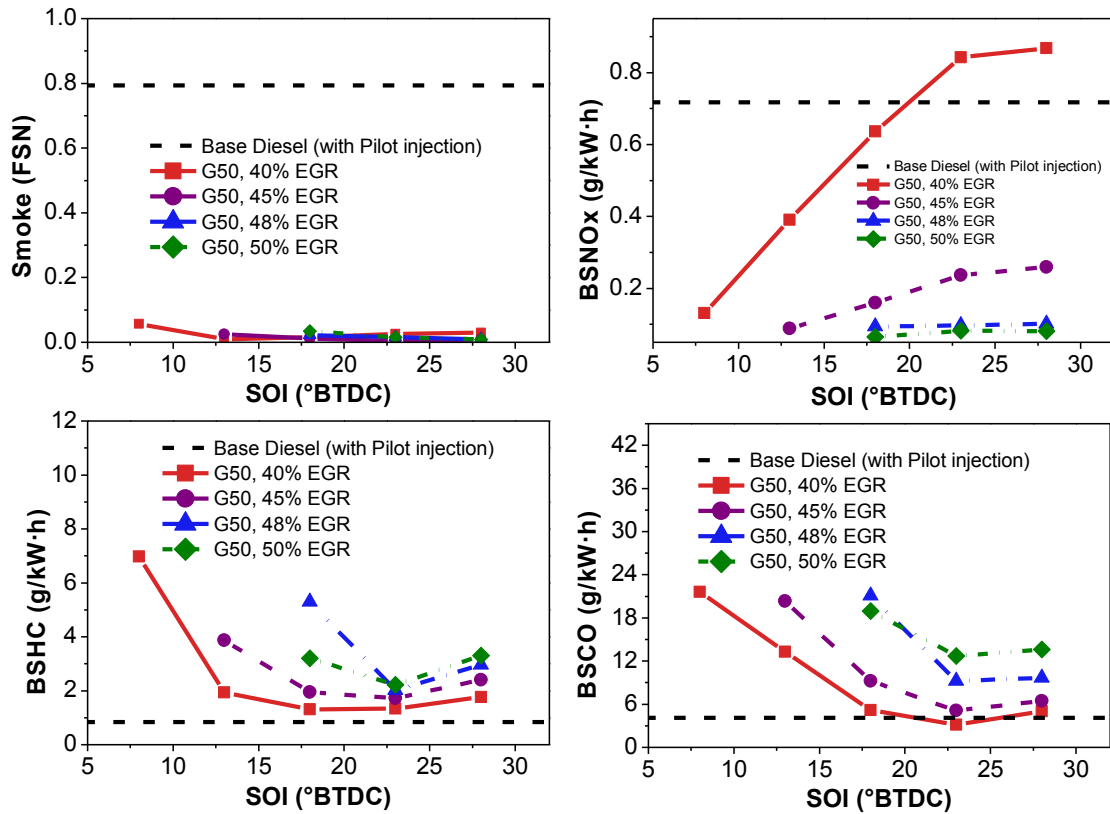


Figure 6.6 Smoke, BSNOx, BSHC and BSCO emissions of G50 fuelled PPCI combustion at varied injection timings and EGR ratios.

Particulate Matter

Generally, for conventional diesel operation, an increased EGR ratio reduces the oxygen concentration and thus weakens the soot oxidization, which results in higher particle emissions. However, it is shown in Figure 6.7 that increasing the EGR ratio from 40% to 50% for G50 fuelled PPCI operation has reduced the particle number total concentration by more than 95% and CMD by 50%, because higher EGR ratios extend the combustion delay, improved the fuel/air mixing and lower the combustion temperature, which largely prevents

soot formation. This may have overwhelmed the deterioration of soot oxidization and resulted in reduced engine-out particle emissions. In particular, as the EGR ratio increased, accumulation mode particles (size over 50 nm) were dramatically reduced while the number of nucleation mode particles (size below 50 nm) increased but in a limited scale.

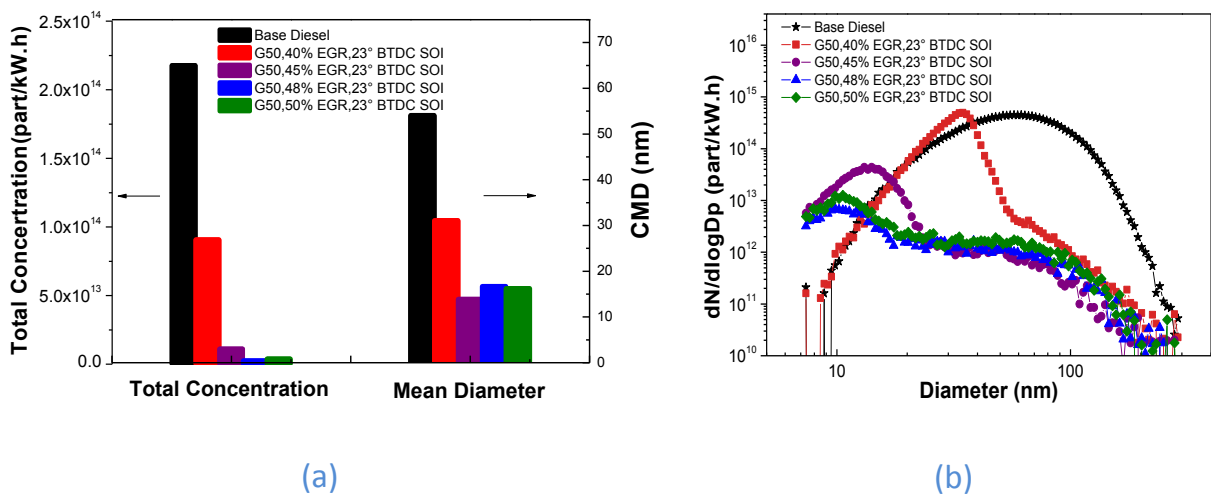
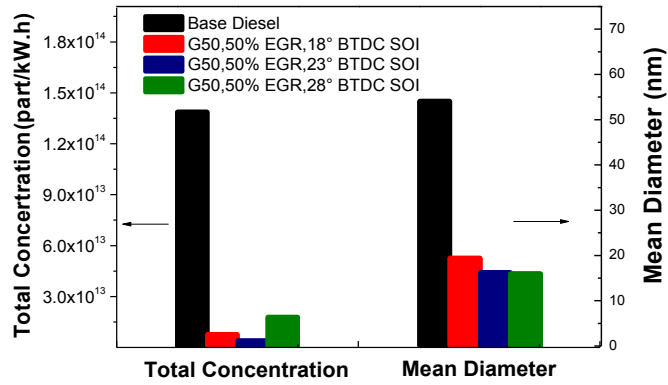
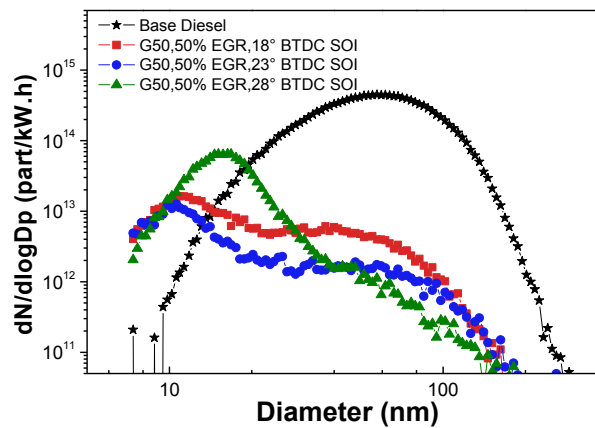


Figure 6.7 Effect of EGR ratios on particle number total concentration. (a) count median diameter (CMD); (b) and size distribution.

Figure 6.8 demonstrates the effect of injection timings on particle emissions. With an EGR ratio of 50%, the injection timing had little effect on particle number total concentration and mean diameter. As shown in Figure 6.8(b), the number of accumulation mode particle was reduced with the advancing of injection timing. In terms of nucleation mode particles, the number increased as injection timing was advanced from 23° to 28° BTDC. This was due to the fuel impingement on the cylinder-wall and fuel/air over mixing, which resulted in an increase of incompletely combusted liquid HC particles, shown in Figure 6.6. Overall, G50 fuelled PPCI operation reduced the particle total number concentration by 99% and CMD from 55 nm to around 20 nm.



(a)



(b)

Figure 6.8 Effect of injection timings on particle number total concentration. (a) count median diameter (CMD); (b) and size distribution.

Trade-off between Smoke and NO_x for Dieseline

Figure 6.9 shows the trade-off between NO_x and smoke emissions as the EGR ratio and injection timing varied for diesel, G50 and G70. Except for points 'A', all of dieseline points (G50 and G70) are located in the low smoke region, regardless of EGR ratio and injection timing. It was found that the SOI of points 'A' were between 8 and 13° BTDC and their injection pressure was 700 bar. Relatively low injection pressure and late injection timing contributed to the high smoke (around FSN 1.0) of points 'A'. With advancing of SOI, the smoke of G50 fell below FSN 0.1. However, for diesel, it was not possible to suppress the

smoke below FSN 1.0 even with advancing the SOI to 20° BTDC. For G70, the smoke stayed at a low level and the NO_x increased significantly when reducing the EGR ratio. To conclude, the NO_x emissions are still mostly decided by EGR ratio for diesel, G50 and G70. Advancing the injection timing for diesel can moderately improve the trade-off between NO_x and smoke. Blending gasoline into diesel (dieseline) can significantly reduce the smoke and thus improve the trade-off between smoke and NO_x.

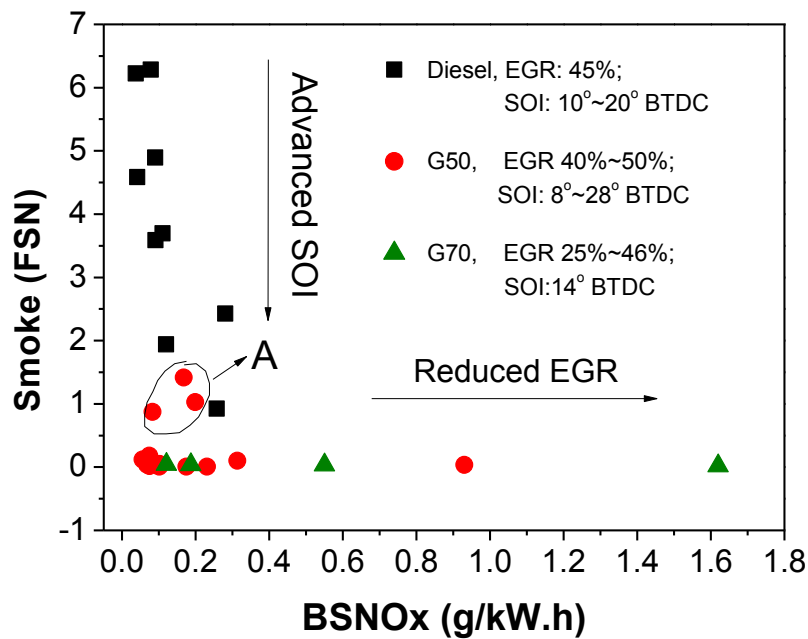


Figure 6.9 Trade-off between smoke and NO_x for diesel, G50 and G70 at 3 bar BMEP.

To Summarise, The experimental results have shown that advanced injection timings and increased EGR ratios provide big benefits in BTE, NO_x and particles' emissions for G50 fuelled PPCI operation, shown in Figure 6.10. Using similar strategies with diesel operation cannot get such good results at the tested load (3 bar BMEP). The main advantages of G50 are its high resistance to auto-ignition and low smoke emissions. The former enables combustion to start ATDC when the injection pulse is placed early (more than 20° BTDC) in order to avoid high in-cylinder temperature region (at around 10° BTDC), which is favoured by soot formation. The latter helps combustion to tolerate a high EGR ratio while low smoke

emissions can be maintained. In summary, the correct combination of combustion delay, combustion phasing and EGR ratio is the key to get optimised results.

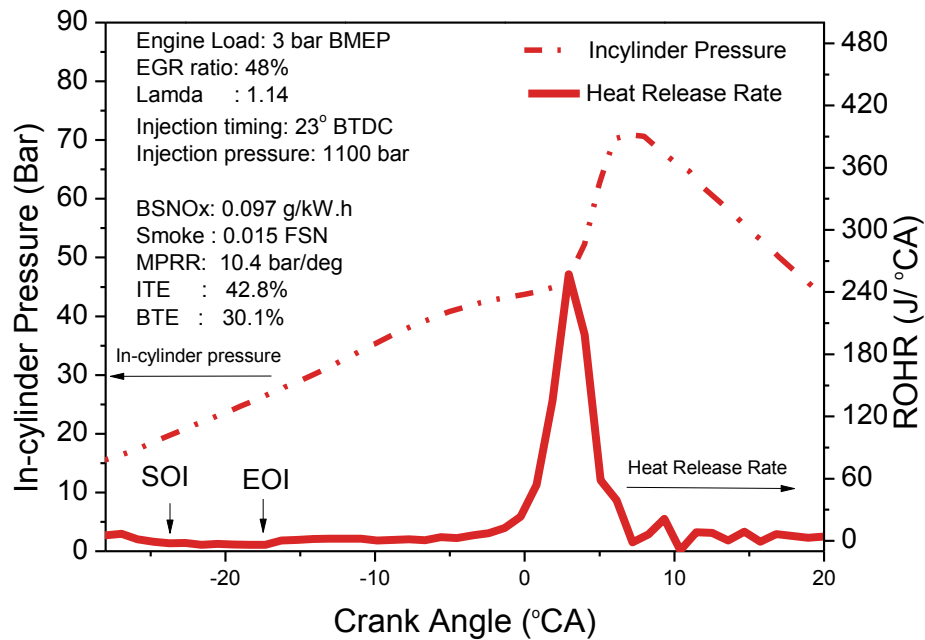


Figure 6.10 Optimised G50 fuelled PPCI operation at 3 bar BMEP

6.2.2. Effect of Injection Pressure

In section 6.2.1, a high injection pressure of 1100 bar was used to achieve PPCI combustion for G50. This section aims to find out how necessary it is to have the high injection pressure. Figure 6.11 compares the effect of 700 bar and 1100 bar injection pressure on combustion and emissions of G50 fuelled PPCI operation (48% EGR, 23° BTDC SOI). It is shown that they presented little difference in terms of combustion phasing, fuel economy, BSNO_x and BSHC emissions. The BSCO of 700 bar injection pressure increased by 93% compared to 1100 bar injection pressure. This should be the result of poor atomization of fuel spray, as discussed in Chapter 4, and more incomplete combustion. Regarding the smoke emissions, they were below 0.05 FSN for both of the two injection pressures as observed in the engine test.

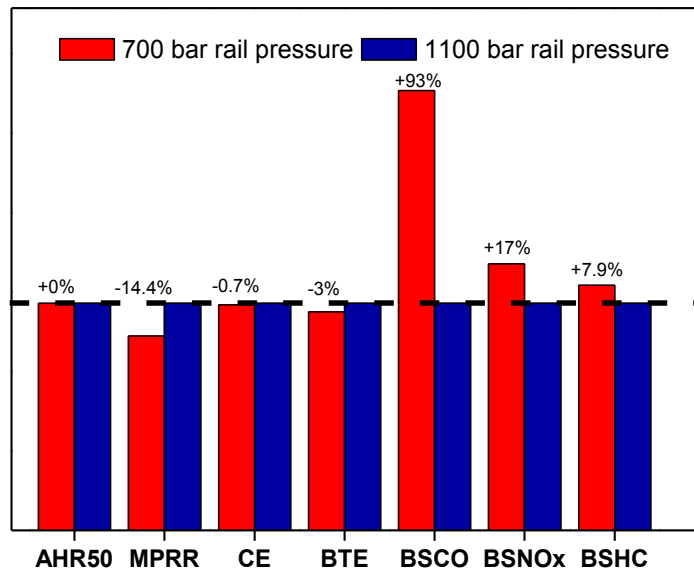


Figure 6.11 Effect of injection pressure on combustion performances and emissions at 48% EGR and 23° BTDC SOI.

More differences between the two injection pressures were observed in the particle number. Figure 6.12 shows that the particle number total concentration increased by 6 times and CMD by 0.8 times as injection pressure was reduced from 1100 bar to 700 bar. In particular, the number of particles of a size between 16 nm and 50 nm, shown in Figure 6.12, mostly contributed to the increase. Higher injection pressure helped to shorten injection duration and improve fuel atomization, which increased entrained air into the fuel jet region and reduced local equivalence ratio [31]. This was the main mechanism that the high pressure injection strategy used to reduce particle emissions. To conclude, G50 fuelled PPCI operation can be achieved with relatively low injection pressure and thus help achieve high fuel economy, while low NO_x and smoke emissions can be maintained. It appears that increasing the injection pressure can effectively further reduce particle number total concentration.

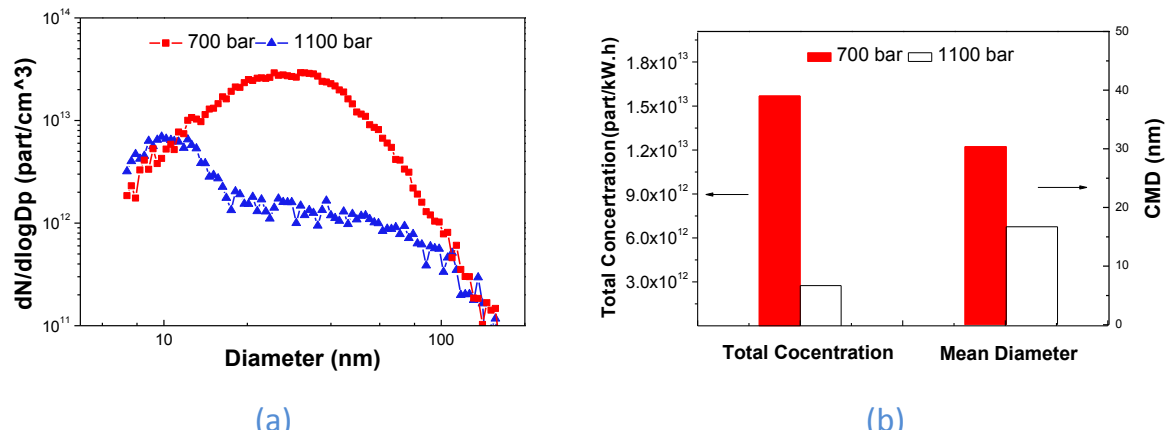


Figure 6.12 Effect of injection pressure on particle emissions. (a) number size distribution; (b) total concentration and CMD.

6.2.3. Engine Load Extension

As discussed in the previous section, PPCI operation can be achieved at 3 bar BMEP in the current engine by using G50. To further extend the PPCI operating load, G70 was tested at a higher load of 5.2 bar BMEP in this section. The main challenge of extending PPCI operation is the limited amount of EGR that can be applied: high EGR ratio causes the overall fuel/air mixture to be too rich. At 5.2 bar BMEP engine load for the current engine, usage of 33% EGR results in an air excess ratio (λ) of 1.09.

Figure 6.13 demonstrates the trade-off between BSNO_x and smoke for G70 fuelled PPCI as the EGR ratio varied from 19% to 33%. The SOI was adjusted to get combustion phasing (AHR50) of -6° BTDC, which gave the engine its best fuel economy. As the EGR ratio increased, the BSNO_x dropped dramatically but the smoke emissions increased. At an EGR ratio of 33%, the smoke was 2.6 FSN, which largely exceeded the diesel baseline, because λ was low (1.09) and injection timing was late, which was around 10° BTDC and the in-cylinder temperature peaked. A compromised result was obtained at an EGR ratio of 25% (marked point A) where the smoke was reduced by 70% compared to the diesel baseline and without the penalty of the BSNO_x emissions. The in-cylinder

pressure, heat release rate and some key results of point ‘A’ are shown in Figure 6.14. It is found that the injection event was separated from the combustion but the gap between them was not as big as shown in Figure 6.10, where engine load was 3 bar BMEP and EGR ratio was 48%. Due to the relatively low EGR ratio and the short gap between injection and combustion, absolutely low smoke (below FSN 0.1) and low BSNO_x (below 0.1 g/kW.h) wasn’t achieved at 5.2 bar BMEP. Retarding the injection timing can simultaneously further reduce smoke and BSNO_x emissions but with a sacrifice of thermal efficiency. Boosting the intake pressure, which was not available in the current test rig, probably helps extend the PPCI operational range, because more EGR can be used and combustion delay can be prolonged.

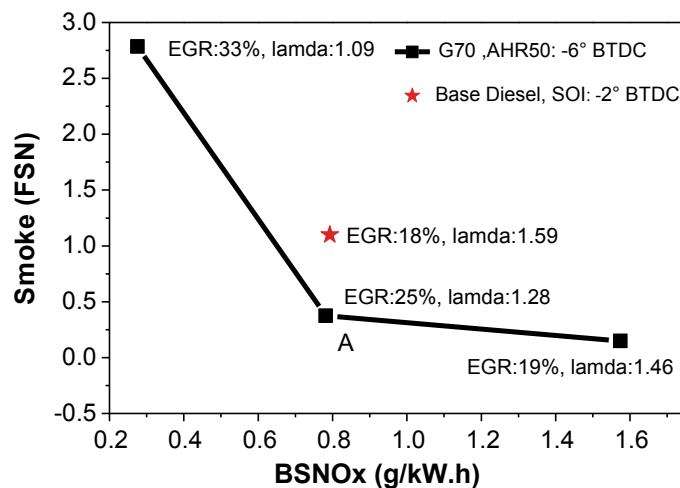


Figure 6.13 Trade-off between BSNO_x and smoke for G50 fuelled PPCI at 5.2 bar BMEP

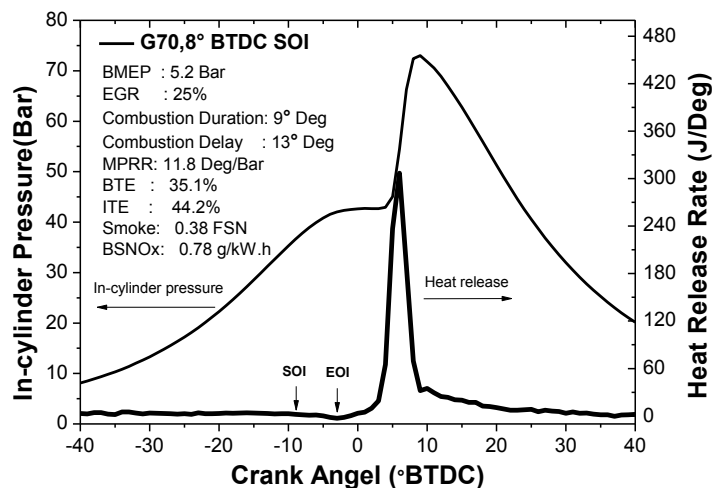


Figure 6.14 G70 fuelled PPCI at 5.2 bar BMEP (marked point A in Figure 6.13)

6.3. Split Injection PPCI

6.3.1. Introduction

It has been introduced in section 6.2 that PPCI combustion can be accomplished by utilising a large amount of EGR and early injection of fuels. A good PPCI combustion needs proper injection timing and combustion phasing: a too early injection may result in advanced combustion phasing (before TDC) which lowers the efficiency and raises the MPRR dramatically; a too late injection (until the in-cylinder temperature peaks) causes short combustion delay and thus high smoke emissions. A probable solution is to split the main injection into two: the first injection starts early to create a homogeneous fuel/air mixture while the second injection is used to control the combustion phasing. The main advantage of split injection strategy is that it provides more flexibility for fuel/air mixing strength and combustion phasing control. However, two main issues should be addressed for diesel split injection strategies. One is the fuel spray wall impingement and the other one is the auto-ignition of first-stage injected fuel. Dieseline has shorter penetration length (shown in Chapter 4), higher volatility and lower cetane number than diesel, which may help to avoid the two issues.

This section investigated split injection strategies of G50 fuelled PPCI combustion at an engine condition of 3 bar BMEP. A higher engine condition of 5.2 bar BMEP was also tried using early first injection timings (e.g. 50° BTDC). However, the results of heat release analysis illustrated two peaks with just moderate first injection-quantity ratios (e.g.15%). This phenomenon was not desirable since the first high temperature heat release peak increased in-cylinder temperature before the second injection started, which significantly increased the smoke emissions. Quick auto-ignition of first-stage injected fuel might be due to limited EGR

ratio and higher residual gas temperature as the engine load increased. A lower fuel CN (e.g. increasing gasoline in the blends), higher EGR ratio and higher boost pressure might help to extend split injection strategies to a higher engine load. However, being limited by the current engine testing rig configuration, engine load higher than 5.2 bar BMEP was not further pursued.

Three injection parameters were examined in this section: split ratio, first injection timing and second injection timing. The EGR ratio was fixed at a high level of 45%. There were two reasons for this: firstly, a high EGR ratio helped to prevent auto-ignition of first-stage injected fuel; secondly, NO_x emissions can be suppressed by a high EGR ratio. The injection pressure was fixed at 600 bar in order to minimize fuel spray impingement on the wall. First injection timings of 68°, 77°, 87° and 97° BTDC and fuel quantity splitting ratios (first injection over total) of 50%, 60% and 70% were tested. Combustion phasing was kept at 3° ATDC by adjusting the second injection timing in this group of experiments. Then the second injection timing was varied from 4° BTDC to 18° BTDC while the first injection timing was fixed at 68° BTDC and the splitting ratio was fixed at 70%. Baseline single injection, which had combustion phasing of 3° ATDC, was also tested and the results are listed in table 6.1.

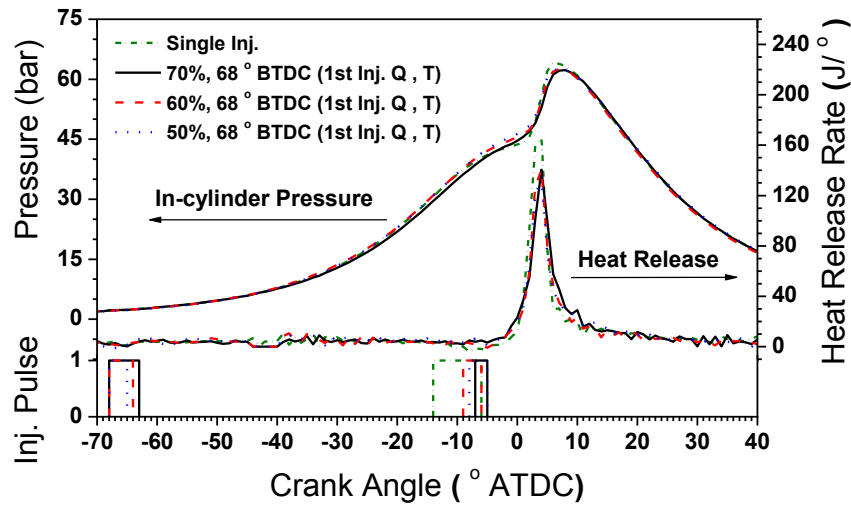
Table 6.1 Baseline single-injection strategy experimental results for 3 bar BMEP, AHR50: 3° ATDC, EGR: 45%

Injec tion Mode	SOI(° BTDC)	BTE (%)	MPRR(bar/deg)	BSNO _x (g/kW.h)	Smoke(FSN)	BSCO (g/kW.h)	BSHC (g/kW.h)
Single	14	29.7	6.4	0.15	3.9	20.80	1.74

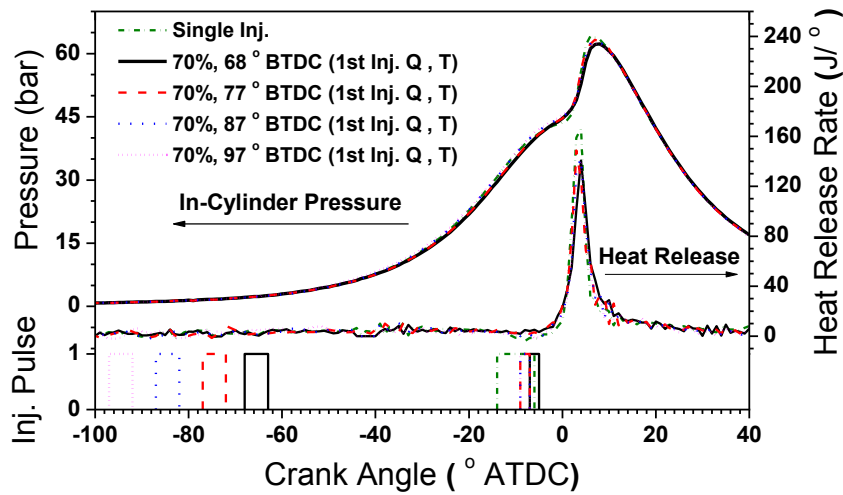
6.3.2. Effect of First Injection Quantity and Timing

Combustion Performance

Figure 6.15 shows the in-cylinder pressure, heat release rate and injection pulse for different first injection quantity ratios and different first injection timings. Single injection strategy had the highest heat release rate peak than any of the split injection strategies. This was due to the first-staged injected fuels being fully mixed with air and forming over-lean mixtures. For split injection strategies, combustion delay was defined as the gap between SOI of the second injection and AHR50. As shown in Figure 6.15, the combustion delay of the single injection was 4° to 6° crank angle longer than the split injections. Low temperature combustion of first-stage injected fuel contributed to the reduced combustion delay of split injections. Under varied first injection quantity-ratios and timings, in-cylinder pressure and HRR were quite similar. Regarding the combustion phasing control, it was found that first injection quantities and timings had a minor effect on combustion phasing.



(a)



(b)

Figure 6.15 In-cylinder pressure, heat release rate and injection pulse for 3 bar BMEP. (a) 70%, 60% and 50% first injection quantity ratio (first injection timing was fixed at 18° BTDC); (b) 70% first injection quantity ratio (first injection timing varied from 68° BTDC to 97° BTDC)

Break thermal efficiency (BTE) and maximum pressure rise rate (MPRR) for different first injection quantity-ratios with respect to the first injection-timings are illustrated in Figure 6.16. With higher first injection quantity-ratios and more advanced injection timings, the BTE decreased. Apparently, that was due to the reduced combustion efficiency, which can be seen from their high concentrations of unburned hydrocarbon emissions, as shown in Figure 6.17. The highest BTE for split injection strategies tested here was 28.32% at a first injection quantity-ratio of 50% and SOI of 68° BTDC. This value was 1.34% (absolute value) lower

than single injection G50 fuelled PPCI combustion (29.66%). For MPRR, there was no specific trend as first injection quantity-ratios and timings varied. However, it was generally lower than single injection strategy. MPRR in the best case (same as the case for BTE) was lowered by 22% compared to the single injection strategy (from 6.4 to 5 bar/deg).

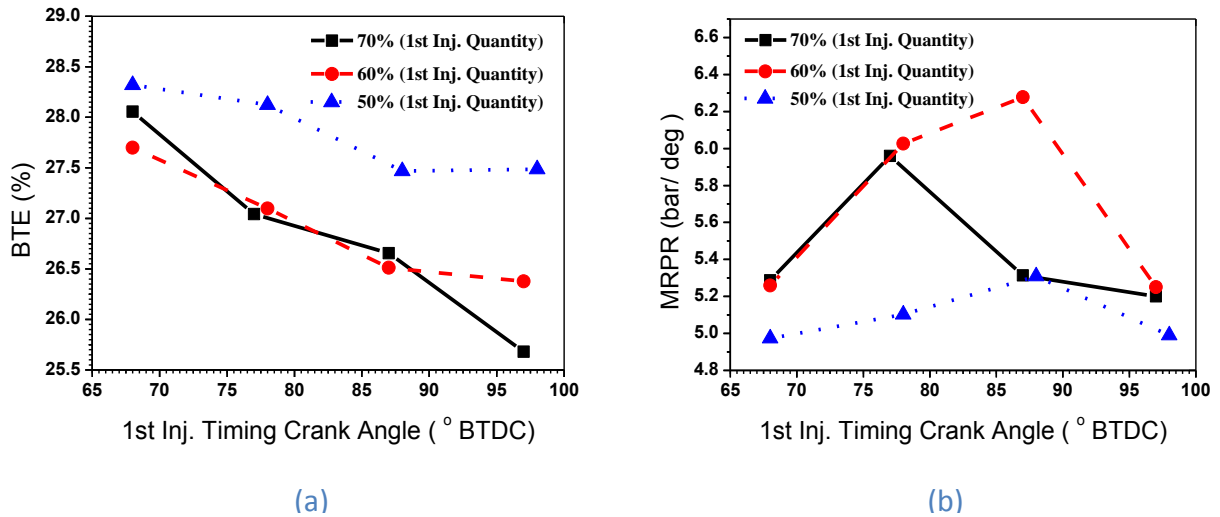


Figure 6.16 Effect of different first injection quantity-ratios on combustion performances, 3 bar BMEP. (a) Brake thermal efficiency; (b) MPRR.

Emissions

Figure 6.17 presents the smoke emissions of different split injection strategies. Higher first injection quantity-ratios resulted in lower smoke. In all of the cases here, smoke should be from the combustion of second-stage injected fuel. As shown in Figure 6.15, there were long intervals between first injection and high temperature heat release. Thus the first-stage injected fuels were almost fully mixed with air when combustion started. For second-stage injected fuel, the combustion delay wasn't long enough to eliminate fuel-rich zones and smoke was generated. It seems the first-injection timing had little effect on smoke emissions. Overall, the smoke emissions were reduced by 85% in the best case compared to single injection. Further reduction of smoke may be achieved by optimisation of second injection timing.

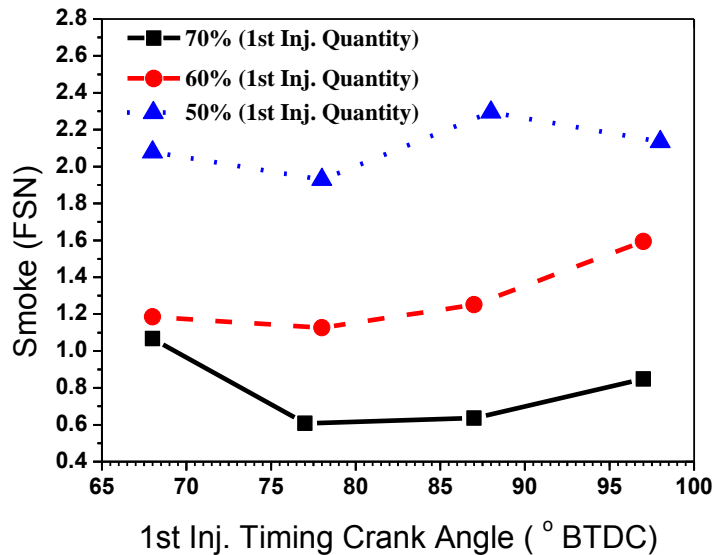


Figure 6.17 Smoke emissions of three different first injection quantity-ratios, 3bar BMEP.

NO_x formation is favoured by a stoichiometric fuel/air mixture and a high temperature environment [25, 36]. Either an over-lean or over rich mixture would result in low NO_x emissions [36]. Figure 6.18 shows that the BSNO_x emissions of split injection strategies were lower than those of the single injection strategy (0.15 g/kW.h). In particular, increasing the first-injection quantity ratio generally reduced BSNO_x. Most NO_x emissions were expected to come from the combustion of the second-stage injected fuels, because the first-stage injected fuels were fully mixed with air and the local mixture packets were close to overall mixing strength, which was over-lean. The combustion delay of the second stage injected fuels was short, which helped to form close to stoichiometric mixture packets; that can explain the lower BSNO_x when the first-injection quantity ratio increased.

BSNO_x was generally increased as the first injection timing was advanced for all injection-quantities. A probable explanation can be made as follows: advancing the first injection reduced brake thermal efficiency, as shown in Figure 6.16, and thus caused load drop; during

the test, the second injection quantity was increased to maintain engine load at 3 bar BMEP; the increased second injection quantity and reduced BTE raised the BSNO_x emissions.

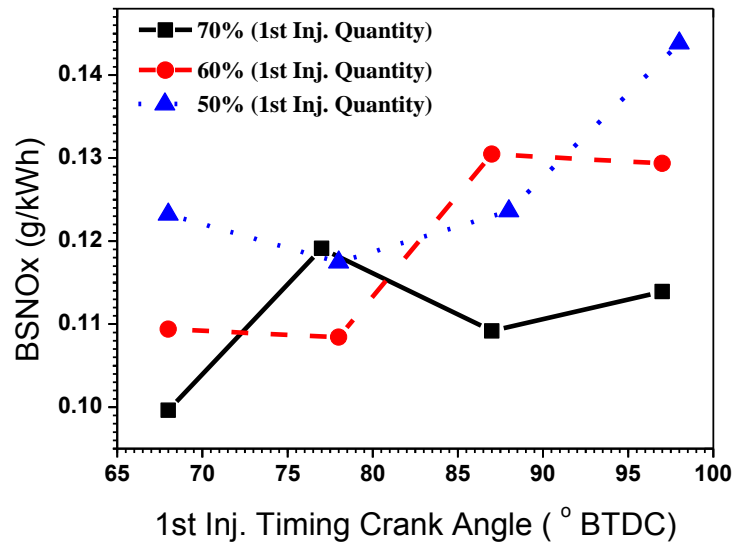


Figure 6.18 Brake specific NO_x of three different first injection quantity-ratios, 3bar BMEP.

Figure 6.19 shows BSHC and BSCO emissions. In the best case, BSHC emissions of the split injection strategies were 5 times higher than in the case of single injection. They went up further as first injection-timing was advanced and the first injection quantity-ratio increased. Wall impingement of fuel spray and over-mixing were the reasons for the high level of BSHC emissions. To resolve these kinds of issues, Sun and Reitz [64, 65] developed a variable injection pressure (VIP) system which was capable of changing injection pressure between low and high in one engine cycle. Low pressure was used for the first injection to reduce spray penetration length and thus wall impingement. Narrow angle direct injection (NADI) technology is another potential solution for the high HC emissions of split injection strategies [124]. BSCO emissions of split injection strategies were slightly lower than single injection (BSCO: 20.8 g/kW.h), as shown in Figure 6.19. In the best case, it was 26% lower compared to single injection. CO mainly forms in fuel-rich combustion [39] and is strongly affected by combustion temperature [38, 39]. It seems that most CO was emitted from the combustion of the second-stage injected fuel, which formed rich mixture with air.

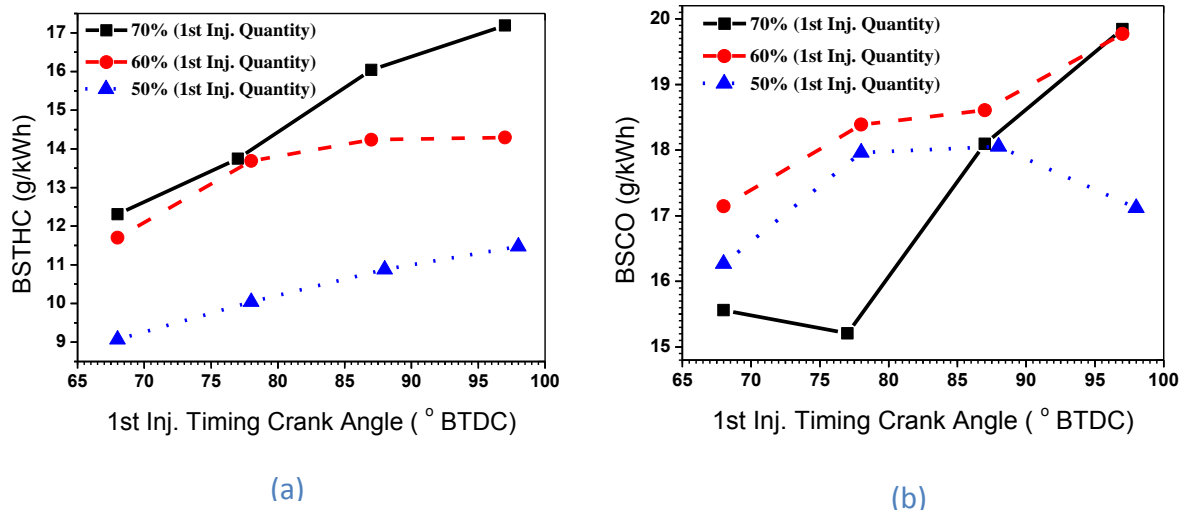


Figure 6.19 Effect of different first injection quantity-ratios on emissions, 3bar BMEP. (a) Brake specific total HC; (b) and brake specific CO.

6.3.3. Effect of the Second Injection Timing

Figure 6.20 shows the in-cylinder pressure, heat release rate and injection pulse for different second injection timings. The first injection-timings were fixed at 68° BTDC while the first injection quantity-ratios were fixed at 30%. It can be seen that the combustion phasing varied with the changing of the second injection timing. Two heat release peaks appeared when the second injection occurred at 4° BTDC. The first peak was caused by the combustion of the first-stage injected fuels while the second peak was due to the combustion of the second-stage injected fuels. It seems the ignition started immediately after the second injection began in this case. With the advancing of the second injection timing, the combustion of two stage injected fuels overlapped with each other and only one heat release peak was observed.

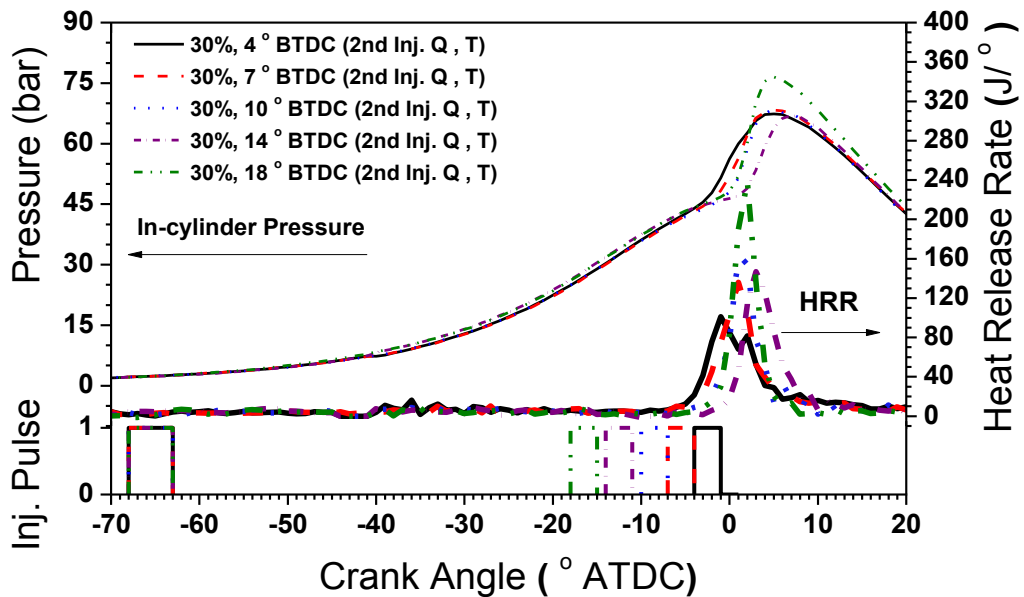


Figure 6.20 In-cylinder pressure, heat release rate and injection pulse for different second injection timings at 3 bar BMEP; second injection quantity ratio: 30%; first injection timing: 68° BTDC

It is shown in Figure 6.21 that the combustion phasing was retarded as the second injection timing was advanced to 14° BTDC. This phenomenon was quite different from the single injection case, introduced in section 6.2, where the combustion phasing was advanced with the advancing of the injection timing. Generally, ignition of high temperature combustion in diesel engines needs a proper combination of local equivalence ratio, temperature and chemical radicals which are produced in low temperature reaction [25]. It was hard to decide from the presented results whether the ignition firstly happened with second-stage or first-stage injected fuels. A possible ignition mechanism for split injection strategy is proposed as follows: the first-stage injected fuels provide a homogeneous lean charge; however, the homogeneous mixture was too lean to be compression auto-ignited like with HCCI combustion; the second-stage injected fuels reduced the equivalence ratio of some local fuel/air mixture packets; combustion started at mixture packets which have proper equivalence ratio and temperature. This proposed ignition mechanism should be studied by optical diagnostics to verify the assumption. As expected, the variation of BSNO_x emissions

followed exactly the trend of combustion phasing when the second injection timing varied, as shown in Figure 6.21.

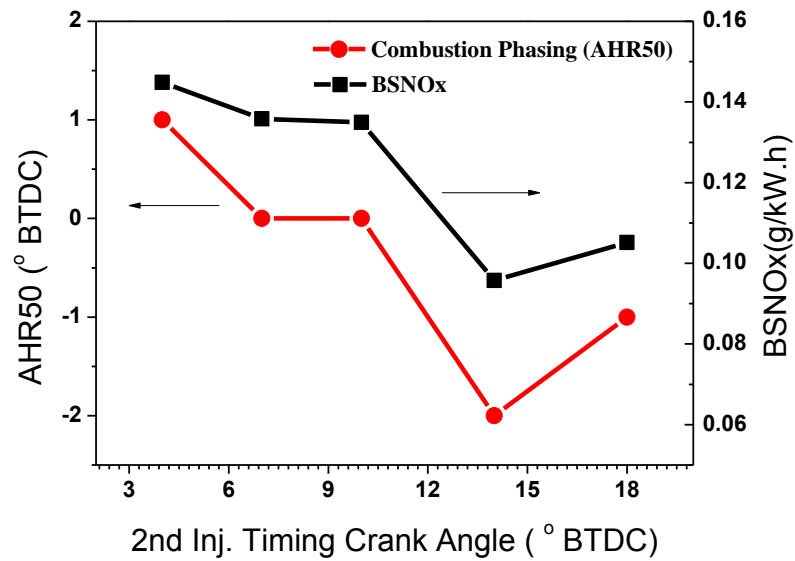


Figure 6.21 Combustion phasing (AHR50) and BSNOx emission for different second injection timings.

It is shown in Figure 6.22 that the combustion delay (interval between SOI of the second injection and AHR50) increased significantly as the second injection timing was advanced, resulting in a dramatic reduction of smoke emissions. In the best case, the smoke was just 0.04 FSN, which was around 98% lower than the single injection. As shown in Figure 6.23, the BSTHC emissions were almost the same at varied second injection timings while the BSCO doubled as the second injection timing was advanced from 10° BTDC to 14° BTDC. To conclude, compared to other injection parameters the second injection timing had the largest effect on smoke, BSNOx and combustion phasing. The first injection timing and quantity ratio had the largest effect on BSTHC and BTE.

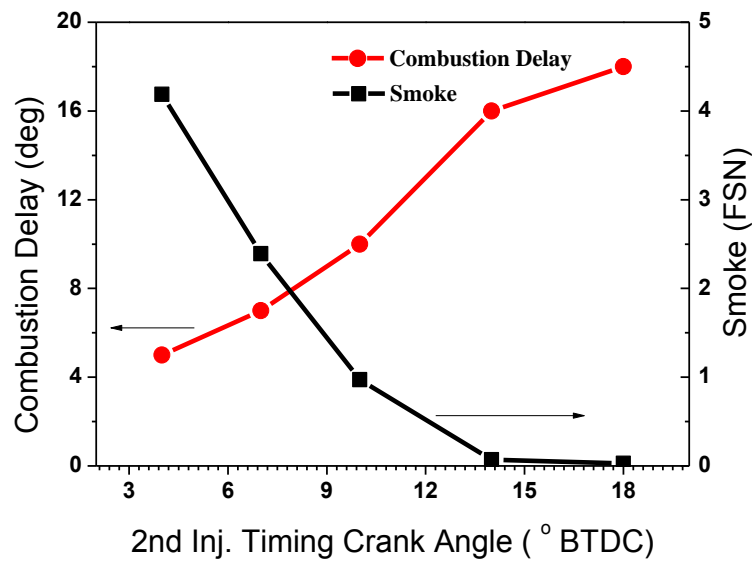


Figure 6.22 Combustion delay and smoke emissions for different second injection timings.

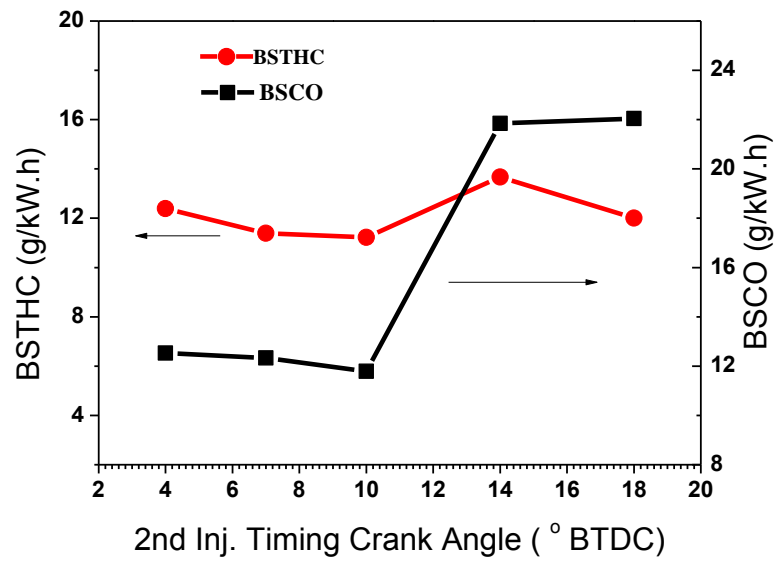


Figure 6.23 BSTHC and BSCO emissions for different second injection timings.

6.4. Conclusions

This chapter investigated different injection strategies in order to achieve PPCI combustion.

Conclusions are made from experimental results and they are as below:

Single injection

1. With advanced injection timing of 23° BTDC, high injection pressure of 1100 bar and large amounts of EGR (48%), optimized PPCI combustion was achieved with G50 at the engine condition of 1800 rpm and 3 bar BMEP. Compared to the case of baseline diesel, smoke, BSNO_x, and particle number are reduced by 98% (from 0.794 to 0.015 FSN), 87% (from 0.72 to 0.097 g/kW.h) and 99% (from 2.2×10^{14} to 2.7×10^{12} part/kW.h) respectively. The brake thermal efficiency was increased from 28.5% to 30.1%. The penalties were slightly higher BSHC (increased from 0.84 to 2.01 g/kW.h), BSCO (increased from 4.13 to 9.22g/kW.h) and MPRR (increased from 2.4 to 10.4 bar/deg). Similar results cannot be achieved with diesel,
2. As the injection timing was advanced beyond 13° BTDC, smoke and particle number emissions were reduced due to the longer combustion delay. Reducing the injection pressure from 1100 to 700 bar increased the particle total number by around 10 times,

Split injection

3. The variation of combustion phasing, smoke and BSNO_x emissions was mostly influenced by the second injection timing at a given EGR ratio. In contrast, the first injection timing and quantity-ratio had a dominating effect on BSHC emissions and brake thermal efficiency,

4. Compared to the single injection strategy, split-injection produced around 50% and 90% less BSNO_x and smoke respectively. The penalty was the reduction of brake thermal efficiency due to increased BSHC emissions,

To summarise, for both single injection and split injection, NO_x reduction depended on EGR ratio and the load extension of G50 fuelled PPCI combustion was limited by the amount of EGR and intake boosting. The experimental results show that a single injection, coupled with high EGR ratio, high injection pressure and an early injection timing of 20° BTDC to 30° BTDC is the best strategy for dieseline fuelled PPCI combustion.

CHAPTER 7

IN-CYLINDER BLENDED DIESEL/GASOLINE COMBUSTION

This chapter examines the in-cylinder blended gasoline/diesel (dieseline) combustion. The engine performance and emissions are investigated. Diesel was injected into the cylinder through a conventional common rail direct injection (DI) system and gasoline through a port fuel injection (PFI) system.

7.1. Introduction

As demonstrated in Chapters 5 and 6, dieseline combustion can significantly reduce smoke emission while the NO_x can be reduced as well if a large amount of EGR is used. This work explored the suitability of the in-cylinder blended dieseline concept, which is a combination of DI and PFI technology. The main advantage is that it allows the flexibility of on-line blending with little hardware modification.

The basic idea was to form a homogeneous gasoline/air mixture through PFI injection and utilise DI diesel to control the combustion phasing. It is slightly similar to the split injection concept in Chapter 6. However, the in-cylinder fuel blending concept avoids wall impingement of fuel spray and gives more flexibility for combustion control. This chapter firstly investigates the effect of the gasoline/diesel blending ratio, EGR ratio, DI injection timing and different engine loads. Following that, a novel stoichiometric dual-fuel compression ignition (SDCI) concept is proposed and series of tests were done. For SDCI, the engine was throttled by an EGR valve and a stoichiometric condition was maintained. This

allows the usage of a three way catalyst for NO_x, THC and CO reduction, while the smoke emission can be handled by increasing the gasoline ratio. All of the tests presented in this chapter were done on a dual-fuel single cylinder diesel engine (introduced in section 3.3), which was modified from the production 4-cylinder Ford engine.

7.2. Dual Fuel Lean Burn

7.2.1 Effect of EGR and G/ (G+D) ratio

Different EGR and gasoline percentages (G/ (G+D) ratio) were tested in this section while the combustion phasing was fixed at 5° ATDC through the adjusting of DI injection timing. The tested EGR ratios were 24%, 30%, 34%, 37% and 40%. The tested G/ (G+D) ratios were 0.25, 0.52 and 0.65 by mass. PFI gasoline injection occurred during the intake stroke (started at - 330° ATDC), which was the same as in the other tests of this chapter. The engine was operated at 1800 rpm and 4.3 bar IMEP. Baseline and optimised (for efficiency) single injection diesel tests were also performed to provide comparisons. The results are shown in table 7.1.

Table 7.1 Baseline and optimised (for efficiency) single injection diesel, 4.3 bar IMEP

EGR	AHR50 (°ATDC)	ITE (%)	MRR (bar/deg)	ISNO _x (g/kW.h)	Smoke (FSN)	ISCO (g/kW.h)	ISHC (g/kW.h)
29%	12	40.0	2.42	0.66	0.74	1.67	0.43
0%	5	42.5	8.6	5.0	0.09	1.56	0.68

Combustion Performances

Figure 7.1 shows in-cylinder pressure and heat release rate of in-cylinder blended dieseline combustion for different EGR and $G/(G+D)$ ratios. At 24% EGR, to achieve the same combustion phasing (5° ATDC), the SOI of the DI diesel were similar for different $G/(G+D)$ ratios. In terms of heat release rate shape, they were also similar to each other at a low EGR ratio (24%). As EGR and $G/(G+D)$ ratio increased, the SOI of the DI diesel needed to be advanced to keep the combustion phasing. At higher than 30% EGR, a higher portion of gasoline in the total fuel resulted in a lower heat release rate peak and longer combustion duration.

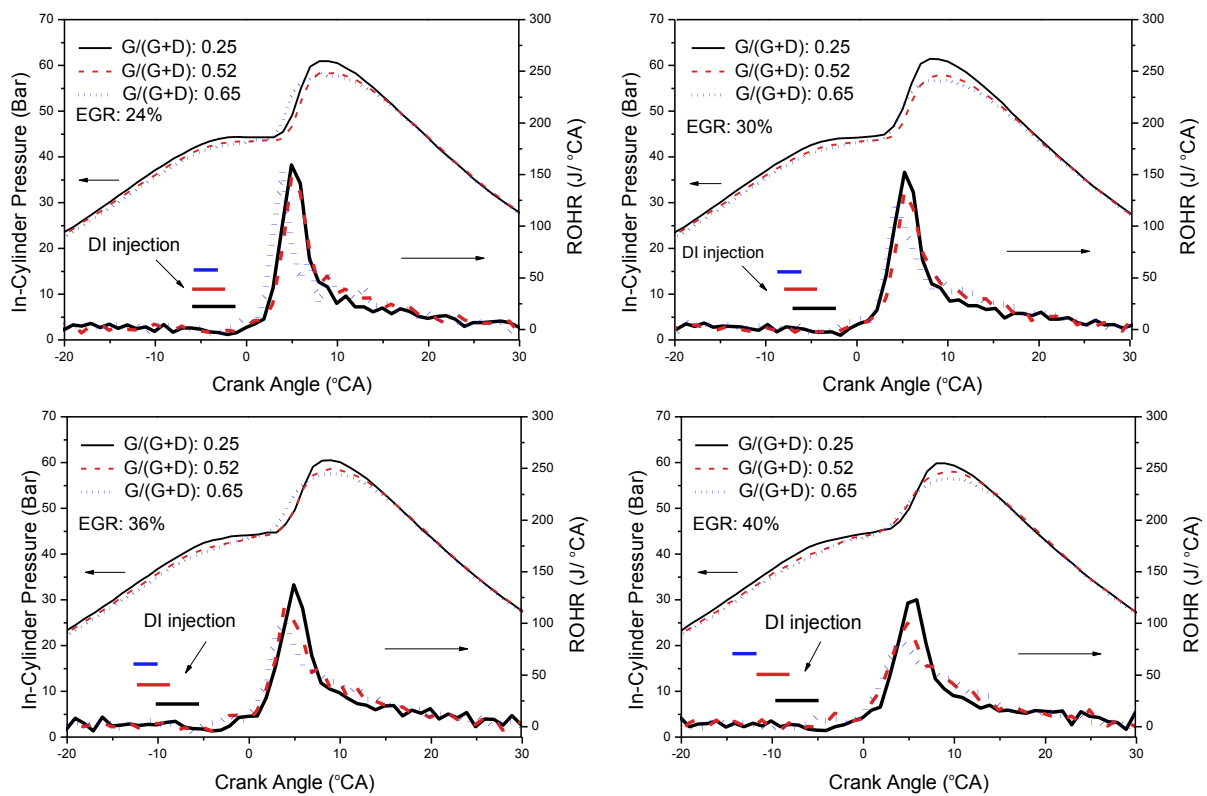


Figure 7.1 In-cylinder pressure and heat release rate of in-cylinder blended dieseline combustion for different EGR and $G/(G+D)$ ratios, IMEP 4.3 bar, AHR50 5° ATDC

Figure 7.2 presents the MPRR and combustion delay for different EGR and G/ (G+D) ratios at a fixed combustion phasing (5° ATDC). Increasing the EGR ratio from 24% to 40% helped to reduce MPRR by 2~2.5 bar/deg. A higher G/ (G+D) ratio also resulted in the reduction of MPRR. In the best case, the MPRR was 2.7 bar/deg, which was close to the case of baseline diesel. MPRR are mainly affected by combustion phasing and burning rate [24]. Since combustion phasing was fixed for all of the testing points here, the different burning rate was expected to cause the differences on MPRR as the EGR and G/ (G+D) ratio varied. A higher EGR ratio brought down MPRR because it reduced intake oxygen concentration and thus slowed the chemical reaction. In the case of higher G/ (G+D) ratio, more gasoline was fully mixed with intake air throughout the combustion chamber. The local gasoline/air mixture packets were close to the overall mixture strength, which was over-lean. The low combustion speed of over-lean gasoline/air mixtures probably reduced the MPRR when a large amount of gasoline was used. As shown in Figure 7.2, the combustion delay was prolonged by increasing the EGR ratio and G/ (G+D) ratio. At 40% EGR, the combustion delay increased from 15 to 19 deg as the G/ (G+D) ratio was raised from 0.25 to 0.65.

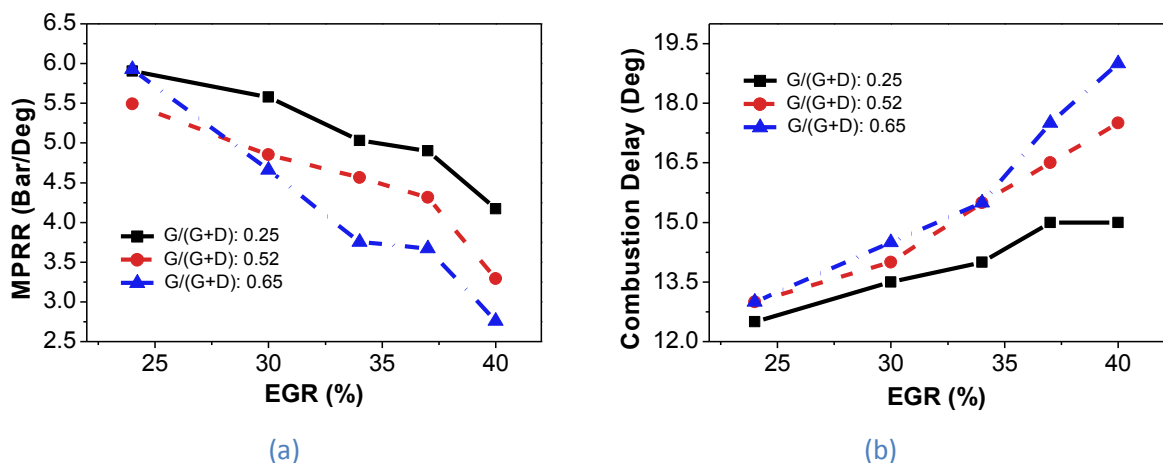


Figure 7.2 Effect of different EGR and G/ (G+D) ratios on combustion performances, IMEP 4.3 bar, AHR50= 5° ATDC. (a) MPRR; (b) combustion delay (deg).

It is shown in Figure 7.3 that, by increasing $G/(G+D)$ ratio from 0.25 to 0.65, the combustion efficiency was reduced from 96.5% to around 93% and the indicated thermal efficiency was reduced by at least 1%. Figure 7.3 indicates that the variation of EGR ratio had little effect on combustion efficiency while the indicated thermal efficiency increased by 1.5% (from 40.8 to 42.3%), at a $G/(G+D)$ ratio of 0.25, as EGR ratio varied from 24% to 37%. This was probably due to the EGR reducing the combustion temperature and thus the heat transfer to the cylinder wall. Further increasing the EGR ratio to 40% reduced the indicated thermal efficiency. For $G/(G+D)$ ratios of 0.52 and 0.65, the effect of varied EGR ratios on indicated thermal efficiency was negligible.

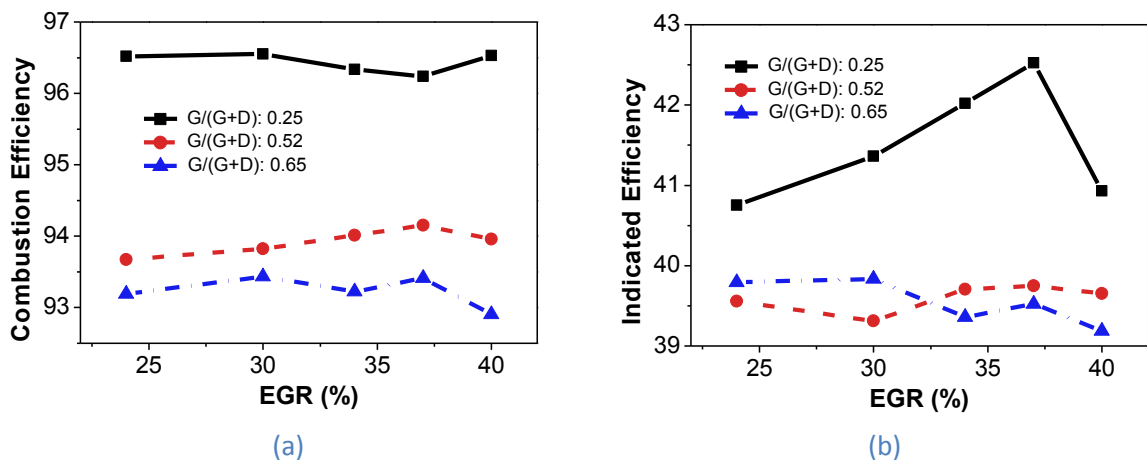


Figure 7.3 Effect of different EGR and $G/(G+D)$ ratios on engine efficiency, IMEP 4.3 bar, AHR50 5° ATDC. (a) Combustion efficiency; (b) indicated efficiency.

Emissions

Figure 7.4 demonstrates the smoke, ISNO_x, ISHC and ISCO emissions of the in-cylinder blended dieseline combustion. Like out-cylinder blending (Chapters 5 and 6), increasing the gasoline ratio of in-cylinder blending effectively reduced smoke emissions. The smoke was below FSN 0.1 over the tested EGR ratios when the gasoline mass fraction was 0.65. At lower gasoline mass fractions, increasing EGR ratios resulted in a quick increase of smoke due to

the weakened soot oxidisation process and reduced exhaust volume flow rate. The ISNO_x was also reduced by increasing the gasoline mass fraction but the reductions were small. In contrast, EGR was a more effective technique for suppressing NO_x emissions. With usage of 37% EGR, the ISNO_x was below 0.1g/kW.h at varied G/ (G+D) ratios. High ISHC and ISCO emissions were the main issues for in-cylinder blended diesel combustion. Compared to diesel baseline, ISHC and ISCO were increased by more than 10 and 4 times respectively when gasoline through PFI injection dominated the fuel energy source (65% gasoline by mass). The incomplete combustion of the over-lean gasoline/air mixture was thought to be the reason for this. Varied EGR ratios showed little effect on ISHC emissions while there was no specific trend for ISCO emissions.

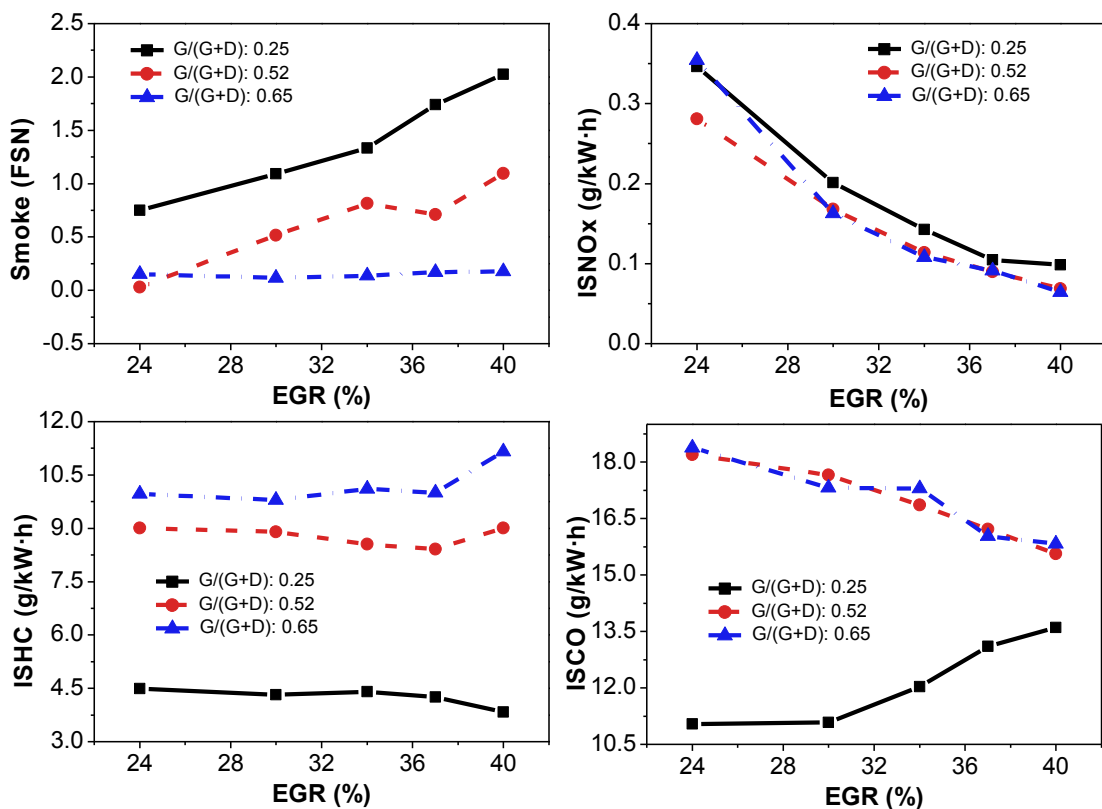


Figure 7.4 Smoke, ISNO_x, ISHC and ISCO for different EGR and G/ (G+D) ratios, IMEP 4.3 bar, AHR50 5° ATDC.

7.2.2. Combustion Phasing Sweep

In this section, the combustion phasing was swept from 1° to 9° ATDC by adjusting the diesel injection timing while the EGR and $G/(G+D)$ ratios were fixed at 36% and 0.52 respectively. It is shown in Figure 7.5 that the start of in-cylinder blended dieseline combustion can be very well controlled by the SOI of the DI diesel. With retarded diesel injection, the combustion phasing was retarded and the maximum in-cylinder pressure (P_{\max}) was reduced by up to 15 bar. A low temperature flame was observed from the heat release rate curve at each testing condition.

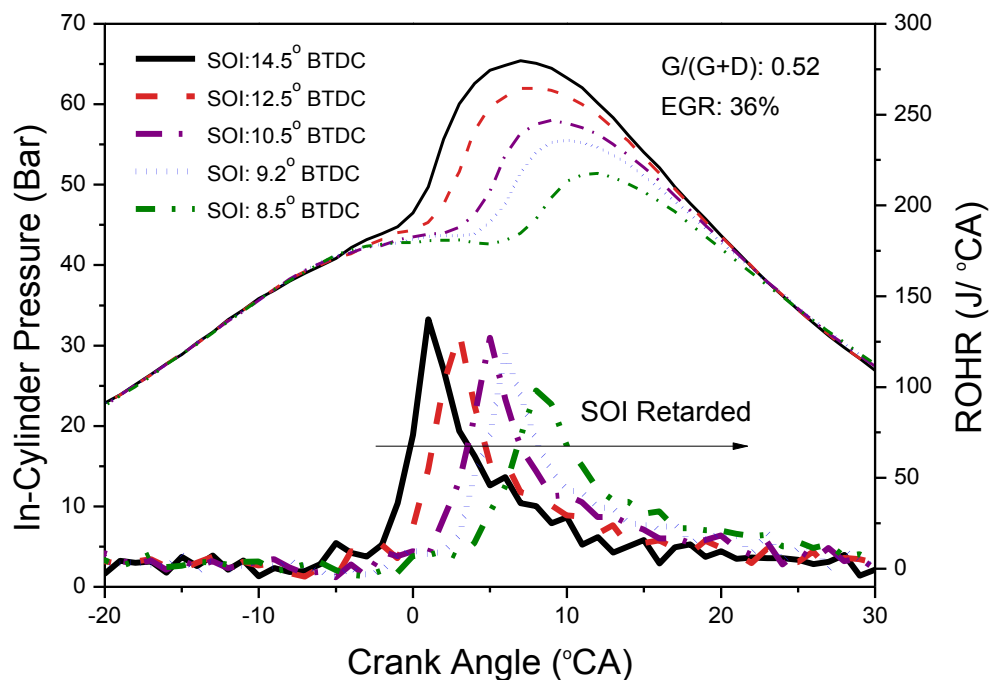


Figure 7.5 In-cylinder pressure and heat release rate for different combustion phasing, IMEP 4.3 bar, EGR 36%, $G/(G+D)$ 0.52.

The main objective of retarding combustion phasing was to reduce MPRR which indicates combustion noise. High combustion noise is unacceptable from a customer's point of view. Figure 7.6 shows that the MPRR was more than halved (from 5.9 to 2.6 bar/deg) by retarding combustion phasing from 1° to 9° ATDC, as pressure rise caused by compression and

combustion were separated from each other when the combustion phasing was retarded to well after TDC. The combustion delay was prolonged by around 2 CAD as combustion phasing was retarded from 1° to 9° ATDC.

The indicated thermal efficiency was penalised by 1.2% (from 40.2 to 39%) as combustion phasing was retarded from 1° to 9° ATDC. The reduced indicated thermal efficiency was due to the lowered expansion ratio when the combustion phasing was well after TDC. It seems that the variation of combustion phasing had little effect on combustion efficiency.

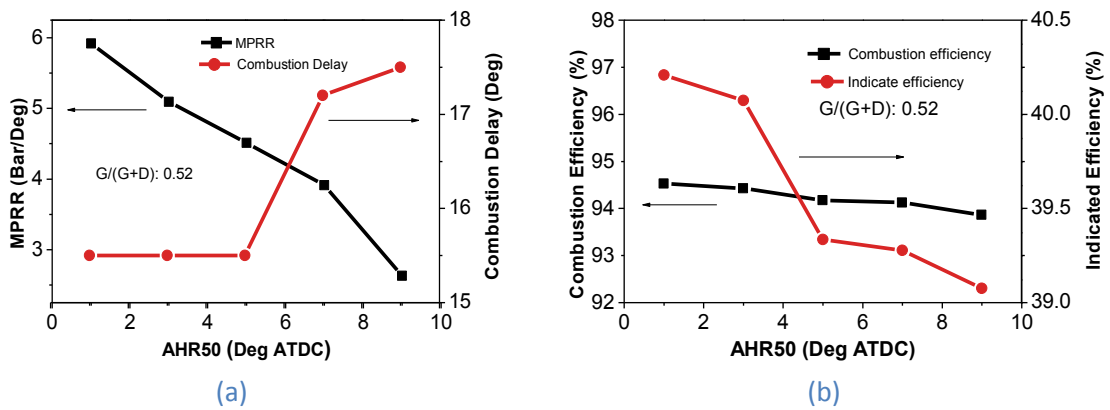


Figure 7.6 Effect of different combustion phasing on engine performances, IMEP 4.3 bar, EGR 36%, G/(G+D)=0.52. (a) MPRR and combustion delay; (b) combustion efficiency and indicated efficiency

Figure 7.7 demonstrates the smoke, ISNO_x, ISCO and ISHC emissions for different combustion phasing. By retarding combustion phasing from 1° to 9° ATDC, the ISNO_x was reduced by 40% due to the lower combustion temperature. Similar to the findings in the previous chapter (Chapter 6, section 6.2.1), the smoke emissions peaked at AHR50 of 5° ATDC. Advanced and retarded combustion phasing reduced the smoke emissions. The ISHC and ISCO emissions increased but on a minor scale as combustion phasing was retarded, due to the lower combustion temperature and incomplete oxidization of the HC and CO.

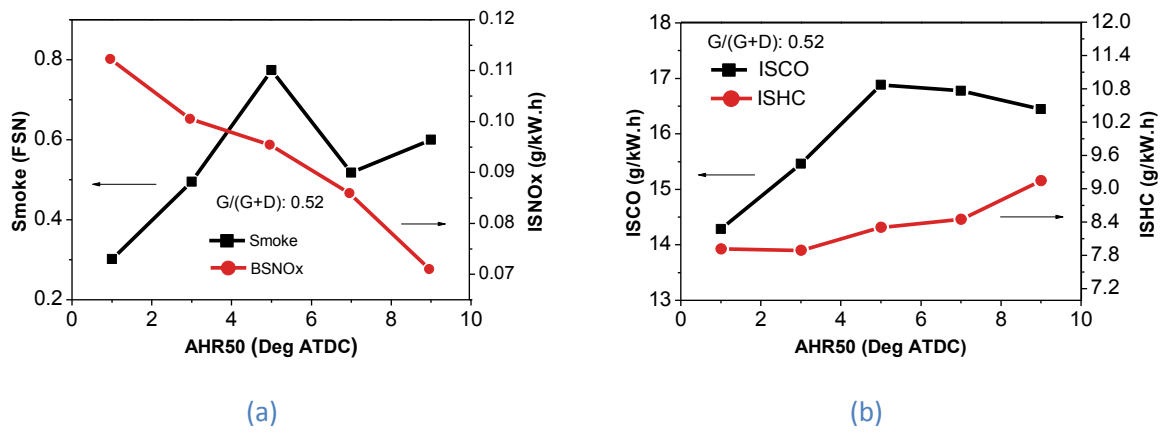


Figure 7.7 Effect of different combustion phasing on emissions, IMEP 4.3 bar, EGR 36%, G/(G+D) 0.52. (a) Smoke and ISNOx; (b) ISCO and ISHC.

7.2.3. Load Sweep

This section examines the performances of in-cylinder blended dieseline combustion at varied loads. The injection quantities of diesel were chosen as 6.2 mg and 7.9 mg per engine cycle. The injection quantities of gasoline were adjusted to achieve 2.1 bar, 3 bar, 4.3 bar, 5.2 bar, 6 bar and 7 bar IMEP respectively. The injection timings of the diesel were fixed at 5° BTDC for 2.1 bar, 3 bar, 4.3 bar and 5.2 bar IMEP. For 6 and 7 bar IMEP, the diesel injection timings were advanced by 2 and 4 CAD respectively to keep the AHR50 within 10° BTDC. Otherwise, the combustion phasing would be too late and the combustion variation was too high (COV of IMEP was more than 6%). The EGR ratios were fixed at 22%. The objective of these tests was to investigate the feasibility of controlling engine load by changing gasoline mass flow rate and the characteristics of combustion and emission when the engine load was varied.

Figure 7.8 presents the G/ (G+D) ratio, AHR50, lambda and MPRR when the engine load was varied by changing the gasoline mass flow rate. At 2.1 bar IMEP, the gasoline mass flow rate was zero and only 7.9 mg/cycle diesel injection quantity was tested. At the highest load of 7 bar IMEP, the gasoline mass fractions were more than 70%. The combustion phasing was

retarded as the engine load increased, because of the reduced intake oxygen concentration. At a higher engine load, the exhaust contained less oxygen. For example, the exhaust oxygen concentration was 15.6% and 1.8% at 2.1 bar and 7 bar IMEP respectively. Since the EGR ratio was fixed at 22%, lower exhaust oxygen concentration brought down the intake oxygen concentration. Another possible reason was the vaporization of gasoline cooled down the charge and reduced the in-cylinder temperature. Due to the retarded combustion phasing, the MPRR decreased as the engine load increased. Lower diesel injection quantity generally brought down the MPRR as well (by a maximum 19%). As the engine load increased to 7 bar IMEP, the air excess ratio (λ) went down to 1.06, which means the engine was almost operated at stoichiometric condition.

Figure 7.9 demonstrates the in-cylinder pressure and heat release rate for an engine condition of 2.1, 4.3 and 7 bar IMEP when the diesel injection quantities were fixed at 7.9 mg per engine cycle. At 2.1 bar IMEP, only diesel was injected into the cylinder. At 4.3 and 7 bar IMEP, the gasoline mass flow rate was increased to achieve the targeted engine load. With higher gasoline mass flow rate, the curve of heat release rate had a longer tail, which was the combustion of the fully premixed gasoline.

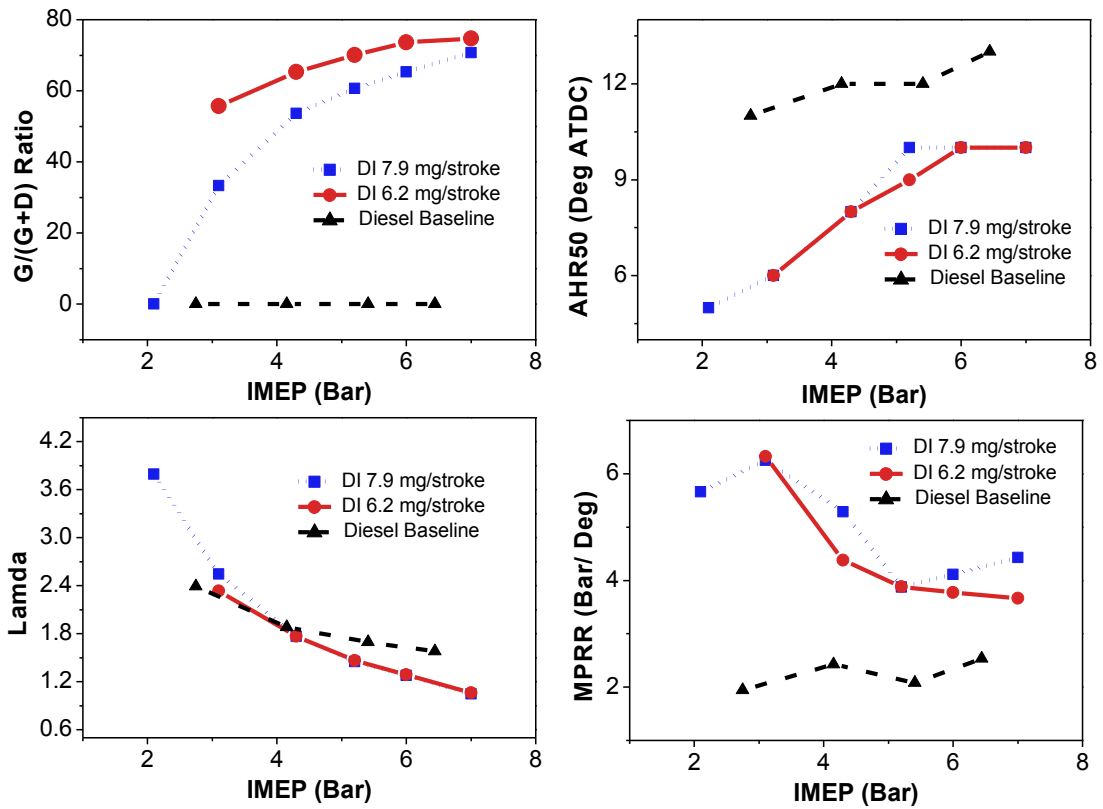


Figure 7.8 Combustion characteristics for varied engine loads, EGR 22%

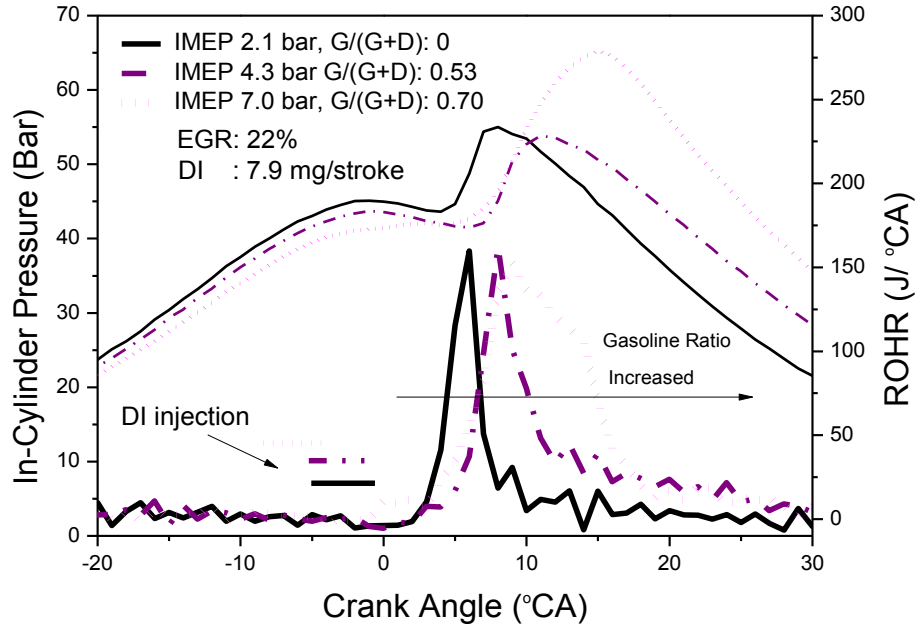


Figure 7.9 In-cylinder pressure and heat release rate for 2.1, 4.3 and 7.0 bar IMEP, EGR 22%, DI quantity 7.9 mg/stroke.

It is shown in Figure 7.10 that the smoke emissions of in-cylinder blended dieseline combustion were below FSN 0.3 for up to 6 bar IMEP engine condition. At 7 bar IMEP, the

smoke was FSN 0.9 for 6.2 mg/cycle diesel injection quantity. This was due to the air excess ratio being low ($\lambda \approx 1$) and diesel was injected when the cylinder temperature almost peaked, which was 9° BTDC. The ISNO_x emissions decreased to less than 0.2 g/kW.h as the engine load increased to 7 bar IMEP, which was due to the reduced intake oxygen concentration and retarded combustion phasing. As expected, the ISHC and ISCO emissions of in-cylinder blended combustion were much higher than the case of diesel baseline. From 2.1 bar (zero gasoline) to 3 bar IMEP (33% gasoline) engine load, the ISHC and ISCO emissions increased by more than 6 and 3 times respectively. However, as the engine load increased further, the ISHC and ISCO emissions decreased, which was due to higher combustion temperature and richer gasoline/air mixture.

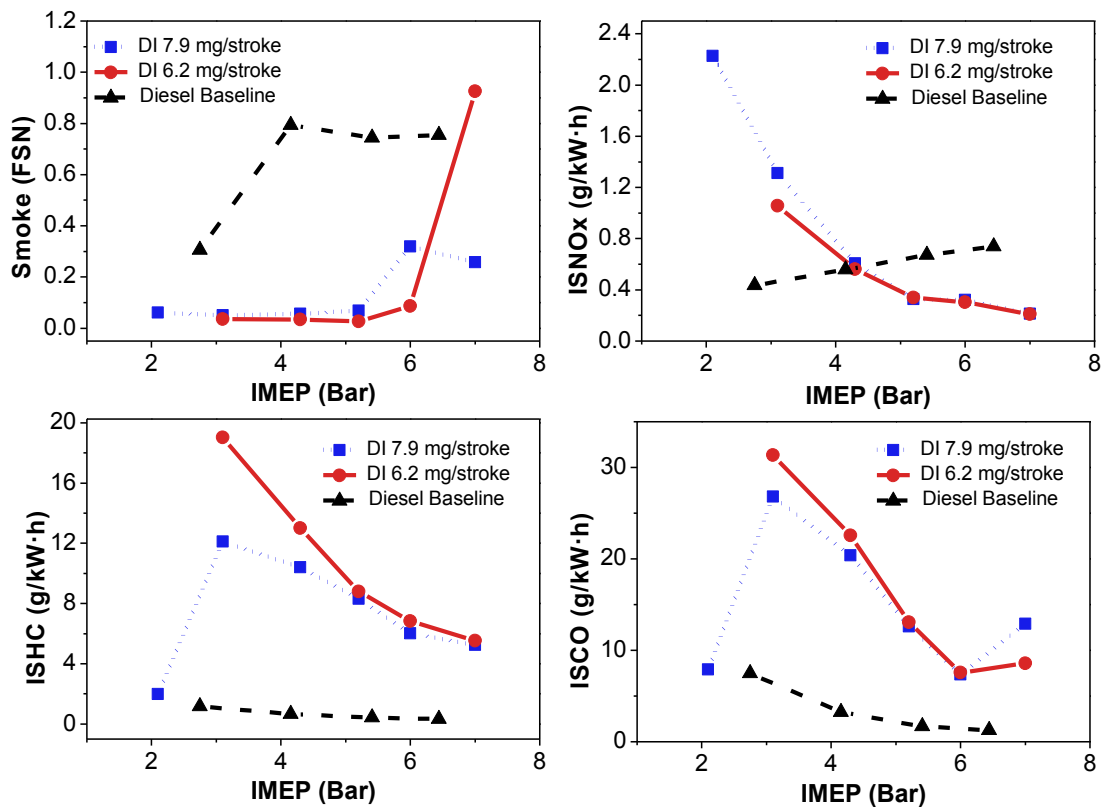


Figure 7.10 Emission characteristics for varied engine loads, EGR 22%.

Figure 7.11 shows the combustion efficiency and indicated thermal efficiency for various engine loads. Generally, the combustion efficiency of in-cylinder blended diesel combustion was 10% to 4% (absolute value) lower than diesel baseline depending on the engine loads and DI injection quantity. As explained in the last paragraph, at low engine loads, the over-lean gasoline/air mixtures resulted in incomplete combustion and low combustion efficiency. At higher loads, the combustion efficiency increased due to the richer gasoline/air mixture and higher combustion temperature. Regarding the indicated thermal efficiency (ITE), below 4.3 bar IMEP, diesel's ITE was 1.5% (absolute value) lower than diesel. Beyond 4.3 bar IMEP, the difference of ITE between diesel and diesel became small. It should be noted that the ITE at 2.1 bar IMEP was high because only diesel was injected and its combustion phasing was advanced by 6 CAD compared to diesel baseline.

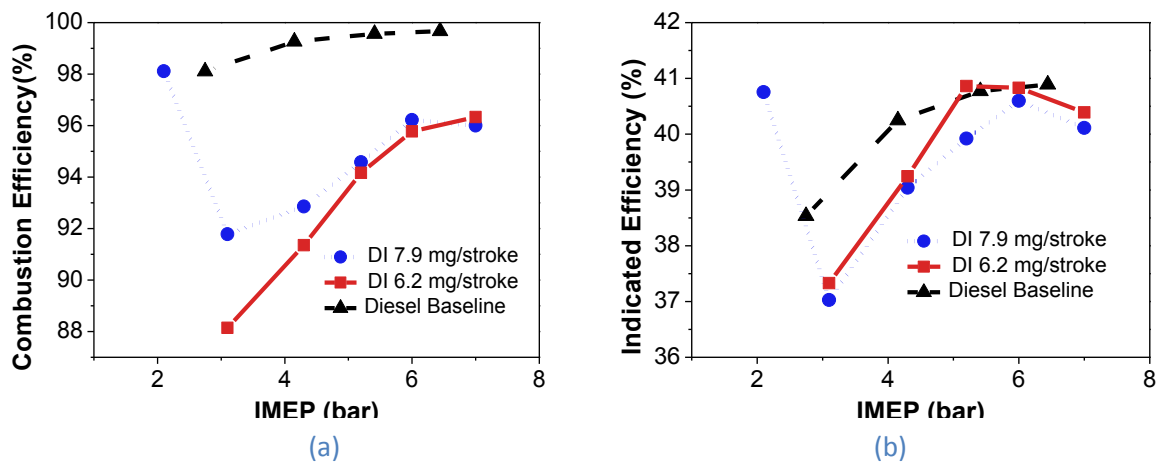


Figure 7.11 Effect of varied engine loads on engine efficiency, EGR 22%. (a) Combustion efficiency; (b) indicated efficiency.

To summarise, in-cylinder blended diesel combustion was proven to be effective in reducing smoke emissions while the combustion phasing was directly controlled by DI injection timing. The NO_x emissions can be reduced significantly as well if a large amount of EGR is used and there were no penalties of efficiency and smoke emission. At low engine loads (below 4.3 bar IMEP), the in-cylinder blended diesel combustion gives 1.5% lower

ITE than diesel baseline but at higher loads the reduction of efficiency for diesel combustion was small and negligible.

7.3. Stoichiometric Dual- Fuel Compression Ignition

7.3.1. Introduction

It has been demonstrated in previous sections of this thesis that the NO_x emissions of compression ignition engines cannot be dramatically reduced by strengthening fuel premixing combustion, either with out-cylinder (Chapters 5 and 6) or in-cylinder (Chapter 7, section 7.2) diesel blending. The NO_x reduction highly relied on increasing the EGR ratio and retarding the combustion phasing. However, the usage of high EGR ratio limited the engine maximum load while the engine efficiency was reduced by retarding the combustion phasing.

In this section, a novel new concept named stoichiometric dual-fuel compression ignition (SDCI) is proposed to handle NO_x emissions without any compromises of maximum engine load, fuel efficiency and smoke emission. The author used EGR in SDCI combustion, not as a conventional way of suppressing NO_x emissions as a main purpose, but as an alternative of throttling to control the intake charge and maintain the engine under stoichiometric operation, which enabled the usage of a three-way catalyst (TWC) for handling NO_x, HC and CO emissions. The cost of a TWC is relatively lower than a DOC and SCR because of the mature mass production. A stoichiometric compression ignition engine using diesel has been researched by several organisations [116-119]. However poor fuel efficiency and high smoke emissions due to the incomplete oxidization were reported as the main challenges. These problems can be resolved by using gasoline through PFI injection as the main fuel energy source. It is presented in section 7.2.1 and 7.2.3 that low smoke emissions and high fuel efficiency can be maintained even at a stoichiometric engine condition if gasoline dominated

the fuel energy source. Therefore in the present section, the engine used the stoichiometric mixture ratio (total λ) with the possible highest gasoline percentage (limited by the hardware and combustion stability), where the diesel was used to create multiple-point ignition to suppress knocking of gasoline combustion.

The current study was carried out on a single-cylinder dual fuel diesel engine as introduced in section 3.3. The engine was operated at 1800 rpm and at least 3-minute running time was conducted before the emission sampling. The coolant temperature was maintained at 80 °C. For each testing point, the EGR ratio was adjusted to control the engine load while maintaining a stoichiometric air-fuel ratio. The fuel economy, thermal efficiency, heat release rates, NO_x/HC/CO emissions and PM emissions were studied. Firstly, an engine load sweep test was conducted and then the effect of gasoline percentage and DI injection timing were examined.

7.3.2. Engine Load Sweep

The SDCl diesel engine was operated in a load range from 4.3 bar to 8 bar IMEP. During the test, the possible minimum amount of diesel (limited by the hardware and the combustion) was used to suppress the smoke emissions while stable and phase-controllable combustion was maintained. AHR50 was monitored and the combustion phasing was always controlled and adjusted to the highest efficiency range, under the constraint of MPRR of 12 bar/°CA or the peak pressure of 100bar. With a fixed DI diesel quantity, the AHR50 can be advanced by earlier injection timing but not beyond a certain range determined by the fuel quantity and the running conditions. Increasing the diesel injection quantity will extend the controllable injection timing range. For example, at 4.3 bar IMEP, the combustion seemed to be chemically kinetic controlled like HCCI and unstable when less than 9.7 mg/cycle DI quantity was used, because the EGR ratio needed to be high (47%) and combustion temperature was

relatively low at that load, which resulted in lower diesel fuel reactivity at a given DI quantity. The optimised DI timing, DI quantity, EGR ratio and gasoline percentage of the load sweep test are listed in table 7.2.

Table 7.2 DI timing and gasoline percentages in the load sweeps.

IMEP (bar)	4.3	5.2	6.2	7.0	8.0
DI Timing (°CA BTDC)	27	27	27	14	9
DI Quantity(mg/cycle)	9.7	7.4	5.7	5.7	5.7
EGR Ratio	47%	38.8%	29.7%	25.0%	19.1%
Gasoline Percentage	40%	63%	77%	79%	81%
AHR50 (° CA ATDC)	4	3	3	3	8

Figure 7.12 shows the in-cylinder pressure and rate of heat release for the different engine loads tested. Using gasoline in a high compression ratio (more than 12:1) is challenging for a spark ignition (SI) engine due to the knocking issue. The pressure traces of SDCI combustion are smooth and indicate no signs of knocking. It is supposed that was due to the volumetric ignition of gasoline/air mixtures through diesel combustion. The AHR50 was controlled within the range from 3° CA to 4° CA after top dead centre (ATDC) except for the load of IMEP 8.0 bar. When the IMEP was 8 bar, the AHR50 was retarded by delaying the injection timing of the diesel in order to limit the peak pressure under 100 bar for this load condition. At 4.3, 5.2 and 6.2 bar IMEP, the heat release rate curve of SDCI combustion appears as a mono-peak profile, where the combustion of diesel and gasoline overlapped. For the cases of 7.0 and 8.0 bar IMEP, two peaks of high temperature heat release were observed. The first peak was the auto-ignited diesel combustion. The second peak was sharp, which is a sign of flame propagation led by multi-point ignition in large areas. The differences between the three lower-load cases and the two higher-load cases resulted from the variations in combustion temperatures, EGR ratios and diesel/gasoline fuel quantity.

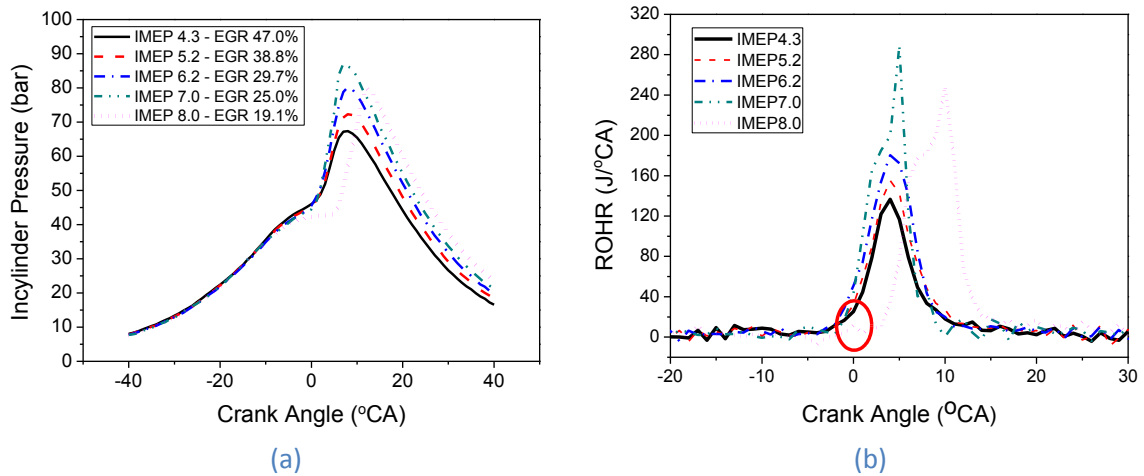


Figure 7.12 SDCl Combustion analysis as the engine load sweeps. (a) In-Cylinder pressure; (b) heat release rate.

Figure 7.13 shows the combustion duration and the MPRR. The shortest combustion duration was 7 $^{\circ}$ CA at 7 bar IMEP while the MPRR peaks at 11 bar/ $^{\circ}$ CA. At lower engine loads, the combustion duration increased and MPRR decreased because of the higher EGR ratio. At 8 bar IMEP, the combustion phasing was retarded by around 5 $^{\circ}$ CA compared to the other loads, for the consideration of mechanical safety, as mentioned above. Thus the case of 8 bar IMEP had longer combustion durations and a lower MPRR of about 7 bar/ $^{\circ}$ CA.

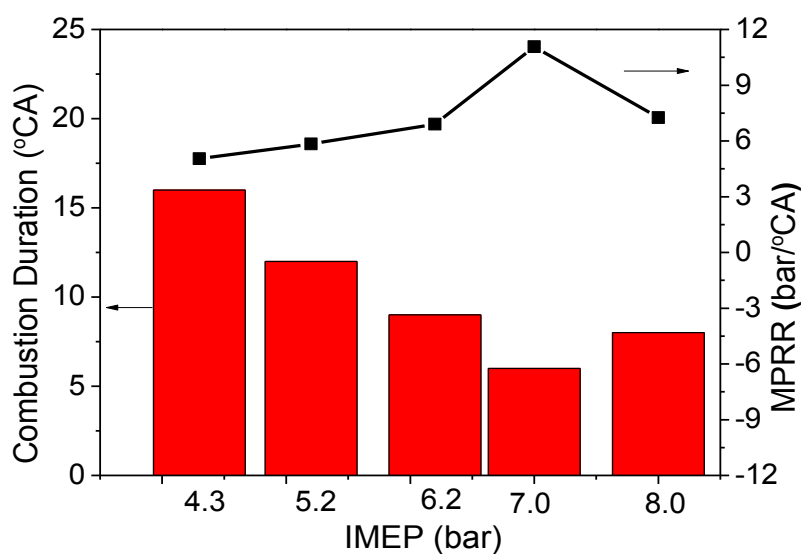


Figure 7.13 Combustion duration and maximum pressure rise rate (MPRR) of load sweeps

Figure 7.14 presents the indicated thermal efficiency (ITE) and ISFC of SDCI combustion at various engine loads. The diesel baseline results are also shown in the figure to provide comparisons between SDCI and conventional diesel combustion. The lowest ITE of SDCI combustion was 39.8% (at 4.3 bar IMEP), which was comparable to diesel baseline. The corresponding ISFC was 209.3 g/kW.h. As the engine load increased, the ITE achieved 43.7% at 7 bar IMEP. The corresponding ISFC was 190.8 g/kW.h, which was 12g/kW.h better than the case of diesel baseline. At 8 bar IMEP, due to the retarded combustion phasing, the ISFC of SDCI combustion increased a bit but was still significantly lower than diesel baseline.

In general, the experimental results showed that the SDCI combustion had better fuel economy than conventional diesel combustion. Given the fact that the current engine configuration was designed for conventional diesel combustion, the fuel efficiency of SDCI combustion can be potentially further improved with engine optimization.

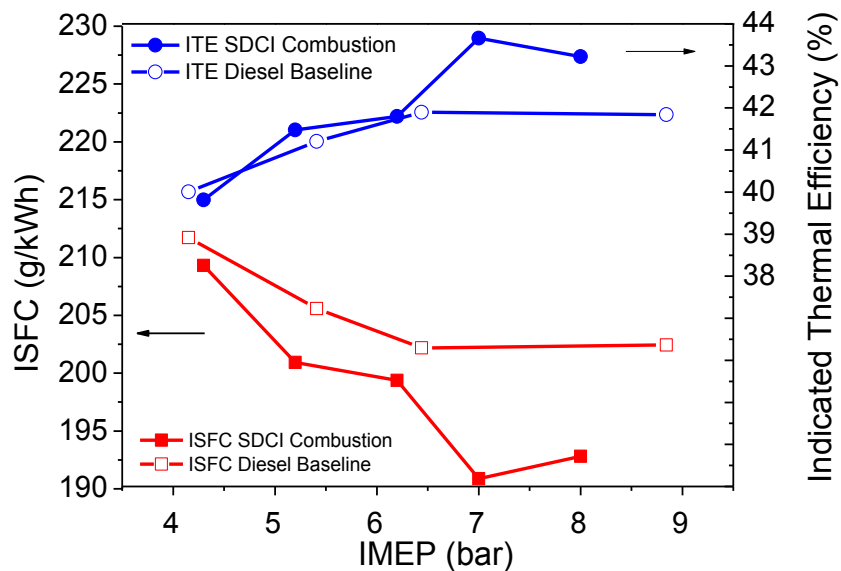


Figure 7.14 Indicate specific fuel consumption (ISFC) and indicated thermal efficiency (ITE)

Figure 7.15 shows the gaseous emissions of SDCI combustion. Due to the fully mixing of gasoline and air, SDCI combustion had higher ISHC and ISCO emissions than diesel baseline. With the increasing of engine load, the ISHC and ISCO emissions decreased because of higher combustion temperature and richer gasoline/air mixture. Until 7 bar IMEP, the NO_x emissions of SDCI combustion were lower than diesel baseline due to the high EGR ratio. At 8 bar IMEP, the NO_x emissions of SDCI combustion were around 0.9g/kW.h and this value was expected to be much higher if the engine load was further increased. The exhaust temperature was found to be above 300 degrees C at all of the tested engine conditions. So the HC, CO and NO_x emissions can be handled by a three-way catalyst since the engine was under stoichiometric operation and the exhaust temperature was higher than the light-off temperature of TWC at tested loads. The gaseous emissions should not be a concern for SDCI combustion here.

The combustion efficiency of SDCI combustion is shown in Figure 7.16. Generally, SDCI had 3% to 6% (absolute value) lower combustion efficiency than the case of diesel baseline depending on the load. For the lower loads, the combustion efficiency was below 94% but at high loads it was generally in the typical range of the combustion efficiency for an SI engine (around 95% ~98%) [24].

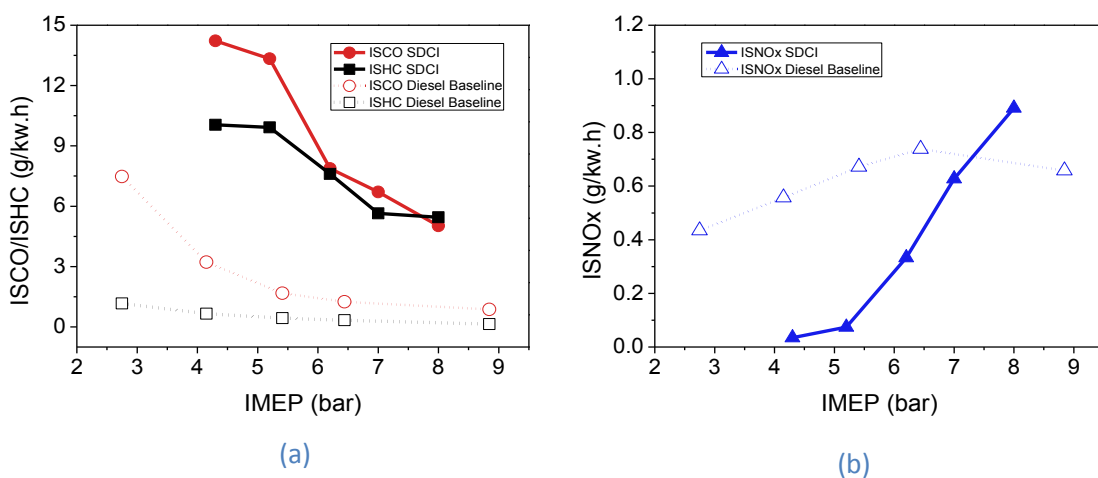


Figure 7.15 Gaseous emissions of SDCI combustion for different engine loads. (a) ISCO and ISHC; (b) ISNO_x

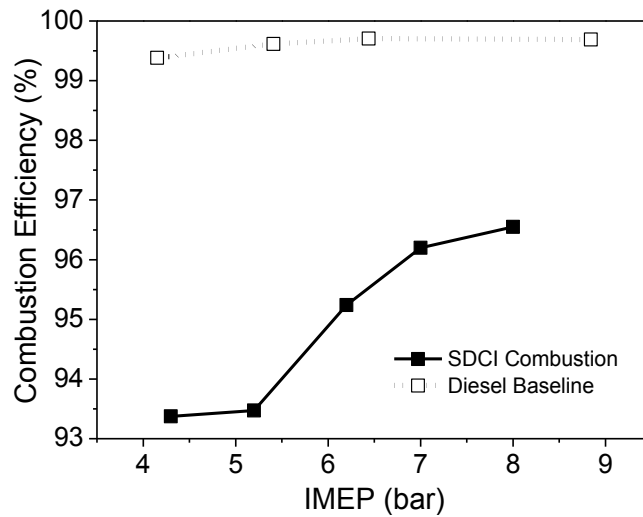


Figure 7.16 Combustion efficiency of SDCI combustion for different engine loads.

Figure 7.17a shows the particle number size distributions of SDCI combustion. The two peaks that appear in every curve generally refer to the nucleation and accumulation mode particles. The three lower load cases were similar to each other: nucleation peak (at particle size 15 nm) was higher than accumulation peak (at particle size of 50 nm). For the two higher IMEP cases (7 and 8 bar), the accumulation peak, which was at 65 nm, was higher than nucleation peak.

Figure 7.17b shows the normalised total number of nucleation and accumulation mode particles. The comparison between SDCI and diesel baseline is only made in terms of accumulation mode particles because the nucleation mode data is less repeatable due to high volatilities [32]. Generally, SDCI combustion produced less accumulation mode particles than diesel baseline, particularly for the three lower load cases. The lowest particle total number was at 6.2 bar IMEP, because the DI quantity was small (5.7 mg/cycle) and injection timing was early (27° BTDC), which resulted in long combustion delay and long mixing time. At 7 and 8 bar IMEP, a small DI quantity (5.7 mg/cycle) was maintained but the particle total number increased by around 10 times. Due to the reduced EGR ratio and increased combustion temperature, the SOI for 7 and 8 bar IMEP was retarded to 14° and 9° BTDC respectively to achieve best fuel economy. As discussed in Chapter 6, the in-cylinder ambient

temperature peaks at around 10° BTDC and the combustion delay would be shortest if fuel injection happens at that time, which causes high smoke emissions.

Figure 7.17c shows that the CMD (accumulation mode) for the three lower load cases are around 45 nm, whereas it is around 60 nm for the two higher load cases. All the SDCI data were lower than the baseline diesel results. The smoke number in Figure 17d shows a similar trend to that of CMD in Figure 17c: the smoke emissions of SDCI combustion were below FSN 0.1 until 6.2 bar IMEP and they increased sharply to FSN 0.3 for 7 and 8 bar IMEP.

It can be expected that the smoke emissions at high engine loads would be significantly reduced if the injection timing was optimised to avoid the high in-cylinder temperature region (around 10° BTDC) and injection pressure was increased (the current test used 600 bar injection pressure). Considering that PM emissions were much lower within a large load range, a smaller DPF can be used to restrict smoke emissions under legislation.

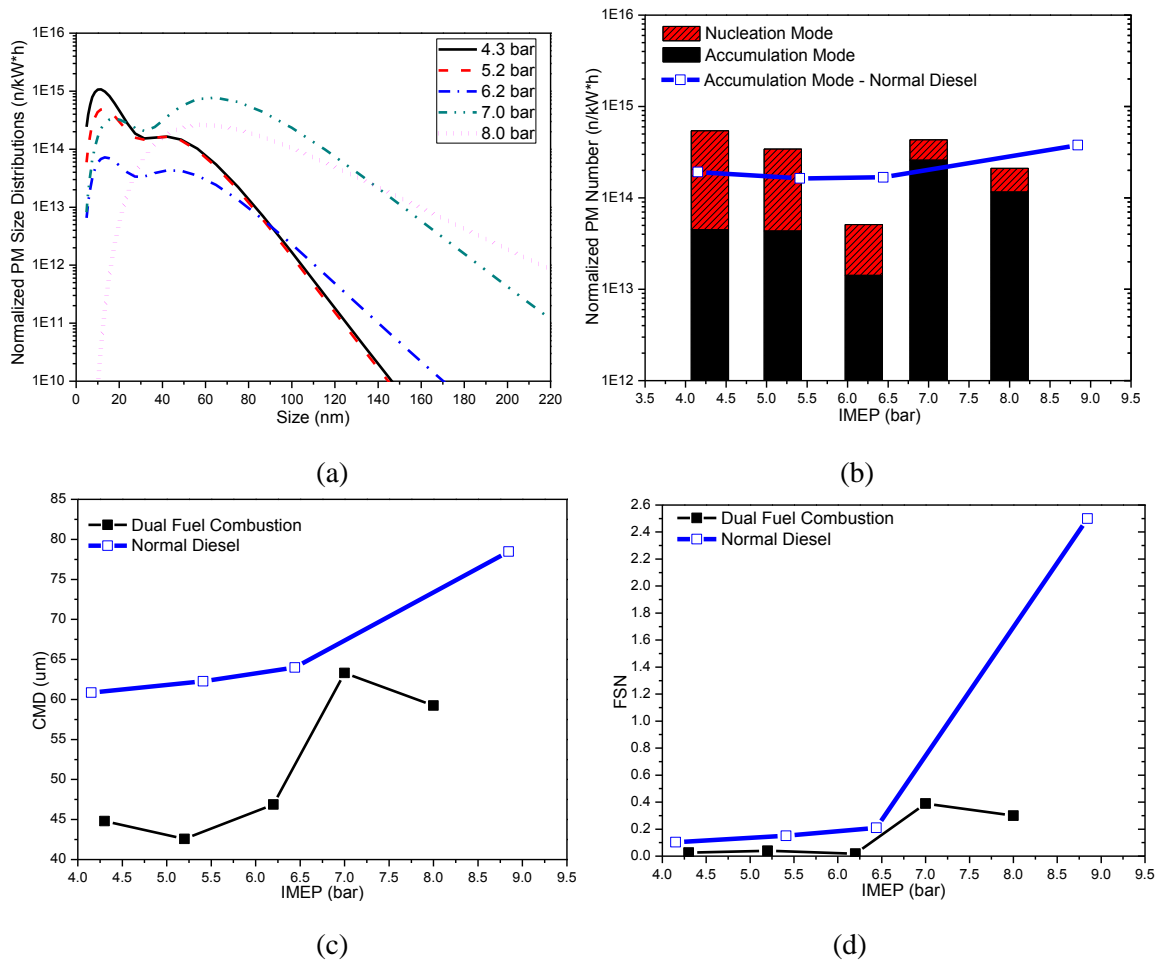


Fig 7.17 PM and FSN data (a) PM size distribution; (b) Particle numbers of the accumulation and nucleation modes; (c) CMD of accumulation mode; (d) FSN.

7.3.3. Impact of the Gasoline Percentage

In order to investigate the effect of gasoline and diesel quantity on SDCI combustion, two groups of experiments were conducted at a load of 6.2 bar IMEP and a fixed EGR ratio of 30%. In the first group, the gasoline percentage was varied with fixed diesel DI timing. In the second group, the DI diesel timing was adjusted to fix the combustion phasing at 3° ATDC while the gasoline percentage was varied. To simplify the expression, 66% gasoline over total fuel is referred to as G66.

Fixed DI Timing

Figure 7.18 shows the in-cylinder pressure traces and heat release rate for various gasoline percentages with a fixed DI injection timing of 27° BTDC. The solid black line corresponds to the case of IMEP 6.2 bar in section 3.1, which is used as the reference case here. With a lowered gasoline percentage the maximum in-cylinder pressure (P_{\max}) increased. Compared to the reference case, P_{\max} of G66 increased by 10 bar, which was caused by the advanced combustion phasing, as shown in Figure 7.18b. Reducing the gasoline percentage from 77% to 66% resulted in 4 CAD advancing of AHR50. As discussed in section 7.2.2, the fuel reactivity increased with a lower gasoline percentage and thus reduced the combustion delay.

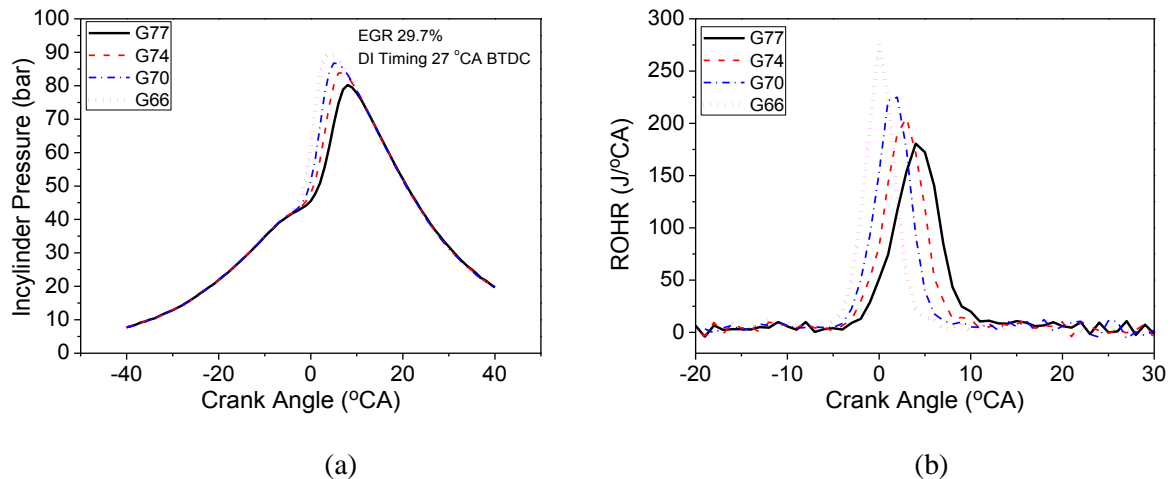


Fig 7.18 Combustion analyses at different gasoline percentages with a fixed injection timing (a) In-cylinder pressure (b) ROHR.

Figure 7.19a shows the efficiencies and ISFC of the four cases. The highest thermal efficiency and lowest ISFC were achieved with G74, which were 42.2% and 197.2 g/kW.h. It is supposed that this was due to the proper combustion phasing for G74. As discussed in Chapter 6, a too early and too late AHR50 reduces the thermal efficiency. Overall, the differences of fuel efficiency between the four cases here are small. Figure 7.19b shows the combustion durations and the MPRR. The three cases, except for the reference case (G77), had similar combustion durations at around 7° CA, indicating that using even less gasoline will not likely bring in significantly shorter combustion duration. The MPRR increased to 12

bar/deg as the gasoline percentage decreased to 66%, which was due to the advanced combustion phasing.

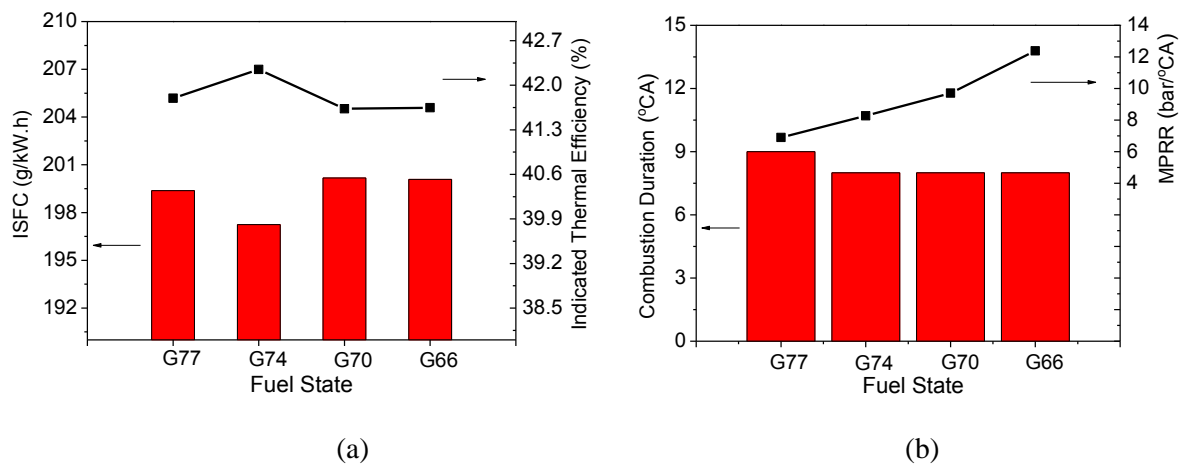


Figure 7.19 Efficiencies and combustion performances for varied gasoline percentages with a fixed DI timing (a) ISFC and ITE (b) Combustion duration and MPRR.

Fig 7.20 presents the measurement of PM emissions for various gasoline percentages. Compared to the reference case (G77) in Fig 20a, a smaller gasoline percentage led to a higher particle total number. Other than that, no significant change was observed in the size distribution trends when the gasoline percentage varied. The particle numbers of the accumulation mode decreased with the higher gasoline percentages. All the CMD results of these cases were around 50 nm and the FSN were around 0.025 and did not change much, as shown in the Figure 20c. In general, the results suggest that the combustion process was dominated by pre-mixed combustion since diesel DI injections were early (27° BTDC) and the smoke emissions were maintained at a low level.

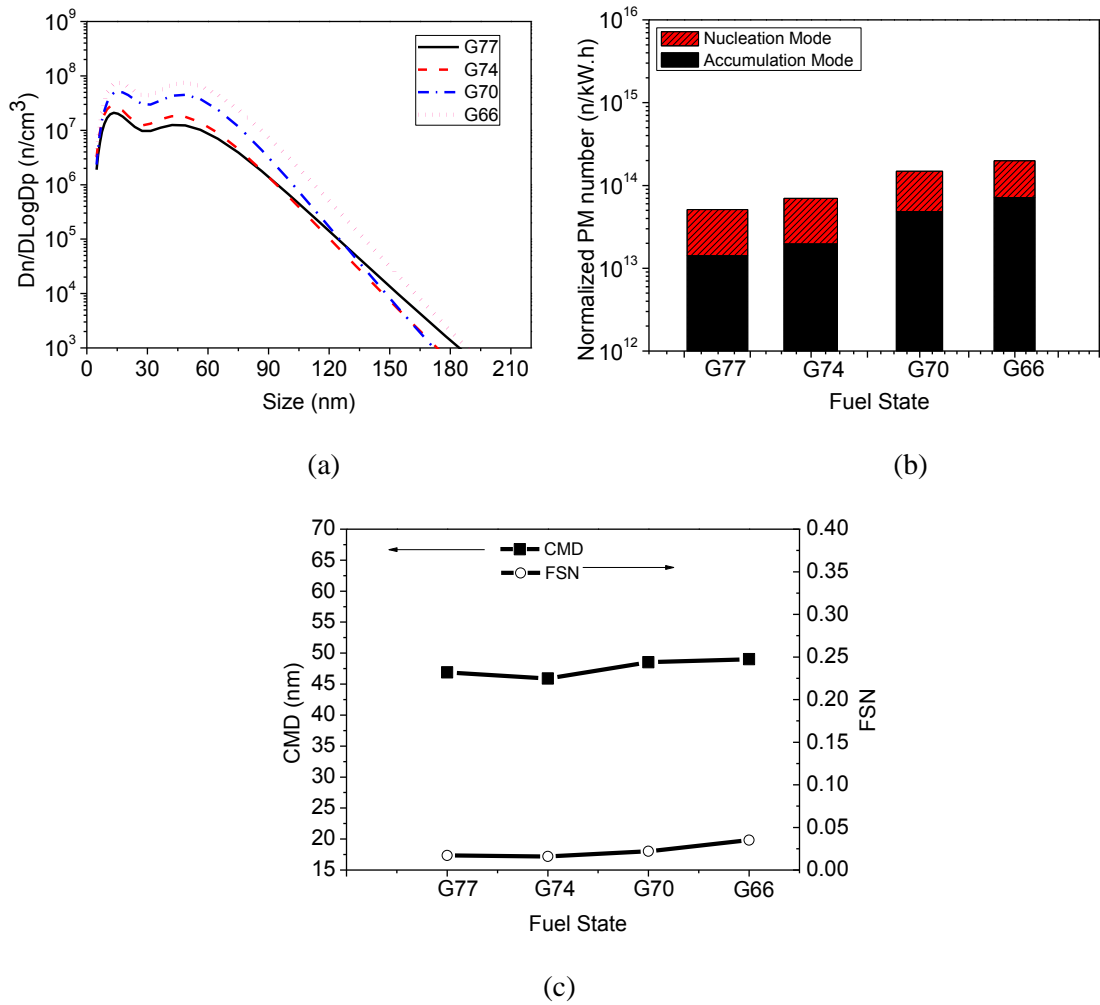


Figure 7.20 PM emissions at different gasoline percentages with a fixed injection timing (a) PM size distribution; (b) Particle number in accumulation and nucleation modes; (c) Particle count median diameter; (CMD) and smoke emission.

Fixed AHR50

To eliminate the effect of varied combustion phasing, AHR50 was fixed at 3° ATDC by adjusting the DI injection timing when the gasoline percentages were changed in this section. The DI injection timings (from the highest gasoline percentages to the lowest) were 27°, 24°, 20° and 18°CA BTDC, respectively. It is shown in Figure 7.21a that the pressure traces of the four cases are quite similar to each other. Figure 7.21b shows that, except for the case of G74, the maximum heat release rate slightly decreased with reduced gasoline percentage. Compared to the results of the previous section, the differences of pressure traces and ROHR

between different gasoline percentages were significantly reduced by fixing the combustion phasing.

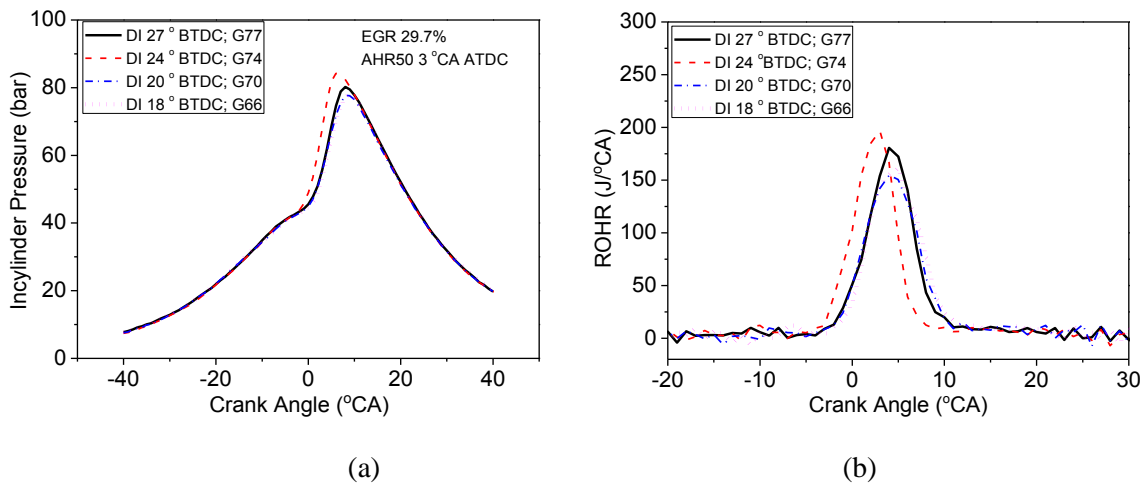


Figure 7.21 Combustion analysis at different gasoline percentages with a fixed AHR50 (a) In-cylinder pressure (b) ROHR.

Figure 7.22a shows the ITE and ISFC of different gasoline percentages with a fixed combustion phasing. In general, there is little difference between the four cases. G74 has the highest indicated efficiency of 42.5%, which was due to its earlier ignition than the other cases, as shown in Figure 7.21a. Figure 7.22b shows that the combustion durations of the four cases were in a range of 9 to 11 CAD. Reducing the gasoline percentage from 77% to 66% reduced the MPRR by 1 bar/CAD.

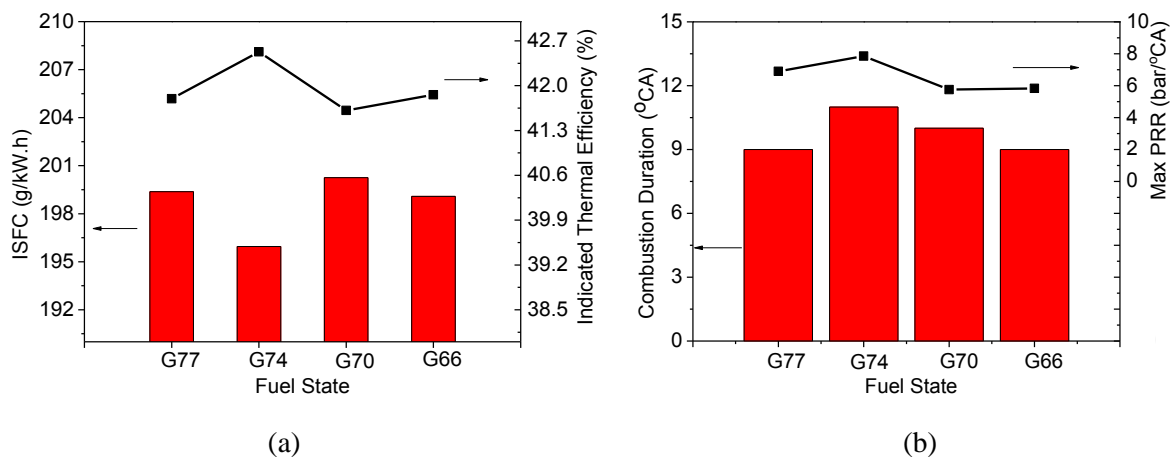


Figure 7.22 Efficiencies and combustion phase data at different gasoline percentages with a fixed AHR50 (a) ISFC and ITE (b) Combustion duration and Max PRR.

Fig 7.23 shows the PM emissions for the different gasoline percentages with the same AHR50. Compared with the reference case, a lower gasoline percentage generally resulted in higher particle numbers. It is shown in Figure 7.23a that both the peak of nucleation mode and accumulation mode particles increased with a lower gasoline percentage. In particular, the total number of accumulation mode particles increased by more than 30 times when the gasoline percentage was reduced from 77% to 66%. A similar result is demonstrated in Figure 7.23c: the smoke emissions increased sharply to 0.38 FSN and CMD increased to 60 nm with G66. The increasing of particle emissions is partly because of the higher DI diesel quantity and also due to the retarded diesel injection timing. However, the latter is the primary reason. It has been shown in the previous section 7 that in the worst case, the particle total number increased by 4 times with a higher gasoline percentage when the DI diesel injection timing was fixed. The retarded DI injection timing reduced the combustion delay of diesel and thus the mixing time.

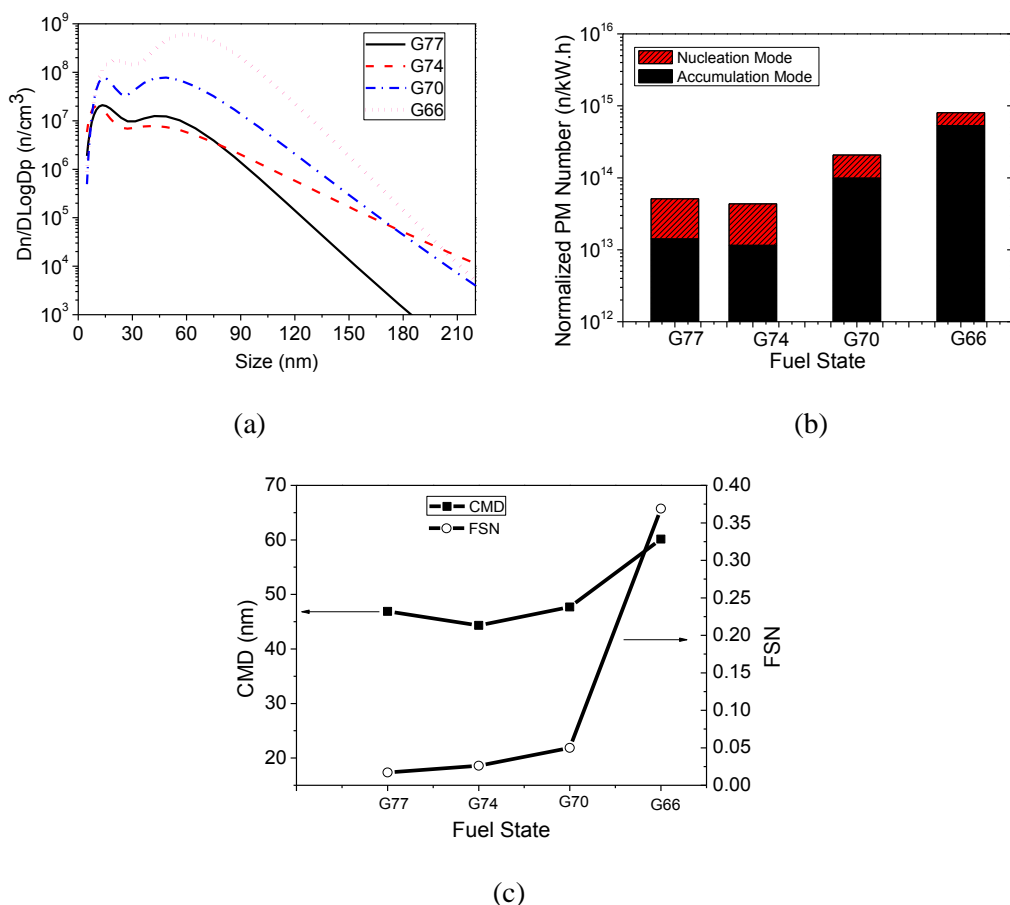


Figure 7.23 PM emissions at different gasoline percentages with a fixed AHR50 (a) PM size distribution (b) Particle number in accumulation and nucleation modes (c) CMD and FSN.

The results in sections 7.3 indicate that the gasoline percentage has a significant impact on the PM emissions of SDCI combustion. Although the DI timing exhibits larger effects, the DI diesel quantity can determine the phase-controllable range. Thus, the gasoline percentages should be carefully considered in reducing the PM emissions while the combustion is controlled for optimization of the thermal efficiency

7.3.4. Impact of DI Timing

The impact of DI timing was studied by adjusting the DI timing directly from the reference case (DI 27° BTDC) without changing the other parameters. The EGR ratio was maintained at 29.5% and the gasoline percentage was maintained at 77%. With retarding the injection timing to 20° and 17° BTDC, the P_{max} were 12 and 17 bar lower respectively, as shown in Figure 7.24a. When the DI timing was 17° BTDC, the peak of ROHR in Fig 7.24b was 40% lower and 5 CAD later than those of the reference case. The AHR50 of the three cases (from the earliest DI timing to the latest) were at 3, 5 and 8° ATDC, respectively. A later DI timing resulted in a longer heat release process in the late combustion, which was apparent in the late stages of the heat release data.

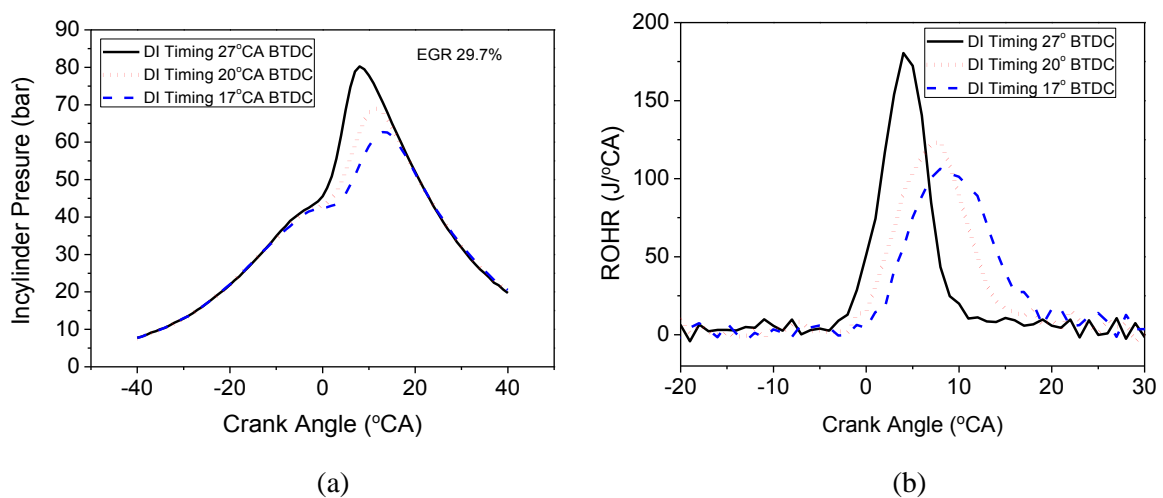


Figure 7.24 Combustion analysis for the different DI injection timings (a) In-cylinder pressure (b)ROHR.

Figure 7.25 shows the fuel efficiency and combustion performances of various DI injection timing. Clearly, retarding the injection timing increased the ISFC and reduced thermal efficiency. In the worst case, the ISFC was 10g/kW.h higher and the ITE was 2% (absolute value) lower than the reference case, as shown in Figure 7.25a. With the latter injection timing, 20° and 17° BTDC, the MPRRs were lower than 4 bar/° CA, which was comparable with a conventional diesel engine's operation.

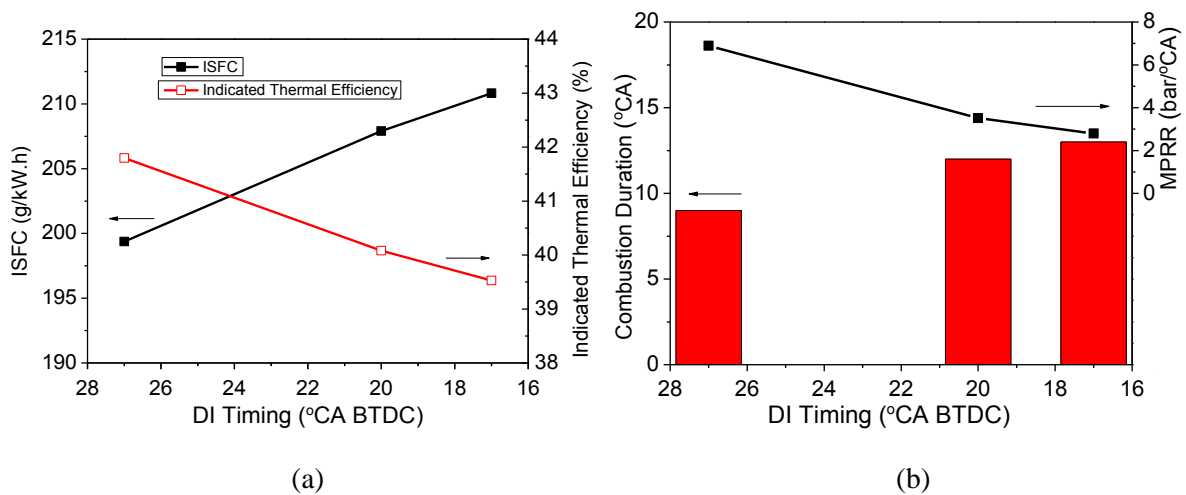
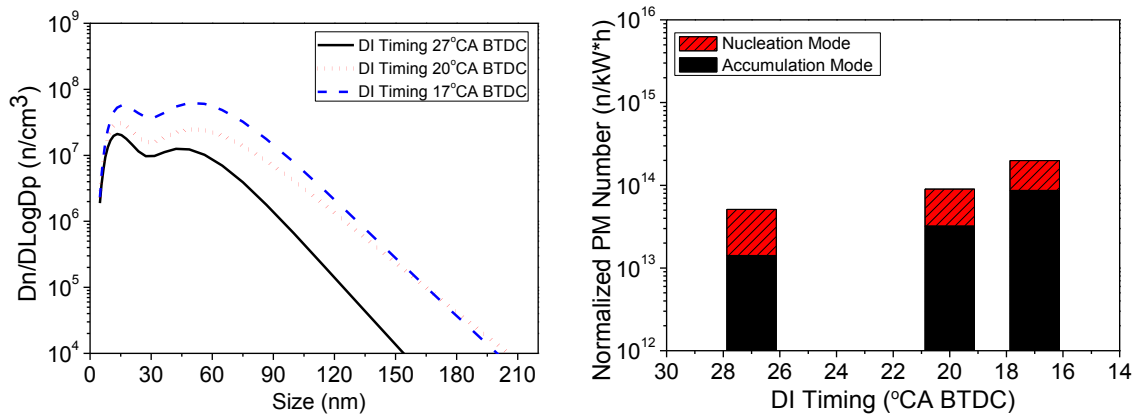


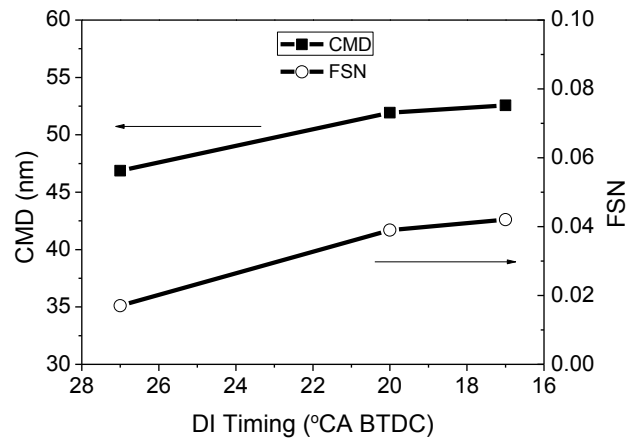
Figure 7.25 Impact of the DI injection timing on the ISFC, indicated thermal efficiency and combustion duration (a) ISFC and ITE (b) Combustion duration and MPRR.

Figure 7.26 shows the PM emissions for different diesel DI timings. Generally, a later DI injection timing (until around 10° BTDC) resulted in higher particle numbers, which coincided with the findings in previous sections. In particular, the particles total number (accumulation mode) increased by around 6 times and the CMD increased from 46 to 52 nm with retarding injection timing from 27° to 17° BTDC. However, the smoke emissions were maintained at a low level (below FSN 0.05) since the particle size was small compared to that of conventional diesel operation whose particles CMD were normally 65 to 75 nm.



(a)

(b)



(b)

Figure 7.26 Impact of the DI injection timing on the PM emissions (a) Normalised PM size distribution (b) Particle numbers of the accumulation and nucleation modes (c) CMD and FSN.

The result of this section indicates the potential of utilising SDCI strategy in industrial developments; which is, controlling the MPRR and P_{max} by optimising DI injection timing to find the compromise among the indicated thermal efficiency, pressure rise rate (related to the NVH) and P_{max} (related to the mechanical failure).

7.4. Conclusions

This chapter investigated the in-cylinder blended dieseline combustion in a modified single cylinder diesel engine. In the first part, the effects of EGR ratio, gasoline percentage, and combustion phasing were studied. Following that, a novel concept named SDCI combustion was proposed and examined. The conclusions that were made from the experimental results are as below:

In-cylinder Blended Dieseline Lean Burn

1. Increasing the gasoline percentages of in-cylinder blended dieseline combustion can effectively reduce the smoke emissions. Raising the EGR ratio can reduce the NO_x emissions and MPRR without compromise of thermal efficiency if the combustion phasing was fixed,
2. With combustion phasing (AHR50) at 5° ATDC, 65% gasoline and 40% EGR, the smoke, ISNO_x, ITE and MPRR of in-cylinder blended dieseline combustion at 4.3 bar IMEP were 0.17 FSN, 0.06 g/kW.h, 39.2% and 2.8 bar/deg respectively. Compared to the case of diesel baseline, the smoke and ISNO_x were reduced by 78% and 90% respectively. The ITE was 1% (absolute value) lower than diesel baseline, which resulted from the reduced combustion efficiency (from 99.6% to 92.9%).
3. Retarding the AHR50 from 1° to 5°ATDC reduced the NO_x emissions by 50% but the ITE was sacrificed by around 1.5% (absolute value),
4. With a fixed EGR ratio and DI diesel quantity, increasing the gasoline flow rate retards the combustion phasing and increases the engine load. At medium engine load (more than 5.2 bar IMEP), the ITE of in-cylinder blended dieseline combustion was close to the diesel baseline,

SDCI Combustion

5. EGR can be used to operate the engine under stoichiometric condition, which thus allows the usage of TWC for handling NO_x emissions. This removes the traditional NO_x-PM trade-off compromise in engine design and has the potential of developing high power density engines and using low-cost after treatments to meet stringent emissions' legislation,
6. The SDCI combustion can achieve better thermal efficiency than diesel engines' in a relatively wide load range (4.3 to 8 bar IMEP). The lowest ISFC of SDCI combustion was 190.8 g/kW.h at a middle load,
7. Gasoline percentage and diesel DI timing is important on the combustion phasing control. More diesel fuel results in an advanced combustion phasing and offers a wide range of ignition timing control, through adjusting DI timing,
8. The PM emissions of SDCI combustion were lower by up to 75% in number than the conventional CI diesel combustion results. Generally, lower gasoline percentage produces more accumulation mode particles. The DI timing also has a large impact on PM emissions: a later DI timing (until 10°BTDC) increases the number of particles. It also reduces the thermal efficiency but suppresses the MPRR, which is important for combustion noise control.

To summarise, the technique of in-cylinder blended dieseline is recommended for its advantage in reducing smoke emission and its flexibility in changing the diesel/gasoline blending ratio on-line. The NO_x emission can be reduced as well without penalty of smoke emission but the operating condition is limited to low loads. Specially, operating the engine under SDCI mode can effectively extend the operation range, increase the fuel efficiency and maintain the advantage of low emissions.

CHAPTER 8

SUMMARY, CONCLUSIONS AND FUTURE WORK

The research work in this thesis has focused on exploring the spray, combustion and emission characteristics of blended diesel and gasoline (dieseline) fuel. Compared to diesel, the higher volatility and auto-ignition resistance make dieseline a promising fuel for low emissions and high efficiency CI engines. However, in order to maximise performance, the difference of fuel spray, burning characteristics, combustion products, injection and blending strategies need to be investigated. This chapter summarizes the main conclusions drawn from experimental studies and provides suggestions for future work.

8.1. Summary and Conclusions

Four experimental chapters are contained in this thesis. The most significant findings are presented as below:

Dieseline Spray Characteristics

The spray of dieseline fuel has similar tip penetration length as diesel at various back pressures and injection pressures while the penetration length of gasoline is shorter than diesel, due to vaporization. At 40 mm downstream of the injector nozzle, with an increase of the gasoline/diesel blending ratio, both the mean diameter and the SMD of the fuel droplets are decreased due to vaporization. However, near the injector nozzle region, the difference of the SMD between blending ratios is small. For dieseline, relatively large droplets appeared near

the jet nozzle region and the diameter is significantly reduced downstream because of the vaporization. As the sampling position moves towards downstream, axial initial velocity of G50 droplets decreased and the final velocity increased.

Overall, the higher atomization quality of dieseline fuel, especially at the jet downstream, can improve the fuel/air mixing and thus produce less particle emissions compared to diesel.

Conventional Dieseline Combustion

With conventional injection and EGR strategies, the particle emissions of dieseline combustion are significantly reduced in terms of mean diameter and total number, at a wide load range (from 1.38 to 7.85 bar BMEP). This is supposedly due to the high volatility and long ignition delay of dieseline fuel. At low loads, G50 has a lower heat release peak and thus lower NO_x emissions than diesel baseline results, due to the partial over-mixing. However, the trend reversed at medium loads. Dieseline has lower BTE than diesel at low loads due to the incomplete combustion but the efficiency is similar at medium loads. The pilot injections can be used to reduce the MPRR of dieseline combustion but with some penalties of increased particle numbers and size (accumulation mode).

Dieseline PPCI Combustion

Dieseline fuelled PPCI combustion can be achieved by utilising advanced injection timings (between 20° and 30° BTDC) and large amounts of EGR (more than 45%) at 3 bar BMEP. Compared to the case of diesel baseline, the smoke, BSNO_x and particles total number were reduced by 98%, 87% and 99% respectively. The BTE increased from 28.5% to 30.1%. Using split injection strategies gave more flexibility, than single injection strategies, for the control

of mixing strength and combustion phasing. The variation of combustion phasing, smoke and BSNO_x emissions were mostly influenced by the second injection timing at a given EGR ratio. In contrast, the first injection timing and quantity-ratio had a dominating effect on BSTHC emissions and brake thermal efficiency.

Ultimately, the NO_x reduction of dieseline combustion largely depends on the EGR ratio. Extending the dieseline PPCI operation to a higher load was limited by the EGR utilisation.

In-cylinder Blended Dieseline Combustion

The gasoline/diesel blending ratio can be real-time controlled by modifying the diesel DI and gasoline PFI injection quantity. Utilising a high gasoline percentage and high EGR ratio reduces the NO_x and smoke emissions simultaneously. EGR can be used to operate the engine under stoichiometric condition, which thus allows the usage of TWC for handling NO_x emissions (SDCI combustion). This removes the traditional NO_x-PM trade-off compromise in engine design and has the potential of being used to develop high power density engines and to take advantage of low-cost after treatments to meet stringent emission legislation. The SDCI combustion can achieve better thermal efficiency than diesel engines in a relatively wide load range (4.3 to 8 bar IMEP). The PM emissions of SDCI combustion are lower by up to 75% in number than the conventional CI diesel combustion results.

Overall, the SDCI concept is a very promising technique for optimising CI engine's efficiency, emissions and noise without compromise of cost and power density.

8.2. Future Work

This thesis has explored a wide variety of dieseline's aspects and it leads to recommendations for future work.

8.2.1. CFD Simulation and Optical Diagnostic

The spray test has shown that dieseline had better atomization quality than diesel while the engine test confirmed dieseline's lower particle emissions. It is unknown whether the long ignition delay or high volatility has mainly led to the low smoke of dieseline. A detailed optical diagnostic and CFD simulation are suggested to answer this question. This could provide the oil industry with guidance on improving fuel quality for smokeless combustion.

8.2.2. Load Extension for PPCI Operation

Low emissions and high efficiency of dieseline fuelled PPCI combustion was achieved at 3 bar BMEP engine condition. A higher load was not further pursued because of the test rig's limitation. In order to extend the PPCI operation to the high load range, the engine should be equipped with an intake boosting system. This can guarantee that the fuel has enough oxygen to burn while the oxygen concentration is reduced by an increased EGR ratio. It would be worth finding out the required boosting pressure and EGR ratio for each engine load of PPCI operation.

8.2.2. Reliability of Using Dieseline in Common Rail Injection System

Gasoline fuel has much higher vapour pressure than diesel. It was observed during the dieseline tests that a lot of vapour bubbles formed in the low pressure fuel line. These vapour bubbles, may damage the high pressure pump and injector. Although no mechanical failure occurred in the present dieseline studies, a long term reliability test is suggested for the dieseline fuel before commercialization.

8.2.3. SDCI Combustion

The SDCI technique has been proven to be very promising for developing a low emission, low cost and high efficiency IC engines. However, due to the limitation of the current engine test rig's configuration, TWC wasn't tested in the present studies. The next step is to equip the engine with a TWC and measure the emissions after TWC. The exhaust temperature, idling and full load engine conditions are the focus for future work.

LIST OF REFERENCES

1. Franklin, Jr., Changing the World's Energy Systems, Stanford University Global Climate & Energy Project, SRI Consulting.
2. US Energy Information Administration, Annual Energy Review [Internet]. 2011[Cited in 2013 Feb 10]. Available from URL: http://www.eia.gov/totalenergy/data/annual/pecss_diagram.cfm.
3. Reiner, R., Cartalos, O., Evrigenis, A. and Viljamaa, K., Challenges for A European Market for Electric Vehicles [Internet]. 2010 [Cited in 2013 Feb 12]. Available from URL:<http://www.europarl.europa.eu/document/activities/cont/201106/20110629ATT22885/20110629ATT22885EN.pdf>.
4. IPCC, Climate Change 2007: The Physical Science Basis. Contribution of Working Group I to the Fourth Assessment Report of the Intergovernmental Panel on Climate Change. Cambridge University Press, ISBN 0521705967, 2007.
5. European Commission. Road Transport: Reducing CO2 emissions from vehicles [Internet]. 2012 [Cited in 2012 Feb 13]. Available from URL: http://ec.europa.eu/clima/policies/transport/vehicles/index_en.htm.
6. Najt, P., "Compression-Ignited Homogeneous Charge Combustion," SAE Technical Paper 830264, 1983.
7. Hiroyasu, H. and Arai, M., (1990) "Structures of Fuel Sprays in Diesel Engines," SAE Paper 900475, 1990.
8. Lefebvre, A.H., Atomization and Sprays. 1989, New York, Hemisphere Publishing Corporation.
9. Reitz, R.D. and Bracco, F.V., MECHANISM OF ATOMIZATION OF A LIQUID JET. Physics of Fluids, 1982. 25(10): pp 1730-1742.
10. Arcoumanis, C., Gavaises, M., and French, B., "Effect of Fuel Injection Processes on the Structure of Diesel Sprays," SAE Technical Paper 970799, 1997.
11. Soteriou, C., Andrews, R., and Smith, M., Direct Injection Diesel Sprays and the Effect of Cavitation and Hydraulic Flip on Atomization. , " SAE Technical Paper 950080, 1995.
12. Faeth, G.M., Hsiang, L.P., Wu, P.K., Structure and breakup properties of sprays. International Journal of Multiphase Flow, 1995. Volume 21(Supplement 1), pp 99-127.

13. Smallwood, G.J., Gulder, O.L. and Snelling, D.R., Views on the structure of transient diesel sprays. *Atomization and Sprays*, 2000. Volume 10(3-5), pp 355-386
14. Naber, J. and Siebers, D., "Effects of Gas Density and Vaporization on Penetration and Dispersion of Diesel Sprays," SAE Technical Paper 960034, 1996.
15. Klein-Douwel, R.J.H., Frijters, P.J.M., Seykens, X.L.J., Somers, L.M.T. & Baert, R.S.G. . Gas density and rail pressure effects on diesel spray growth from a heavy-duty common rail injector. *Energy & Fuels*, 2009, 23(4), pp 1832-1842.
16. Chang, C. T. and Farrel, P.V., "A Study on the Effects of Fuel Viscosity and Nozzle geometry on High Injection Pressure Diesel Spray Characteristics", SAE Technical Paper 970353, 1997.
17. Zink, M., Raatz, T., Wintrich, T., and Eilts, P., "A New Approach for Characterization of Fuel Property Influence on Spray Formation in Diesel Engines," SAE Technical Paper 2010-01-2249, 2010.
18. Matsuoka, H., Yamashita, H., Hayashi, T., and Kitano, K., "Effects of Fuel Properties on Diesel Spray Behavior under High Temperature and High Pressure Conditions," SAE Technical Paper 2009-01-0834, 2009.
19. Payri, R., Garcia, A., Domenech, V., Durett, R., Plazas, A.H., " An experimental study of gasoline effects on injection rate, momentum flux and spray characteristic using a common rail diesel injection system", *Fuel*, Vol.97, pp 390-399, 2012.
20. Mugele, R., and EEvans, H.D., Droplet Size Distribution in Sprays, *Ind. Eng. Chem.*, Vol.43, No.6, 1951, pp. 1317-1324.
21. Tabata, M., Fujii, H., Arai, M and Hiroyasu, H., (1991) "Mean Drop Diameter of a Diesel Spray in a Vaporizing process", *JSME International Journal, Series II*, Vol. 34, No.3, pp 369-378.
22. Gulder, O.L. and Smallwood, G.J., Time-resolved structure of full cone diesel sprays. *Proceedings of the Second International Workshop on Advanced Spray Combustion*, pp. 1-10, 1998.
23. Yule, A., Akhtar, P., Shrimpton, J., Wagner, T., Rickeard, D.J and Duff, J.L.C., "PDA Measurements of Fuel Effects on Atomization and Spray Structure from a Diesel Engine Injector," SAE Technical Paper 982544, 1998.
24. Heywood, J. B., *Internal Combustion Engine Fundamentals*, McGraw Hill International Editions, ISBN 0-07-100499-8, 1988.

25. Dec, J.E., "A Conceptual Model of DI Diesel Combustion Based on Laser-Sheet Imaging", SAE Technical Paper 970873, 1997.
26. Dec, J.E., "Advanced compression-ignition engines-understanding the in-cylinder processes", Proceedings of The Combustion Institute, Issue 32, pp. 2727-2742, 2009.
27. Kittelson, D.B. "Engines and nanoparticles: A review". Journal of Aerosol Science 29, pp. 575-588, 1998.
28. Zhang, J., Zhang, F., Tian, G., Xu, H. et al., "The Particle Emission Characteristics of a Light Duty Diesel Engine by Using Different Pilot Injections," SAE Technical Paper 2010-01-1959, 2010.
29. Zhang, J., Xu, H., Tian, G., Zhang, F. et al., "The Particle Emissions Characteristics of a Light Duty Diesel Engine with 10% Alternative Fuel Blends," *SAE Int. J. Fuels Lubr.* 3(2):438-452, 2010.
30. Ehleskog, M., Gjirja, S., and Denbratt, I., "Effects of High Injection Pressure, EGR and Charge Air Pressure on Combustion and Emissions in an HD Single Cylinder Diesel Engine," *SAE Int. J. Engines* 2(2):341-354, 2010.
31. Pickett, L.M and Siebers, D.L., Soot in diesel fuel jets: effects of ambient temperature, ambient density, and injection pressure, *Combustion and Flame*, Volume 138, Issues 1–2, pp. 114-135, 2004.
32. Eastwood, P., *Particulate Emissions from Vehicles*, John Wiley & Sons Ltd, ISBN 978-0-470-72455-2, 2008.
33. Zhang, J., Tian, G.H., Xu, H.M., Zhang, F and Daniel., R., "The Application of Two Closely Coupled DPFs as the After-treatment System," SAE Technical Paper 2010-01-1939, 2010.
34. Zeldovich, Y. B and Sadovnikov., P. Y., *Oxidation of Nitrogen in Combustion*. Academy of Sciences, USSR. 1947.
35. Badami, M., Millo, F. and D'Amata, D. D., "Experimental Investigation on Soot and NOx Formation in a DI Common Rail Diesel Engine with Pilot Injection". SAE Technical Paper 2001-01-0657, 2001.
36. Hildingsson, L., Johansson, B., Kalghatgi, G., and Harrison, A., "Some Effects of Fuel Autoignition Quality and Volatility in Premixed Compression Ignition Engines," *SAE Int. J. Engines* 3(1):440-460, 2010.
37. Kim, D., Ekoto, I., Colban, W., and Miles, P., "In-cylinder CO and UHC Imaging in a Light-Duty Diesel Engine during PPCI Low-Temperature Combustion," *SAE Int. J. Fuels Lubr.* 1(1):933-956, 2009.

38. Sjöberg, M. and Dec, J.E., An investigation into lowest acceptable combustion temperatures for hydrocarbon fuels in HCCI engines, Proceedings of the Combustion Institute, Volume 30, Issue 2, pp. 2719-2726, 2005.
39. Khan, I.M., Greeves, G. and Wang, C.H.T., "Factors Affecting Smoke and Gaseous Emissions from Direct Injection Engines and a Method of Calculation," SAE paper 730169, 1973.
40. Takeda, Y., Keiichi, N., and Keiichi, N., "Emission Characteristics of Premixed Lean Diesel Combustion with Extremely Early Staged Fuel Injection," SAE Technical Paper 961163, 1996.
41. André, M., Walter, B., Bruneaux, G., Foucher, F. and Mounaim-Rousselle, C., "Optimizing Early Injection Strategy for Diesel PCCI Combustion," SAE Technical Paper 2009-01-2731, 2009.
42. (Bill) Gray, A. and Ryan, T., "Homogeneous Charge Compression Ignition (HCCI) of Diesel Fuel," SAE Technical Paper 971676, 1997.
43. Ryan, T. and Callahan, T., "Homogeneous Charge Compression Ignition of Diesel Fuel," SAE Technical Paper 961160, 1996.
44. Kook, S., Bae, C., Miles, P., Choi, D. and Pickett., L.M., "The Influence of Charge Dilution and Injection Timing on Low-Temperature Diesel Combustion and Emissions," SAE Technical Paper 2005-01-3837, 2005.
45. Pickett, L. and Siebers, D., "Non-Sooting, Low Flame Temperature Mixing-Controlled DI Diesel Combustion," SAE Technical Paper 2004-01-1399, 2004.
46. Pickett, L.M., Caton, J.A., Musculus, M. P. B. and Lutz, A. E., "Evaluation of the equivalence ratio-temperature region of diesel soot precursor formation using a two-stage Langrangian model. International Journal of Engine Research," Volume 7, pp.349-370, 2006.
47. Helmantel, A., "Reduction of NOx Emissions from a Light Duty DI Diesel Engine in Medium Load Conditions with High EGR Rates," SAE Technical Paper 2008-01-0643, 2008.
48. Kiplimo, R., Tomita, E., Kawahara, N., Zhou, S. and Yokobe, S., "Effects of Injection Pressure, Timing and EGR on Combustion and Emissions Characteristics of Diesel PCCI Engine," SAE Technical Paper 2011-01-1769, 2011.
49. Genzale, C., Reitz, R., and Musculus, M., "Effects of Piston Bowl Geometry on Mixture Development and Late-Injection Low-Temperature Combustion in a Heavy-Duty Diesel Engine," *SAE Int. J. Engines*1(1):913-937, 2009.

50. Cao, L., Bhave, A., Su, H., Mosbach, S., Kraft, M., Dris, A., and McDavid, R.M., et al., "Influence of Injection Timing and Piston Bowl Geometry on PCCI Combustion and Emissions," *SAE Int. J. Engines* 2(1):1019-1033, 2009.
51. Musculus, M.P.B., Pickett, L.M., Miles, P., Dec, J. and Oefelein, J., "A Conceptual Model for Partially Premixed Low-Temperature Diesel Combustion Based on In-Cylinder Laser Diagnostics and Chemical Kinetics Modeling," Directions in Engine-Efficiency and Emissions Reduction Research Conference, Michigan, 2012.
52. Keeler, B., Constraints on the Operation of a DI Diesel Engine in Partially-premixed Combustion Mode, PHD thesis, University of Nottingham, 2009.
53. Zhao, H., Advanced direct injection combustion engine technologies and development, volume 2: Diesel engines, 2010, Cambridge, Woodhead Publishing Limited.
54. Kimura, S., Aoki, O., Kitahara, Y. and Aiyoshizawa, E. "Ultra-Clean Combustion Technology Combining a Low-Temperature and Premixed Combustion Concept for Meeting Future Emission Standards," SAE Technical Paper 2001-01-0200, 2001.
55. Kimura, S., Ogawa, H., Matsui, Y. and Enomoto, Y., An Experimental Analysis of Low-Temperature and Premixed Combustion for Simultaneous Reduction of NO_x and Particulate Emissions in Direct Injection Diesel Engines. *International Journal of Engine Research*, Volume 3 (4), pp. 249-259, 2002.
56. Kimura, S., Aoki, O., Ogawa, H., Muranaka, S. and Enomoto, Y., New Combustion Concept for Ultra-Clean and High-Efficiency Small DI Diesel Engines, SAE Technical Paper 1999-01-3681. 1999.
57. Weall, A. and Collings, N., "Highly Homogeneous Compression Ignition in a Direct Injection Diesel Engine Fuelled with Diesel and Biodiesel," SAE Technical Paper 2007-01-2020, 2007.
58. Araki, M., Umino, T., Obokata, T., Ishima, T. et al., "Effects of Compression Ratio on Characteristics of PCCI Diesel Combustion with a Hollow Cone Spray," SAE Technical Paper 2005-01-2130, 2005.
59. Beatrice, C., Giacomo, N., and Guido, C., "Benefits and Drawbacks of Compression Ratio Reduction in PCCI Combustion Application in an Advanced LD Diesel Engine," *SAE Int. J. Engines* 2(1):1290-1303, 2009
60. Siebers, D., "Scaling Liquid-Phase Fuel Penetration in Diesel Sprays Based on Mixing-Limited Vaporization," SAE Technical Paper 1999-01-0528, 1999.
61. Cao, L., Bhave, A., Su, H., Mosbach, S. et al., "Influence of Injection Timing and Piston Bowl Geometry on PCCI Combustion and Emissions," *SAE Int. J. Engines* 2(1):1019-1033, 2009.

62. Hasegawa, R. and Yanagihara, H., "HCCI Combustion in DI Diesel Engine ," SAE Technical Paper 2003-01-0745, 2003.
63. Yanagihara, H., "Ignition Timing Control at Toyota 'UNIBUS' Combustion System," Proceedings of the IFP International Congress on a New Generation of Engine Combustion Processes of the Future, pp.34-42, 2001.
64. 13. Sun, Y. and Reitz, R.D., "Adaptive Injection Strategies (AIS) for Ultra-Low Emissions Diesel Engine," SAE Technical Paper 2008-01-0058, 2008.
65. Sun, Y. and Reitz, R.D., "Adaptive Engine Injection for Emissions Reduction," University of Wisconsin WARF Patent Application P07342US, March, 2007.
66. Kokjohn, S., Swor, T.A., Andrie, M.J. and Reitz, R.D., "Experiments and Modeling of Adaptive Injection Strategies (AIS) in Low Emission Diesel Engines," SAE International Journal of Engines, vol. 2, no. 1, pp .16-32, 2009.
67. Pesant, L., Forti, L., and Jeuland, N., "Effect of Fuel Characteristics on the Performances and Emissions of an Early-injection LTC / Diesel Engine," SAE Technical Paper 2008-01-2408, 2008.
68. Cheng, A.S., Fisher, B.T., Martin, G.C., Mueller, C.J., Effects of fuel volatility on early direct-injection, low-temperature combustion in an optical diesel engine. *Energy Fuel* 2010; 24(3): 1538-51.
69. Kalghatgi, G.T., Hildingsson, L., Johansson, B., Harrison, A.J., "Low-NOx, low-Smoke Operation of a Diesel Engine Using 'Premixed Enough' Compression Ignition – Effects of Fuel Auto-Ignition Quality, Volatility and Aromatic Content," Proceedings of THIESEL 2010, Thermo and fluid dynamic processes in diesel engines, UPV Valencia, 14–17 September, 2010.
70. Hildingsson, L., Johansson, B., Kalghatgi, G., and Harrison, A., "Some Effects of Fuel Autoignition Quality and Volatility in Premixed Compression Ignition Engines," *SAE Int. J. Engines* 3(1):440-460, 2010.
71. Ickes A.M, Bohac, S.V., Assanis, D.N., Effect of fuel cetane number on a premixed diesel combustion mode. *Int J Engine Res* 2009; 10(4): 251-63.
72. Warey, A., Hardy, J., Hennequin, M., Tatur, M. et al., "Fuel Effects on Low Temperature Combustion in a Light-Duty Diesel Engine," SAE Technical Paper 2010-01-1122, 2010.
73. Butts, R., Foster, D., Krieger, R., Andrie, M. et al., "Investigation of the Effects of Cetane Number, Volatility, and Total Aromatic Content on Highly-Dilute Low Temperature Diesel Combustion," SAE Technical Paper 2010-01-0337, 2010.

74. Zheng, M., Han, X., Tan, Y., Kobler, M. et al., "Low Temperature Combustion of Neat Biodiesel Fuel on a Common-rail Diesel Engine," SAE Technical Paper 2008-01-1396, 2008.
75. Veltman, M., Karra, P., and Kong, S., "Effects of Biodiesel Blends on Emissions in Low Temperature Diesel Combustion," SAE Technical Paper 2009-01-0485, 2009.
76. Northrop, W., Bohac, S., and Assanis, D., "Premixed Low Temperature Combustion of Biodiesel and Blends in a High Speed Compression Ignition Engine," *SAE Int. J. Fuels Lubr.* 2(1):28-40, 2009.
77. Fang, T., Lin, Y., Foong, T., and Lee, C., "Spray and Combustion Visualization in an Optical HSDI Diesel Engine Operated in Low-Temperature Combustion Mode with Bio-diesel and Diesel Fuels," SAE Technical Paper 2008-01-1390, 2008.
78. Kalghatgi, G.T., Risberg, P., and Ångström, H.E., "Advantages of a fuel with high resistance to auto-ignition in late-injection, low-temperature, compression ignition combustion," SAE Technical Paper 2006-01-3385, 2006.
79. Kalghatgi, G.T., Risberg, P., and Ångström, H.-E., "Partially pre-mixed auto-ignition of gasoline to attain low smoke and low NO_x at high load in a compression ignition engine and comparison with a diesel fuel," SAE Technical Paper 2007-01-0006, 2007.
80. Kalghatgi, G., Hildingsson, L., and Johansson, B., "Low NO_x and low smoke operation of a diesel engine using gasoline-like fuels", Proceedings of the ASME Internal Combustion Engine Division 2009 Technical Conference, ICES2009-76034, 2009.
81. Kalghatgi, G., Hildingsson, L., Harrison, A.J. and Johansson, B., "Some effects of fuel auto-ignition quality and volatility in premixed compression ignition engines", SAE Technical paper 2010-01-0607.
82. Kalghatgi, G., Hildingsson, L., Johansson, B., "Low NO_x and Low Smoke Operation of a Diesel Engine Using Gasoline like Fuels," *Journal of Engineering for Gas Turbines and Power*, Vol. 132(9), Article 1, 092803, 2010.
83. Hildingsson, L., Kalghatgi, G., Harrison, A. J., and Johansson, B. Auto-ignition quality of gasoline fuels in partially premixed combustion in diesel engines. *Proc. Combust. Inst.*, 2011, 33, 3015–3021.
84. Kalghatgi, G.T., "Is gasoline the best fuel for advanced diesel engines? - Fuel effects in "premixed-enough" compression ignition (CI) engines", Conference on Towards Clean Diesel Engines, Aachen, June 4-5, 2009.
85. Kalghatgi, G., Hildingsson, L., Harrison, A. J., and Johansson, B. Low NO_x and low smoke operation of a diesel engine using premixed enough compression ignition: effects of fuel auto-ignition quality and volatility and aromatic content. In Proceedings of the

THEISEL 2010 Conference on Thermo- and Dynamic Processes in Diesel Engines
Valencia, Spain, 14–17 September 2010, pp. 409–420.

86. Manente, V., Johansson, B., Tunestal, P., Gasoline partially premixed combustion: High efficiency, low NO_x and low soot by using an advanced combustion strategy and a compression ignition engine, *International Journal of Vehicle Design*. Volume 59, Issue 2-3, pp. 108-128.
87. Manente, V., Johansson, B., and Tunestål, P., “Partially Premixed Combustion at High Load using Gasoline and Ethanol, a Comparison with Diesel,” SAE Technical Paper 2009-01-0944, 2009.
88. Manente, V., Johansson, B., and Tunestål, P., “Half Load Partially Premixed Combustion, PPC, with High Octane Number Fuels. Gasoline and Ethanol Compared with Diesel”, *SIAT* 2009 295, 2009.
89. Manente, V., Johansson, B., and Tunestål, P., “Characterisation of partially premixed combustion with ethanol: EGR sweeps, low and maximum loads”, *Proceedings of the ASME Internal Combustion Engine Division 2009 Technical Conference, ICES2009-76165*, 2009.
90. Tunér, M., Fröjd, K., Seidel, L., Mauss, F. et al., "Diesel-PPC engine: Predictive Full Cycle Modeling with Reduced and Detailed Chemistry," SAE Technical Paper 2011-01-1781, 2011.
91. Fridriksson, H., Sundén, B., Hajireza, S., and Tunér, M., "CFD Investigation of Heat Transfer in a Diesel Engine with Diesel and PPC Combustion Modes," SAE Technical Paper 2011-01-1838, 2011.
92. Borgqvist, P., Tuner, M., Mello, A., Tunestal, P. et al., "The Usefulness of Negative Valve Overlap for Gasoline Partially Premixed Combustion, PPC," SAE Technical Paper 2012-01-1578, 2012.
93. Sellnau, M., Sinnamon, J., Hoyer, K., and Husted, H., "Gasoline Direct Injection Compression Ignition (GDCI) - Diesel-like Efficiency with Low CO₂ Emissions," *SAE Int. J. Engines* 4(1):2010-2022, 2011
94. Sellnau, M., Sinnamon, J., Hoyer, K., and Husted, H., "Full-Time Gasoline Direct-Injection Compression Ignition (GDCI) for High Efficiency and Low NO_x and PM," *SAE Int. J. Engines* 5(2):300-314, 2012.
95. Ciatti, S. A., Subramanian, S., “An Experimental Investigation of Low Octane Gasoline in Diesel Engines,” *ASME Journal of Engineering for Gas Turbines and Power Systems*, New York, NY, 2011.
96. Ra, Y., Yun, J.E., and Reitz, R., “Numerical Simulation of Diesel Engine Operation with Gasoline,” *Combustion, Science, and Technology*, Volume 181, 2009.

97. Hansen, R., Splitter, D., and Reitz, R., "Operating a Heavy-Duty Direct-Injection Compression Ignition Engine with Gasoline for Low Emissions," SAE Technical Paper 2009-01-1442, 2009.
98. Weall, A.J., and Collings, N., "Gasoline Fuelled Partially Premixed Compression Ignition in a Light Duty Multi Cylinder Engine: A Study of Low Load and Low Speed Operation," SAE Technical Paper 2009-01-1791, 2009.
99. Zhong, S., Wyszynski, M., Megaritis, A., Yap, D. and Xu, H., "Experimental Investigation into HCCI Combustion Using Gasoline and Diesel Blended Fuels," SAE Technical Paper 2005-01-3733, 2005.
100. Turner, D., Tian, G., Xu, H., Wyszynski, M. et al., "An Experimental Study of Dieseline Combustion in a Direct Injection Engine," SAE Technical Paper 2009-01-1101, 2009.
101. Zhang, F., Xu, H., Zhang, J., Tian, G. et al., "Investigation into Light Duty Dieseline Fuelled Partially-Premixed Compression Ignition Engine," *SAE Int. J. Engines* 4(1):2124-2134, 2011.
102. Zhang, F., Xu, H., Zeraati Rezaei, S., Kalghatgi, G. et al., "Combustion and Emission Characteristics of a PPCI Engine Fuelled with Dieseline," SAE Technical Paper 2012-01-1138, 2012.
103. Weall, A. and Collings, N., "Investigation into Partially Premixed Combustion in a Light-Duty Multi-Cylinder Diesel Engine Fuelled with a Mixture of Gasoline and Diesel," SAE Technical Paper 2007-01-4058, 2007.
104. Han, D., Ickes, A., Assanis, D. N., Zhen, H., Bohac, S.V., "The Attainment and Load Extension of High-Efficiency Premixed Low-Temperature Combustion with Dieseline in a Compression Ignition Engine," *Energy & Fuels*, 24, pp. 3517-3525, 2010.
105. Han, D., Ickes, A., Bohac, S.V., Zhen, H., Assanis, D.N., Premixed low-temperature combustion of blends of diesel and gasoline in a high speed compression ignition engine, *Proceedings of the Combustion Institute*, Volume 33, Issue 2, 2011, pp. 3039-3046.
106. Bessonette, P.W., Schleyer, C.H., Duffy, K.P., Hardy, W.L. et al., "Effects of Fuel Property Changes on Heavy-Duty HCCI Combustion," SAE Technical Paper 2007-01-0191, 2007.
107. Kokjohn, S.L., Hanson, R.M., Splitter, D.A., and Reitz, R.D., "Experiments and Modeling of Dual-Fuel HCCI and PCCI Combustion Using In-Cylinder Fuel Blending," *SAE Int. J. Engines* 2(2):24-39, 2009.

108. Hanson, R.M., Kokjohn, S.L., Splitter, D.A., and Reitz, R.D., "An Experimental Investigation of Fuel Reactivity Controlled PCCI Combustion in a Heavy-Duty Engine," SAE Int. J. Engines 3(1):700-716.
109. Splitter, D., Kokjohn, S., Rein, K., Hanson R. et al., "An Optical Investigation of Ignition Process in Fuel Reactivity Controlled PCCI Combustion," SAE Int. J. Engines 3(1):142-162, 2010.
110. Splitter, D., Hanson, R., Kokjohn, S., and Reitz, R., "Reactivity Controlled Compression Ignition (RCCI) Heavy-Duty Engine Operation at Mid-and High-Loads with Conventional and Alternative Fuels," SAE Technical Paper 2011-01-0363, 2011.
111. Alger, T., Hanhe, S., Roberts, C., and Ryan, T., "The Heavy Duty Gasoline Engine - A Multi-Cylinder Study of a High Efficiency, Low Emission Technology," SAE Technical Paper 2005-01-1135, 2005.
112. Alger, T. and Mangold, B., "Dedicated EGR: A New Concept in High Efficiency Engines," *SAE Int. J. Engines*2(1):620-631, 2009.
113. Roberts, C., Snyder, J., Stovell, C., Dodge, L. et al., "The Heavy-Duty Gasoline Engine - An Alternative to Meet Emissions Standards of Tomorrow," SAE Technical Paper 2004-01-0984, 2004.
114. Jiang, H., Wang, J., and Shuai, S., "Visualization and Performance Analysis of Gasoline Homogeneous Charge Induced Ignition by Diesel," SAE Technical Paper 2005-01-0136, 2005.
115. Yu, C., Wang, J.X., Wang, Z. and Shuai, S.J., Comparative study on Gasoline Homogeneous Charge Induced Ignition (HCII) by diesel and Gasoline/Diesel Blend Fuels (GDBF) combustion, *Fuel*, Available online 15 November 2012, ISSN 0016-2361.
116. Lee, S., Gonzalez, D. M. A., and Reitz, R. D., 2006, "Stoichiometric Combustion in a HSDI Diesel Engine to Allow Use of a Three-Way Exhaust Catalyst," SAE Technical Paper 2006-01-1148, 2006.
117. Lee, S., Gonzalez D. M. A., and Reitz, R. D., 2007, "Effects of Engine Operating Parameters on Near Stoichiometric Diesel Combustion Characteristics," SAE Technical Paper 2007-01-0121, 2007.
118. Kim, j., Reitz, R.D., Park, S.W. and Sung, k., Reduction of NO_x and CO Emissions in Stoichiometric Diesel Combustion Using a 3-Way Catalyst, ASME Conf. Proc. 2009, pp. 389-397.
119. Chase, S., Nevin, R., Winsor, R., and Baumgard, K., 2007, "Stoichiometric Compression Ignition SCI Engine," SAE Technical Paper 2007-01-4224, 2007.

120. Muether, M., Lamping, M., Kolbeck, A., Cracknell, R. Rickeard, D.J., Aritegui, J., Rose, K.D., "Advanced Combustion for Low Emissions and High Efficiency Part 1: Impact of Engine Hardware on HCCI Combustion," SAE Technical Paper 2008-01-2405, 2008.
121. Musculus, M., "Multiple Simultaneous Optical Diagnostic Imaging of Early-Injection Low-Temperature Combustion in a Heavy-Duty Diesel Engine," SAE Technical Paper 2006-01-0079, 2006.
122. Eastwood, P., Particulate Emissions from Vehicles, John Wiley & Sons Ltd, ISBN 978-0-470-72455-2, 2008.
123. Noehre, C., Andersson, M., Johansson, B., Hultqvist, A., "Characterization of Partially Premixed Combustion," SAE Technical Paper 2006-01-3412, 2006.
124. Walter, B. and Gatellier, B., "Development of the High Power NADI™ Concept Using Dual Mode Diesel Combustion to Achieve Zero NOx and Particulate Emissions", SAE Technical Paper 2002-01-1744, 2002.
125. Papagiannakis, R., Rakopoulos, C, Hountalas, D., et al. Emission characteristics of high speed, dual fuel, compression ignition engine operating in a wide range of natural gas/diesel fuel proportions. Fuel 2010; 89:1397-1406.
126. Wakuri, Y., Fujii, M., Amitani, T. and Tsuneva, R., Studies of the penetration of a fuel spray in a diesel engine. J Soc Mech Eng 1960;3:123–30.
127. Dent, J.C., "A basis for the comparison of various experimental methods for studying spray tip," SAE Technical Paper 660749, 1966.
128. Li, Y.F., Experimental study on spray and combustion characteristics of diesel like fuel, PhD Thesis, University of Birmingham, 2012.
129. Measurement principles of PDA [Internet]. 2013 [cited in 2013 Feb 12]. Available from URL: <http://www.dantecdynamics.com/Default.aspx?ID=1058>.
130. Zhao, H. and Ladammatos, N., Engine Combustion Instrumentation and Diagnostics. Warrendale: Society of Automotive Engineers; 2001.
131. Zhang, J., Particle Matter Emission Control and Related Issues for Diesel Engines. PhD Thesis, University of Birmingham, 2011.
132. Specification of D-type flip-flop ACT374 [Internet]. 2013 [cited in 2013 Feb 12]. Available from URL: <http://www.ti.com/lit/ds/schs290/schs290.pdf>.

133. Model 3936 SMPS (Scanning Mobility Particle Sizer) [Internet]. 2003 [cited in 2013 Feb 12]. Available from URL: <http://www.univ-tln.fr/Recherche/unites/lepi/instruments/smeps3936.pdf>.
134. Jonathan P.R.S., Jason, S.O. and Kingsley S.J.R., Sample Line Efficiency Measured with a Real Time Particulate Size Spectrometer. Poster, Cambustion, 2007.

APPENDIX

A. Literature Review

A1. Criteria of Jet Break-up Regimes and Definitions

Liquid Weber Number (We):

$$We = \frac{\text{inertia}}{\text{surface tension}} = \frac{\rho_l D V_d^2}{\sigma}$$

Reynolds Number (Re):

$$Re = \frac{\text{inertia}}{\text{viscosity}} = \frac{\rho_l V_d L}{\mu} = \frac{V_d L}{\nu}$$

Ohnesorge Number (Oh):

$$Oh = \frac{\sqrt{We}}{Re}$$

Where ρ_l is the liquid density, D is the droplet diameter, V_d is the droplet relative velocity, σ is the liquid surface tension, μ is the dynamic viscosity, ν is the kinematic viscosity, L is the nozzle length

B. Experimental Setup

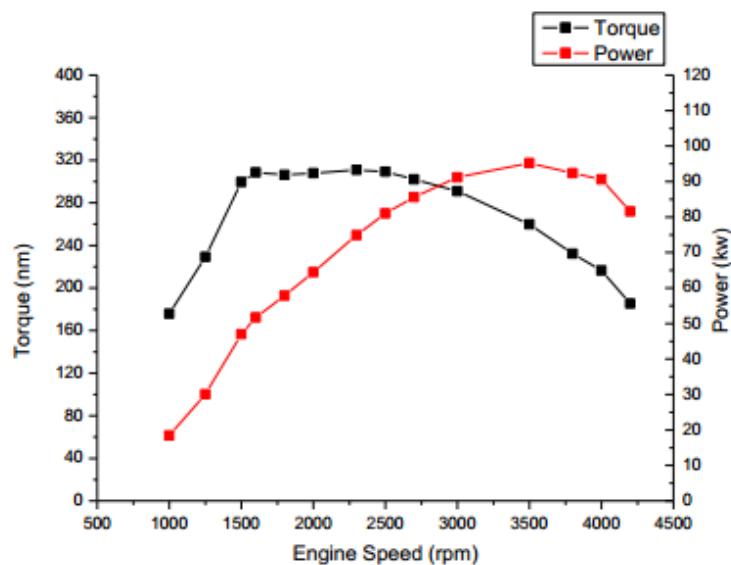


Figure B1 The torque and power characteristics of PUMA engine [131]

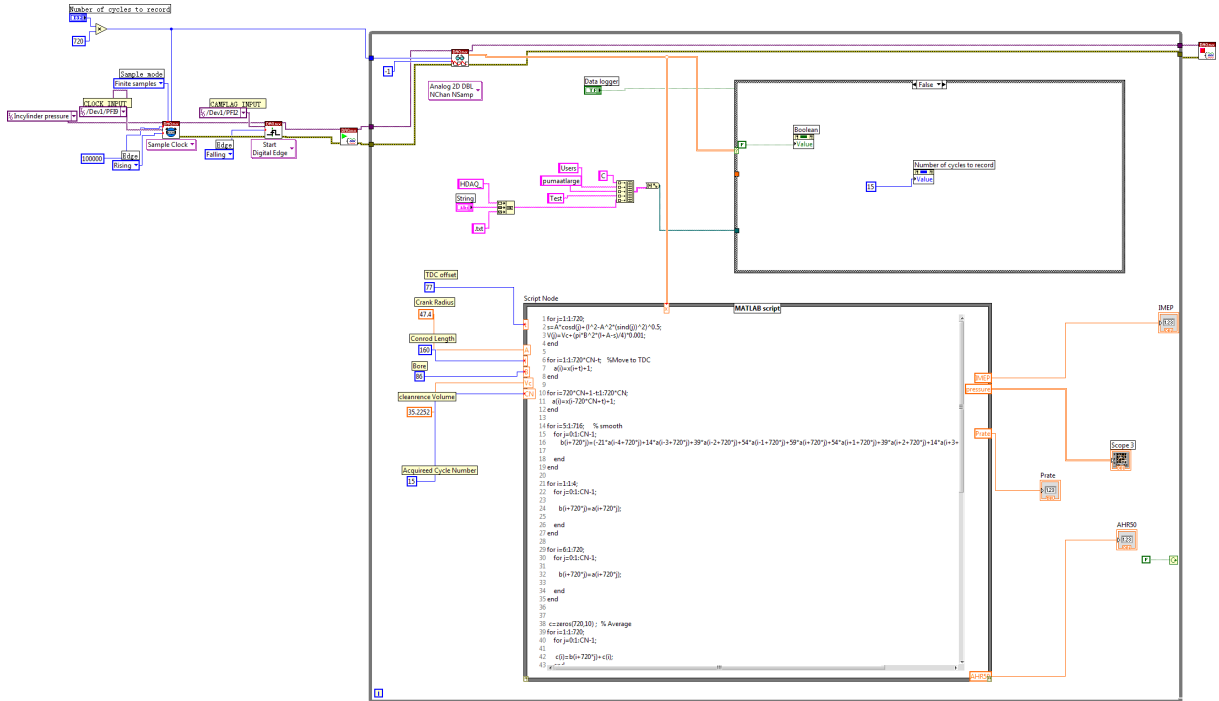


Figure B2 The block diagram of real time combustion analysing program

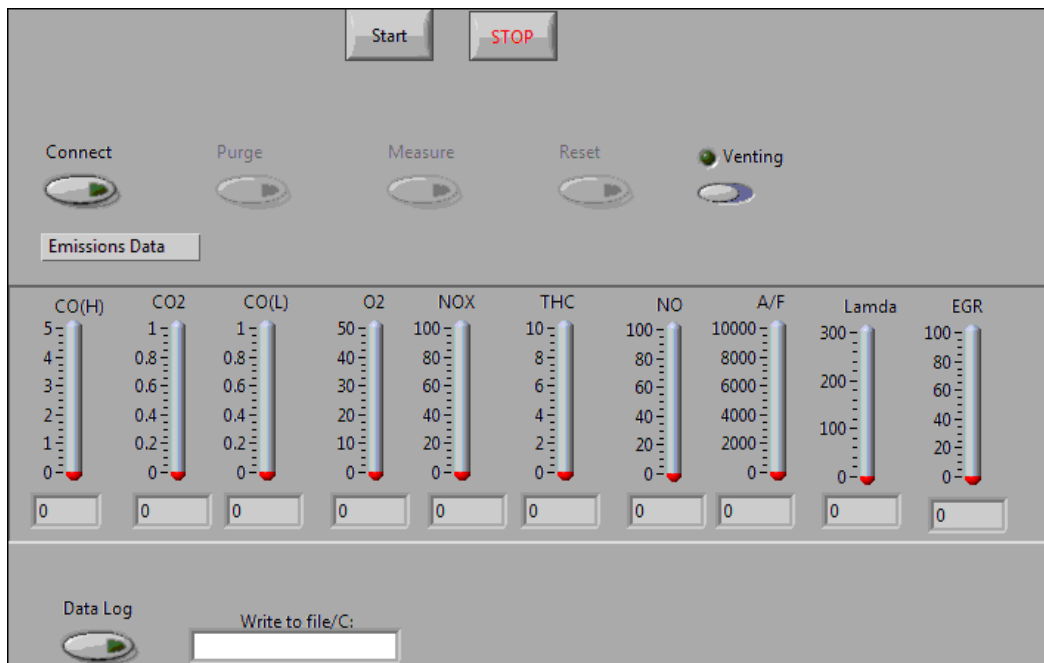


Figure B3 The front panel of Horiba remote control program



Figure B4 The block diagram of Horiba remote control program

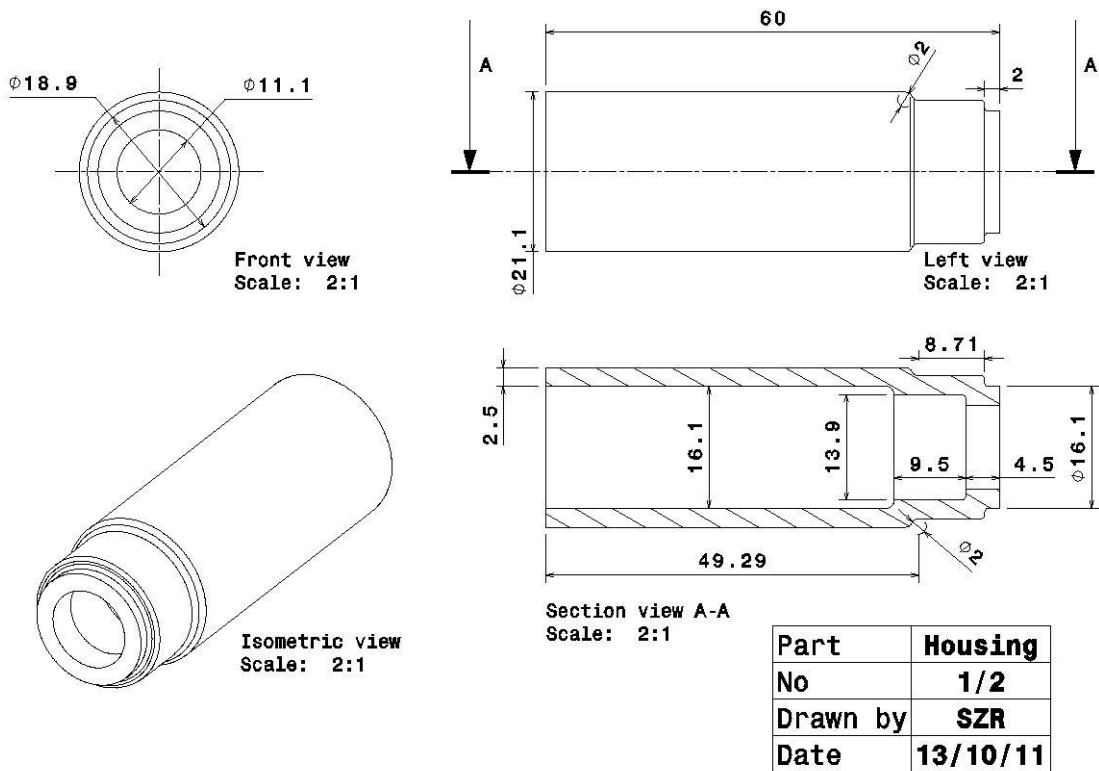


Figure B5 The engineering drawing of PFI injector housing